



ΕΘΝΙΚΟ ΜΕΤΣΟΒΙΟ ΠΟΛΥΤΕΧΝΕΙΟ

ΣΧΟΛΗ ΜΗΧΑΝΟΛΟΓΩΝ ΜΗΧΑΝΙΚΩΝ

ΤΟΜΕΑΣ Μ.Κ. & Α.Ε.

Εργαστήριο Αυτομάτου Ελέγχου

Διπλωματική Εργασία

**Design of Upper limb prosthesis:
Experimental Comparison of the Classic and Biomechatronic Extended Physiological
Proprioception**

**Σχεδιασμός Άνω Προσθετικού Άκρου:
Πειραματική Σύγκριση Κλασσικής και Βιο-Μηχανοτρονικής Εκτεταμένης
Φυσιολογικής Ιδιοδεκτικότητας**

Ζαχαρίας Βαγγελάτος

Επιβλέπων Καθηγητής: Ε. Γ. Παπαδόπουλος

ΑΘΗΝΑ 2017

Περίληψη

Τα προσθετικά άκρα έχουν σημειώσει σπουδαία πρόοδο τα τελευταία χρόνια. Παρόλα αυτά το κομμάτι του ελέγχου αποδεικνύεται ακόμη και σήμερα προβληματικό, κυρίως εξαιτίας της έλλειψης ανάδρασης από τον χρήστη (συγκεκριμένα έλλειψη αίσθησης). Η Εκτεταμένη Φυσιολογική Ιδιοδεκτικότητα (Extended Physiological Proprioception- EPP) έχει προκύψει ότι είναι η καλύτερη μέθοδος ελέγχου προσθετικών αφού παρέχει την δυνατότητα ασυναίσθητου ελέγχου θέσης του άκρου, καθώς τα σήματα ανάδρασης που παρέχει στον ακρωτηριασμένο, ενεργοποιούν την ιδιοδεκτική του αισθητικότητα. Όμως, ο κλασικός έλεγχος EPP είναι πολύ δύσκολο να πραγματοποιηθεί, αφού απαιτεί απευθείας μηχανική σύνδεση με το προσθετικό άκρο μέσω αντιαισθητικών ντιζών, καθώς και ειδικό χειρουργείο κινησιοπλαστικής για να επιτευχθεί αυτή η σύνδεση. Τα παραπάνω μειονεκτήματα οδήγησαν σταδιακά στην εγκατάλειψή του, και την διάδοση του μυοηλεκτρικού ελέγχου, που αποτελεί μη επεμβατική μέθοδο. Στο εργαστήριο Αυτομάτου Ελέγχου της Σχολής Μηχανολόγων Μηχανικών προτάθηκε μια προσέγγιση που βασίζεται στην τεχνολογία της τηλερομποτικής, με την οποία φιλοδοξείται να επιτευχθεί έλεγχος προσθετικών ισοδύναμος με τον κλασικό EPP, αλλά χωρίς την χρήση ντιζών και χειρουργείου κινησιοπλαστικής. Το προτεινόμενο σύστημα περιλαμβάνει χρήση εμφυτευμάτων χαμηλής ισχύος, συνδεδεμένα σε σειρά με συγκεκριμένους εναπομείναντες μύες του ακρωτηριασμένου, τα οποία εμφυτεύονται κατά την αρχική χειρουργική επέμβαση του ακρωτηριασμού. Τα εμφυτεύματα αυτά, αποτελούν τα κύρια (master) ρομπότ του συστήματος τηλεχειρισμού, και δέχονται απευθείας εντολές δυνάμεων από τους μύες. Οι εντολές αυτές μεταφέρονται ασύρματα στο ρομπότ-υπηρέτη (slave), που είναι το προσθετικό άκρο, το οποίο κινείται στο χώρο. Ο ελεγκτής του συστήματος εγγυάται την δυναμική σύζευξη των master και slave ρομπότ, παρέχοντας στον ακρωτηριασμένο ιδιοδεκτική ανάδραση κάθε χρονική στιγμή. Αυτή η αρχιτεκτονική θα προσφέρει ισοδύναμα αποτελέσματα ελέγχου με την κλασική EPP διάταξη, αλλά χωρίς τα μειονεκτήματα που την χαρακτηρίζουν. Αποδείχτηκε ότι θεωρητικά η κλασική μέθοδος εκτεταμένης φυσιολογικής ιδιοδεκτικότητας είναι ισοδύναμη με την καινούργια μέθοδο που επινοήθηκε, η οποία ονομάστηκε Biomechatronic EPP, καθιστώντας την εφαρμόσιμη για προσθετικά άκρα. Σκοπός αυτής της εργασίας είναι ο σχεδιασμός (με βάση την διπλωματική του Ανέστη Μαμπλέκου) και η κατασκευή της πειραματικής διάταξης που θα εξετάσει αν αυτές οι δυο μέθοδοι είναι πειραματικά ισοδύναμες ή όχι και ποιές είναι οι αιτίες. Επιπλέον αντικείμενο της εργασίας είναι ο σχεδιασμός του συστήματος ελέγχου με την βοήθεια του DS1103 και του περιβάλλοντος του ControlDesk. Επομένως μεγάλο μέρος της διπλωματικής θα αναλωθεί στο να ξεδιαλυθούν τα μυστήρια αυτού του hardware και software. Τέλος θα αναπτυχθεί ένα πρωτόκολλο πειραμάτων που πρέπει να ακολουθείται για τα πειράματα που θα ακολουθήσουν που θα καθιστούν τα εξαγόμενα αποτελέσματα επαναλήψιμα και αξιολογήσιμα.

Abstract

Prosthetic limbs have faced significant progress through the last two decades. However, the controller design still remains strenuous. The main reason is the lack of feedback provided to the user (insufficient sensing in particular). The Extended Physiological Proprioception (EPP) has been proved to be the best control method for prosthetic limbs, because it stimulates his/her proprioceptive sense, enabling subconscious control. Nevertheless, Classic EPP is very arduous to be implemented, due to the fact that it requires the connection of the prosthetic to unaesthetic Bowden cables, as well as an extra plastic surgery to achieve that connection. These drawbacks led to the waiving of this method and the spread of myoelectric control, which is a totally non invasive method. At the Control Systems laboratory of the School of Mechanical Engineering a new method was proposed that is inspired by the teleoperation theory. The goal is to achieve a control scheme that is equivalent to the Classic EPP, but without the use of Bowden Cables and the extra plastic surgery. In the proposed system, low power devices are implanted and connected to specific muscles during the required initial amputation surgery. The muscles exert forces to the implants, which correspond to the master robots of the teleoperation system. Those forces are wirelessly transmitted to the prosthesis which is the slave robot. The controller of the topology guarantees the dynamic conjunction of the master and slave robots, enabling amputee's proprioception. The proposed system is expected to provide a modern EPP-equivalent control scheme for upper-limb prostheses without the disadvantages of previous EPP configurations, but with the control advantages of proprioceptive feedback. Before the dawn of this thesis, it had been proved that theoretically the Classic EPP control method and the new one, which for this thesis will be called Biomechatronic EPP, are equivalent. This renders the new method suitable for limb prosthetics. The purpose of this thesis is the design and the construction of the experimental setup. This setup will be used to inquire whether the two control methods are equivalent, or the reality is much more ruthless and the new innovative method has been proved to be a dubious dream. Furthermore, a primary objective of this thesis is the design of the control systems with the DS1103 and the ControlDesk environment. Ergo, a significant part of this thesis will be related to the unraveling of the mysteries of this uncharted territory of hardware and software. Finally, for the experiments that must be conducted a protocol must be stated. The reason is that the experimental data must be repeatable and effortlessly evaluated.

"Ay, now the Plot thickens very much upon us"
The Rehearsal (1671)
George Villiers, 2nd Duke of Buckingham

Preface

Prosthetics is a vast field of knowledge with open arms for everyone willing to study it meticulously. It consists of various research areas such as Biology, Medicine, Control Systems and Manufacturing Design and as a multidisciplinary field it intertwines the fate of doctors, engineers, designers and most importantly, the people who have lost a part of their body and need the assistance of modern technology to make their lives easier. These are the main reasons that I decided to choose this diploma thesis. Feeling that you do something that in the future will probably help someone is a great motive to move forward, regardless of the tides faced through the course. This thesis forced me to deal with the design process, the manufacturing process and implement controllers. Control systems engineering is a field requiring theoretical skills, for finding and evaluating alternative design solutions, as well as practical skills necessary for the implementation of experiments, manufacturing processes, prototyping and getting accustomed to electrical and mechanical components, such as drivers, h-bridges, motors and controllers. Therefore, working for this project provided me the skills previously inferred. During my research for this Thesis I had to use Machine Tools, e.g. mill and lathe, for the processing of components, 3D printer and Solidworks for prototyping, the LDKF for the construction of boards and adapters for the electronic parts of the plant, but most importantly extensively Matlab and Simulink for the use of the dSpace DS1103 and ControlDesk, a powerful tool for control systems implementation and experimentation. As the only one in the lab using DS1103, I had to solve various problems by myself, theoretical and practical, but for the evaluation of designing options and the use of the laboratory equipment I collaborated with MS students, PhD students and also fellow undergraduate students. Also, due to the lab's teamwork spirit, I helped or provided advice to fellow students of the lab when asked for some assistance, in Solidworks, ANSYS, design problems, the use of the 3D printer and in soldering.

These experiences provided a sufficient material for the plot of the play that I am jolly to present. What a Devil is the plot good for, but to bring in fine things? I have to warn the possible reader that during his/her reading session he /she will notice (or not) references to songs, English literature, philosophical questions, modern Japanese literature and even more! Even though an obvious reason is to show off (how abruptly), the main reason is to render the reading easier and more enjoyable for everyone, whether or not he/she is a mechanical engineer!

At this point it would be appropriate to thank my supervisor, Prof. Evangelos Papadopoulos, who gave me the opportunity to deal with this thesis and at his laboratory I had the chance to meet and collaborate with magnificent people and every single one of his subordinates that helped me through this thesis. Furthermore, I would like to thank Postdoctoral Fellow Georgios A. Bertos for his advising during the stages of this thesis.

Finally, I would like to pay special tribute to Konstantinos Asimakopoulos, who created the EAGLE files for the boarding prototyping stage of this thesis (read the related chapter) and taught me how the LPKF works. Without his assistance this thesis would be delayed at least for two months and he has my gratitude for his magnanimous efforts.

Chapters

Περίληψη	3
Abstract.....	5
Preface.....	7
FIGURE INDEX.....	12
TABLE INDEX	19
1 Introduction	20
1.1 Purpose	20
1.2 Review of references	22
1.3 Thesis Structure	24
2 Design of the experimental setup	25
2.1 Classic EPP initial process setup design.....	25
2.2 Biomechatronic EPP initial process setup design.....	28
2.3 Final Design Proposal	30
3 Design and implementation of Reference Input	42
4 Boarding Prototyping - Hardware Selection	53
5 Preliminary Data Processing.....	64
5.3 Correlating the duty cycle with the output of the controller.....	69
5.4 Noise filtering.....	71
5.5 System identification of the master motors	80
5.6 Controller Design	82
6 Final Setup for Experimentation	84
6.1 Hardware Connection.....	84
6.2 Simulink Program.....	94
6.3 Reading the FSR Sensors	95
7 Experimental Verification	103
7.1 Experiment 1 Transparency – Equivalence	103
7.2 Experiment 2 Target – Experiment	122
7.3 Case study Presentation – Pilot Test.....	125
7.4 Experimental Data Evaluation.....	139
7.5 Target Experiment 2.....	147
7.5 Experimental Data Evaluation vol. 2.....	152
7.6 Experiment 3 Force	158
8 Conclusions and Continuation - Legacy.....	162
8.1 Conclusions	162
8.2 Continuation - Legacy	163
9 REFERENCES.....	165

10 APPENDIX A BASICS ON dSPACE.....	168
10.1 dSpace and Simulink - Basic Concepts	168
11 APPENDIX B DATASHEETS.....	195
11.1 Biomechatronic Power Screw	195
11.2 Master Motor Coupling	196
11.3 Slave Motor Coupling.....	197
11.4 Slave Motor Bearing.....	198
11.5 Slave Motor Pulley	199
11.6 Slave Motor Drive	200
11.7 Master Motor h - bridge.....	206
11.8 Slave Motor	209
11.9 Slave Motor Gearhead	210
11.10 Slave Motor Encoder	211
11.11 Master Motor	212
11.12 Master Motor Encoder.....	213
12 APPENDIX C ENGINEERING DRAWINGS	214

FIGURE INDEX

Figure 1.1.	Schematic sketch of the mechanical connection of the limb with the user	21
Figure 1.2.	Setup of Biomechatronic EPP in an upper limb prosthetic	22
Figure 2.1.	Schematic design of the Bidirectional Classic EPP configuration	25
Figure 2.2.	Setup for the Classic EPP configuration	26
Figure 2.3.	Potential pulleys used for the setup	27
Figure 2.4.	Bearings and their housings	27
Figure 2.5	Couplings	27
Figure 2.6.	Setup for the master motors position control.....	28
Figure 2.7.	Biomechatronic Setup Configuration	29
Figure 2.8.	Power screw with its nut	29
Figure 2.9.	"Mini" Coupling	29
Figure 2.10.	Final Design for the whole setup.....	30
Figure 2.11.	Flange 1	30
Figure 2.12.	Flange 2	31
Figure 2.13.	The two flanges assembled in the setup	31
Figure 2.14.	Guide Rod	31
Figure 2.15.	The guide rods supporting the power screw nut.....	32
Figure 2.16.	Slave motor support flange.....	32
Figure 2.17.	Assembly of the flange with the slave motor and the base.....	33
Figure 2.18.	Master Motor flange support	33
Figure 2.19.	Assembly of the flange with the master motor and the base	34
Figure 2.20.	String guide for the connection of the screw nuts with the force sensors.....	34
Figure 2.21.	String guide assembly with the screw nuts.....	35
Figure 2.22.	Master Motors coupling	36
Figure 2.23.	Slave motor coupling	36
Figure 2.24.	The pulley that connects the slave motor with the Bowden cables	37
Figure 2.25	.Power screw for the transformation of rotary motion to translation.....	37
Figure 2.26	.Bearing with its housing for the support of the shaft of the pulley	38
Figure 2.27.	Final setup (view 1).....	38
Figure 2.28.	Final Setup (view 2)	39
Figure 2.29.	Final setup (view 3).....	39
Figure 2.30.	Initial concept of the design	40
Figure 2.31	.Bowden cable with cover of hoses	40
Figure 2.32.	Cover for bicycle brakes (up) and cover for hydraulic hoses (down)	41
Figure 2.33.	Final assembly of the Bowden cables	41
Figure 3.1.	Control Schemes for both Proprioception Methods. For both cases measurement of the force to control the system is required.....	42
Figure 3.2 .	the Force Sensitive Resistor used in the setup.....	43
Figure 3.3.	Operational amplifier MCP6002	43

Figure 3.4.	Signal Conditioning Circuit.....	44
Figure 3.5.	Force applying setup for the integrated circuits calibration	45
Figure 3.6.	Final Setup	45
Figure 3.7.	Setup for the circuit's calibration.....	46
Figure 3.8.	Resulting Output - Weight Curves for different resistance R13.....	47
Figure 3.9.	Press plate of the final circuit support	48
Figure 3.10.	Housing of the final circuit support.....	48
Figure 3.11.	Assembly of the two parts	48
Figure 3.12.	Step one. Place the FSR to the housing.....	49
Figure 3.13.	Step two. Place on the pressure surface some rubber to avoid sticking	49
Figure 3.14.	Step three. Place the pressure place.....	50
Figure 3.15.	Place the board of the electronic circuit	50
Figure 3.17.	FSR connection with the Bowden cables of the motors setup.....	52
Figure 4.1.	Slave motor drawing	53
Figure 4.2.	Master motor CAD.....	53
Figure 4.3.	Encoder of the slave motor.....	54
Figure 4.4.	Master motor encoder.....	54
Figure 4.5.	Master motors hbridge	55
Figure 4.6.	Analog Servo Drive AZBDC10A4	55
Figure 4.7.	Initial solution of the connectivity problem	56
Figure 4.8.	Commercial mounting for the drive AZBDC10A4.....	56
Figure 4.9.	LPKF setup.....	57
Figure 4.10.	The schematic drawing view of the mounting of the driver	57
Figure 4.11.	The board view of the mounting of the driver	58
Figure 4.12.	Final mounting prototype	58
Figure 4.13.	Header pin 1.27 mm	59
Figure 4.14.	Screw terminal connector 2.54 mm.....	59
Figure 4.15.	Final mounting prototype	59
Figure 4.16.	The driver attached to the mounting.....	60
Figure 4.17.	The mounting with cables attached to it to connect with the setup	60
Figure 4.18.	ENX 10 EASY connector.....	61
Figure 4.19.	Adapter EASY Absolute Part number 488167	61
Figure 4.20.	The schematic drawing view of the encoder adaptor	62
Figure 4.21.	The board view of the encoder adaptor	62
Figure 4.22.	Adaptor prototype for the encoder connector.....	63
Figure 5.1.	The slave motor encoder specifications	64
Figure 5.2.	The master motor encoder specifications	65
Figure 5.3.	Number of counts identification scheme	66
Figure 5.4.	Position Response	66
Figure 5.5.	Electronic Optical Tachometer.....	67
Figure 5.6.	Signal pins of Servo Drive AZBDC10A4	68
Figure 5.7.	The pins of the L293D Quadruple Half-H Drivers.....	68

Figure 5.8.	Slave motor direction control scheme	69
Figure 5.9.	Slave motor direction control scheme	69
Figure 5.10.	Illustration of the closed loop diagram which will be used for the master motors	70
Figure 5.11.	Duty Cycle - Current experimental curve	71
Figure 5.12.	Current response.....	71
Figure 5.13.	FSR Sensor 1 response.....	72
Figure 5.14.	FSR Sensor 2 response.....	72
Figure 5.15.	current spectrum.....	73
Figure 5.16.	FSR Sensor 1 Spectrum.....	73
Figure 5.17.	FSR Sensor 2 Spectrum.....	74
Figure 5.18.	Responses comparison	75
Figure 5.19.	Zoom in on the responses. The time range of the zoom is presented on the x-axis.....	75
Figure 5.20.	Focus on the higher frequencies of the sensor 1.....	76
Figure 5.21.	Focus on the higher frequencies of the sensor 2.....	76
Figure 5.22.	Simulink scheme for filtering response recording.....	77
Figure 5.23.	Sensor 1 response comparison using G_1	78
Figure 5.24.	Zoom in to distinguish the response delay of G_1 . The time range of the zoom is presented on the x-axis	78
Figure 5.25.	Sensor 1 response comparison using G_1	79
Figure 5.26.	Zoom in to distinguish the response delay of G_2 . The time range of the zoom is presented on the x-axis	79
Figure 5.27.	Linear graph of the motor - power screw system	80
Figure 5.28.	Closed loop P control response	81
Figure 6.1.	Analog Servo Drive AZBDC10A4 Pins description	84
Figure 6.2.	HEDS 5540 500 Counts per turn encoder pins mapping.....	85
Figure 6.3.	Connectivity schematic view of the ENCODER HEDS 5540	86
Figure 6.4.	Ground Connection of the encoder.....	87
Figure 6.5.	L293d Quadruple Half-H Driver pins description.....	87
Figure 6.6.	The ENX10 EASY 512IMP encoder pins mapping	88
Figure 6.7.	Connector P1A pins mapping.....	90
Figure 6.8.	Connector P1B pins mapping.....	91
Figure 6.9.	Connector P2A pins mapping.....	91
Figure 6.10.	Connector P2B pins mapping.....	92
Figure 6.11.	Connector P3A pins mapping.....	92
Figure 6.12.	Connector P3B pins mapping.....	93
Figure 6.13.	The connectors of the DS1103 expansion box	93
Figure 6.14.	Bidirectional Classic EPP.....	94
Figure 6.15.	Bidirectional Biomechatronic EPP.....	95
Figure 6.16.	Upper and Lower Bounds of the FSR sensor Output	95
Figure 6.17.	Measurement of the FSR sensor block diagram.....	96
Figure 6.18.	Logic gate circuit of the position - force control	97
Figure 6.19.	Defining the position limits and the normalization of the input to duty cycle	98

Figure 6.20	.Motor Velocity Response with duty cycle 1 as being displayed at ControlDesk. x axis is time (s) and y axis is the velocity (deg/s)	99
Figure 6.21.	Reading of the encoder position and velocity	99
Figure 6.22.	Biomechatronic EPP control scheme	100
Figure 6.23.	Biomechatronic EPP Simulink program for the Master Motors (Part 1).....	100
Figure 6.24.	Biomechatronic EPP Simulink program for the Master Motors (Part 2).....	101
Figure 6.25.	Biomechatronic EPP Simulink program for the Master Motors (Part 3).....	101
Figure 6.26.	Side view of the setup	102
Figure 6.27.	Front view of the setup.....	102
Figure 7.1.	ControlDesk environment for the Transparency test.....	103
Figure 7.2.	Delay Time between the FSR sensor and the slave motor	104
Figure 7.3.	Response of the slave motor for a specific time range	105
Figure 7.4.	FSR 1 response for the same time range	105
Figure 7.5.	FSR 2 Response for the same time range	106
Figure 7.6.	Slave motor velocity for the same time range	106
Figure 7.7.	Slave motor Current for the same time range.....	107
Figure 7.8.	Delay between the slave motor and the master motor	108
Figure 7.9.	Velocity of the slave motor	108
Figure 7.10.	Velocity of the Master 1 motor	109
Figure 7.11.	Velocity of the Master 2 motor	109
Figure 7.12.	FSR 1 response.....	110
Figure 7.13.	FSR 2 response.....	110
Figure 7.14 .	Master Motor 1 error	111
Figure 7.15.	Master Motor 2 Error	111
Figure 7.16.	Power screws before (left) and after the improvement of the assembly	104
Figure 7.17.	New Controller implementation on Simulink	113
Figure 7.18.	Delays between the master motors and the slave motor (case 1)	114
Figure 7.19.	Zoom in to examine the range of the delays depending of the position of the motor (case 1) ..	114
Figure 7.20.	Master Motor 1 error (case 1).....	115
Figure 7.21.	Master Motor 2 error (case 1).....	115
Figure 7.22.	Master Motor 1 normalized current (converted to d.c.) (case 1)	116
Figure 7.23.	Master Motor 2 normalized current (converted to d.c.) (case 1)	116
Figure 7.24.	Delays between the master motors and the slave motor (case 2)	117
Figure 7.25.	Zoom in to examine the range of the delays depending of the position of the motor (case 2) ..	117
Figure 7.26.	Master Motor 1 error (case 2).....	118
Figure 7.27.	Master Motor 2 error (case 2).....	118
Figure 7.28.	Master Motor 2 normalized current (converted to d.c.) (case 2)	119
Figure 7.29.	Master Motor 1 normalized current (converted to d.c.) (case 2)	119
Figure 7.33.	ControlDesk environment for the supervisor.....	122
Figure 7.34.	Record button on ControlDesk 5.6.....	123
Figure 7.35.	Setting the Control Gains of the Master Motors to zero for the Classic EPP target position experiment.....	124
Figure 7.36.	Slave motor path during the phase 1 of Biomechatronic EPP test	126

Figure 7.37.	Slave motor velocity during the phase 1 of Biomechatronic EPP test	126
Figure 7.38.	FSR 1 output during the phase 1 of Biomechatronic EPP test	127
Figure 7.39.	FSR 2 output during the phase 1 of Biomechatronic EPP test	127
Figure 7.40.	Slave motor current during the phase 1 of Biomechatronic EPP test	128
Figure 7.41.	Master 1 Motor error during the phase 1 of Biomechatronic EPP test	128
Figure 7.42.	Master 2 Motor error during the phase 1 of Biomechatronic EPP test	129
Figure 7.43.	.Slave - Master Motor positioning during the phase 1 of Biomechatronic EPP test.....	129
Figure 7.44.	Slave motor path during the phase 2 of Biomechatronic EPP test	130
Figure 7.45.	Slave motor velocity during the phase 2 of Biomechatronic EPP test	130
Figure 7.46.	FSR 1 output during the phase 2 of Biomechatronic EPP test	131
Figure 7.47.	FSR 2 output during the phase 2 of Biomechatronic EPP test	131
Figure 7.48.	Slave motor current during the phase 2 of Biomechatronic EPP test	132
Figure 7.49.	Master 2 Motor error during the phase 2 of Biomechatronic EPP test	132
Figure 7.50.	Master 1 Motor error during the phase 2 of Biomechatronic EPP test	133
Figure 7.51.	Slave - Master Motor positioning during the phase 2 of Biomechatronic EPP test.....	133
Figure 7.52.	Slave motor path during the phase 1 of Classic EPP test	134
Figure 7.53.	Slave motor velocity during the phase 1 of Classic EPP test	134
Figure 7.54.	FSR 1 output during the phase 1 of Classic EPP test	135
Figure 7.55.	FSR 2 output during the phase 1 of Classic EPP test	135
Figure 7.56.	Slave motor current during the phase 1 of Classic EPP test	136
Figure 7.57.	Slave motor path during the phase 2 of Classic EPP test	136
Figure 7.58.	Slave motor velocity during the phase 2 of Classic EPP test	137
Figure 7.59.	FSR 1 output during the phase 2 of Classic EPP test	137
Figure 7.60.	FSR 2 output during the phase 2 of Classic EPP test	138
Figure 7.61.	Slave motor current during the phase 2 of Classic EPP test	138
Figure 7.62.	Movement time comparison curve (phase 1)	140
Figure 7.63.	Movement time comparison curve (phase 2)	140
Figure 7.64.	Duel time comparison curve (phase 1)	141
Figure 7.65.	Duel time comparison curve (phase 2)	142
Figure 7.66.	Reach target error (phase 1)	142
Figure 7.67.	Reach target error (phase 2)	143
Figure 7.69.	Biomechatronic EPP with connection master motor 1 closed loop error.	148
Figure 7.70.	Biomechatronic EPP with connection master motor 1 closed loop error.	149
Figure 7.73.	Biomechatronic EPP with connection master motor 1 closed loop error.	150
Figure 7.74.	Biomechatronic EPP with connection master motor 2 closed loop error.	151
Figure 7.68.	Redesigned CAD of the pulley with a hole to hold the fishing line	158
Figure 7.69.	3D printed pulley on the shaft of the setup	158
Figure 7.70.	CAD of the rectangular shaft	159
Figure 7.71.	Standard weight placed in a base connected to the 3D printed pulley	159
Figure 7.72.	Assembly of the 3D printed shaft to the setup	160
Figure 7.73.	The flanges that are used as bounds for the shaft	160
Figure AA.1.	Block diagram of the architecture of DS1103	169

Figure AA.2.	DS1103ADC_Cx.....	169
Figure AA.3.	Channels 18 and 20 pins.....	170
Figure AA.4.	Channels 17and 19 pins.....	171
Figure AA.5.	DS1103MUX_ADC_CONx block.....	171
Figure AA.6.	Correspondence of pins. Converter 1 (green), Converter 2 (red), Converter 3 (blue) and Converter 4 (orange)	172
Figure AA.7.	The pins on the connector. Converter 1 (green), Converter 2 (red), Converter 3 (blue) and Converter 4 (orange)	173
Figure AA.8.	DS1103DAC_Cx block.....	173
Figure AA.9.	The pins on the connector.	174
Figure AA.10.	The pins on the connector	174
Figure AA.11.	The DS1103SL_DSP_PWM3 block	175
Figure AA.12.	Options window for the DS1103SL_DSP_PWM3 block.....	176
Figure AA.13.	The DS1103SL_DSP_PWM block	177
Figure AA.14.	Options window for the DS1103SL_DSP_PWM block.....	178
Figure AA.15.	The PWM pins on the connector	179
Figure AA.16.	The PWM pins on the connector	179
Figure AA.17.	The DS1103ENC_SETUP block.....	180
Figure AA.18.	The DS1103ENC_POS_Cx block.....	180
Figure AA.19.	The DS1103ENC_SET_POS_Cx block.....	181
Figure AA.20.	The DS1103ENC_SW_INDEX_Cx block.....	182
Figure AA.21.	The DS1103ENC_SW_INDEX_Cx block output.....	183
Figure AA.22.	The mapping for the inverse channels of the first two channels	183
Figure AA.23.	The mapping for the original channels of the first two channels.....	184
Figure AA.24.	Encoder with differential signals connection	184
Figure AA.25.	Encoder with single - ended signals connection.....	185
Figure AA.26.	Single - ended 1 Vpp signals connection, case 1	185
Figure AA.27.	Single - ended 1 Vpp signals connection, case 2.....	186
Figure AA.28.	Connection of the encoder using external supply.....	187
Figure AA.29.	Connectors of the expansion box	187
Figure AA.30.	Use of Dynamic Dead Zone and Dynamic Saturation block.....	188
Figure AA.31.	Example of using math and logic operations with the Convert block	188
Figure AA.32.	Closed loop scheme.....	189
Figure AA.33.	The register platform window.	190
Figure AA.34.	Creating the code from Simulink	190
Figure AA.35.	Choosing the .sdf file to execute the program	191
Figure AA.36.	The ControlDesk environment	191
Figure AA.37.	Record option.....	192
Figure AA.38.	Changing the duration of the displayed signals.....	192
Figure AA.39.	Exporting data	193
Figure AA.40.	Changing the properties of the slider instrument.....	193

TABLE INDEX

Table 6.1.	Analog Servo Drive AZBDC10A4 connectivity map	85
Table 6.2.	ENCODER HEDS 5540 500 Counts per turn connectivity map.....	86
Table 6.3.	L293d Quadruple Half-H Driver connectivity map	88
Table 6.4.	Sensor - ENX10 EASY 512IMP connectivity map for Master Motor 1	89
Table 6.5.	Sensor - ENX10 EASY 512IMP connectivity map for Master Motor 2	89
Table 6.6.	Connectivity schematic view of the Sensor - ENX10 EASY 512IMP encoder	89
Table 6.7.	FSR Sensors connectivity map.....	90
Table 6.8.	Power requirements of the setup	94
Table 6.9.	Definition of the logic variables	97
Table 6.10.	Truth table of the logic circuit	98
Table 7.1.	Case Study Target Positions	125
Table 7.2.	Results of statistical tests for Phase 1 duel time random variable	145
Table 7.3.	Results of statistcal tests for Phase 2 duel time random variable	145
Table 7.4.	Results of statistical tests for Phase 1 error random variable	146
Table 7.5.	Results of statistical tests for Phase 2 error random variable	146

1 Introduction

1.1 Purpose

The replacement of the human upper limbs by mechanical ones is a solemn scientific challenge. The mechanical demands and constraints of this aim are significant; however, the most crucial factor for the proper function of the upper limb is its control. Elaborating, the controller design defines the communication - connection between the impaired and the upper limb prosthetic. This hindrance is related to the lack of sufficient communication that is restrained only to communication with visual feedback, between the mutilated and the alien upper limb prosthetic.

In the case of the upper limbs of the human body the control is achieved by practically an infinite number of sensors provided. These sensors are called mechanoreceptors and provide data to the neural system on any variations in the state of the upper limb. The ability to sense using these mechanoreceptors is called proprioception, and its absence renders the control of the limbs impossible.

Thus, it is pellucid that even though a prosthetic could be highly advanced from an engineering perspective, it would not be functional unless proprioception is achieved. A control method that dominated the field of prosthetics and was widely used is Proportional myoelectric control. A proportional myoelectric control system utilizes a microcontroller or computer that inputs electromyography (EMG) signals from sensors on the leg muscle(s) and then activates the corresponding joint actuator(s) proportionally to the EMG signal. Sensors on the skin detect electromyography (EMG) signals from the muscles of the wearer's leg(s). EMG signals can be measured from just one muscle or many, depending on the type of the exoskeleton and how many joints are actuated. Each signal measured is then sent to a controller, which is either an onboard microcontroller (mounted to the exoskeleton) or to a nearby computer. Onboard microcontrollers are used for long-term assistive devices since the wearer must be able to walk in different locations while wearing the exoskeleton, whereas computers not carried by the exoskeleton can be used for therapeutic or research purposes since the wearer does not have to walk very far in a clinical or lab environment. The controller filters out noise from the EMG signals and then normalizes them so as to better analyze the muscle activation pattern. The normalized EMG value of a muscle represents its activation percentage, since the EMG signal is normalized by dividing it by the maximum possible EMG reading for the muscle it came from. The maximum EMG reading is generated when a muscle is fully contracted. An alternative method to normalization is to proportionally match the actuator power to the EMG signal between a minimum activation threshold and an upper saturation level. During the last couple of years, at the Control Systems Lab, where this thesis was supervised, research was conducted in this field and a new, innovative control proposal was introduced. This proposal was about a novel control topology, with activation of proprioception as well. To be more precise, the core of this concept is based on the field of Telerobotics - Teleoperation. In this field, a master - slave control scheme is designed, using implants that activate the receptors of the limb. This scheme guarantees the connection between the remaining intact muscles of the limb with its prosthetic.

The theoretical foundations of this notion have been established in a previous diploma thesis^[4]. To examine whether a new idea is functional, it has to be compared to an old one that is primarily used. The objective of this thesis is the design of an experimental setup for two upper – limb control methods, as well as the experimental comparison of these two methods. In prosthetics, the control method which has shown superiority over myoelectric control which is used most often is the Classic Extended Physiological Proprioception (Classic EPP)^[5], in which the tendons of the arm are connected to cables with the prosthetic limb. More precisely, the limb prosthetic is connected directly to the muscles of the impaired mechanically, using links such as Bowden Cables. Thus, the alien prosthetic becomes an extension of the remaining limb. Consequently, the position, the velocity and the forces that are applied to the prosthetic are transferred from the cables to the muscles, stimulating the neural receptors of the body, activating the proprioception to a certain degree. The EPP control resembles to the hydraulic steering. The driver "feels" the state of the wheels and simultaneously assistance is provided for more effortless driving. Nevertheless, the most important factor is that the drive and the wheels are synchronized. This mechanical connection provided by the EPP control is presented in Figure 1.1.

However, this control method has the disadvantage that it is not aesthetic for the human user, it has often has control constraints (related to the direction of the movement) and finally a plastic surgery is required^[6]. The new control method that has to be tested, using a master – slave topology, will be called by the research team of the laboratory as Biomechatronic Extended Physiological Proprioception (Biomechatronic EPP). The main advantage of this method is the fact that feedback is provided to the system and thus a closed loop system is created (minimizing the systems position error) and not an open loop system as in the previous method. A layout of the setup as it is going to be implemented is presented in Figure 1.2.

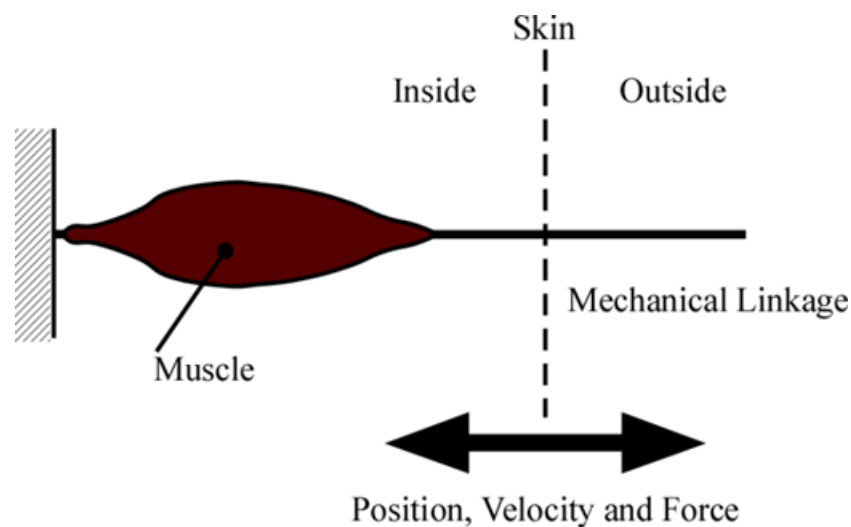


Figure 1.1. Schematic sketch of the mechanical connection of the limb to the user. (Copied from [1]).

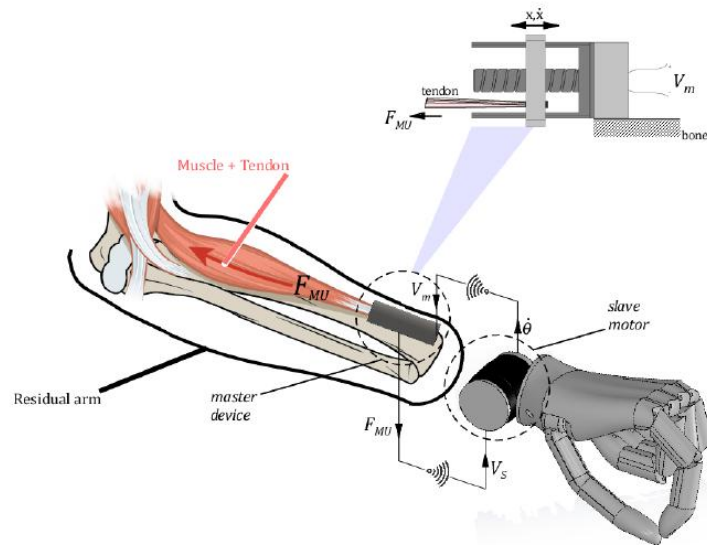


Figure 1.2. Setup of Biomechatronic EPP in an upper limb prosthetic. (Copied from [4]).

It has to be noted that the degrees of freedom of both the master and the slave devices must be the same. This topology is considered a successful one, if the impedance of the environment is the same for the user, as if he or she was controlling the slave motor without the master. In this case, the control system is called transparent [7].

To clarify if the two control methods are equivalent, the experiments to be conducted are the following three:

The transparency test, which was described previously.

The target positioning test. In this test the user must apply the necessary force to the sensors in order to rotate the slave motor to a desired target, while the target keeps changing position. The data that have to be processed is the error of the final distance from the target, the time it took to reach the target, and for how long the user can stay on the target.

The force test. In this test for various loading cases the user must perceive the change of the load and respond accordingly. For instance, if the load applied to the slave motor is increased, the force applied to the Force Sensors must increase as well. The data that have to be processed are the output of the sensors for various loading cases, and the current of the slave motor. With the current the torque produced by the motor can be calculated.

1.2 Review of references

Childress D.S. had presented the the desired for the control scheme of upper limb prosthesis [14].

- Subconscious control. The mutilated must apply the minimum mental effort for the use of the prosthetic.
- User - friendly through the procedure of learning how to use the prosthetic.
- Independent control schemes for different tasks.

- Simultaneous control for different independent tasks of the prosthetic.
- Design that is aesthetic.

Thus, the main trait of the prosthetic is the ability toathom the position of the prosthetic to the environment, as well as its position in comparison to the other limbs of the body ^[12 - 15]. The most crucial factor is the control scheme of the prosthetic. The one that was inquired in this thesis is the Extended Physiological Proprioception-EPP.

Extended Physiological Proprioception-EPP

Simpson D.C. at 1974, trying to preserve the proprioception of the mutilated patients, suggested a topology known as Extended Physiological Proprioception-EPP ^[5]. He was inspired by aircraft engineering, and he used Bowden cables and pneumatic actuators for the construction of prosthetic limbs for children ^[5]. He was the first that used the phrase "Extended Physiological Proprioception", to imply the use of the sensors of the human body to move the prosthetic limb.

The main notion is that the prosthetic limb is connected directly to the muscles of the disfigured using links, such as Bowden Cables. This mechanical connection converts the alien prosthetic limb to an extension of the remaining human body. Thus, the data for the position, the velocity and the forces applied to the prosthetic limb are transferred directly to the muscles, stimulating the neural receptors of the body, activating the proprioception of the user. Furthermore, prosthetic limbs that stimulate the proprioception are "friendlier" during their use, leading to subconscious. The classic EPP control resembles to the hydraulic driving. The driver understands the state of the wheels and at the same time assistance during driving is provided for less effort. However, the most important factor is that the vehicle is synchronized with the moves of the driver.

Telerobotics - Teleoperation (TT)

TT is the control of a machine or an actuator in a distant area. The result is the increase of the visual sense of the user in this area. A system like this consists of the following:

- A master device controlled by the user
- A slave device that its function depends on the master device
- A controller that is the link between the master and the slave devices, allowing the correlation of their displacement and applied forces respectively.

It has to be noted that the degrees of freedom of both the master and the slave devices must be the same. This topology is considered a successful one, if the impedance of the environment is the same for the user, as if he or she was controlling the slave motor without the master. In this case, the control system is called transparent ^[7].

To clarify if the two control methods are equivalent, the experiments to be conducted are the following three:

- The transparency test, which was described previously.
- The target positioning test. In this test the user must apply the necessary force to the sensors in order to rotate the slave motor to a desired target, while the target keeps changing position. The data that have to be processed is the error of the final distance from the target, the time it took to reach the target, and for how long the user can stay on the target.
- The force test. In this test for various loading cases the user must perceive the change of the load and respond accordingly. For instance, if the load applied to the slave motor is increased, the force applied to the Force Sensors must increase as well. The data that have to be processed are the output of the sensors for various loading cases, and the current of the slave motor. With the current the torque produced by the motor can be calculated.

1.3 Thesis Structure

At this point the structure of this thesis will be presented. At first it will be thoroughly presented the design and the construction of the setup of both the Classic EPP configuration and the Biomechatronic EPP. Furthermore, the design of the various adjustable parts of the setup will be presented, such as the Force Sensors, the mountings of the motor drivers and the adaptors of the encoders. The design of the controller for the two schemes will be implemented with the use of the dSpace DS1103 ^[8]. The DS1103 is an all-rounder in rapid control prototyping to test new control functions. Used with ControlDesk, the controller board is fully programmable from the Simulink® block diagram environment. This is a quick and easy way to implement your control functions on the board. It provides the user with D/A and A/D converters, pwm signals, position and velocity measurement from encoders and the use of all of Simulink Block Diagrams for real – time implementations (such as PID controllers, Signal Generation and Filtering etc) and makes controller design and implementation in any setup much easier. To design the controllers, preliminary data processing will be conducted, such as system identification and the calculation of the controller gains. With the mysteries of the DS1103 and the ControlDesk unraveled the Simulink program design will be presented for the conducted experiments. The experiments will be the three that were previously described and their results will define if the new method is indeed equivalent to the old one or a counterfeit. Finally, the conclusions of this thesis will be presented, with potential recommendations for future research.

2 Design of the experimental setup

In this chapter the design process and the final setup will be inquired. Moreover, the aims of the setup will be resolute and cheap and easy ways that these aims would be achieved will be presented. The fundamental purpose of the setup is to simulate the two control schemes that have to be compared, the old one which is the Classic Extended Physiological Proprioception (EPP), and the new one, the Biomechatronic Extended Physiological Proprioception.

2.1 Classic EPP initial process setup design

A common setup used in prosthetics with the Classic EPP configuration is displayed in Figure 2.1.

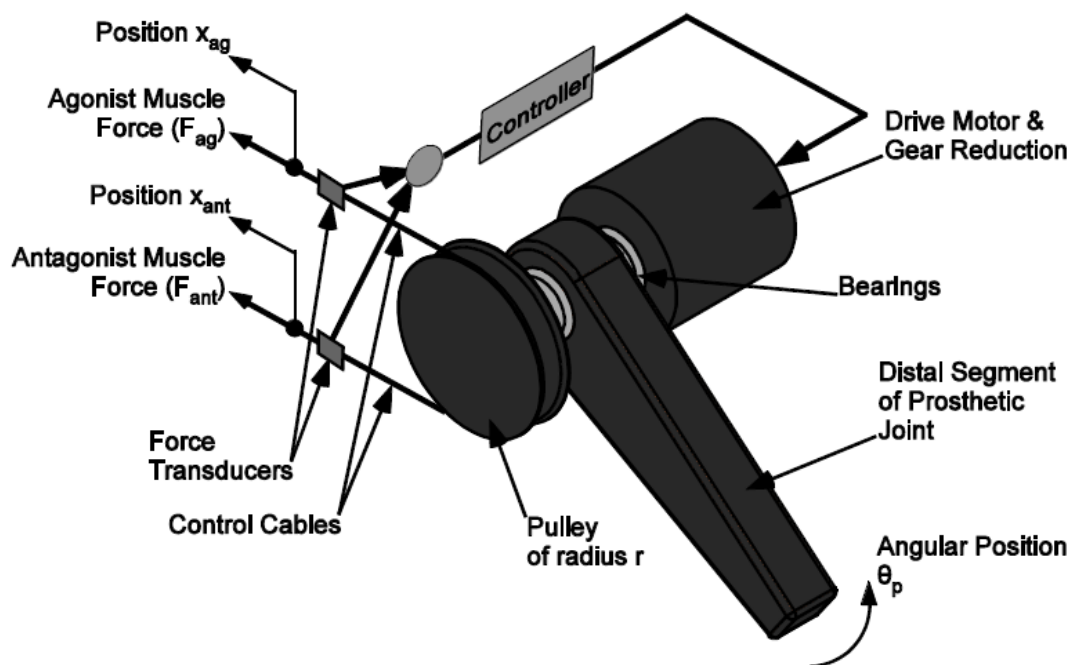


Figure 2.1. Schematic design of the Bidirectional Classic EPP configuration. (Modified from [1]).

Thus, in the design process for the Classic EPP a method must be considered to apply force for a prosthetic joint to be rotating. The force mechanism must be connected to the joint; however the rotation of the joint must be driven by the electromechanical system (motor) of the configuration, which will be controlled by the controller of the scheme. The controller will have as input the measured force applied to the system. The way that the force will be applied and be measured will be examined thoroughly on the following chapter. All things considered, the motor must be connected to the joint. The force will be applied in the same way as in the prosthetics in which the muscle is connected to mechanical linkages, which in most cases are Bowden cables. The cable will be intertwined with a pulley, which will be

connected to the motor and the joint with a coupling. Ergo the final setup is presented in Figure 2.2.

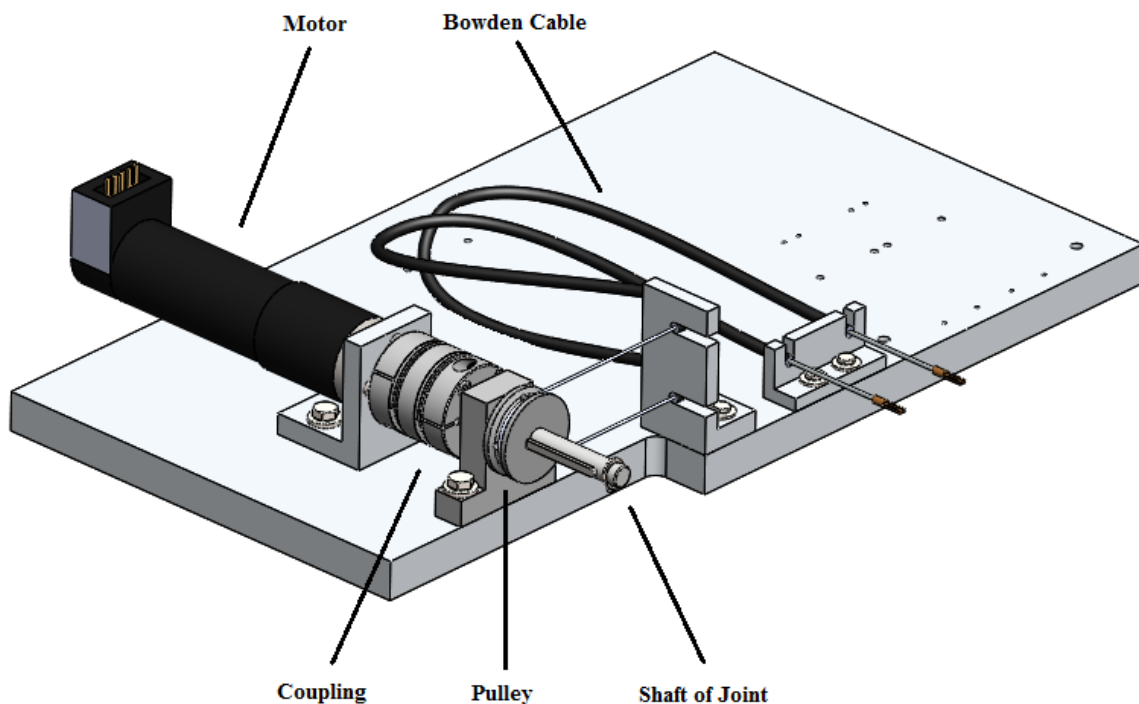


Figure 2.2. Setup for the Classic EPP configuration. Modified from [4].

The shaft provides an effortless way to assemble in the setup a joint of various shapes, which can easily be designed and prototyped using 3D printing for instance. As a result, disturbances can be included in the experiments to come. The shaft and the pulley will be supported in the setup using a bearing. Distinctive examples of a coupling, a bearing with its housing and a pulley are presented in the following Figures.

It was decided that it was more judicious that the flanges which will support the motor and the Bowden cables to be constructed using the labs equipment. Further details about the final assembly will be presented after the design solution for the Biomechatronic EPP is presented. To inspect each component thoroughly, the datasheets are provided on APPENDIX B DATASHEETS.



Figure 2.3. Potential pulleys used for the setup. See Chapter 11.5.



Figure 2.4. Bearings and their housings. See Chapter 11.4.



Figure 2.5. Couplings. See Chapter 11.3.

It was decided that it was more judicious that the flanges which will support the motor and the Bowden cables to be constructed using the labs equipment. Further details about the final assembly will be presented after the design solution for the Biomechatronic EPP is presented.

2.2 Biomechatronic EPP initial process setup design

Apropos of the Biomechatronic EPP the aim is to implement the force to a displacement mechanism, which will be displaced by the master motors whose input will be the displacement of the slave motor. Thus, a transformer that will convert the rotary displacement of the master motors to translation is required, as well as a support attached to it that will be connected to the sensor in which the force is to be applied. The constraint that has to be taken into consideration is the small size of the master motors. The final design solution for the master motors positioning is displayed in Figure 2.6. It has to be noted that the force sensor used for the force measurements and it is presented in the Figure is presented just as an example of a potential setup, and it will be meticulously examined in the following chapter.

Furthermore, it must be considered how the slave motor will be placed in the setup. Due to the fact that space constraints of the setup should be taken into account, it was erudite to exploit the setup of the Classic EPP configuration, as shown in Figure 2.7.

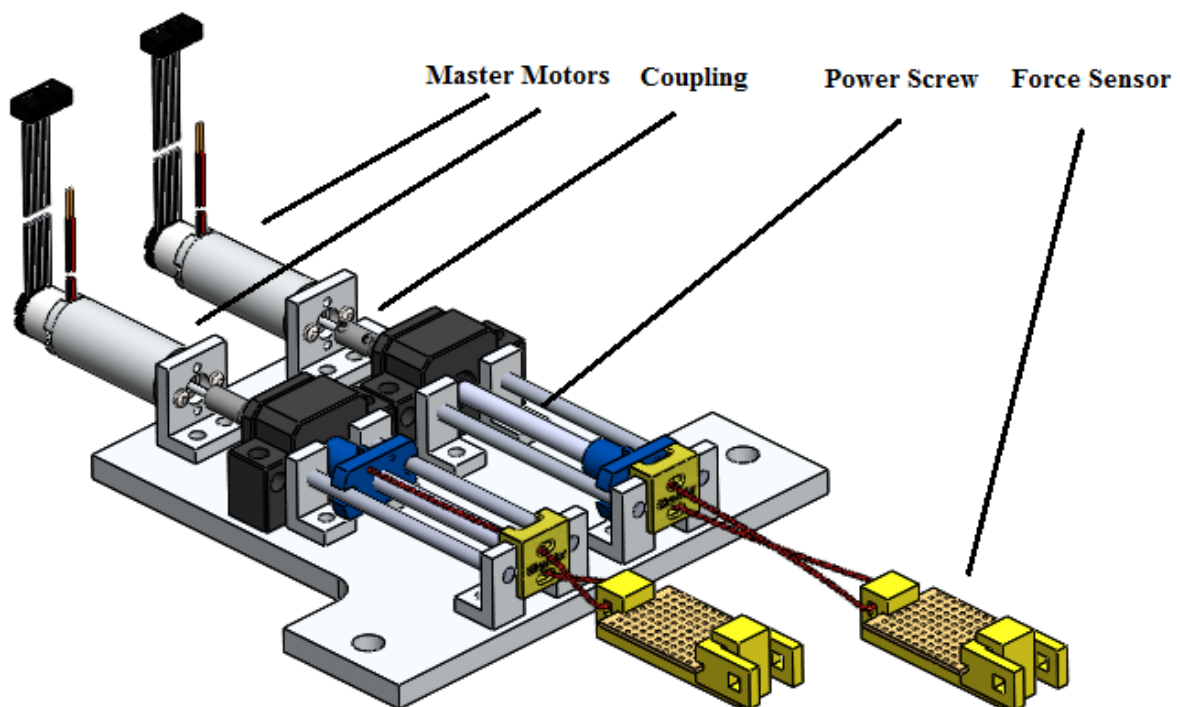


Figure 2.6. Setup for the master motors position control. Modified from [4].

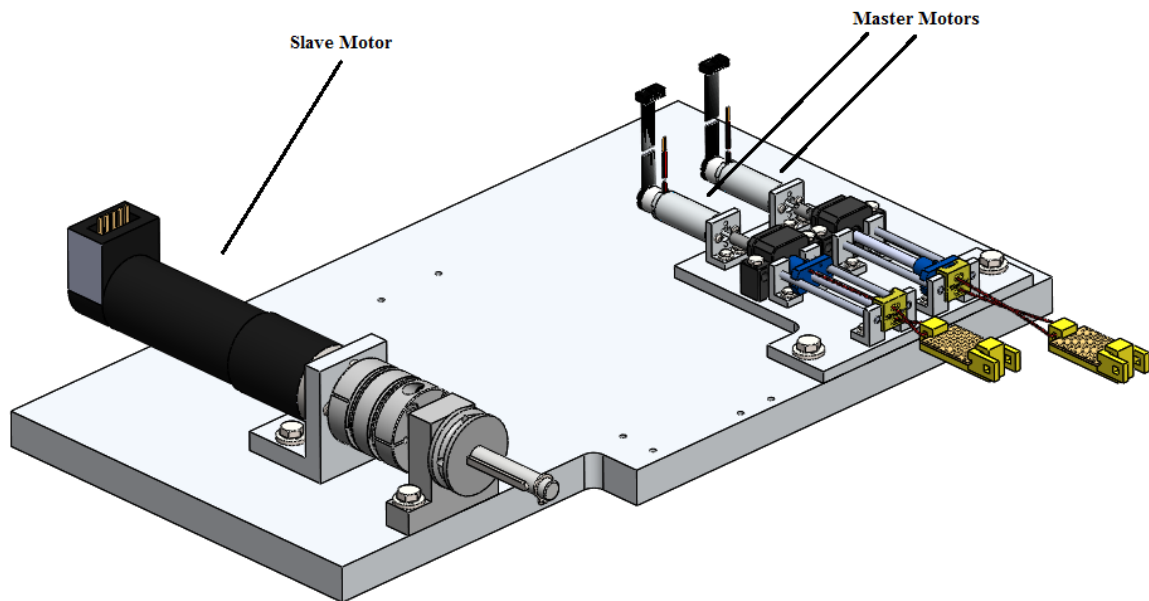


Figure 2.7. Biomechatronic Setup Configuration. Modified from [4].

The most challenging demand that must be satisfied is the size of the components the setup of the master motors. Thus couplings small enough must be found, as well as proper power screws, as the ones displayed in the following Figures.



Figure 2.8. Power screw with its nut. See Chapter 11.1.



Figure 2.9. "Mini" Coupling. See Chapter 11.1.

2.3 Final Design Proposal

All in all, the final CAD of the whole setup is displayed in Figure 2.10.

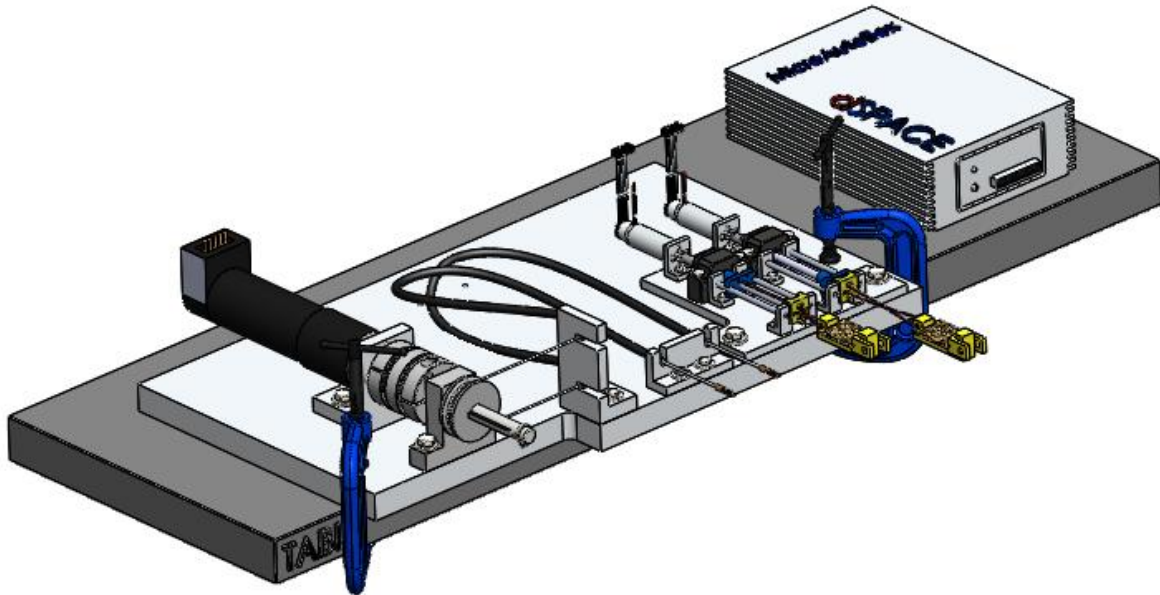


Figure 2.10. Final Design for the whole setup. Modified from [4].

The exact dimensions of the assembly, as well as its parts will be presented in the APPENDIX C ENGINEERING DRAWINGS.

2.4 Construction of the Setup

For the construction of the setup some parts were ordered, while some others were required to be constructed using the tool machines of the laboratory or be constructed at a workshop. Next it will be presented which parts were constructed at the laboratory.

Using the milling machine and the electrical saw of the laboratory the parts that were constructed were the flanges that are supporting the Bowden cables, presented in Figures 2.11, 2.12. Their mating with the setup is displayed in Figure 2.13.

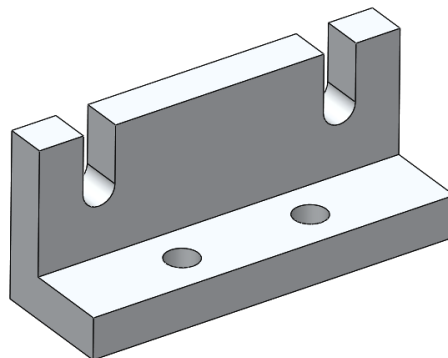


Figure 2.11. Flange 1.

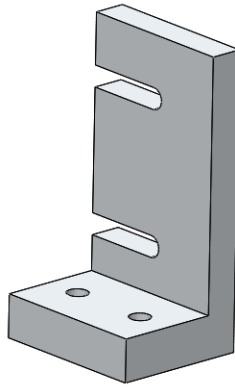


Figure 2.12. Flange 2.

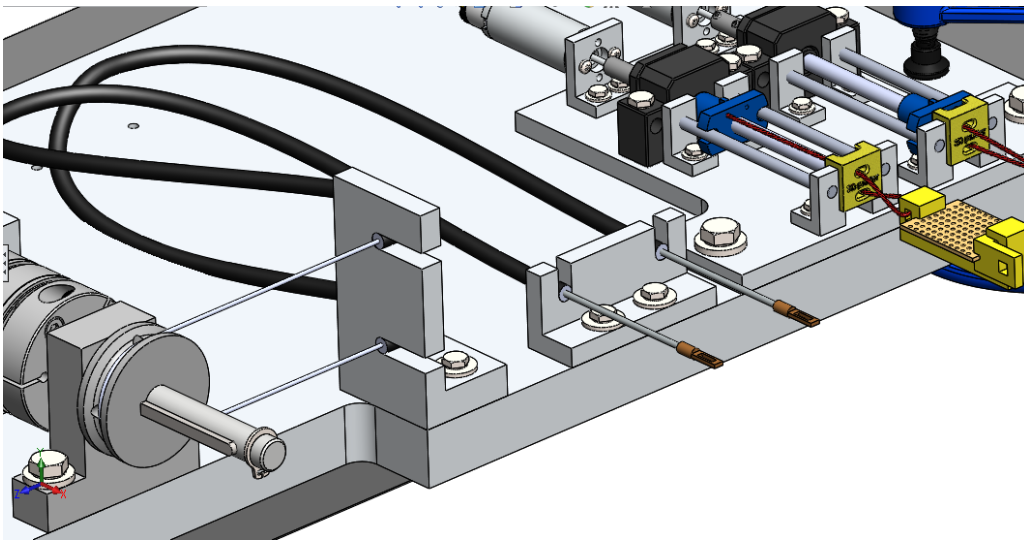


Figure 2.13. The two flanges assembled in the setup. Modified from [4].

Moreover, the parts that were constructed using the lathe of the laboratory were the rod guides of the power screw nut, as shown in Figures 2.14 and 2.15.

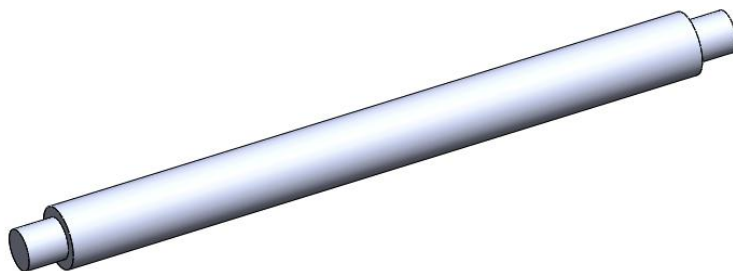


Figure 2.14. Guide Rod.

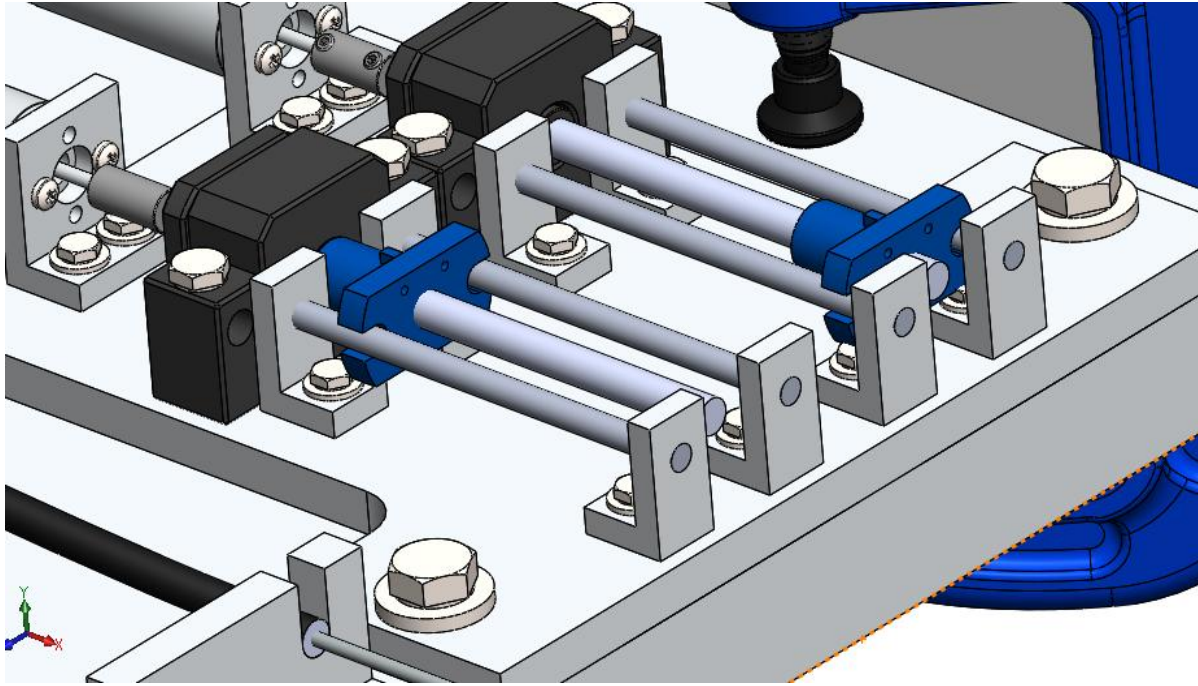


Figure 2.15. The guide rods supporting the power screw nut. Modified from [4].

The parts that were constructed at an external workshop, because of the required precision of their dimensions, were the base, the flanges that are supporting the master motors and the slave motor respectively, as well as guides supports for the rod guides of the power screw nuts. Each of the parts previously referred is displayed in the following Figures.

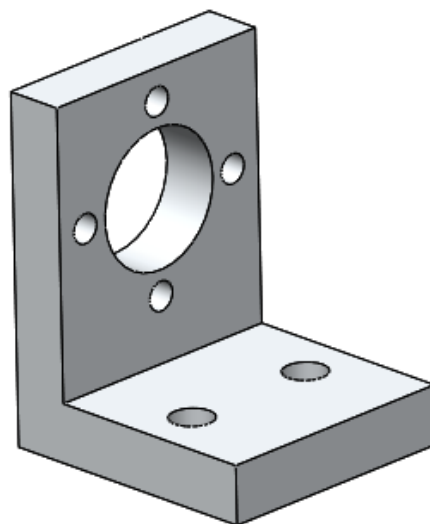


Figure 2.16. Slave motor support flange. Modified from [4].

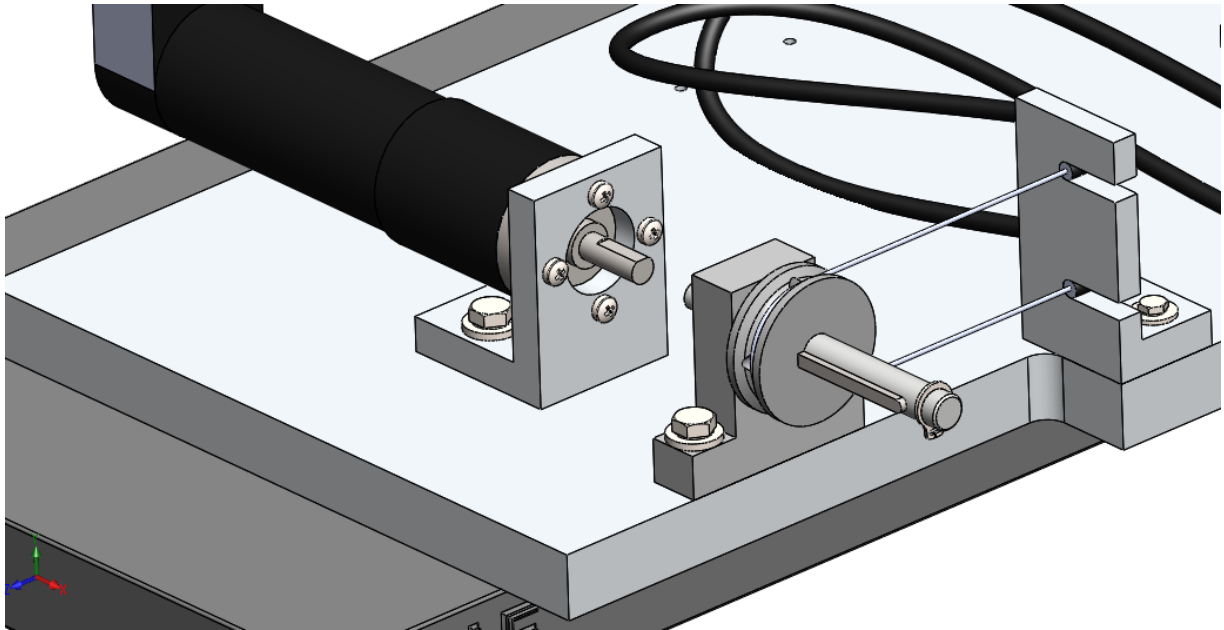


Figure 2.17. Assembly of the flange with the slave motor and the base. Modified from [4].

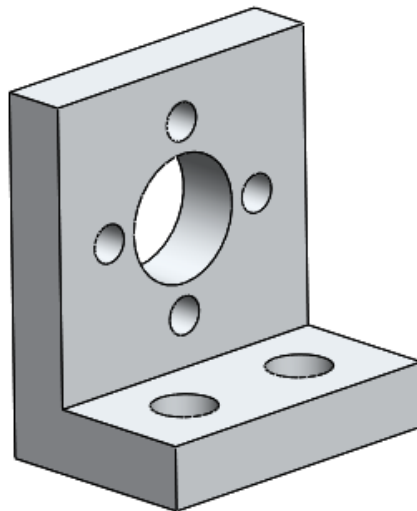


Figure 2.18. Master Motor flange support. Modified from [4].

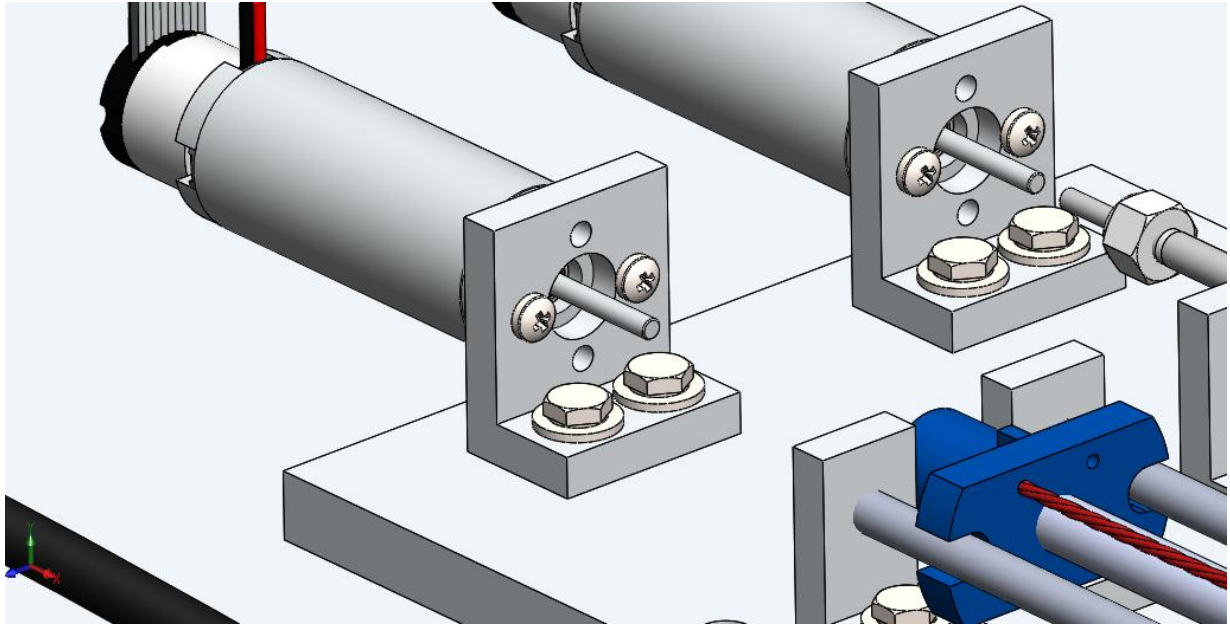


Figure 2.19. Assembly of the flange with the master motor and the base. Modified from [4].

An easy way to connect the potential force sensor with the screw nut was determined to be a string guide, which is displayed in Figure 2.20. In Figure 2.21 it is displayed the way it is assembled in the whole setup. This specific part was constructed with the use of the 3D printer of the laboratory.

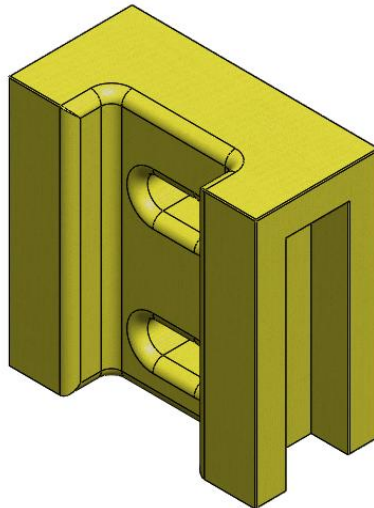


Figure 2.20. String guide for the connection of the screw nuts with the force sensors. Modified from [4].

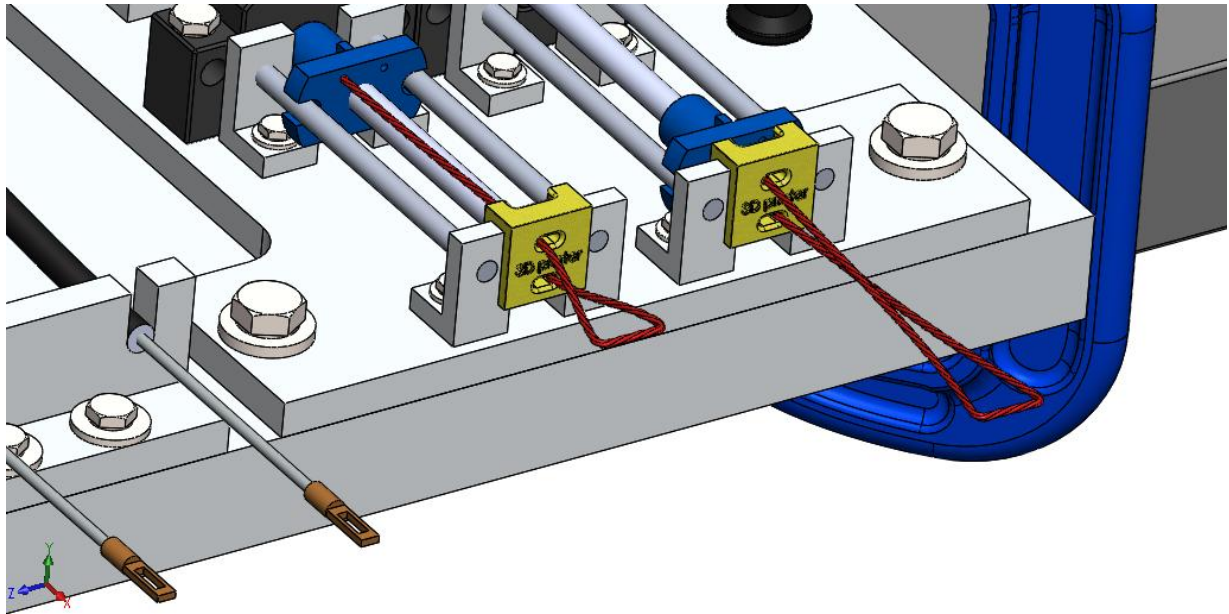


Figure 2.21. String guide assembly with the screw nuts. Modified from [4].

Finally, it is presented the list of the parts that ordered because of their standardized dimensions required to fit with the electromechanical systems of the setup. In this chapter only the codes of the parts and some specific characteristics will be presented. For further details, it is advised to read the APPENDIX B DATASHEETS.

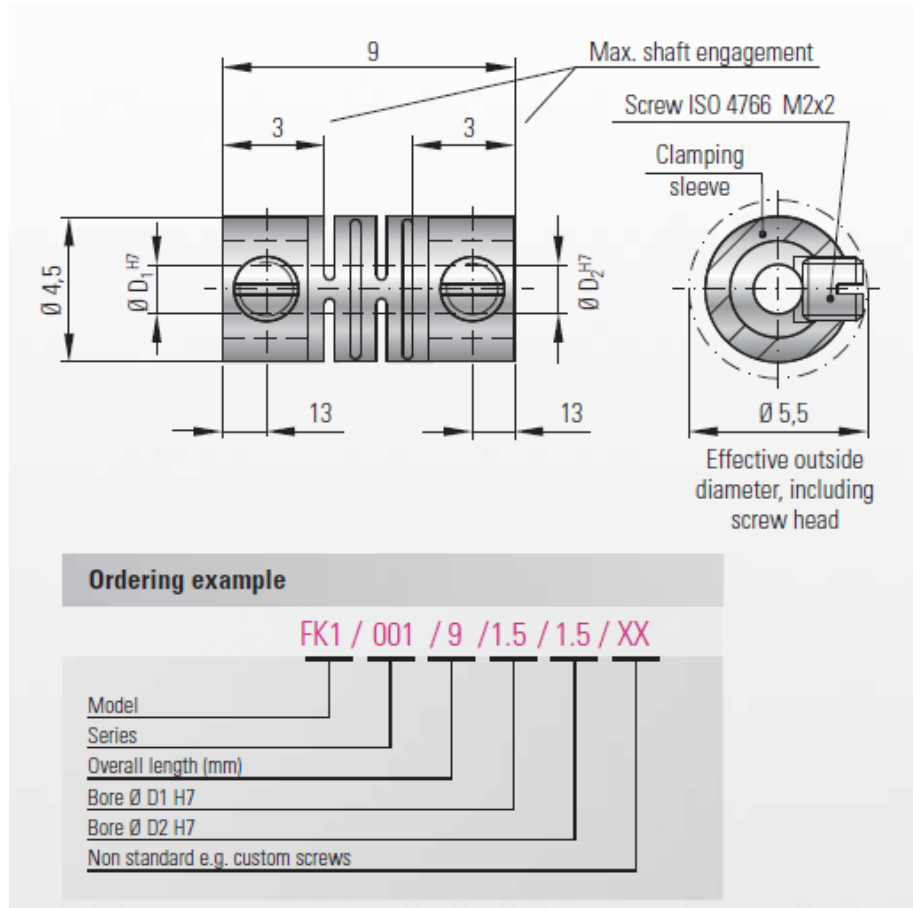


Figure 2.22. Master Motors coupling. See Chapter 11.2.

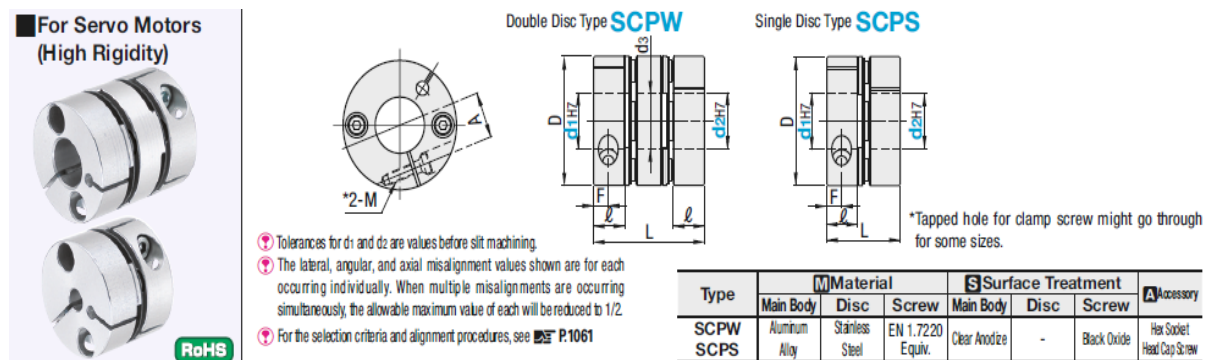


Figure 2.23. Slave motor coupling. See Chapter 11.3.

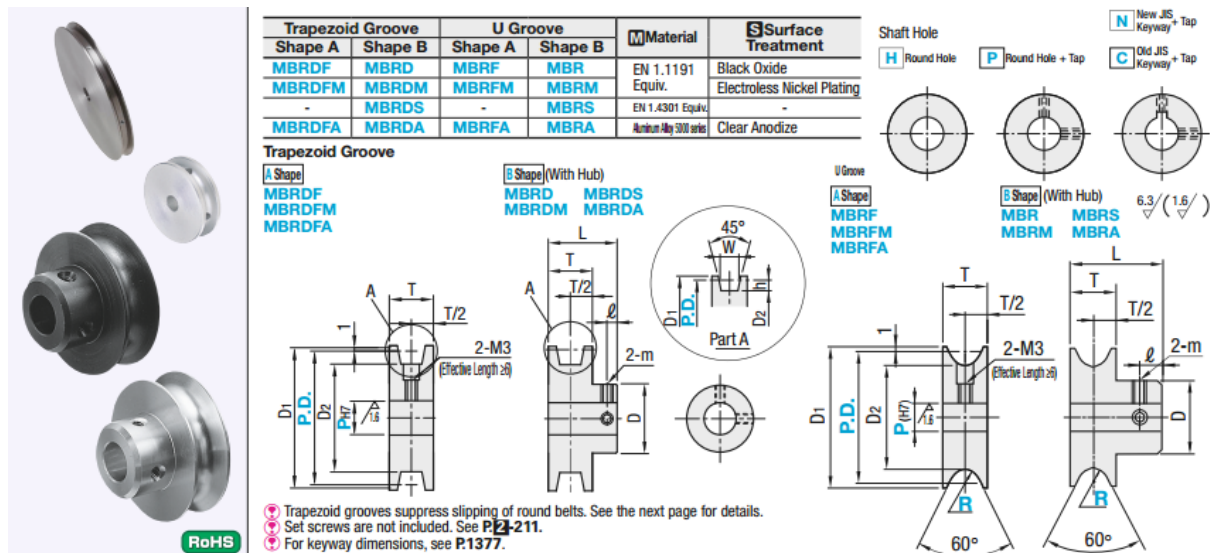


Figure 2.24. The pulley that connects the slave motor with the Bowden cables. See Chapter 11.5.



Metric Flanged Standard Lead Screw Assembly 4 mm x 1.22 mm S

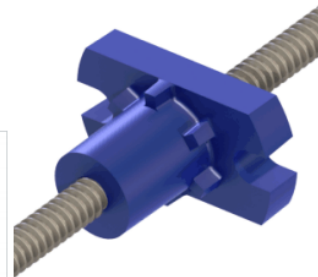
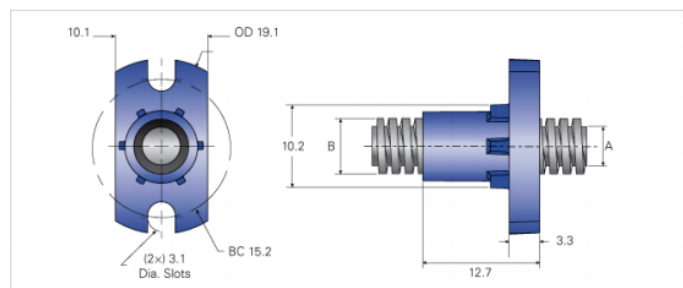


Figure 2.25. Power screw for the transformation of rotary motion to translation. See Chapter 11.1.

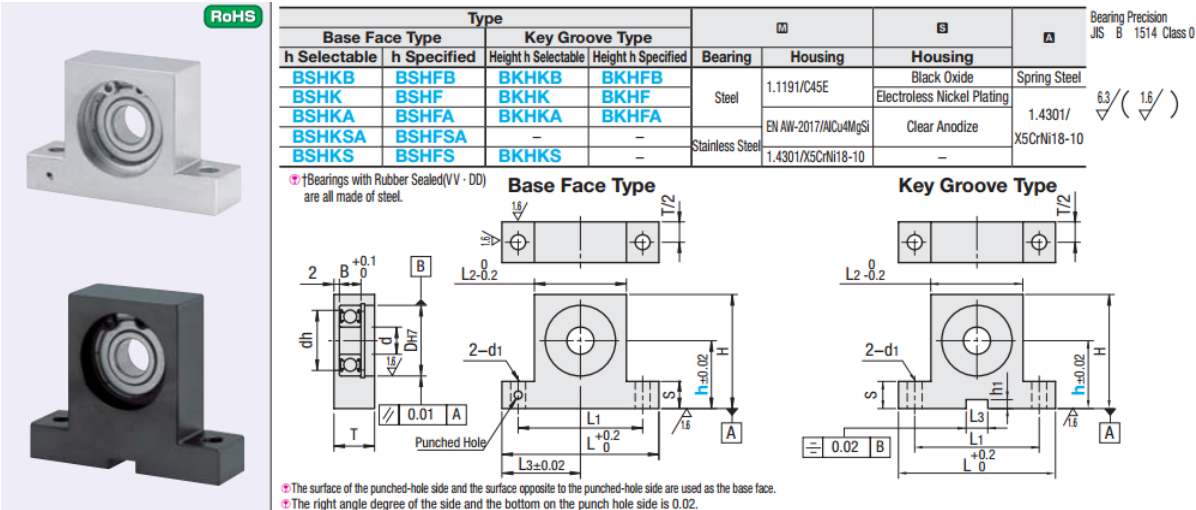


Figure 2.26. Bearing with its housing for the support of the shaft of the pulley. See Chapter 11.4.

2.5 Final Design

The final assembly is presented in the following Figures.

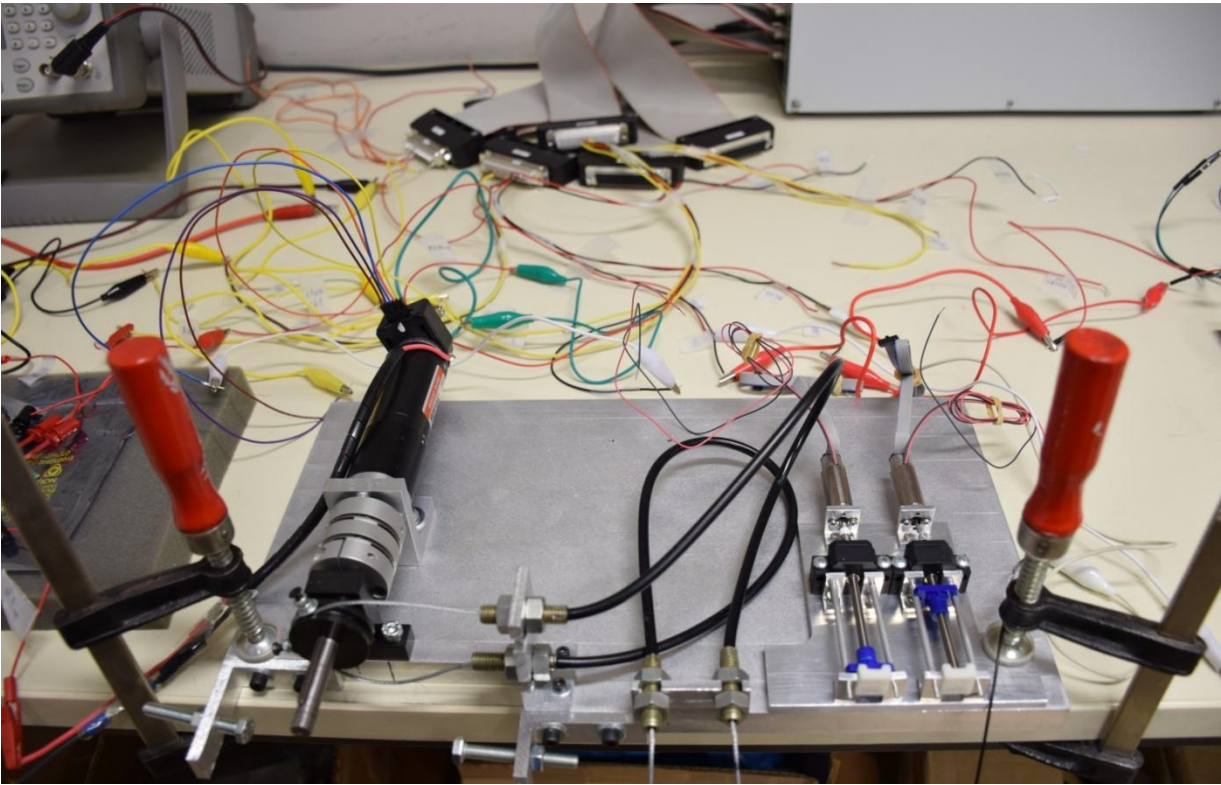


Figure 2.27. Final setup (view 1).

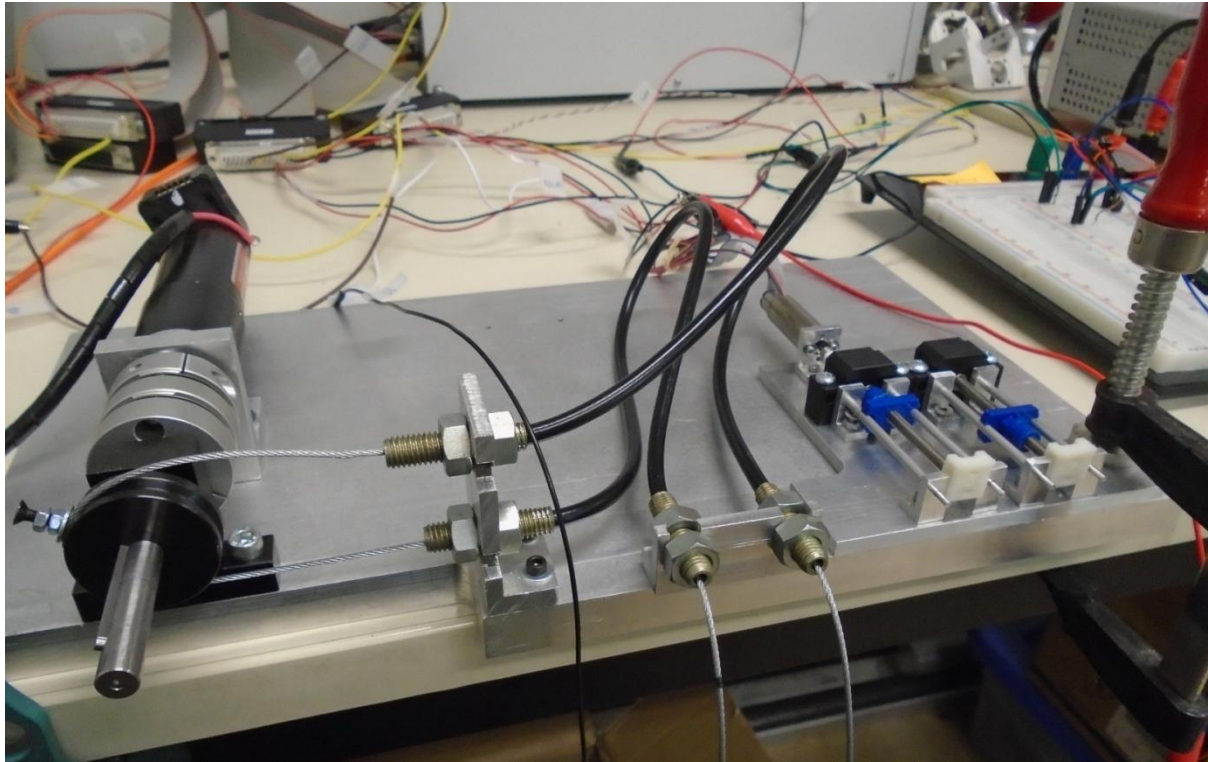


Figure 2.28. Final Setup (view 2).

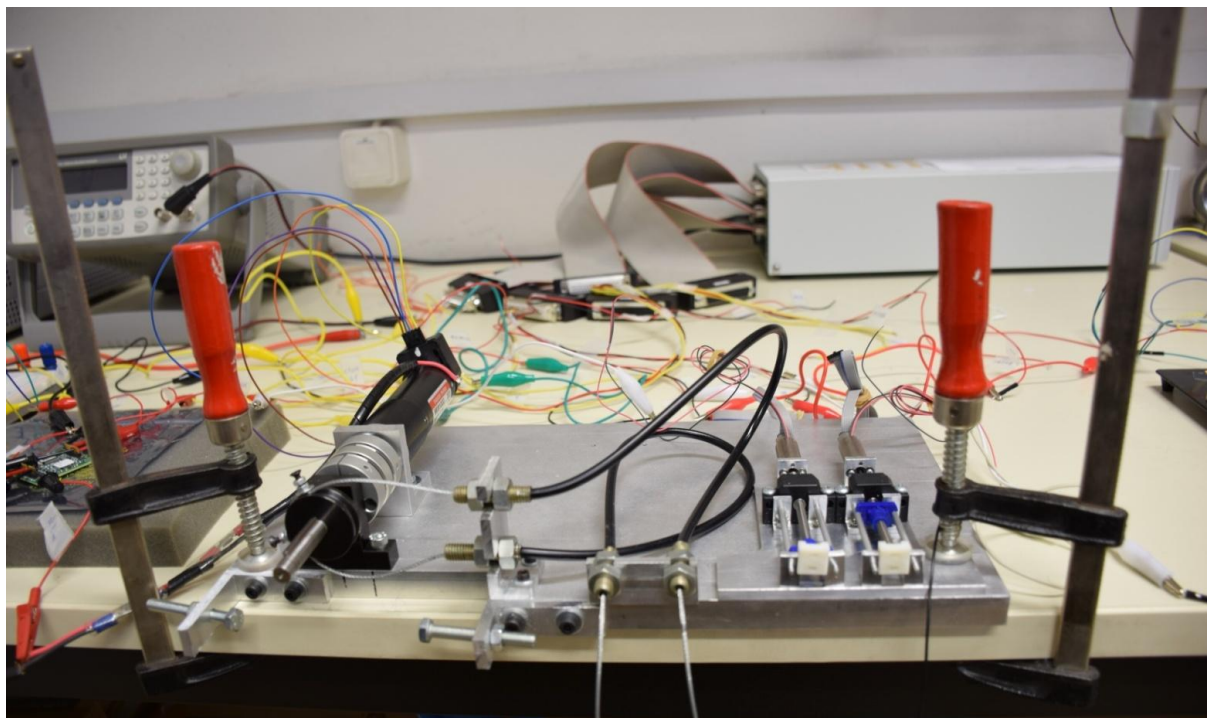


Figure 2.29. Final setup (view 3).

2.6 Troubleshooting

It has to be noted that the most arduous part of the setup paradoxically was the construction of the Bowden cables. Even though it seems insignificant in contrast with the rest of the setup, because of the time it consumed, it should be mentioned **Honoris Causa**. At the initial

steps of the concept, as presented in Figure 2.29, the notion was to make the Bowden cables stiff enough to preserve their shape using the same cover which is used to protect hydraulic hoses. The cables would be supported to the rest of the setup using the flanges previously mentioned and nuts. An outline of this idea is presented in Figure 2.30.

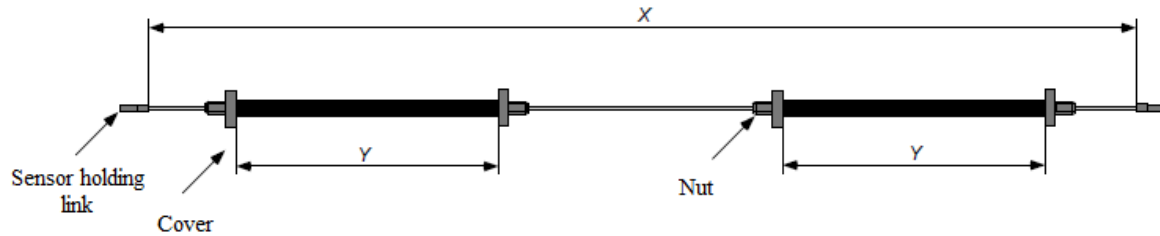


Figure 2.30. Initial concept of the design.

Thus, the first Bowden cable that was going to be used was constructed at an external workshop and it is presented in Figure 2.31.

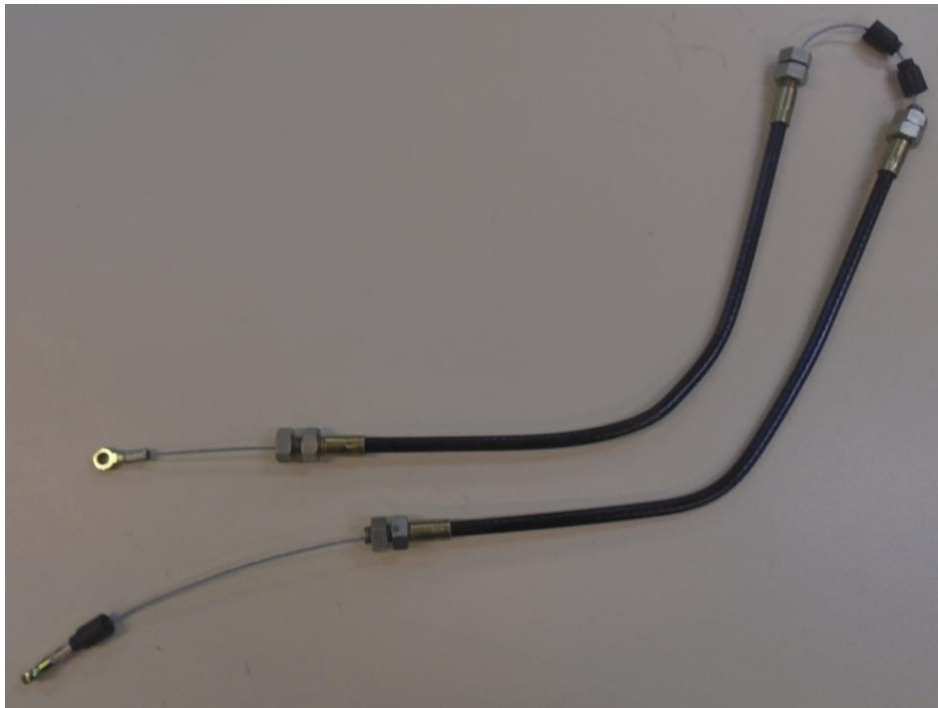


Figure 2.3. Bowden cable with cover of hoses.

Nevertheless, at the first trials to assemble it to the setup, the stiffness of the cover was so high that for the required distances of the setup the cable could not be bended. Even though with enough force and with the nuts the cable could be placed, it was volatile and if a significant load was applied, it could be freed from the supports, making the setup dangerous for the user. The Bowden cable is the most crucial part of the Classic EPP configuration, because it connects the pulley and the motor with the force sensors. Thus, an alternative solution was mandatory. However, the best solutions are sometimes found in the plainest ideas. The design concept was right, but the problem was the cover of the cables. Another option that was considered then was instead of using cover for hoses, to use cover for

Bowden cables that is applied to bicycle brakes, something that at the workshop because it was familiar with industrial applications was considered uncommon. In Figure 2.31 the two covers are presented.



Figure 2.4 Cover for bicycle brakes (up) and cover for hydraulic hoses (down)

Fortunately, with this cover the stiffness diminished significantly, and as it was presented in Figures 2.28 and 2.29 the assembly of the setup was achieved.

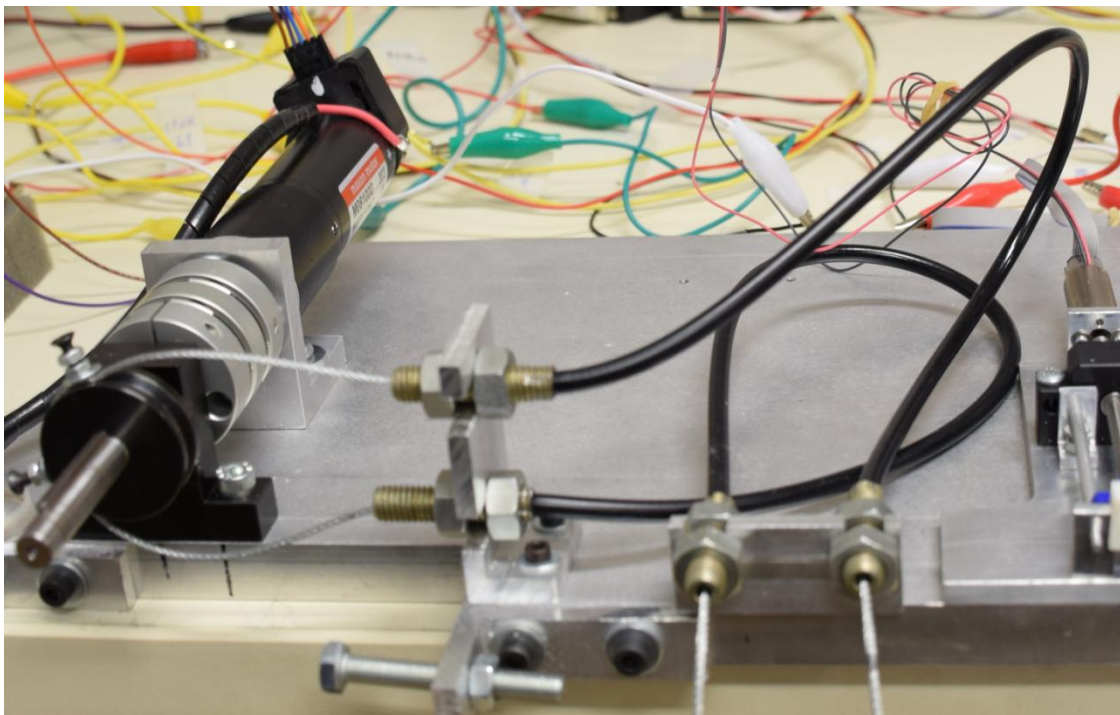


Figure 2.5. Final assembly of the Bowden cables.

3 Design and implementation of Reference Input

An essential part of the experimental setup, as for the implementation of Classic Extended Physiological Proprioception setup, as well as the Biomechatronic Extended Physiological Proprioception is the design of the setup that will provide the reference input to the system, for both cases will be the force of the muscles, as it is displayed in Figure 3.1.

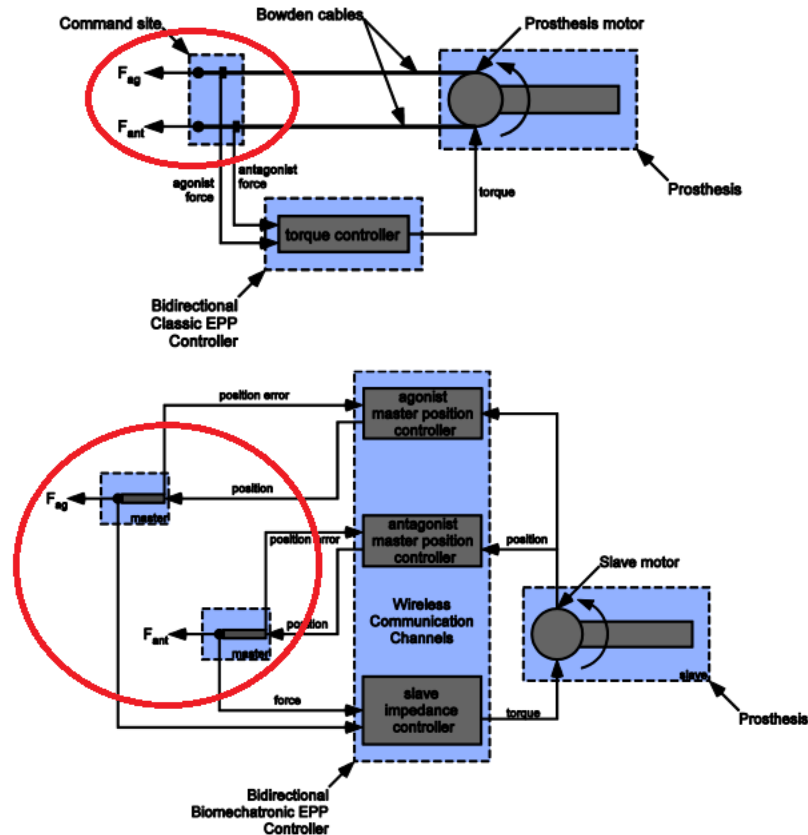


Figure 3.1. Control Schemes for both Proprioception Methods. For both cases measurement of the force to control the system is required. Modified from [4].

Thus, the design of a setup is required, which depending on the force which is applied to the Bowden cables in the case of Classic EPP, or at the screws, in the case of Biomechatronic EPP, it will determine the duty cycle of the PWM pulse. This will determine the current input of the slave motor, as shown in Figure 3.1, and as a consequence, the displacement of the master motors.

For this specific application the most appropriate means to convert the applied force to a measured signal was the Force Sensitive Resistor (FSR) displayed in Figure 3.2. The FSR's resistance depends on the applied pressure on its surface hence it is ideal for the purpose of the setup.

However, FSR has two considerable drawbacks. The first one is its high sensitivity to noise, rendering it inaccurate for precision measurements, and the second one is the fact that the properties of the resistance will vary significantly through continuous use. About the first

problem the most reasonable solution was to design an integrated circuit, which would reduce the noise using operational amplifiers, such as the ones shown in Figure 3.3 which are the MCP6002.



Figure 3.2. The Force Sensitive Resistor used in the setup.

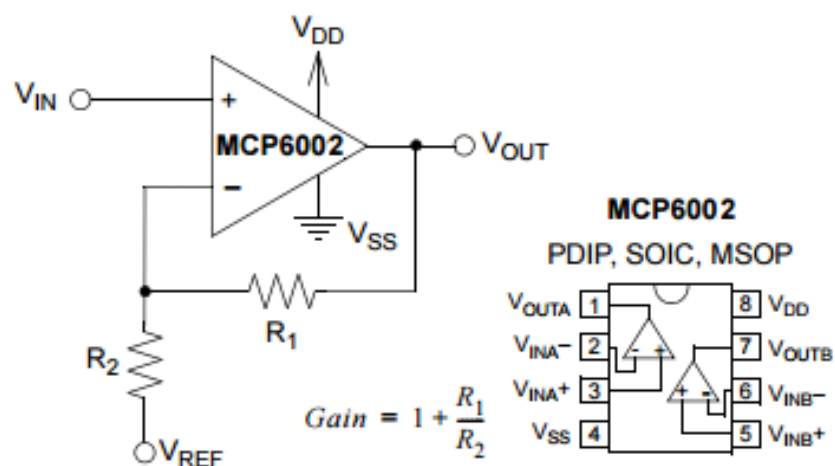


Figure 3.3. Operational amplifier MCP6002.

The final signal conditioning circuit that was constructed is presented in Figure 3.4.

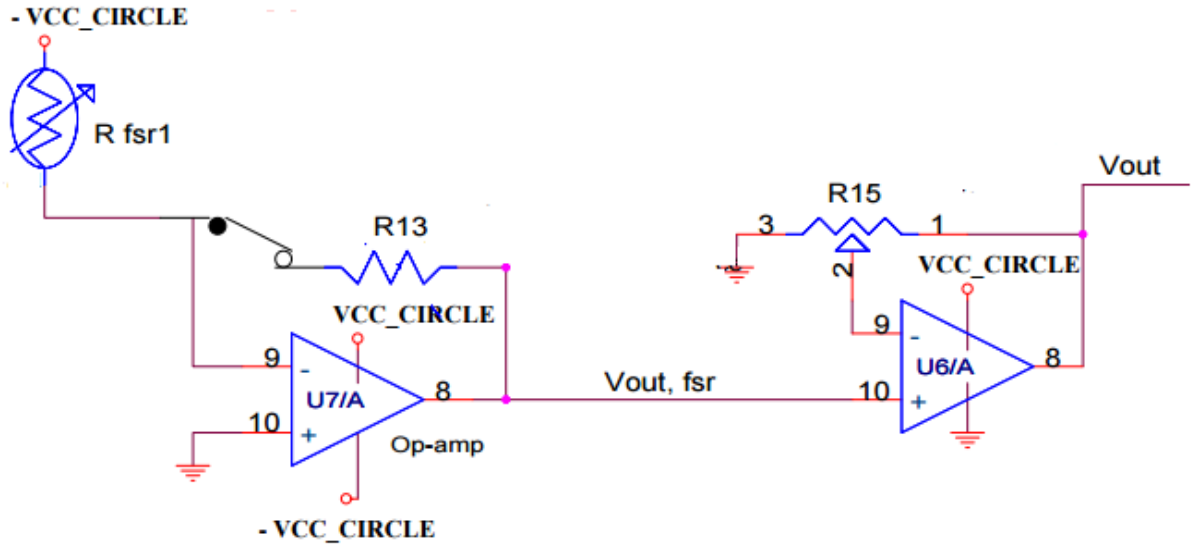


Figure 3.4. Signal Conditioning Circuit. Modified from [1].

Applying the Kirchhoff's laws the transfer function that relates the V_{CC_CIRCLE} (Power Supply) to the circuits output is the equation 3.1.

$$V_{out} = -V_{ccircle} \frac{R_{fsr1}}{R_{13}} \left(1 + \frac{R_{15_{23}}}{R_{15_{21}}}\right) \quad (3.1)$$

The output voltage of the FSR signal conditioning circuit (and input to the A/D port of the controller) is slightly less than +5V. Depending on the values of the circuit's resistances $R_{13}, R_{15_{23}}, R_{15_{21}}$ the force resolution is different. Varying values display force capability ranges that muscle cineplasty amputees and exteriorized tendons amputees can produce ^[1]. For further experiments to be conducted, it was necessary to define the maximum force under which the saturation of the output would occur. Ergo in the stage of prototyping it was essential to find the optimum values of the resistances, such that the maximum force that would be applied. For the experiment's implementation, the setup of Figure 3.5 was designed, with which for various values of resistance the Voltage - Force curve could be calculated. The exact dimensions of the setup are presented on the APPENDIX C ENGINEERING DRAWINGS.

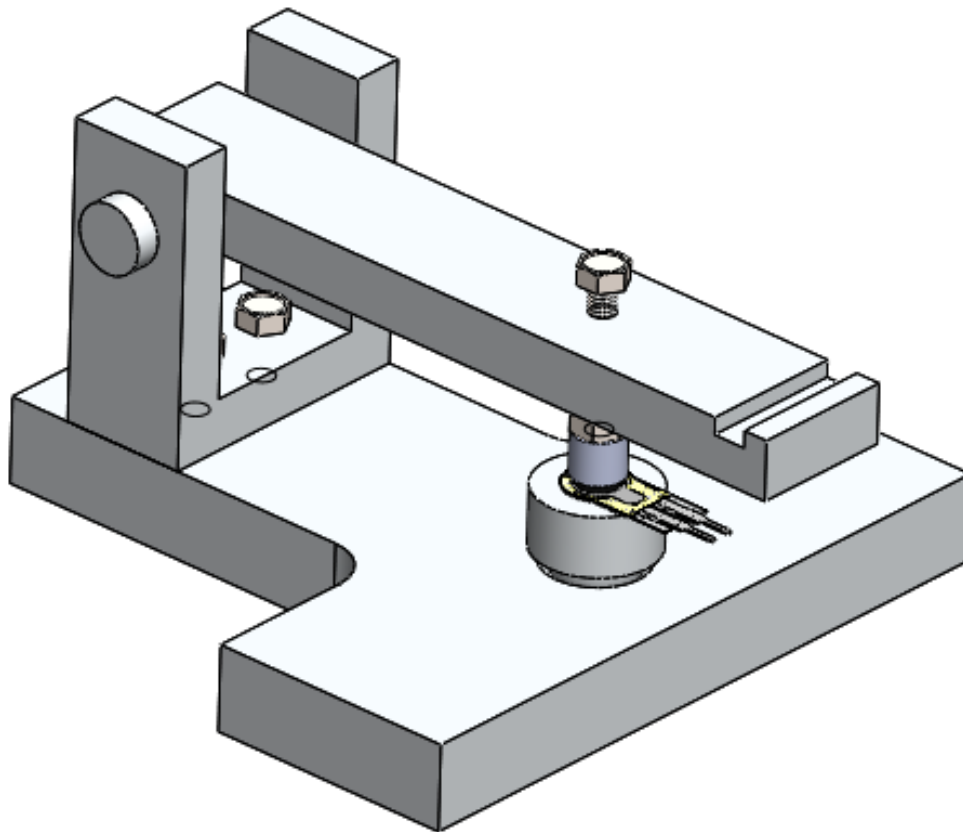


Figure 3.5. Force applying setup for the integrated circuits calibration. Modified from [4]

The design of this specific setup was completed in a previous diploma thesis ^[4] and some of its parts were ordered, while others were manufactured with the laboratory's lathe and milling machine for this diploma thesis. The final design with the use of test weights to record the exact force value is presented in Figure 3.6.



Figure 3.6. Final Setup of the FSR characterization module.

In the stage of prototyping, the circuit was designed on a breadboard and the various values of resistance were tested with the use of a potentiometer. A potentiometer is used to cope with the second disadvantage, that of the varying properties. An increase of the circuits output without the application of load is noted with the potentiometer. Then changing the potentiometer's parameter value is an easy and cheap solution, because in other case it would be required to change FSRs too often, which could be proved very costly for the whole setup. The setup is shown in Figure 3.7.

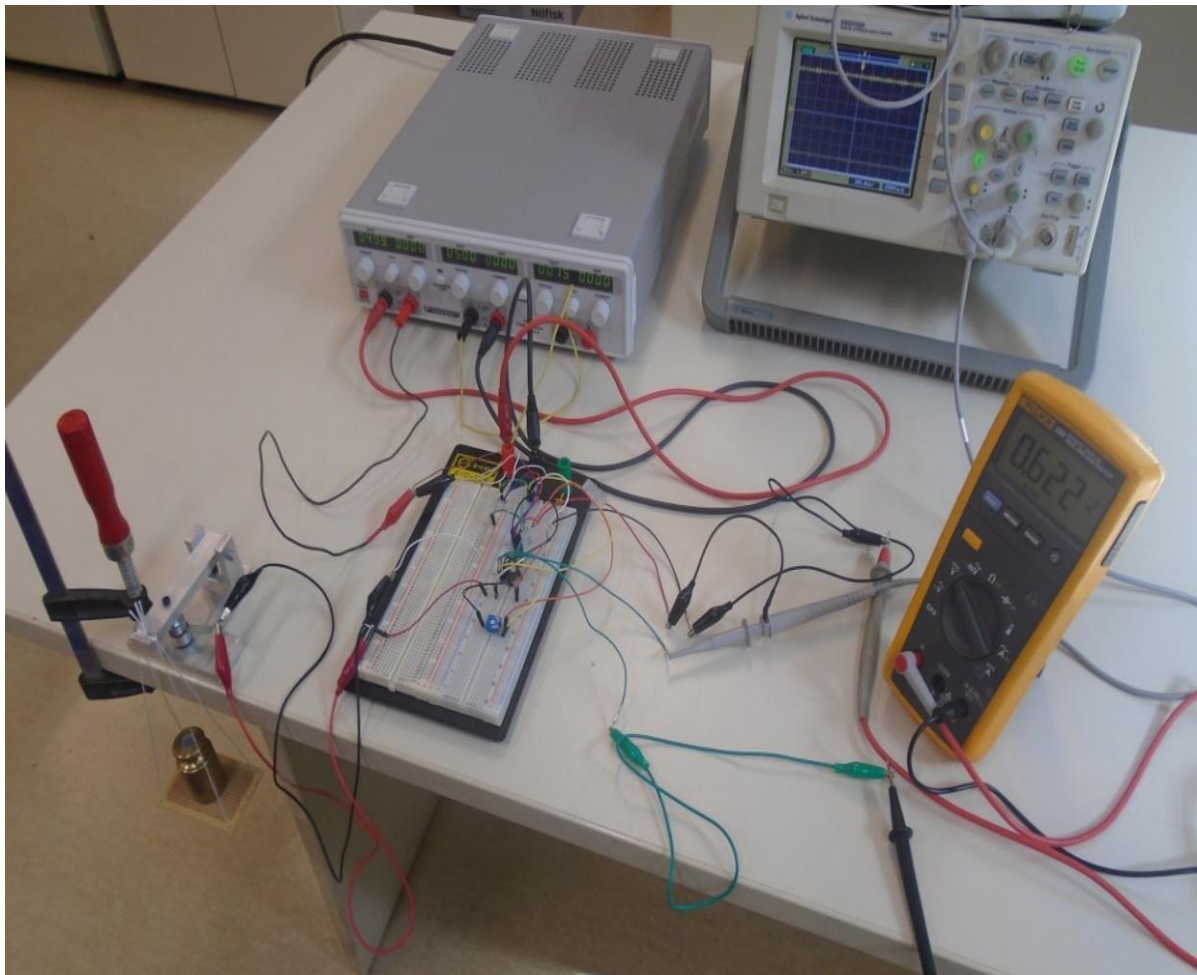


Figure 3.7. Setup for the circuit's calibration.

Some distinctive results are presented in Figure 3.8. It has to be noted that the potentiometer's value had to be variable, for the previously stated reason that through the experiments the properties of the FSR changed and it was mandatory to change it for different cases.

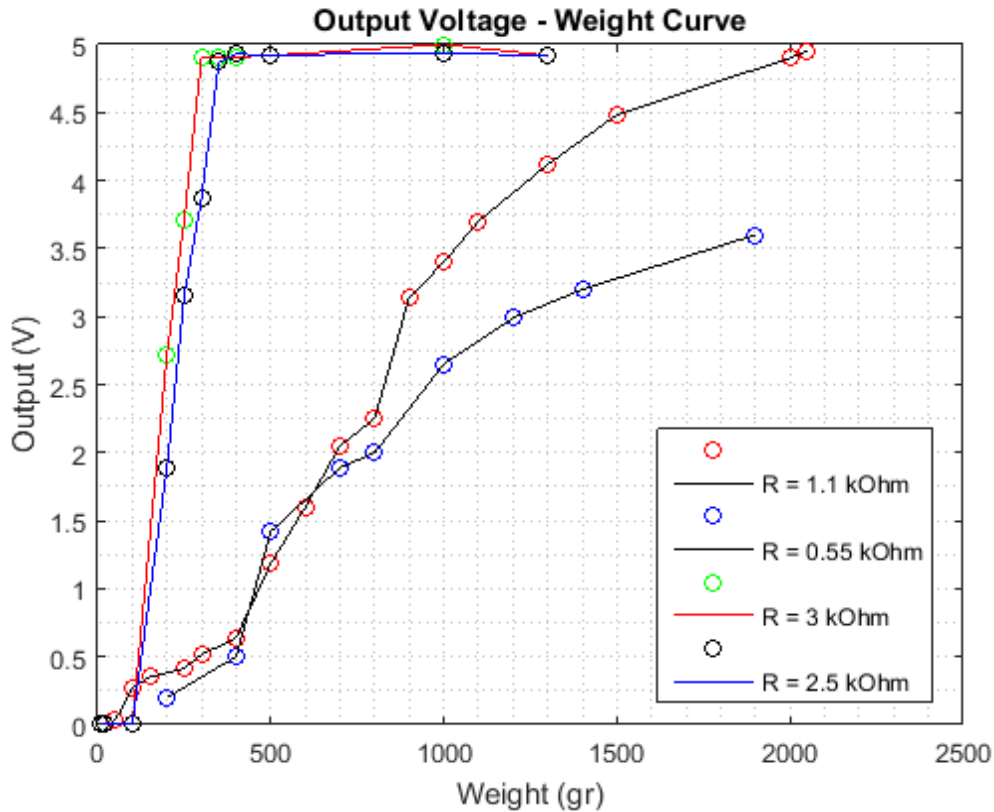


Figure 3.8. Resulting Output - Weight Curves for different resistance R13.

From the experimental results it can be derived that the slope of the curve decreases as the parameter value of the resistance decreases as well. Taking into account the maximum load that should be applied until the 5V upper bound is reached, and also the mean force that can be applied by an individual, the best option that was selected was the value of 1.1 kOhm, and when considered necessary, to change the value of the potentiometer when significant changes in the circuit's output value is observed.

After the calibration, the next stage is to construct the circuit in a way that the potential user can apply force to the FSR on one hand and on the other hand the FSR and the circuit to be close to each other, in contrast with the prototyping stage shown in Figure 3.7. Moreover, a way to connect it with the cables has to be found. It was decided to construct the circuit in a board with soldering, instead of the use of LPKF, for swift modifications if required and effortless change of the operational amplifiers in the case of erroneous use. Moreover, it has to be considered the fact that the user has to apply the necessary force though the whole surface of the FSR, without leaving any unloaded area. All things considered, the parts that were designed that would support the board are presented in Figures 3.9, 3.10 and 3.11. The exact dimensions of the setup are presented on the APPENDIX C ENGINEERING DRAWINGS.

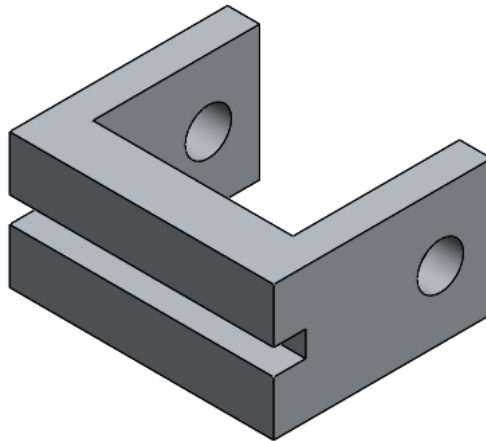


Figure 3.9. Press plate of the final circuit support.

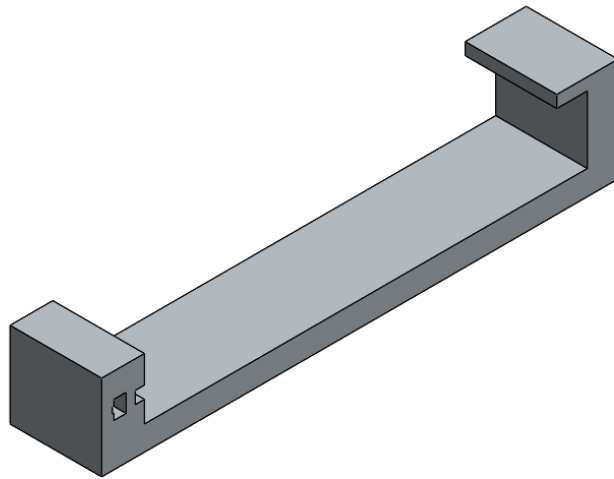


Figure 3.10. Housing of the final circuit support.

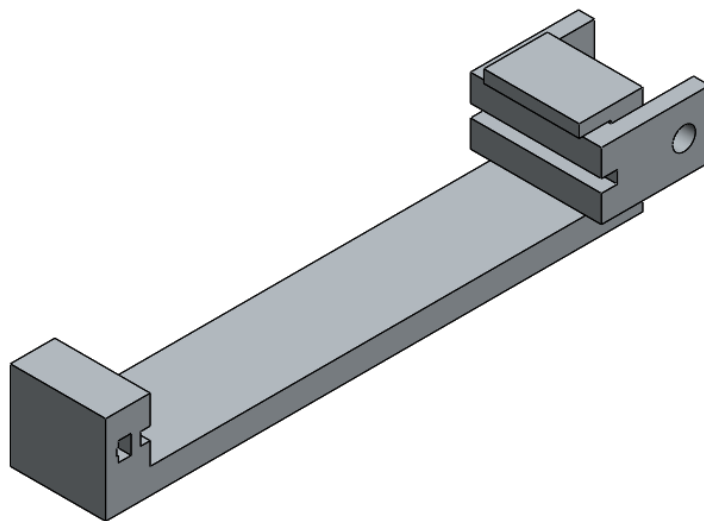


Figure 3.11. Assembly of the two parts.

These parts were designed in Solidworks and they were constructed in the laboratory's 3D printer. The final dimensions were opted so that a conventional board could be placed, as it is shown in the following Figures.

The assembly procedure is presented step by step in the following Figures.

Step 1

Bend the FSR (without hurting the pressure surface) and place it on the housing, as shown in Figure 3.12.

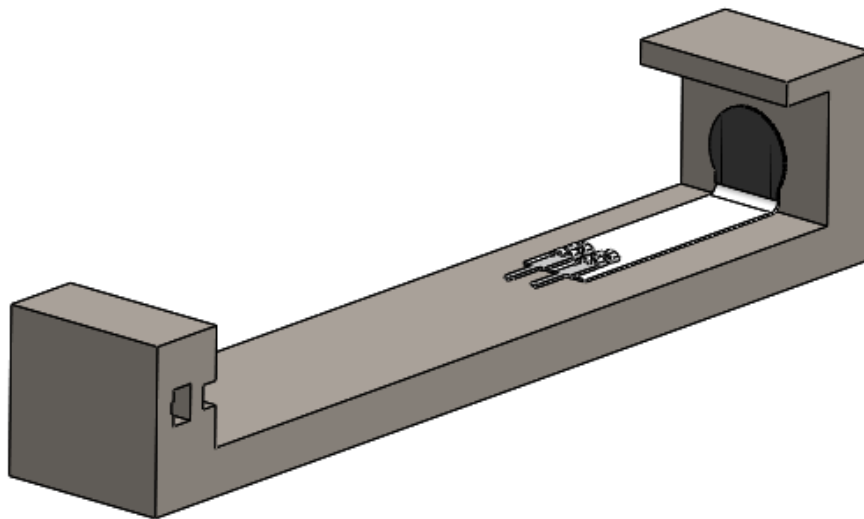


Figure 3.12. Step one. Place the FSR to the housing.

Step 2

During the first experiments it was observed that the stick and slip phenomenon occurred between the FSR and the pressure plate. To avoid it, it should be advised to place between the two of them some rubber, as shown in Figure 3.13.

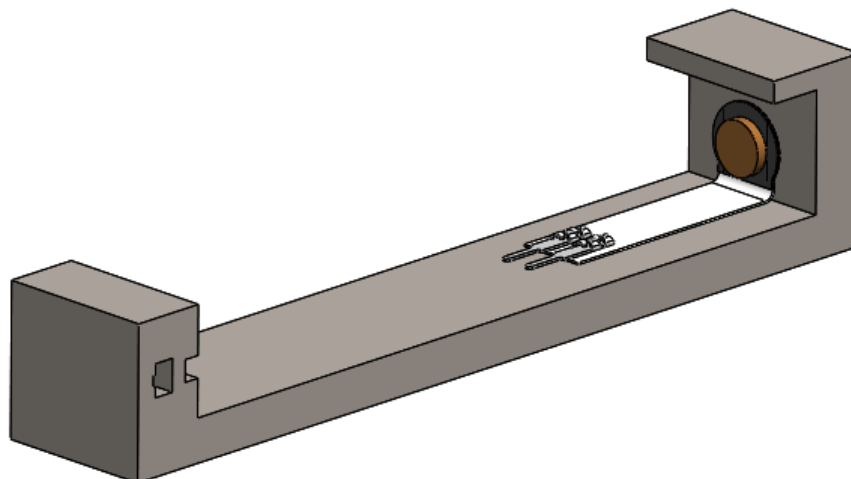


Figure 3.13. Step two. Place on the pressure surface some rubber to avoid sticking.

Step 3

Place the pressure plate, as shown in Figure 3.14.

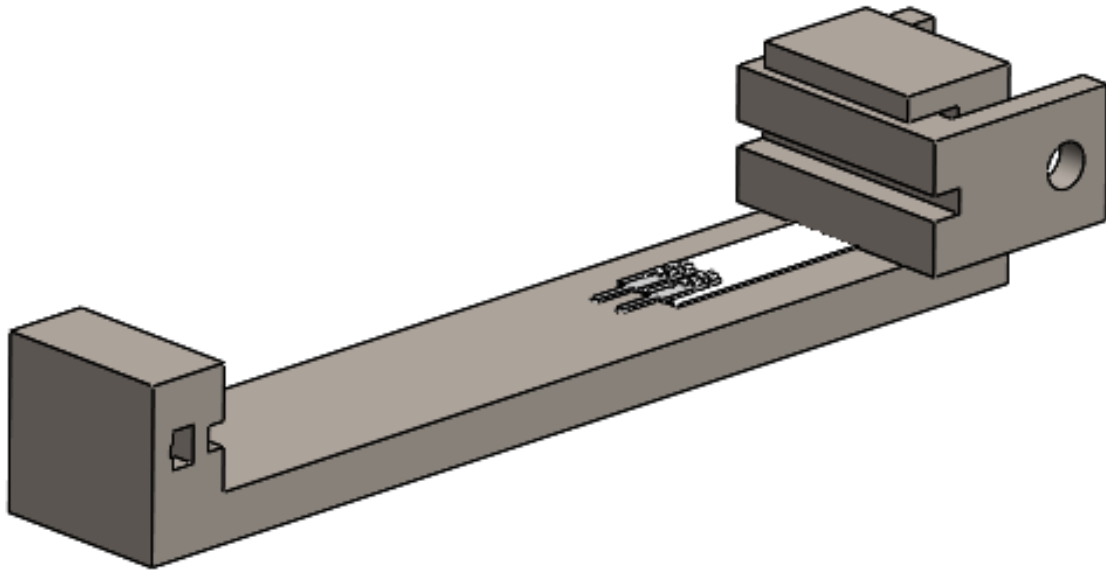


Figure 3.14. Step three. Place the pressure place.

Step 4

Place the board with the electronic circuit, as shown in Figure 3.15. To keep the board fixed and to constrain its movements, it can be attached to the housing with glue.

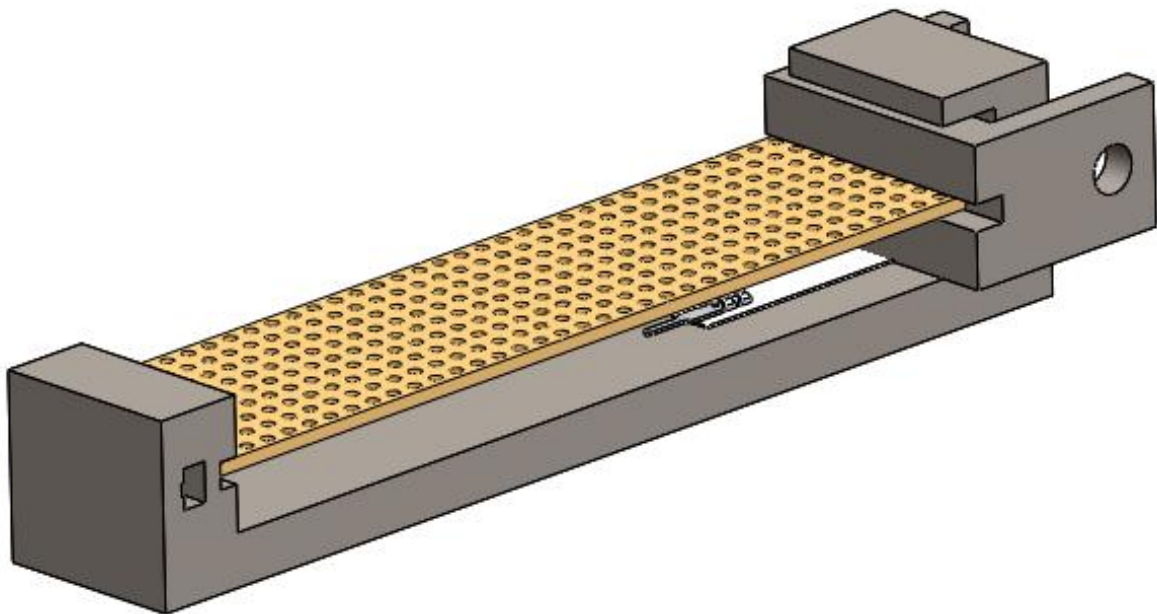


Figure 3.15. Place the board of the electronic circuit.

The final force sensor is presented in Figure 3.12. In Figure 3.13 the way the sensors are to be connected to the Bowden cables is presented.

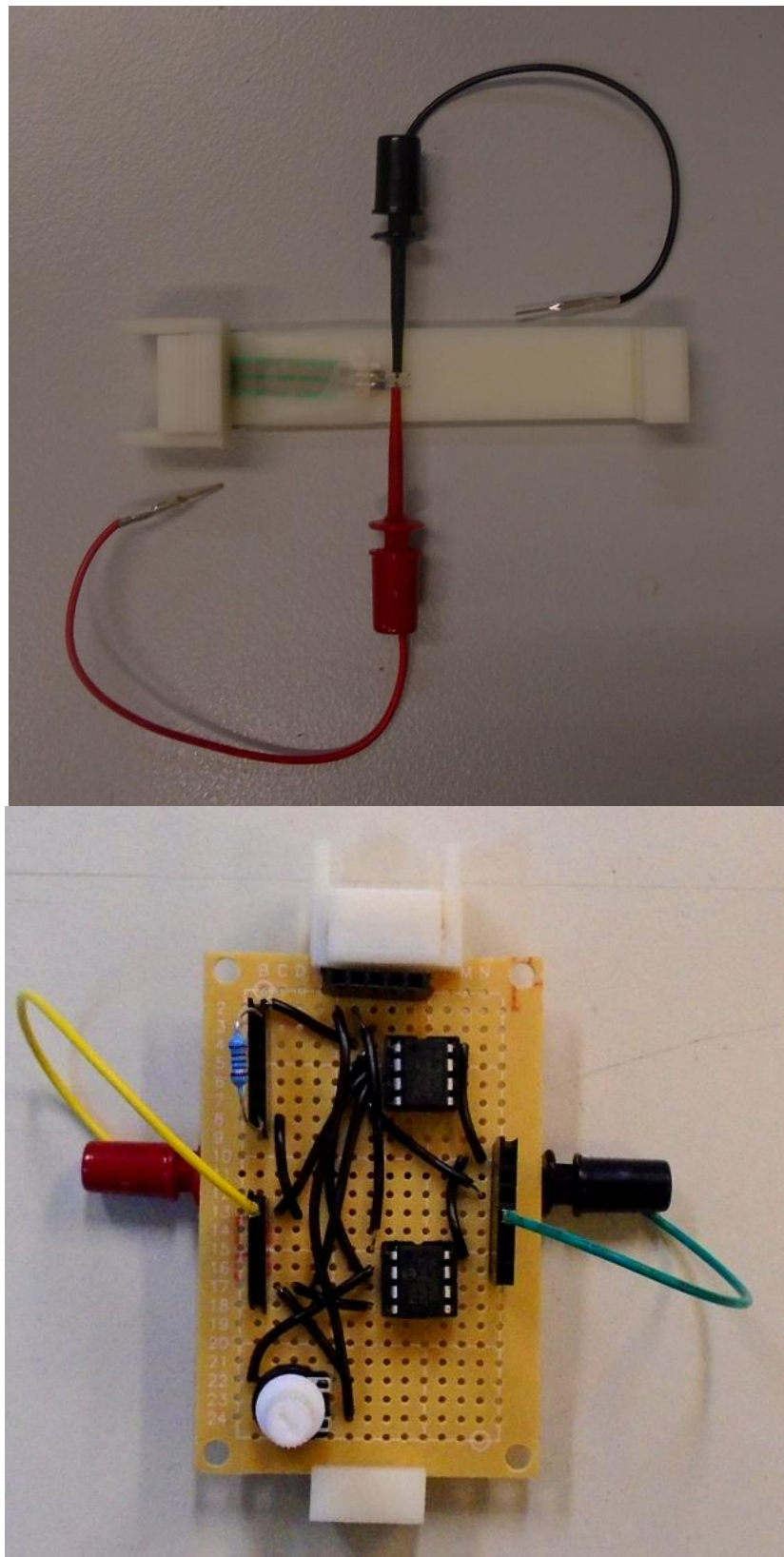


Figure 3.16. Force Sensor Front View and FSR's connection.

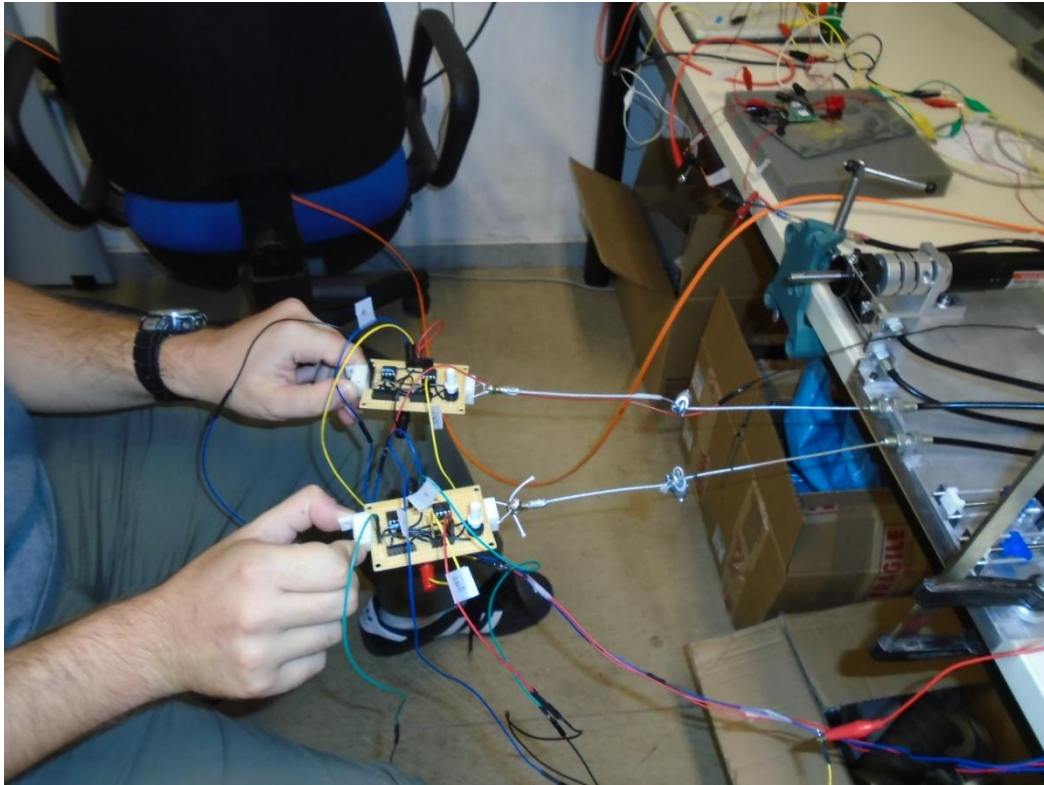


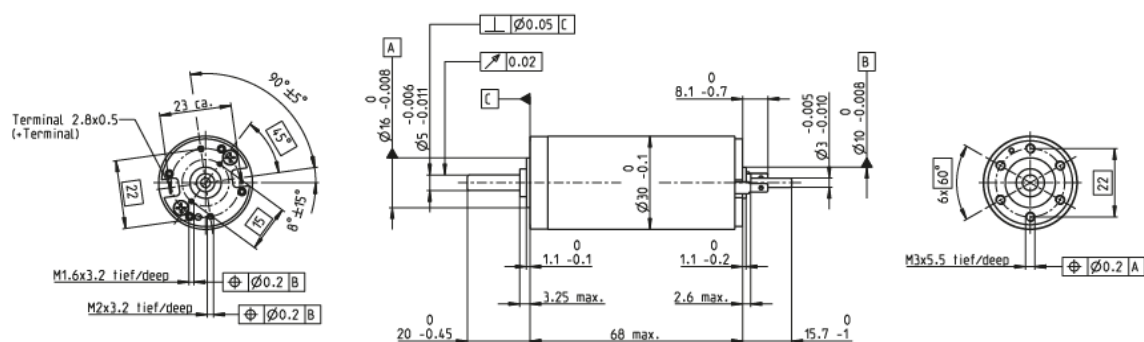
Figure 3.17. FSR connection with the Bowden cables of the motors setup.

Thus, the demand of a functional way to measure the applied force and measure the input force was solved with these sensors and they were used for the prototyping of the control schemes for the tests to come. However, the nature of these tests and the route that was followed to be implemented will be presented to the next installments.

4 Boarding Prototyping - Hardware Selection

The most vital part of the setup is the electromechanical equipment, which consists of the motors, the encoders and the drivers. The slave motor is the one that will be responsible for the imitation of the upper limb motion, because it must provide the necessary force of the end effector. Thus, the user of the upper limb can hold or grab an object. For this task the motor that was selected was the RE 30 Ø30 mm, Graphite Brushes, 60 Watt displayed in Figure 4.1.

RE 30 Ø30 mm, Graphite Brushes, 60 Watt



M 1:2

Figure 4.1. Slave motor drawing. See Chapter 11.8.

For the master motors it was required small size and fast response, thus it was selected the Motor - DCX12L EB KL 4.5V, displayed in Figure 4.2.

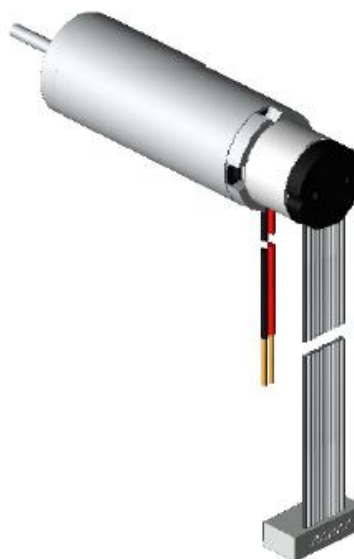


Figure 4.2. Master motor CAD. See Chapter 11.11.

For the feedback of the control schemes, the measurement of the position of the encoders was required. For the slave motor, the encoder that was selected was the Encoder HEDS 5540 500 Counts per turn, 3 Channels, displayed in Figure 4.3.

Encoder HEDS 5540 500 Counts per turn, 3 Channels



Figure 4.3. Encoder of the slave motor. See Chapter 11.10

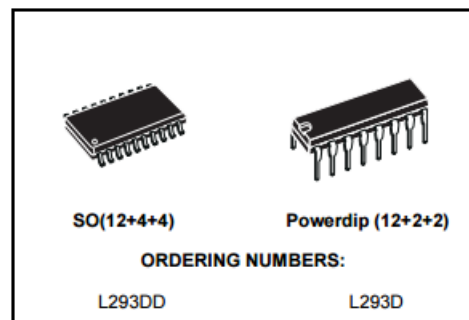
For the master motors their encoders were already attached to the motors, and they were of type Sensor - ENX10 EASY 512IMP, displayed in Figure 4.4.

Sensor - ENX10 EASY 512IMP



Figure 4.4. Master motor encoder. See Chapter 11.12

For the control of the master motors, the hbridge was selected taking into account the maximum Supply Voltage and maximum current of the motors. The one that was selected was the A3959 DMOS Full-Bridge PWM Motor Driver, displayed in Figure 4.5.



- 600mA OUTPUT CURRENT CAPABILITY PER CHANNEL
- 1.2A PEAK OUTPUT CURRENT (non repetitive) PER CHANNEL
- ENABLE FACILITY
- OVERTEMPERATURE PROTECTION
- LOGICAL "0" INPUT VOLTAGE UP TO 1.5 V (HIGH NOISE IMMUNITY)
- INTERNAL CLAMP DIODES

Figure 4.5. Master motors H-bridge.

For the slave motor the driver that was selected was the Analog Servo Drive AZBDC10A4, displayed in Figure 4.6, because its Supply Voltage range fulfills the required desire of the Nominal Voltage of the motor.

Power Range	
Peak Current	10 A
Continuous Current	5 A
Supply Voltage	10 - 36 VDC



Figure 4.6. Analog Servo Drive AZBDC10A4. See Chapter 11.6.

However, the main drawback of these drivers is the distance between their pins. Unlike the common standardization of 2.54 mm distance between the pins, in this specific driver the distance is 1.27 mm. One short -termed solution was the one displayed in Figure 4.7. The simplest way to connect the driver with the setup was to connect the pins with the smallest hook clips available (1.7" Hook Clip Grabbers), so that short circuit is avoided.

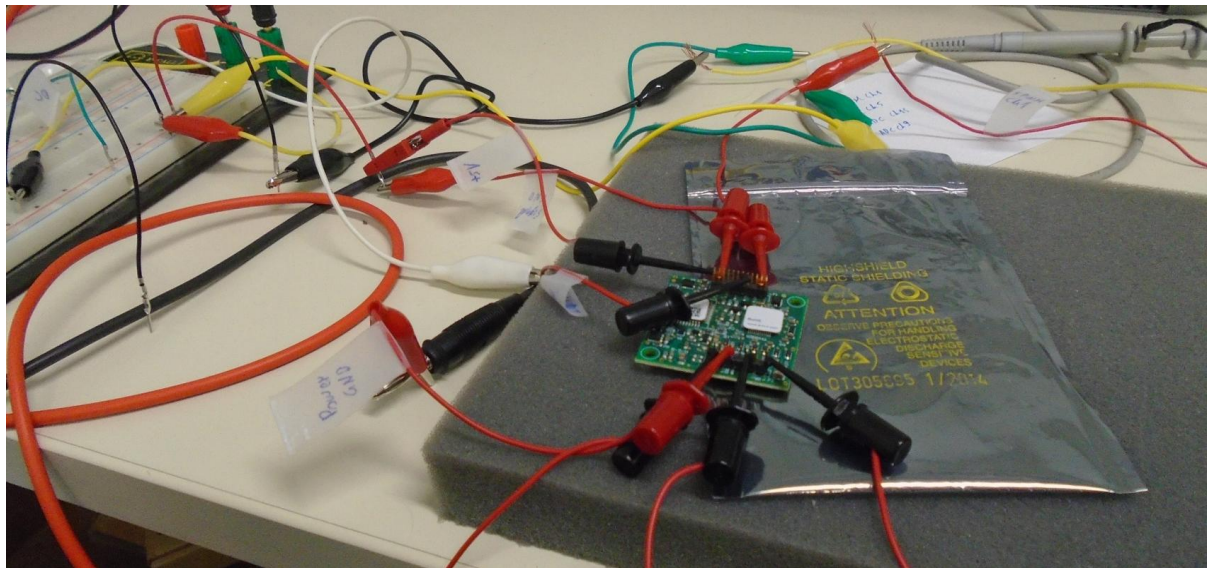


Figure 4.7. Initial solution of the connectivity problem.

However, the risks of connectivity problems, short circuit and augmented noise in the measurements were still imminent; and it was required to make the connection between the driver and the setup easier increasing the distance among the pins. The commercial option of the manufacturer of the drivers was the AZ Drive Family Mounting Card MC1XAZ02, displayed in Figure 4.8.


Description	Drive Compatibility
<p>The MC1XAZ02 mounting card is designed to host a μZ-style AZ series analog servo drive. This mounting card offers convenient screw-terminal connectors. Easily accessible test points are available for I/O monitoring. The MC1XAZ02 can be screw-mounted directly to a PCB when assembled with a μZ-style AZ drive, and is ideal for both prototyping and production. The mounting card also features a keyed connector to prevent misaligned connections.</p>	<p>μZ-style AZ 40 V Models 10A</p>
	

Figure 4.8. Commercial mounting for the drive AZBDC10A4.

Even though it was a decent option, the high cost and the time required to transverse it from abroad made it prohibitive. Thus, it was decided that the board mounting could be constructed using the resources and the equipment of the laboratory, and especially the LPKF PCB prototyping.



Figure 4.9. LPKF setup.

First, the LPKF requires the CAD files of the board that will be constructed, that are the schematic drawing and the board view, displayed in Figures 4.10 and 4.11. They were designed using the EAGLE PCB design software.

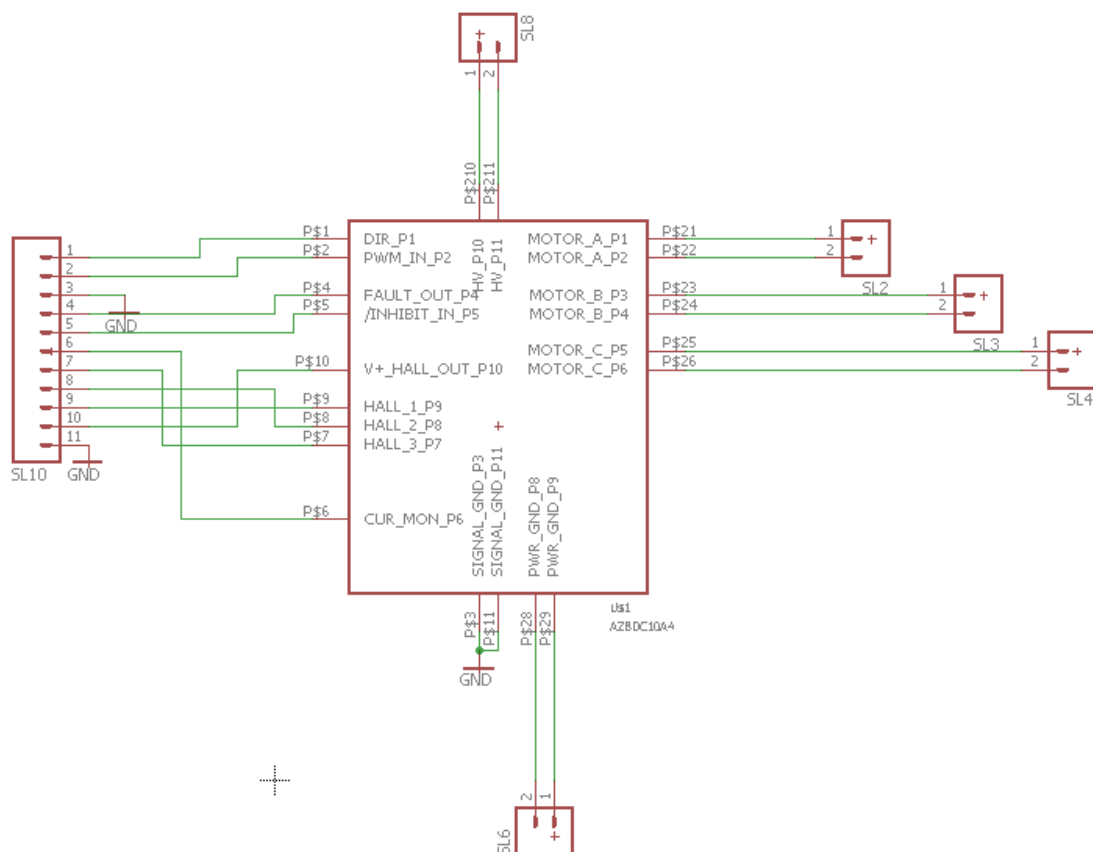


Figure 4.10. The schematic drawing view of the mounting of the driver.

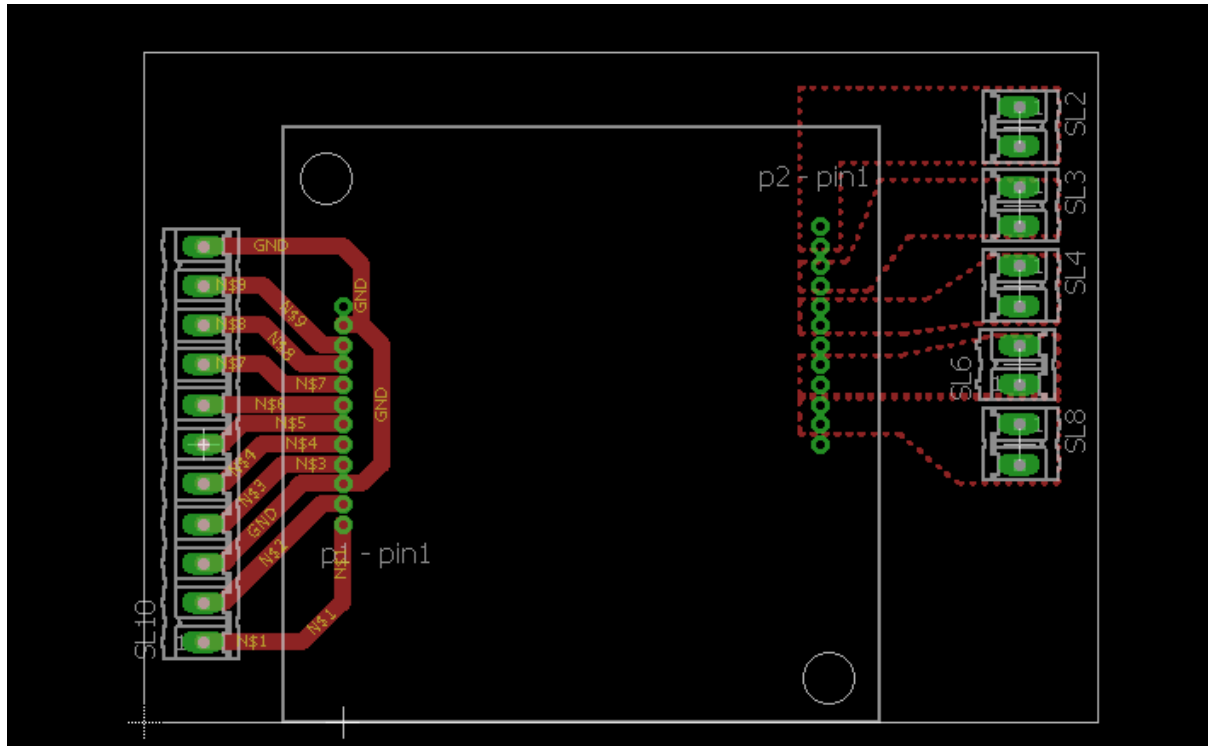


Figure 4.11. The board view of the mounting of the driver.

The final mounting prototype that was constructed using the LPKF is displayed in Figure 4.12.

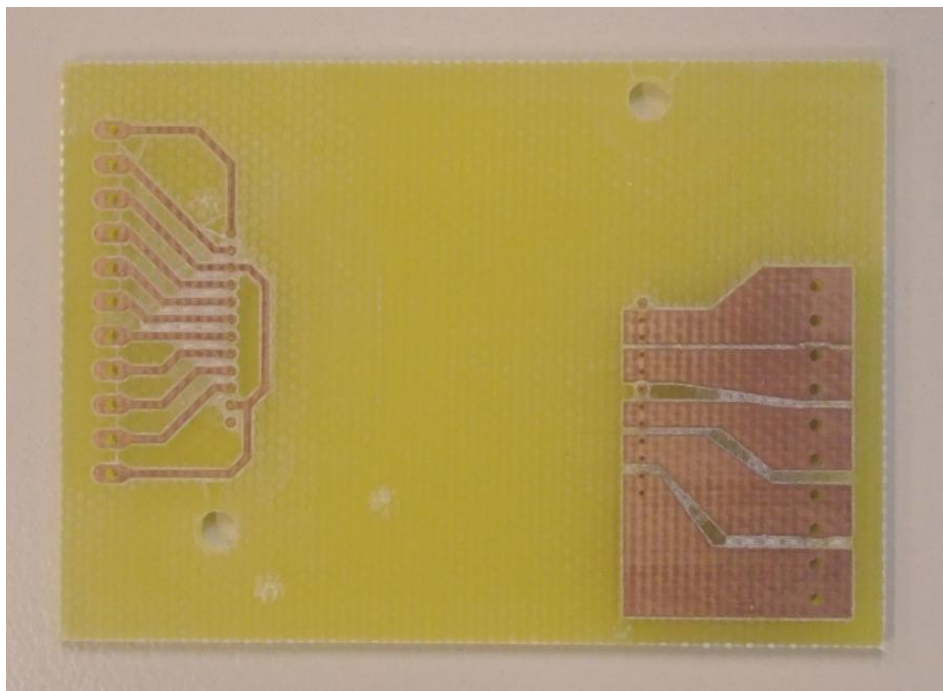


Figure 4.12. Final mounting prototype.

To mount the board to the prototype, header pins 1.27 mm and screw terminal connectors 2.54 mm were soldered, and the final result is presented in Figure 4.15.



Figure 4.13. Header pin 1.27 mm.



Figure 4.14. Screw terminal connector 2.54 mm.

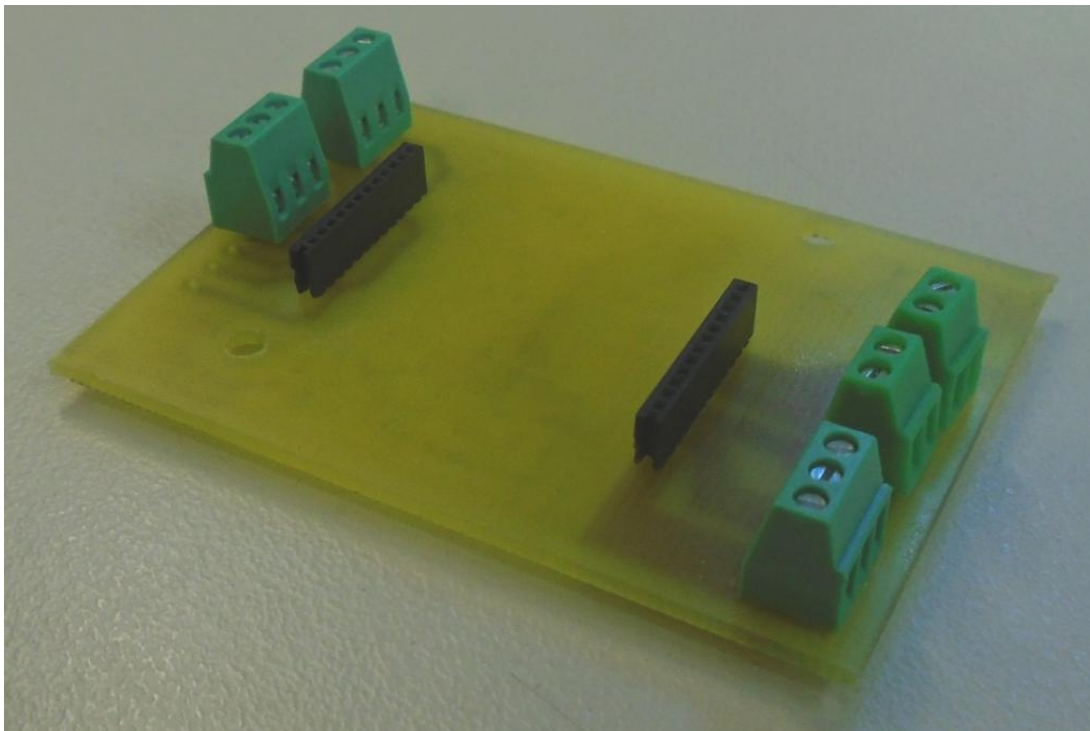


Figure 4.15. Final mounting prototype.

In the following Figures the driver attached to the mounting is presented.

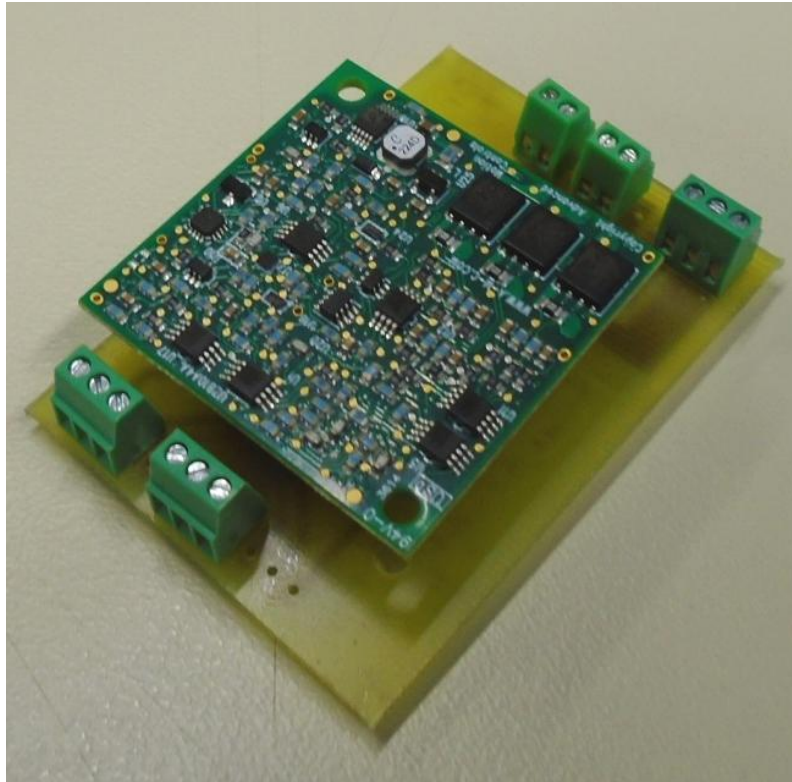


Figure 4.16. The driver attached to the mounting.

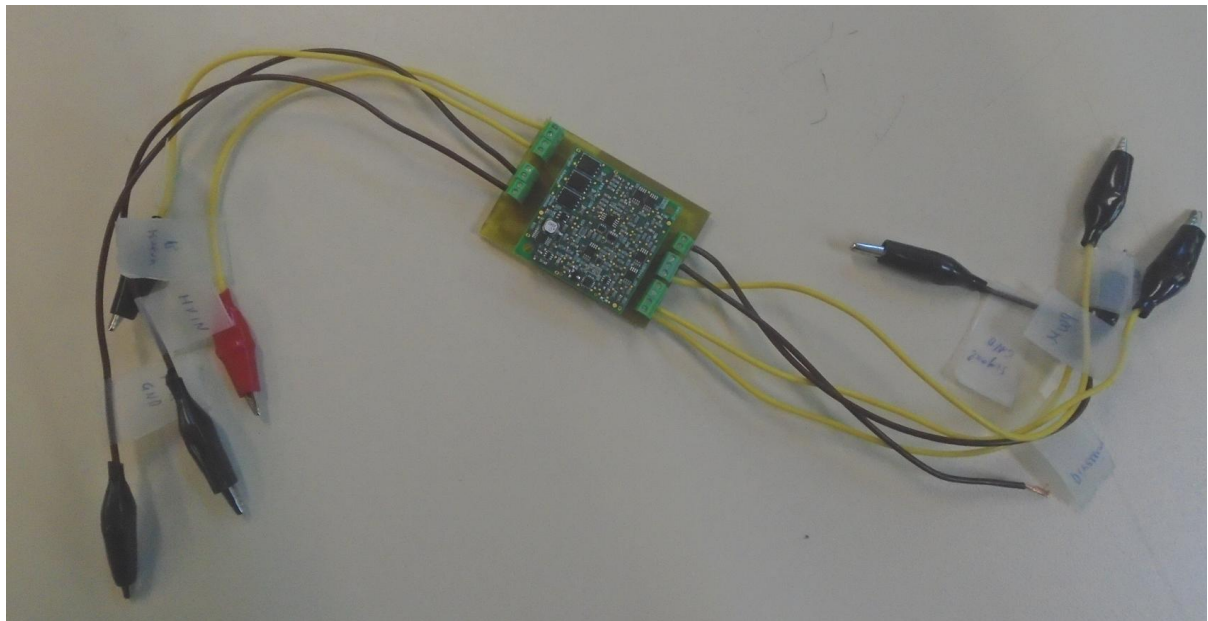


Figure 4.17. The mounting with cables attached to it to connect to the setup.

Thus, the connectivity constraints were resolved and the short circuit was avoided.

The next hindrance that had to be overcome was the connection of the master motor encoder to the setup. The problem was the very same, as the connector of the encoder had pins with distance 1.27 mm, thus making the connection with the setup very hampering. The connector is displayed in Figure 4.18.

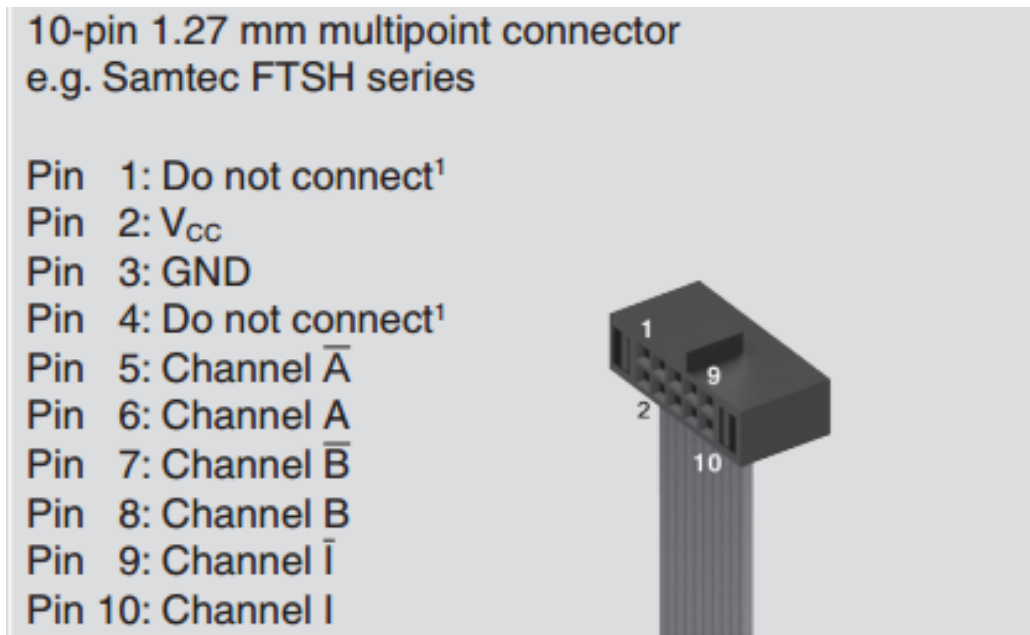


Figure 4.18. ENX 10 EASY connector. See Chapter 11.12.

Likewise, the manufacturer proposes the use of a commercial adaptor, presented in Figure 4.19, however the price and the transportation time prevented this option, and as a result the LPKF was used again. The schematic drawing and the board view, displayed in Figures 4.20 and 4.21. They were designed using the EAGLE PCB design software.

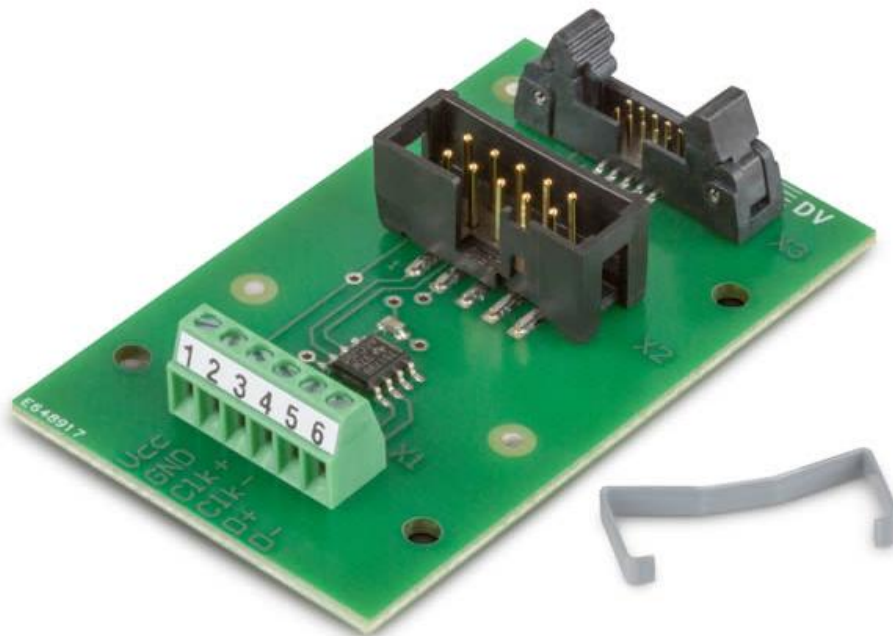


Figure 4.19. Adapter EASY Absolute Part number 488167.

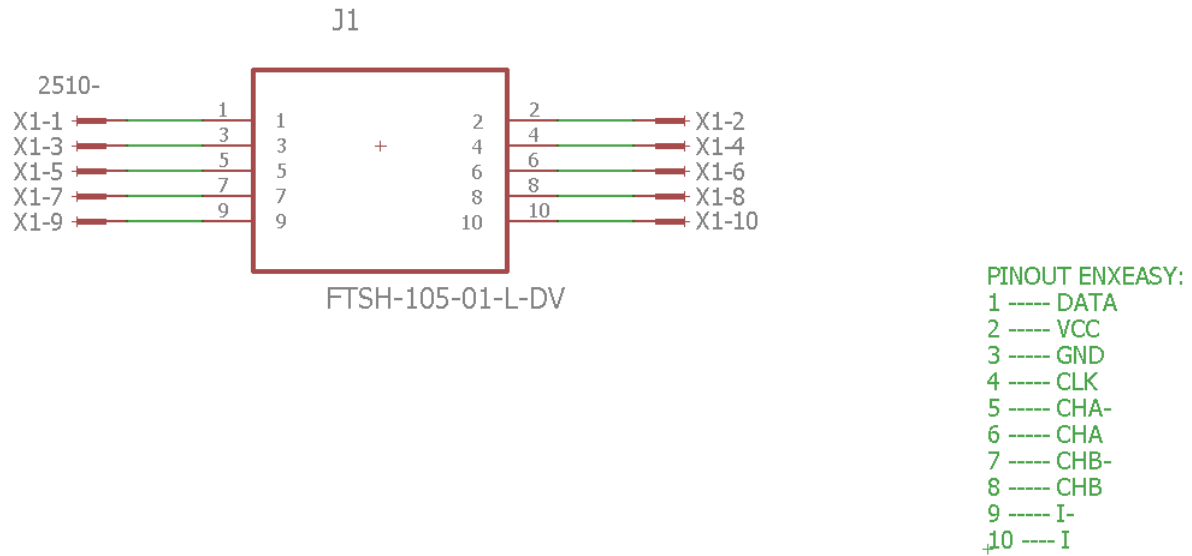


Figure 4.20. The schematic drawing view of the encoder adaptor.

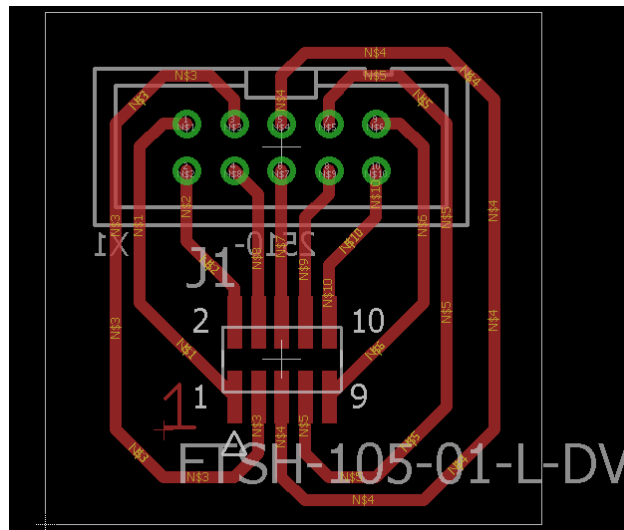


Figure 4.21. The board view of the encoder adaptor.

The final adaptor prototype is displayed in Figure 4.22. To connect the connector with the adaptor the Samtec FTSH Series, 1.27mm Pitch 10 Way 2 Row Straight Pin Header, Surface Mount, Solder Termination was soldered. The soldering procedure had to be extremely meticulous, because the copper lines were too close to each other, and a mistake because of fidgeting could prove fatal.

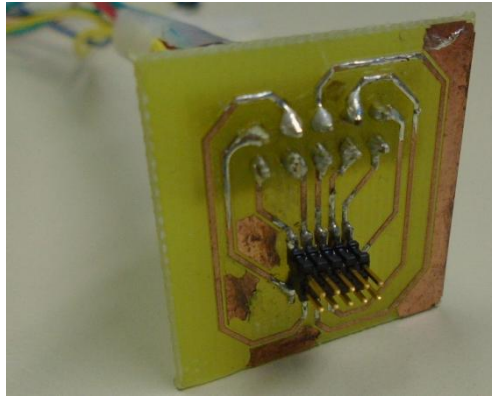


Figure 4.22. Adaptor prototype for the encoder connector.

Thus, the hardship of the connection of the master motor encoder with the setup was resolved. How the hardware will be used for the setup will be presented to the next installment.

5 Preliminary Data Processing

In this chapter it will be presented the required data processing for the identification of the system, as well as the techniques that were used to improve the quality of the measurements of the sensors of the setup. Furthermore, the theoretical foundations for the dynamic analysis of the system of the setup and the closed loop design are presented. Even though these topics seem unrelated to each other, what they share is that all of them are required steps to make the final Classic EPP and the Biomechatronic EPP function properly, even though this is not the final stage of the experimental validation.

System Identification

In this section it will be presented how the various parameters of the system, mandatory for the control of the setup, were identified.

5.1 Unit conversion of the outputs of the encoders

One vital aspect of the control system is the correct measurement of the output. dSpace provides the user with the necessary tools to measure the position and the velocity of the actuators of the system; however, the user is obliged to convert the measurements to the correct units. In this specific setup it is required to measure the position of two different motors, thoroughly presented in Chapter 4. Boarding prototyping – Hardware Selection . According to the instructions of ControlDesk 5.6 to convert the output of the DS1103ENC_POS_Cx block the counts per revolution of the encoder of the motor are required. The counts per revolution are provided in the datasheet of the motor. In Figures 5.1 and 5.2 the number of counts per revolution for the master and the slave motors are presented.

Encoder HEDS 5540 500 Counts per turn, 3 Channels

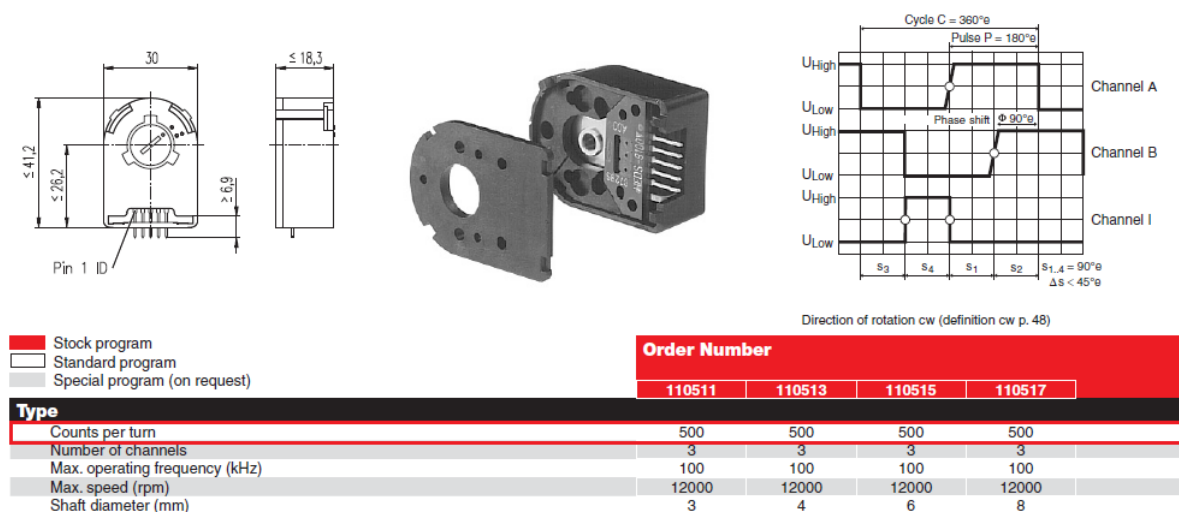


Figure 5.1. The slave motor encoder specifications. See Chapter 11. 8.

Summary of your selected configuration

Motor - DCX12L EB KL 4.5V
Sensor - ENX10 EASY 512IMP

Total weight of the drive: 27 g

Functions		
Commutation	Precious metal brushes	
Spark suppression (CLL)	with CLL	
Supply voltage	Nominal voltage 4.5 V	*
Motor bearings	Preloaded ball bearing	
Counts per turn	512	*
Hysteresis	0.17°m	
Form and Fit		
Flange, front	Flange with thread hole	*
Pitch circle diameter TK	9 mm	
Thread diameter	M1.6	
Amount of threads	2	
Shaft, front	straight	*
Shaft length L1	10 mm	*
Electrical connection, motor	Cable	
Connector type, motor	No connector	
Cable length L1 for motor	500 mm	*
Cable type	AWG26	
Electrical connection, encoder	configured	*
Cable length L1 for encoder	500 mm	*
Cable type for encoder	TPE ribbon cable	
Connector type, encoder	10-pol 1.27mm pin header	
Connection orientation (motor)	0 degree	
Connection orientation (encoder)	0 degree	
Add-ons		
Labeling	Standard labeling	

Figure 5.2. The master motor encoder specifications. See Chapter 11.11.

To measure the velocity a gain block is used as well, but this time apart from the term (360/# of counts per revolution), the inverse of the sample rate. For instance, if the sampling rate is 0.001 sec, then to measure the value in deg/s the gain block must have the value $(0.001)^{-1} \cdot (360/\# \text{ of counts per revolution})$. Thus the equations (5.1) and (5.2) must be used:

$$\theta[\text{deg}] = \text{EncPosition} \cdot \frac{360}{\text{countsperrevolution}} \quad (5.1)$$

$$\frac{d\theta}{dt} \left[\frac{\text{deg}}{\text{sec}} \right] = \text{EncDeltaPosition}(\text{samplingrate})^{-1} \cdot \frac{360}{\text{countsperrevolution}} \quad (5.2)$$

However, during the first experiments to define the necessary block scheme for Simulink, it was observed that the position of the slave motor measured at ControlDesk differed from the real rotation of the motor. Thus, it was considered that probably a more thorough examination of the gain values for the units conversion is required. The first Simulink scheme used is presented in Figure 5.3. To measure when one revolution is completed the DS1103ENC_SW_INDEX_C1 block is used. When its input is 0, then the output is 1, thus triggering the DS1103ENC_SET_POS_C1 block to reset the encoder. To control the motor in open loop mode the DS1103_DSP_PWM3 block is used. The resulted responses are presented in Figure 5.4.

It was calculated that for one complete revolution the output of the Slave motor encoder is 528 count and not 500 provided by the datasheet, something that might be related to the way the DS1103 reads the single – ended signals. Ergo the experimental was decided to be used for the experiments to come.

To validate whether the velocity measurement is correct the Electronic Optical Tachometer of the laboratory was used (Compact Instruments Ltd CT6), presented in Figure 5.5, and its

measurement was compared to the velocity measured by ControlDesk. It has to be noted that the encoder measured the velocity of the shaft of the motor, however the desired velocity is the one of the output shaft. The output shaft is attached to a planetary gearbox with gear ratio 343/17576.

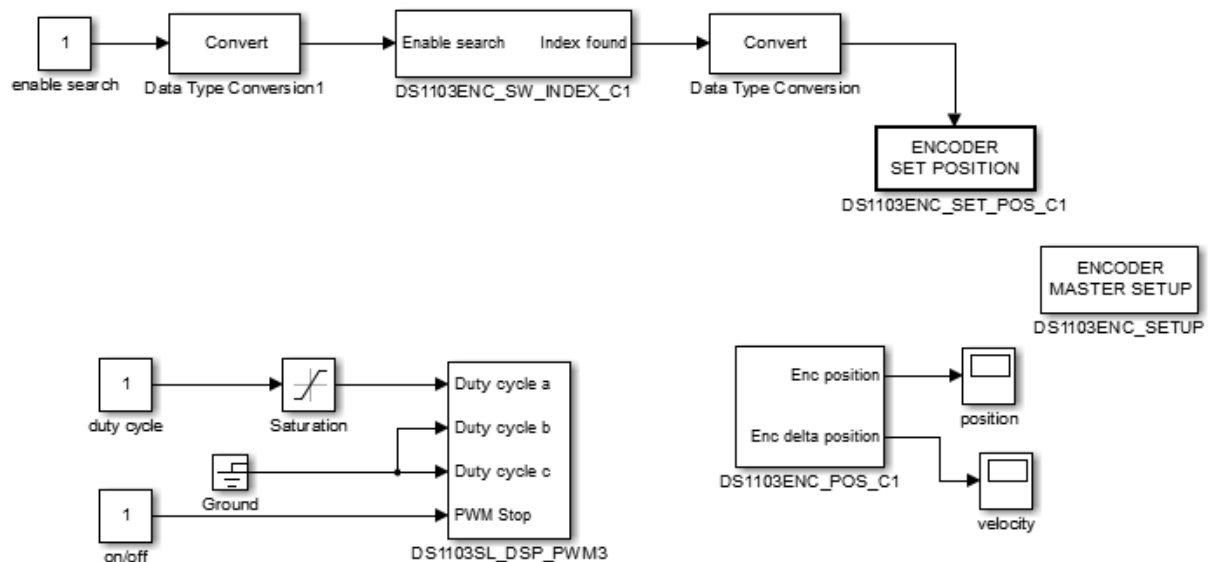


Figure 5.3. Number of counts identification scheme.

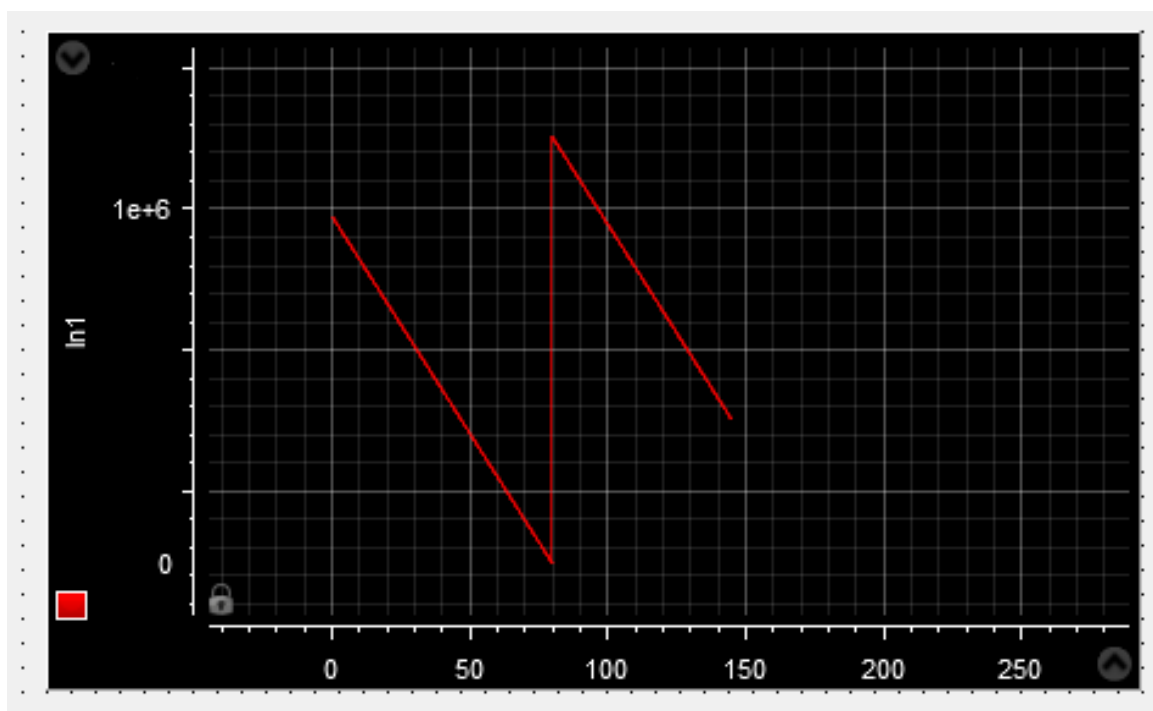


Figure 5.4. Position Response.



Figure 5.5. Electronic Optical Tachometer.

Having the beam of the tachometer focused on the coupling of the slave motor, the measurement of the tachometer was approximately 570 deg/sec. At ControlDesk the measured enc position was 41 counts/sec. The equation which relates the two velocities is the following is the equation (5.3). i is the gear ratio of the gearbox.

$$\omega_{coupling} = \frac{\omega_{motorshaft}}{i} \quad (5.3)$$

In this specific experiment the sampling rate was 10^{-3} s, thus using the equation (5.2) the velocity is 578.82 deg/s:

The error between the value measured by ControlDesk and the one measured by the tachometer is approximately 1.5 %, thus it was deduced that the measurements presented at ControlDesk are the right ones.

5.2 Inquiring the clockwise/counterclockwise rotation

As it was presented in Chapter 4. Boarding prototyping – Hardware Selection one of the gravest factors that will define whether the bidirectional configurations of the control schemes are either successful or doomed, is the fact that the motors must be able to change direction depending on the measured force. The drivers used for the setup provide specific pins for the direction control of the motor, presented in Figures 5.6 and 5.7. For more information it is advised to check the whole datasheets provided at the APPENDIX B DATASHEETS. These pins receive either a high level logic signal (+5 V) to rotate at one direction, or they are attached to the ground, making the motors rotate at the other direction. Thus, which direction is considered the clockwise and which one is the counterclockwise must be found. To achieve it the following Simulink schemes were used, presented in Figures 5.8 and 5.9.

P1 - Signal Connector				
Pin	Name	Description / Notes	I/O	
1	DIRECTION	Direction Input (+5V)	I	
2	PWM / IN	10 – 25 kHz pulse width modulated digital input command (+5V). Input duty cycle commands the output current.	I	
3	SIGNAL GND	Signal Ground (Common With Power Ground).	GND	
4	FAULT OUT	TTL level (+5 V) output becomes high when power devices are disabled due to at least one of the following conditions: inhibit, invalid Hall state, output short circuit, over voltage, over temperature, power-up reset.	O	
5	INHIBIT IN	TTL level (+5 V) inhibit/enable input. Leave open to enable drive. Pull to ground to inhibit drive. Inhibit turns off all power devices.	I	
6	CURRENT MONITOR	Current Monitor. Analog output signal proportional to the actual current output. Scaling is 2 A/V. Measure relative to signal ground.	O	
7	HALL 3	Single-ended Hall/Commutation Sensor Inputs (+5 V logic level)	I	
8	HALL 2*		I	
9	HALL 1		I	
10	+V HALL OUT	Low Power Supply For Hall Sensors (+5 V @ 30 mA). Referenced to signal ground. Short circuit protected.	O	
11	SIGNAL GND	Signal Ground (Common With Power Ground).	GND	
12	RESERVED	Reserved	-	

Figure 5.8. Signal pins of Servo Drive AZBDC10A4. See Chapter 11. 6.

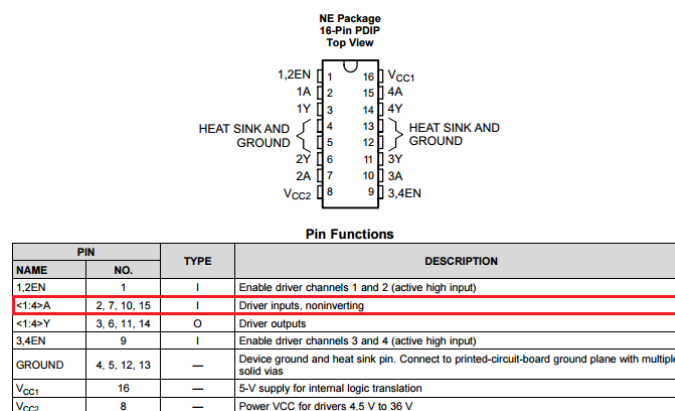


Figure 5.9. The pins of the L293D Quadraple Half-H Drivers. See Chapter 11.7.

In these schemes the duty cycle is provided by the DS1103_DSP_PWM3 block and the DS1103L_DSP_PWM block are used. To define the direction of the motors the direction pins are connected to the D/A converter channels of DS1103. In the case of the slave motor, only one pin is required, while the master motor requires two. It must be underscored that the direction control also requires that the ground of DS1103 is connected to the ground pins of the drivers, while in other applications it is not prerequisite, such as using Arduino Uno for instance. If the rotation of the motor and the measurement of ControlDesk are not the desired ones, for instance the clockwise rotation is negative. One easy way to change the signs is to change the connection of the encoder pins. For example, if the channel one is selected on Simulink and previously the Channel A of the encoder is connected to the PHI90(1) pin of the Connector 3B and the Channel B of the encoder is connected to the PHI0(1) pin of the Connector 3B, then the user can simply reverse the connection. This fundamental concept will be the core of the direction control of the upcoming Simulink schemes for the final experiments.

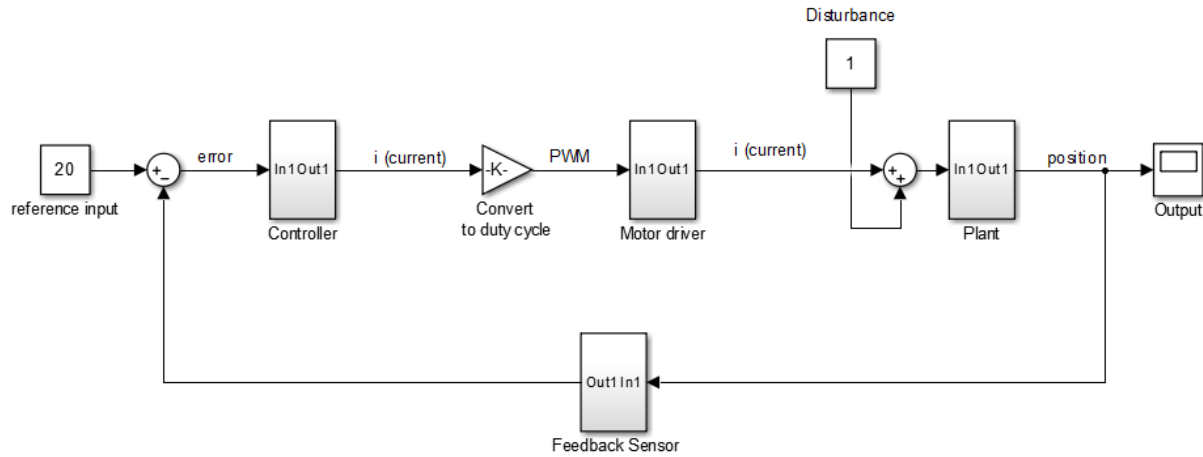


Figure 5.12. Illustration of the closed loop diagram which will be used for the master motors.

The range of the duty cycle is [0 1]. For the slave motor, which will have open loop control, the solution is relatively easy. The current provided to the motor depends on the difference of the outputs of the force sensors, and the maximum output value is +5V, then the range of the input will be [0 5]. Thus the input can just be divided to the maximum value (Gain 1/5) and the desired range will be [0 1]. However, for the master motors control scheme this cannot be applied because closed loop control will be implemented. Thus, the relationship between the current of the motor and the duty cycle provided to the hbridge must be found.

The setup that was used is the following. Using a precision resistance 2.5 Ohm $\pm 1\%$ in series with the motor for various duty cycle values the motor had been held still, thus the velocity was zero and the torque was the maximum. For every value of the duty cycle, the voltage of the resistance was noted and using the Ohm formula the current of the motor was calculated. In Figure 5.11 the experimental data and the interpolated curve are presented. It can be observed that apart from very low duty cycles, the curve is a line with constant slope. Calculating the slope of this line the result is:

$$\lambda = 114.2857 \frac{mA}{d.c.} \quad (5.4)$$

Thus, the conversion gain that must be used for the closed loop control scheme will be the inverse value. It has to be noted that it was found peculiar that the at the end of the experiments the slope slightly changed. When the resistastance was measured, it had slightly changed, and thus it was deduced that this was the reason for this occurrence.

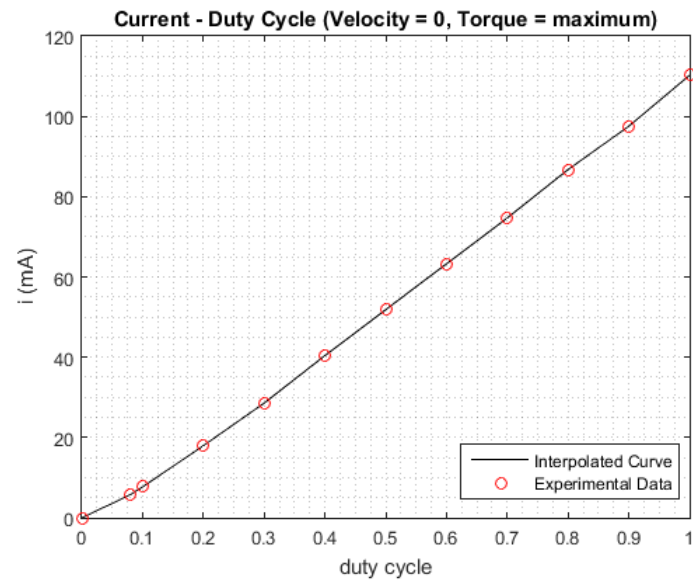


Figure 5.13. Duty Cycle - Current experimental curve.

5.4 Noise filtering

During the first tests to examine how CotrolDesk functions the FSR sensors values and the current of the slave motor were displayed and are presented in Figures 5.12, 5.13 and 5.14.

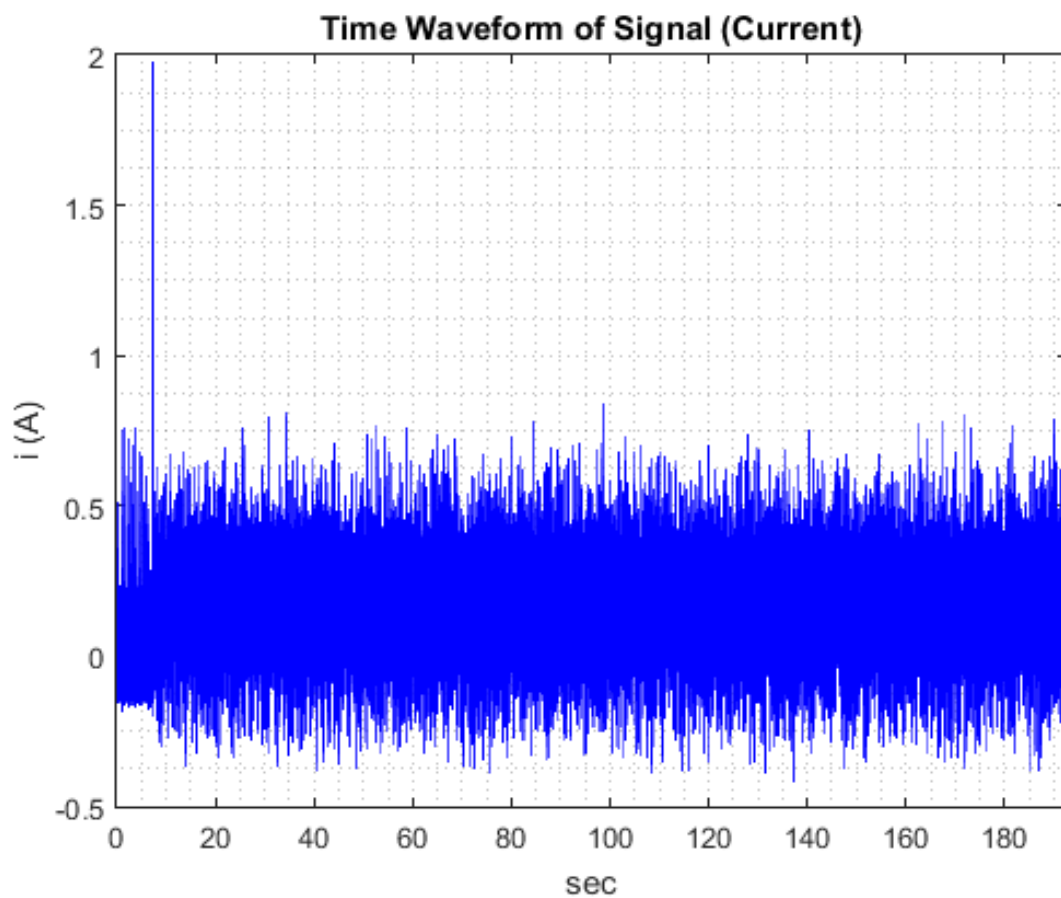


Figure 5.14. Current response.

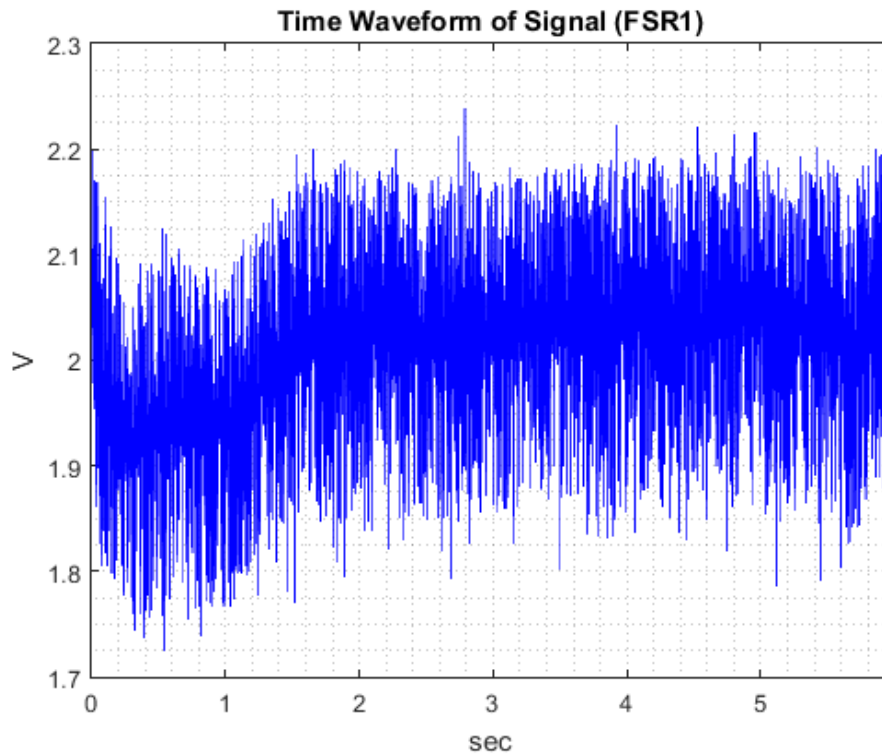


Figure 5.13. FSR Sensor 1 response.

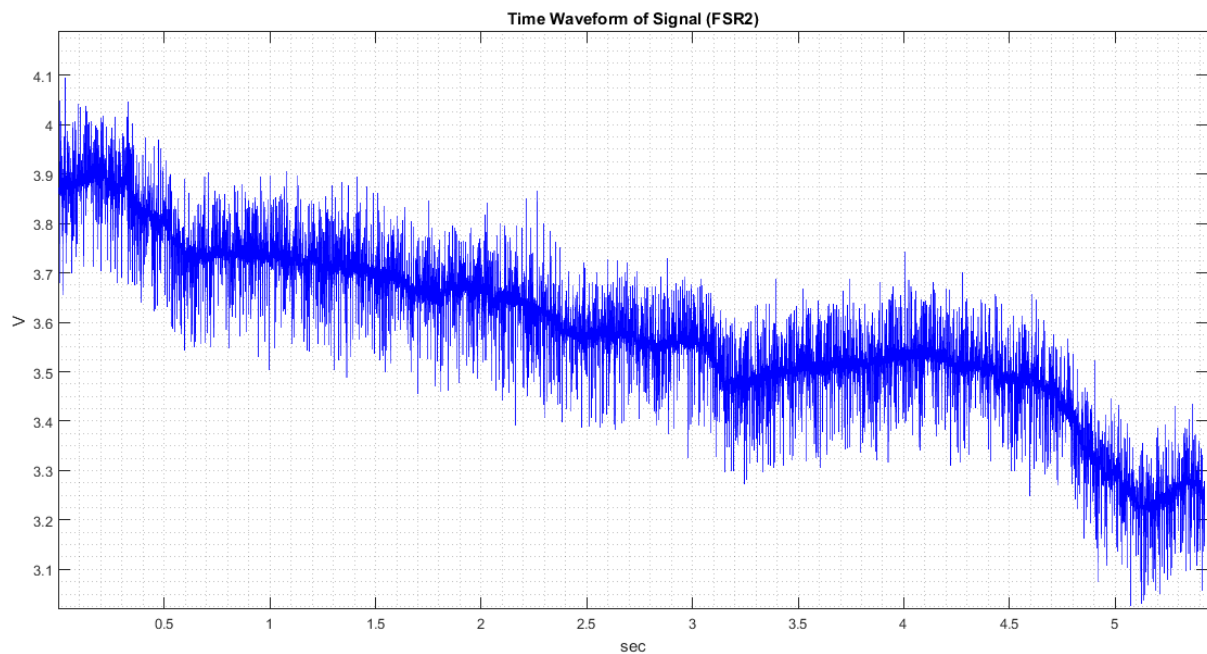


Figure 5.14. FSR Sensor 2 response.

For the current the noise filtering is mandatory because the response is not distinguishable, but for the FSR sensors neither the amplitude was affected dramatically or the use of the sensor was hampering the user. However, one potential problem is the delay that will be increased because of the filter. In this chapter the spectral analysis will be

presented and the final results of the filtering process. In the following chapters, the possible use of the filters for FSR sensors will be examined.

For the design of the filters it is necessary to plot the spectrum of the signals. Using Fourier transformation the spectrum of the three time responses respectively are presented in Figures 5.15, 5.16 and 5.17. For the current recording the sampling rate was 1 kHz and for the FSR sensors the sampling rate was 10 kHz.

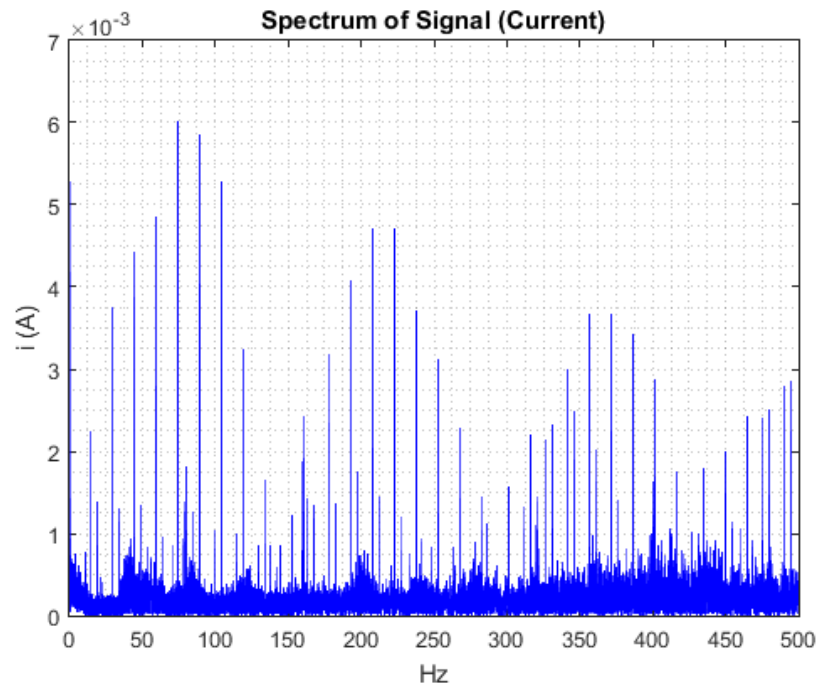


Figure 5.15. current spectrum.

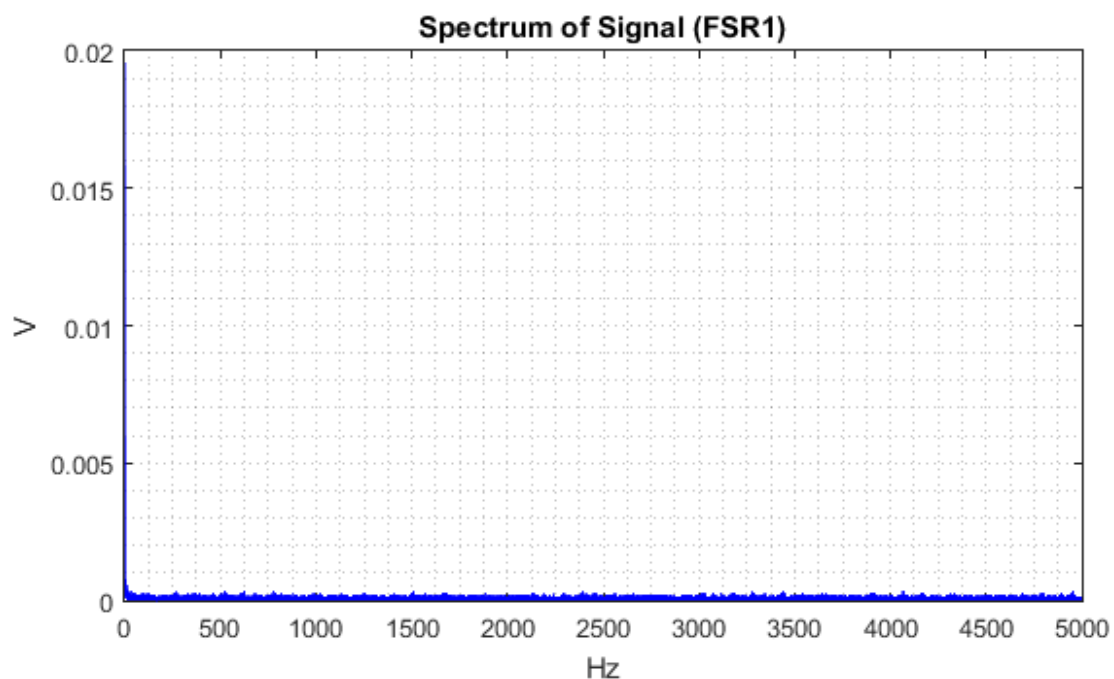


Figure 5.16. FSR Sensor 1 Spectrum.

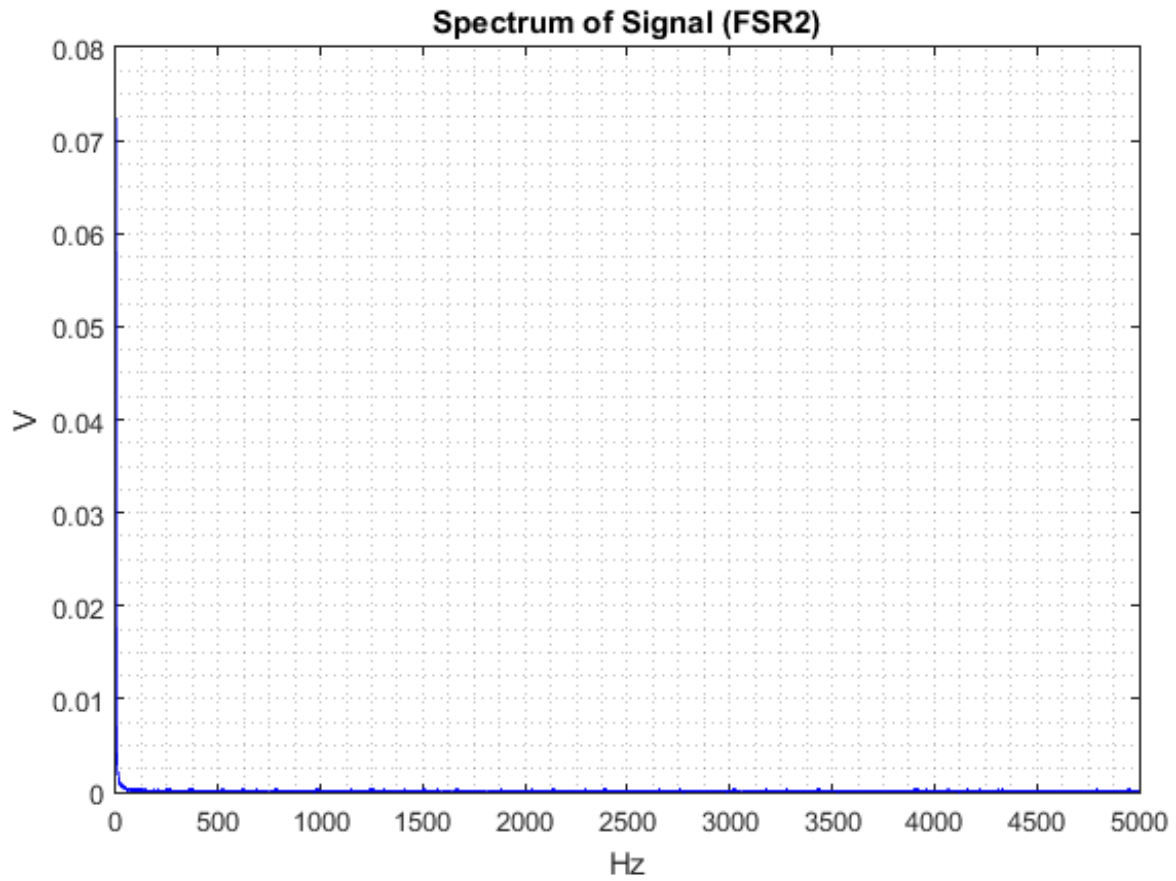


Figure 5.17. FSR Sensor 2 Spectrum.

Figure 15 shows that apart from the dc component, higher frequencies have high energy levels as well. These frequencies were sub harmonics of the PWM frequency of 15000 Hz. Thus, the design of a filter was mandatory. The frequency of the low pass filter was decided to be 15 Hz and the transfer function of the filter is the following:

$$G(s) = \frac{1}{\frac{1}{2\pi 15} s + 1} \quad (5.5)$$

Moreover, a 4th order filter was used with the same frequency, the transfer function of which is the following:

$$G(s) = \frac{1}{\left(\frac{1}{2\pi 15} s + 1\right)^4} \quad (5.6)$$

The responses compared to the signal without filtering is presented in Figures 5.18 and 5.19.

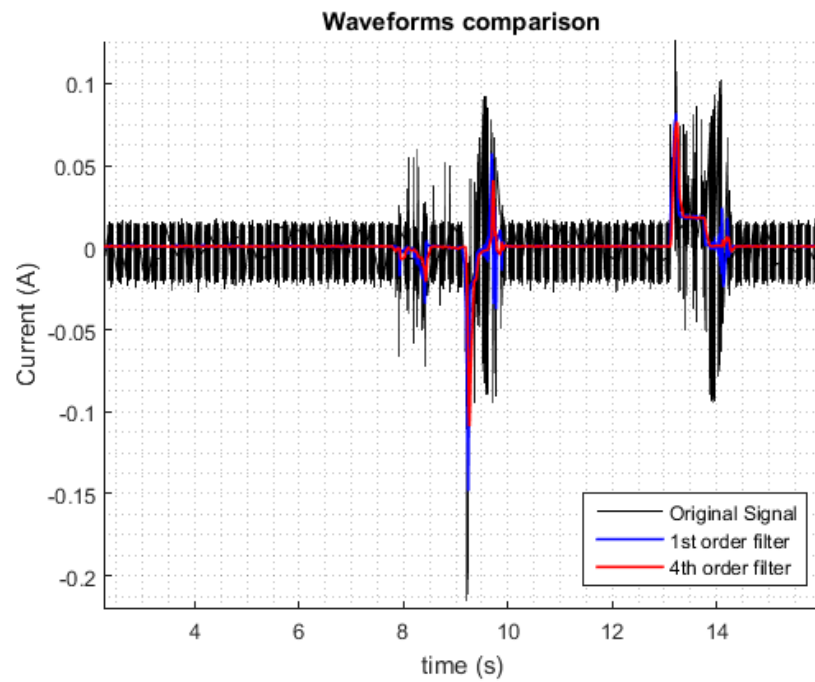


Figure 5.18. Responses comparison.

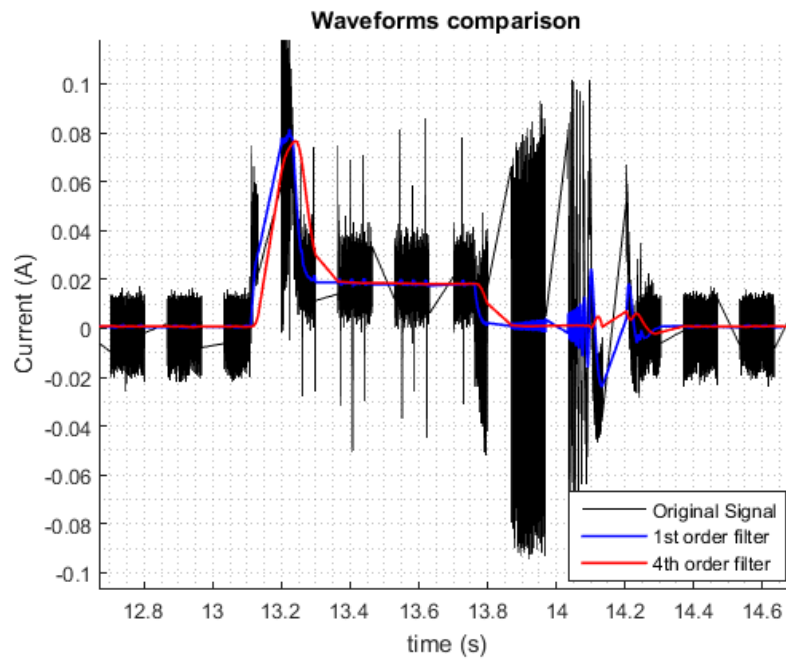


Figure 5.19. Zoom in on the responses. The time range of the zoom is presented on the x-axis.

From the experimental results it can be observed that with the first order filter the response continued to have noise, thus it was decided to use a 4th order filter. As for the FSR sensors the spectral illuminated that only the energy level of the dc component was high. In the following Figures it can be observed that the higher frequencies have insignificant contribution, however the noise caused by these components should be removed.

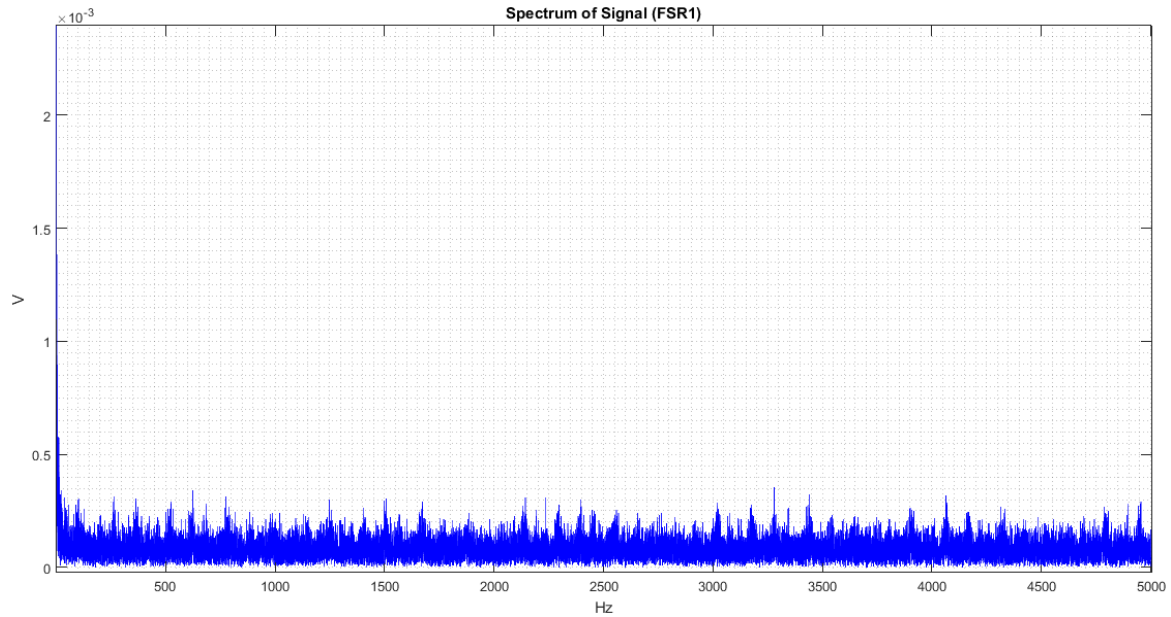


Figure 5.20. Focus on the higher frequencies of the sensor 1.

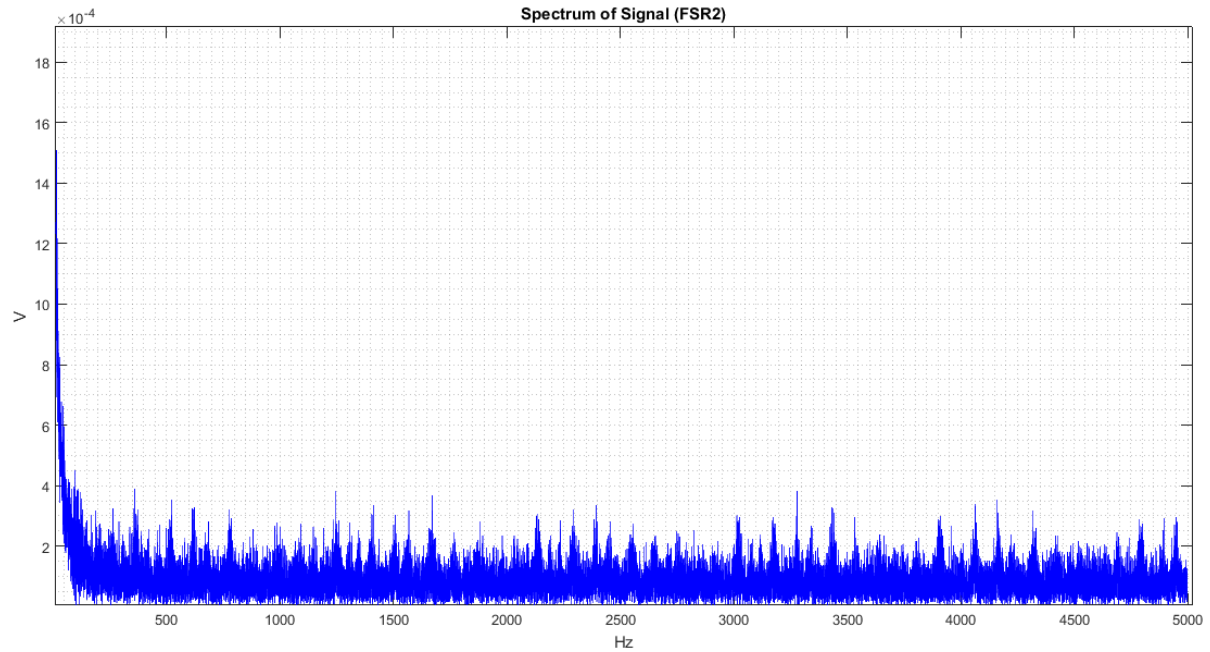


Figure 5.21. Focus on the higher frequencies of the sensor 2.

To diminish the energy leakage of the dc component presented in Figures 5.20 and 5.21 it was decided to test two low pass filters of various order for two different frequencies, 2.766 Hz and 1.106 Hz. The filters transfer functions are the following:

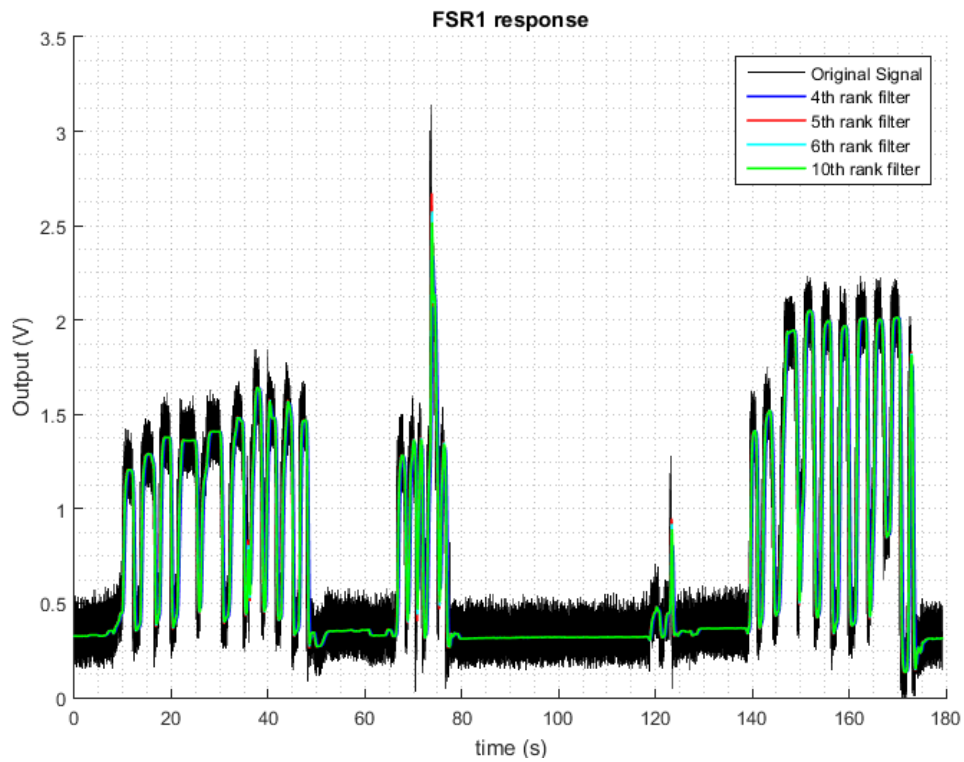


Figure 5.23. Sensor 1 response comparison using G_1 .

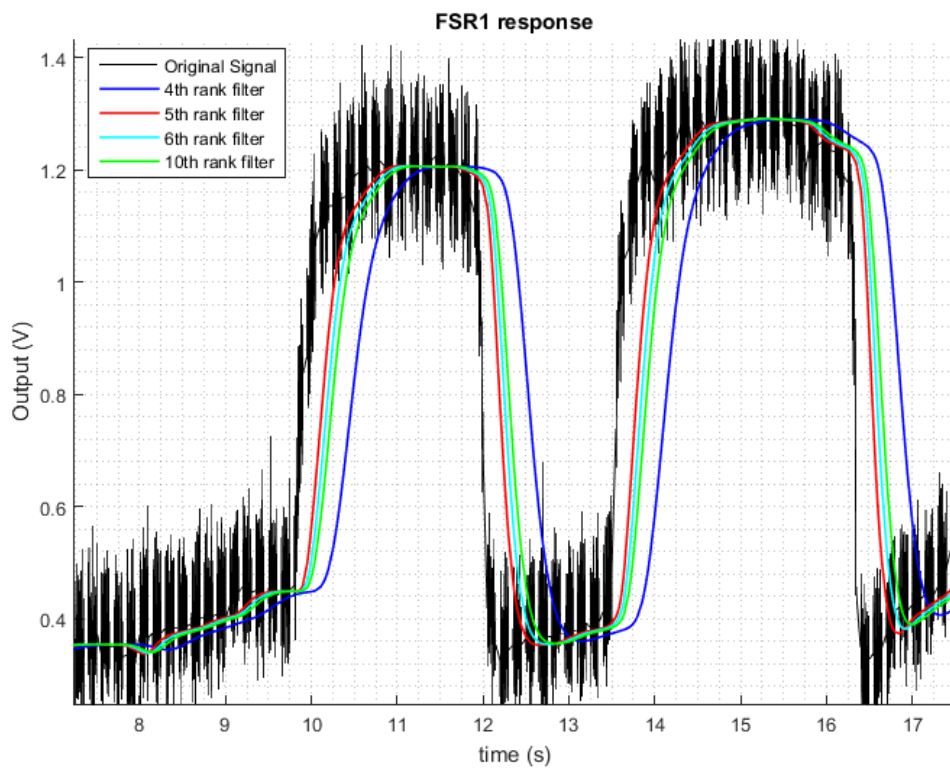


Figure 5.24. Zoom in to distinguish the response delay of G_1 . The time range of the zoom is presented on the x-axis.

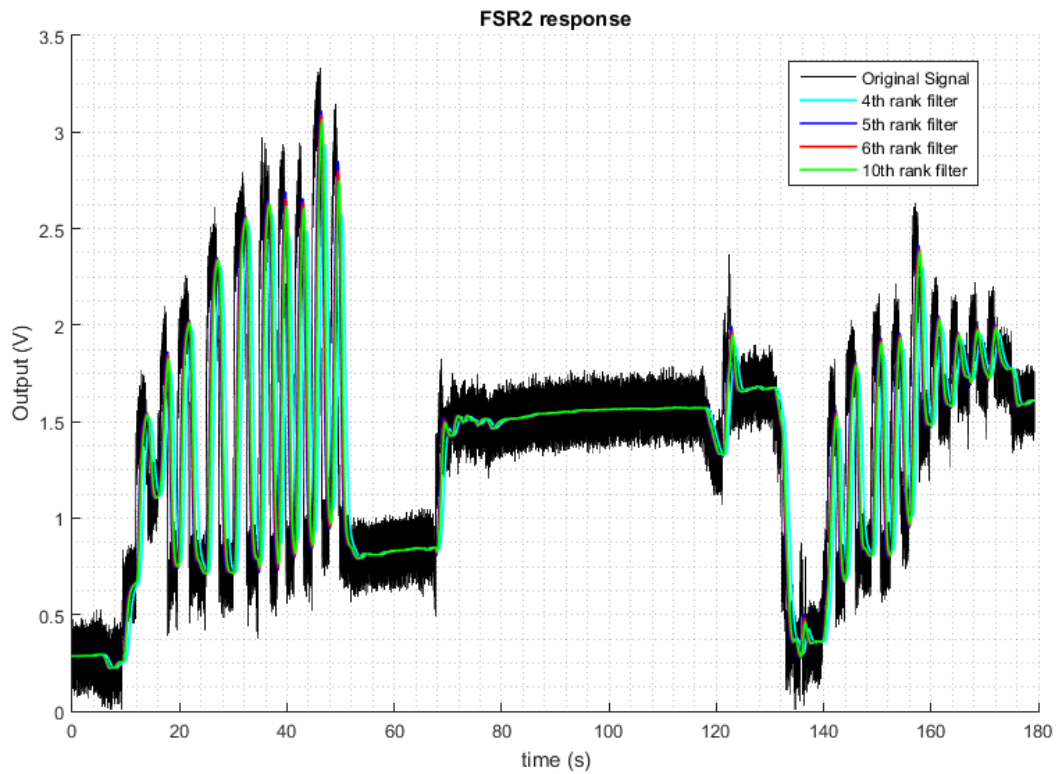


Figure 5.25. Sensor 1 response comparison using G_1 .

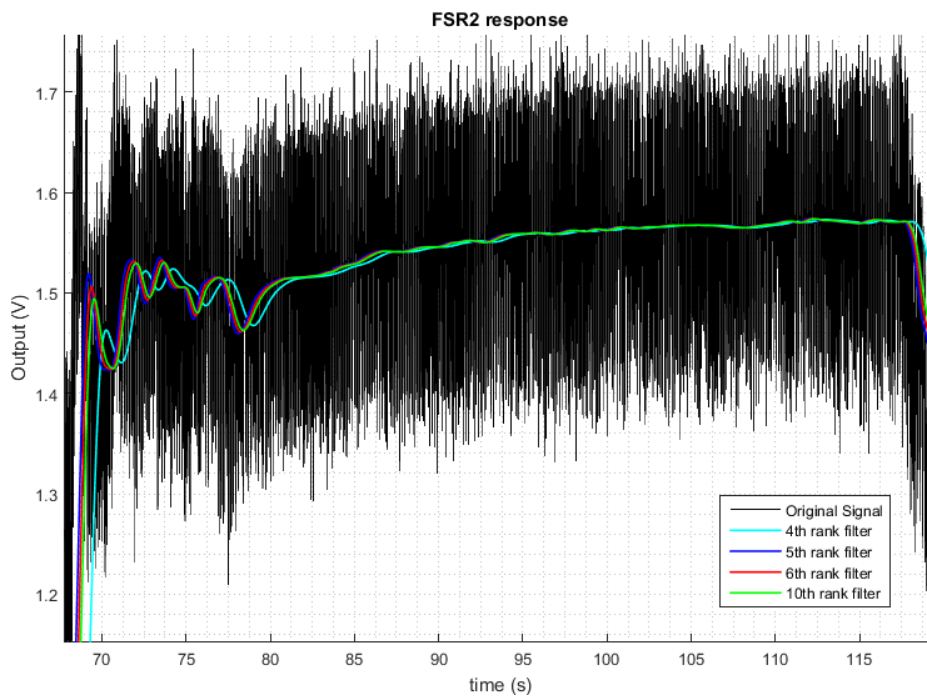


Figure 5.26. Zoom in to distinguish the response delay of G_2 . The time range of the zoom is presented on the x-axis.

Evaluating the delay caused by the filter it was decided that the optimal solution was the 5th order filter applied at the response of sensor 2. However, this solution is not absolute and will be analyzed more thoroughly in the following chapters.

5.5 System identification of the master motors

For the design of the controller it is required to identify the transfer function of the plant. The closed loop control will be applied for the control of the master motors. This subsystem consists of a motor and a motor and a power screw. The transfer function of the system will be calculated using the linear graph theory. Due to the fact that the input is a current source the inductance of the motor is not a state variable, this element can be eliminated. The linear graph representation of the system is presented in Figure 5.27.

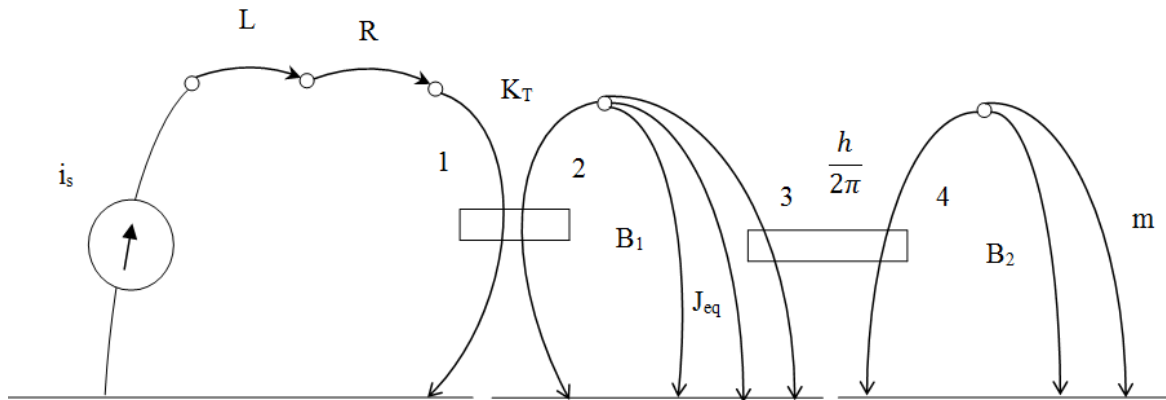


Figure 5.27. Linear graph of the motor - power screw system.

B_1 is the damping of the mechanical parts of the motor, J_{eq} the equivalent moment of inertia of the motor and the power screw, B_2 the damping of the nut and m the mass of the nut. K_T is the torque constant of the motor and h is the lead of the screw. From the datasheets K_T is $4.9 \text{ N}\cdot\text{A}^{-1}\cdot\text{mm}$ and h is 1.22 mm .

According to the linear graph theory ^[3], the system consists of one flow source ($i_s(t)$) and one state variable, which is either the angular velocity of the motor or the power screw shaft. It has an electrical, a rotational and translational energy domains. It can be deduced easily that the final state equation is the following:

$$\begin{aligned} \frac{dv_m}{dt} \left(m + \left(\frac{2\pi}{h} \right)^2 J_{eq} \right) + v_m \left(B_2 + B_1 \left(\frac{2\pi}{h} \right)^2 \right) &= K_T \frac{2\pi}{h} i_s(t) \rightarrow \\ \frac{dv_m}{dt} m_{eq} + v_m B_{eq} &= K_T \frac{2\pi}{h} i_s(t) \end{aligned} \quad (5.9)$$

The constants m_{eq} , B_{eq} and $K_T \frac{2\pi}{h}$ are dependent of the parameters the system. Making the assumption that the initial conditions of the system are set to zero, applying the Laplace transform to the ordinary differential equation (5.9), the resulting transfer function is the following:

$$\frac{x_m}{i_s} = G_p(s) = \frac{K_T \frac{2\pi}{h}}{s(m_{eq}s + B_{eq})} \quad (5.10)$$

A simplest form of the equation (9) is the following:

$$G_p(s) = \frac{K}{s(\tau s + 1)} \quad (5.11)$$

The constants of the system are the following:

$$\begin{cases} K = K_T \frac{2\pi}{hB_{eq}} \\ \tau = \frac{m_{eq}}{B_{eq}} \end{cases} \quad (5.12)$$

K is a gain and τ is the time constant of the system. After the acquisition of the transfer function the values of the parameters must be found. To achieve this, a simple P control was applied to the system. The gain that was selected was $K_p = 16000 \cdot 8.75 \cdot 10^{-6}$. The response is presented in Figure 5.28. From the measured angle of the motor the desired displacement of the screw can be obtained.

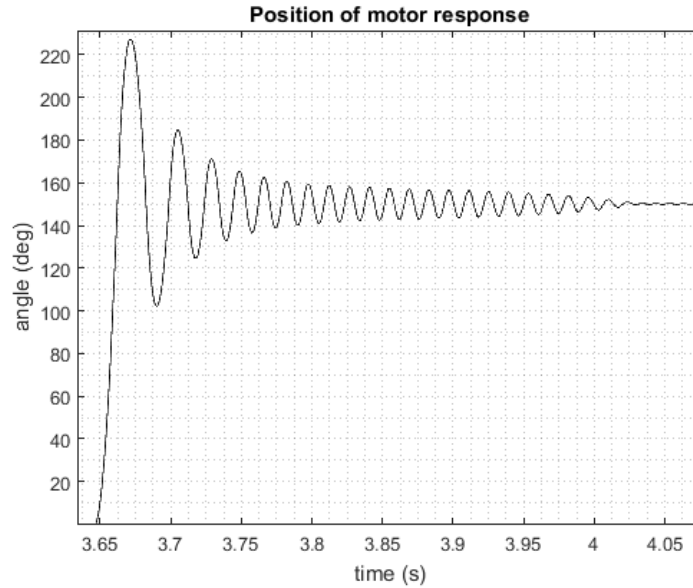


Figure 5.6. Closed loop P control response.

The closed loop transfer function is the following:

$$G_{cl} = \frac{K_p G_p}{1 + K_p G_p} \quad (5.13)$$

Equation (5.11) can be reformed to the following one:

$$K_p G_p = \frac{G_{cl}}{1 + K_p G_{cl}} \quad (5.14)$$

Using Figure 5.28 the overshoot and the settling time can be obtained. The overshoot can be calculated using the following equation [2]:

$$PO = \frac{\theta_{\max} - \theta_{ss}}{\theta_{ss}} 100\% = 100e^{\left(-\frac{\zeta\pi}{\sqrt{1-\zeta^2}}\right)} \quad (5.15)$$

Thus the damping ratio is 0.20668. The settling time can be calculated using the following equation:

$$t_s = \frac{4}{\zeta \omega_n} \quad (5.16)$$

Using the equation 14 the natural frequency is 50.2737204 r/s. The closed loop transfer function for P control and a second order plant is the following:

$$G_{cl} = \frac{\omega_n^2}{s^2 + 2\zeta\omega_n s + \omega_n^2} \quad (5.17)$$

Using the equations (5.10), (5.12) and (5.14) it can be obtained:

$$\frac{K_p K}{s(\tau s + 1)} = \frac{\frac{\omega_n^2}{2\zeta\omega_n}}{s(\frac{s}{2\zeta\omega_n} + 1)} \quad (5.18)$$

Thus, the parameters of the motor were calculated. The gain constant was 2.94 mm/A and the time constant 0.048125 s.

From these data the damping of the system can be obtained. The equivalent mass of the system can be calculated from the datasheets of the parts. The mass of the screw is $1.7 \cdot 10^{-3}$ kg. The equivalent inertia of the rotational domain is the sum of the inertia of the motor, the coupling and the power screw. Their values are $0.533 \cdot 10^{-8}$ kg·m², $5.39 \cdot 10^{-7}$ kg·m² and $3.4 \cdot 10^{-8}$ kg·m². Thus, the equivalent mass of the system is 16.613722 kg. From the time constant of the system the equivalent damping constant is 41.53 Kg/s. From equation (11) the theoretical value of the gain K is 3.2115 mm/A, thus the percentage difference with the experimental value is approximately 9%, a result that can be considered decent.

5.6 Controller Design

With the model of the plant obtained the controller of the system can be designed. For this application the most appropriate controlled is the PD controller for quick response and small errors. The equation of the controller is the following ^[2]:

$$G_c = K_p + sK_D \quad (5.17)$$

The closed loop transfer function is the following:

$$G_{cl} = \frac{(K_p + sK_D)G_p}{1 + (K_p + sK_D)G_p} \quad (5.18)$$

Thus, substituting the G_p it is obtained:

$$G_{cl} = \frac{\frac{K}{\tau}(K_p + sK_D)}{s^2 + \frac{(1 + K_D K)}{\tau}s + \frac{K_p K}{\tau}} \quad (5.19)$$

The natural frequency of the system is:

$$\omega_n = \sqrt{\frac{K_p K}{\tau}} \quad (5.20)$$

The damping ratio of the system is:

$$\zeta = \frac{1}{2} \frac{(1 + K_p K)}{\tau} \left(\frac{K_p K}{\tau} \right)^{-\frac{1}{2}} \quad (5.21)$$

Using these equations at the stage of the experiments the control system will be designed real time at the Controldesk environment. The answer to the question how it will be done will be presented in the following installments.

6 Final Setup for Experimentation

In this Chapter it will be presented the final preparation of the Setup, the connectivity of the hardware parts and the Simulink file used for the experiments. For further details about the DS1103 it is advised to read the APPENDIX A BASICS ON dSPACE.

6.1 Hardware Connection

For the connection of the hardware it is required to connect the slave motor and its driver, the master motors, their respective encoders and its drivers and the FSR sensors to the power supply and the DS1103 as well. Next the correct connectivity will be presented.

Slave Motor Division

The slave motor system division of the setup consists of the RE 30 Ø30 mm slave motor, the HEDS 5540 500 Counts per turn encoder and the Analog Servo Drive AZBDC10A4. In Figures 6.1 and 6.2 the Pins of the Drive and the encoder are presented.

P1 - Signal Connector			
Pin	Name	Description / Notes	I/O
1	DIRECTION	Direction Input (+5V)	I
2	PWM / IN	10 – 25 kHz pulse width modulated digital input command (+5V). Input duty cycle commands the output current.	I
3	SIGNAL GND	Signal Ground (Common With Power Ground).	GND
4	FAULT OUT	TTL level (+5 V) output becomes high when power devices are disabled due to at least one of the following conditions: inhibit, invalid Hall state, output short circuit, over voltage, over temperature, power-up reset.	O
5	INHIBIT IN	TTL level (+5 V) inhibit/enable input. Leave open to enable drive. Pull to ground to inhibit drive. Inhibit turns off all power devices.	I
6	CURRENT MONITOR	Current Monitor. Analog output signal proportional to the actual current output. Scaling is 2 A/V. Measure relative to signal ground.	O
7	HALL 3	Single-ended Hall/Commutation Sensor Inputs (+5 V logic level)	I
8	HALL 2*		I
9	HALL 1		I
10	+V HALL OUT	Low Power Supply For Hall Sensors (+5 V @ 30 mA). Referenced to signal ground. Short circuit protected.	O
11	SIGNAL GND	Signal Ground (Common With Power Ground).	GND
12	RESERVED	Reserved	-

P2 - Power Connector			
Pin	Name	Description / Notes	I/O
1	MOTOR A	Motor Phase Outputs. Current output distributed equally across 2 pins per motor phase, 3A continuous current carrying capacity per pin.	O
2	MOTOR A		O
3	MOTOR B		O
4	MOTOR B		O
5	MOTOR C		O
6	MOTOR C		O
7	NC (KEY)	No Connection. Keyed pin.	-
8	PWR GND	Power Ground (Common With Signal Ground). 3A Continuous Current Rating Per Pin	GND
9	PWR GND		GND
10	HV IN	DC Power Input. 3A Continuous Current Rating Per Pin. Requires a minimum of 47 µF external capacitance between HV IN and PWR GND pins.	I
11	HV IN		I
12	RESERVED	Reserved	-

Figure 6.1. Analog Servo Drive AZBDC10A4 Pins description. See Chapter 11.6.

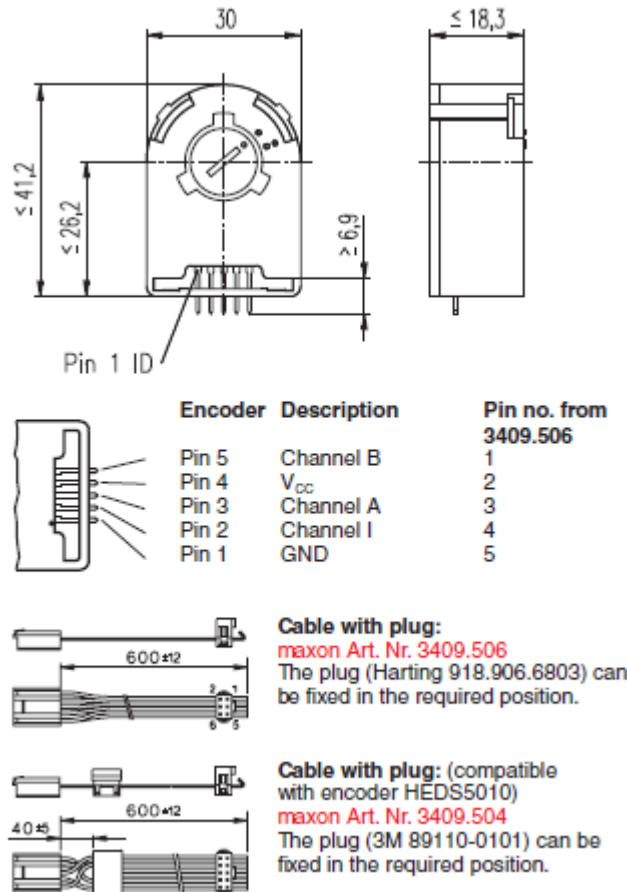


Figure 6.2. HEDS 5540 500 Counts per turn encoder pins mapping. See Chapter 11.10.

The connectivity map of this division is presented in the following tables accompanied by comments, mandatory to follow to the letter for the proper function of the setup.

Table 6.1. Analog Servo Drive AZBDC10A4 connectivity map.

Analog Servo Drive AZBDC10A4 Mapping		
a/a	Hardware Pin	dS1103 Pins / Power Supply
1	P1 – Pin 1	P1B25 DACH1
2	P1 – Pin 2	P2B28 SPWM1
3	P1 – Pin 6	P1A2 ADCH4
4	P1 – Pin 8	Drive Signal Ground
5	P1 – Pin 11	Drive Signal Ground
6	P2 – Pin 1	Motor Phase 1(red)
7	P2 – Pin 3	Motor Phase 2 (black)
8	P2 – Pin 8	Power Ground
9	P2 – Pin 10	Power Supply (+13.5 V)

The P1 Pin 1 is the Direction Pin that enables the motor to change its direction. To achieve it, apart from P1B25 (or any other D/A converter channel), a GND pin of the Connector P1B of DS1103 must be connected to the Signal GND pin of the drive (P1 - Pin 11). The Power GND pin (P2 – Pin 8) must have a minimum 47 µF external capacitance between it and the

HV IN pin (P2 – Pin 10). The HV IN is the power supply pin. For this specific motor of the setup the range of the Supply is 13.5 – 24 V. To measure the current of the motor (and implicitly the torque), the Current Monitor Pin of the drive must be connected to an A/D converter channel of DS1103. Moreover, a GND pin of Connectors P1A (for the A/D converter), P1B (for the D/A converter) and P2B (for the PWM pulse).

Table 6.2. ENCODER HEDS 5540 500 Counts per turn connectivity map.

ENCODER HEDS 5540 500 Counts per turn		
a/a	Hardware Pin	dS1103 Pins / Power Supply
1	Pin 1	P3B12 GND
2	Pin 2	P3B28 IDX(3)
3	Pin 3	P3B11 PHI0(3)
4	Pin 4	Power Supply (+5)
5	Pin 5	P3B44 PHI90(3)

This specific encoder is single - ended, thus its connection with DS1103 must be the one presented in Figure 6.3. For further details about the DS1103 connections, the user must search for the help provided by HelpDesk, which is also provided with ControlDesk 5.6.

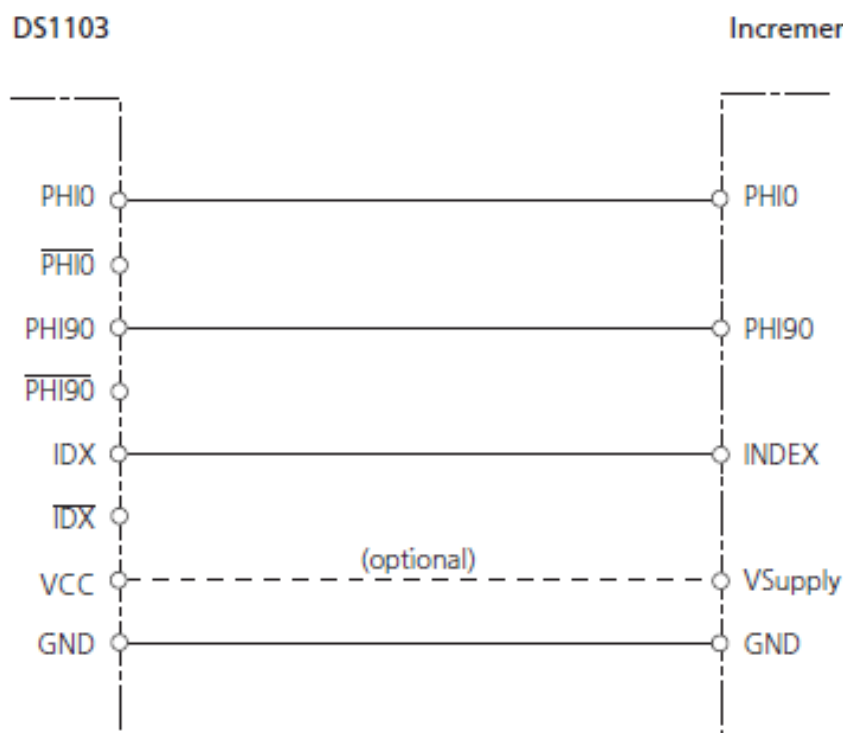


Figure 6.3. Connectivity schematic view of the ENCODER HEDS 5540.

The equivalent PHI0 pin of the encoder is the Channel A, and the PHI90 pin is the Channel B respectively, however, it is not absolute. If the user reverses the connection the measurement will be reversed as well. Furthermore, it is crucial for the power supply connection, if the Power Supply pins of DS1103 are not used, to connect the GND pin of the encoder to both the supply GND and the GND pin of DS1103, as presented in Figure 6.4.

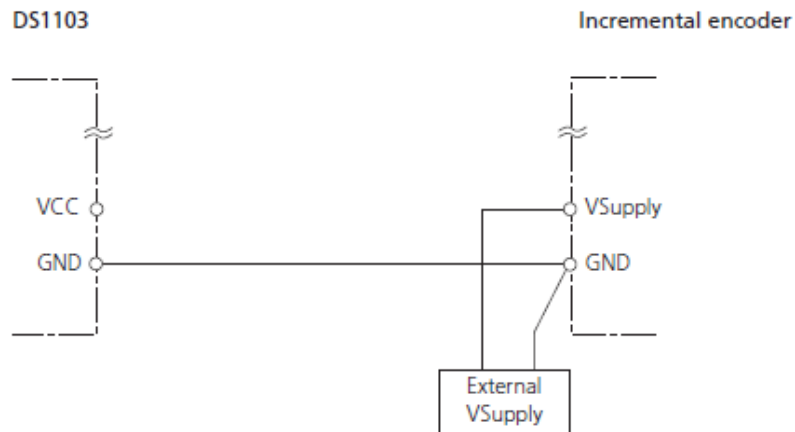
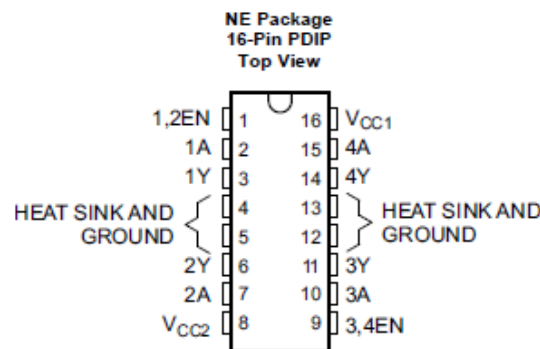


Figure 6.4. Ground Connection of the encoder.

Master Motor Division

The master motors system division of the setup consists of the master motor - DCX12L EB KL 4.5V, the L293d Quadruple Half-H Driver and the Sensor - ENX10 EASY 512IMP. In Figures 6.5 and 6.6 the Pins of the Drive and the encoder are presented.



Pin Functions

PIN		TYPE	DESCRIPTION
NAME	NO.		
1,2EN	1	I	Enable driver channels 1 and 2 (active high input)
<1:4>A	2, 7, 10, 15	I	Driver inputs, noninverting
<1:4>Y	3, 6, 11, 14	O	Driver outputs
3,4EN	9	I	Enable driver channels 3 and 4 (active high input)
GROUND	4, 5, 12, 13	—	Device ground and heat sink pin. Connect to printed-circuit-board ground plane with multiple solid vias
V _{CC1}	16	—	5-V supply for internal logic translation
V _{CC2}	8	—	Power VCC for drivers 4.5 V to 36 V

Figure 6.5. L293d Quadruple Half-H Driver pins description. Reference ?

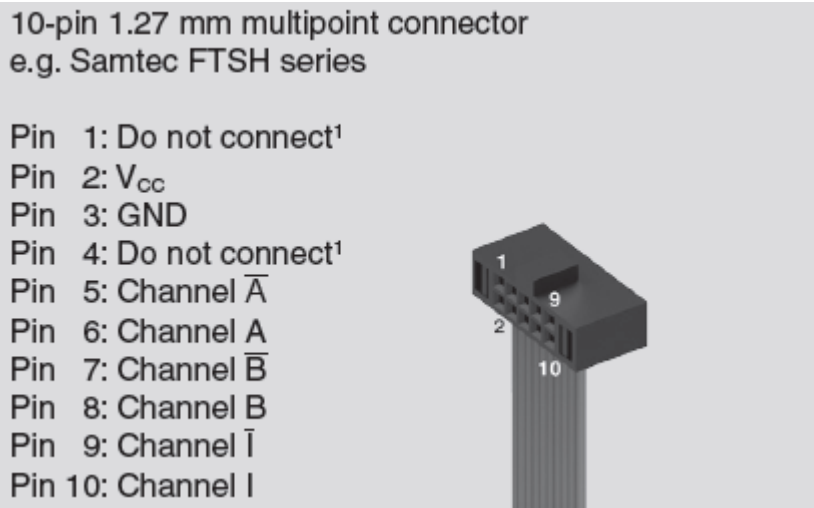


Figure 6.6. The ENX10 EASY 512IMP encoder pins mapping. See Chapter 11.12.

The connectivity map of this division is presented in the following tables.

Table 6.3. L293d Quadruple Half-H Driver connectivity map.

L293d Quadruple Half-H Driver		
a/a	Hardware Pin	dS1103 Pins / Power Supply
1	1,2 EN	P2A27 ST2PWM
2	1A	P1A10 DACH6
3	1Y	Motor Phase 1 (red)
4	GND	P2A GND Pin (PWM) - P1A GND Pin (D/A Converter)
5	GND	Transl. Supply GND – Power Supply GND
6	2Y	Motor Phase 2 (black)
7	2A	P1A42 DACH4
8	V _{cc2}	Power Supply (+ 4.5 V)
9	V _{cc1}	Translation Supply (+ 5 V)
10	4A	P1A27 DACH8
11	4Y	Motor Phase 2 (black)
12	GND	P2A GND Pin (PWM) – P1A GND Pin (D/A Converter)
13	GND	Transl. Supply GND – Power Supply GND
14	3Y	Motor Phase 1 (red)
15	3A	P1A25 DACH2
16	3,4EN	P2B29 SPWM7

The pins 1, 2 EN and 3, 4 EN must be connected to a PWM pulse channel of DS1103. The pins 1A, 2A, 3A and 4A are the direction pins (the pairs are 1A - 2A and 3A - 4A). To define the direction of the motor, one must be HIGH, with the other must be LOW. The pins 1Y, 2Y, 3Y and 4Y are the output pins that must be connected to the motor (the pairs are 1Y - 2Y and 3Y - 4Y). For the proper function of the drive, it is mandatory to connect the ground of

the PWM, the Direction signals, the power and the translation supply to the GND pins of the drive.

Table 6.4. Sensor - ENX10 EASY 512IMP connectivity map for Master Motor 1.

Sensor - ENX10 EASY 512IMP (Master Motor 1)		
a/a	Hardware Pin	dS1103 Pins / Power Supply
1	Pin 2	Power Supply (+5V)
2	Pin 3	Power Ground - P3B27 GND (1) - P3A27 GND (1)
3	Pin 5	P3A41 PHI0(1) (Inverse)
4	Pin 6	P3B41 PHI0(1)
5	Pin 7	P3A25 PHI90(1) (Inverse)
6	Pin 8	P3B25 PHI90(1)

Table 6.5. Sensor - ENX10 EASY 512IMP connectivity map for Master Motor 2.

Sensor - ENX10 EASY 512IMP (Master Motor 2)		
a/a	Hardware Pin	dS1103 Pins / Power Supply
1	Pin 2	Power Supply (+5V)
2	Pin 3	Power Ground P3A42 GND (2) - P3B42 GND(2)
3	Pin 5	P3A26 PHI0(2) (Inverse)
4	Pin 6	P3B26 PHI0(2)
5	Pin 7	P3A10 PHI90(2) (Inverse)
6	Pin 8	P3B10 PHI90(2)

The Sensor - ENX10 EASY 512IMP is differential encoder. Ergo its connection with DS1103 must be the one presented in Figure 6.7.

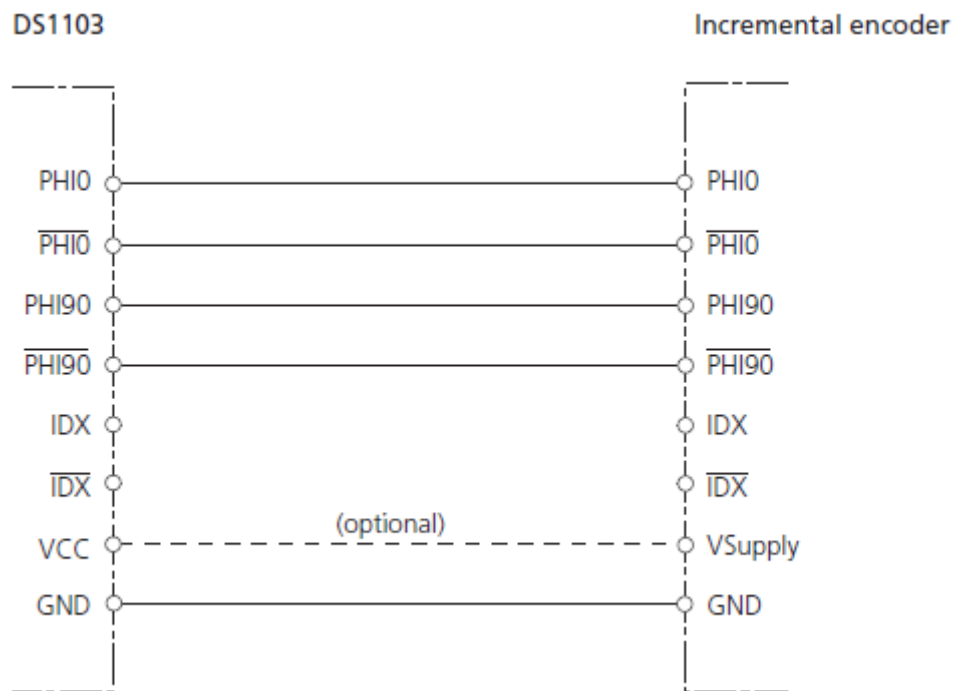


Figure 6.7. Connectivity schematic view of the Sensor - ENX10 EASY 512IMP encoder.

The power supply connection is the same with the one that was presented previously in Figure 6.4. The reversing of the pin connections can also be applied to this case as well.

FSR Sensor Division

The connection of the FSR Sensors is the least arduous one. It just requires two analog to digital channels and it is presented in the following table.

Table 6.6. FSR Sensors connectivity map.

FSR Sensor		
a/a	Hardware Pin	dS1103 Pins
1	Sensor 1 Output	P1A34 ADCH2
2	Sensor 2 Output	P1A19 ADCH6

The FSR sensors require two power supply sources. A +5 V and a -5 V. Moreover, the ground of the Sensor must be connected to the ground pins of the P1A connector of DS1103. The Channels of the connectors for all the divisions of the setup that must be used are presented in the following Figures.

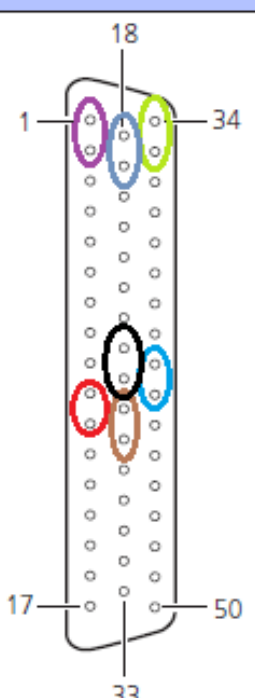
Connector P1A	Pin	Signal	Pin	Signal	Pin	Signal
	1	GND			34	ADCH2
	2	ADCH4	18	GND	35	GND
	3	GND	19	ADCH6	36	ADCH8
	4	ADCH10	20	GND	37	GND
	5	GND	21	ADCH12	38	ADCH14
	6	ADCH16	22	GND	39	GND
	7	GND	23	ADCH18	40	ADCH20
	8	GND	24	GND	41	GND
	9	GND	25	DACH2	42	DACH4
	10	DACH6	26	GND	43	GND
	11	GND	27	DACH8	44	GND
	12	SADCH2	28	GND	45	GND
	13	GND	29	SADCH4	46	SADCH6
	14	SADCH8	30	GND	47	GND
	15	GND	31	SADCH10	48	SADCH12
	16	SADCH14	32	GND	49	GND
	17	GND	33	SADCH16	50	GND

Figure 6.8. Connector P1A pins mapping.

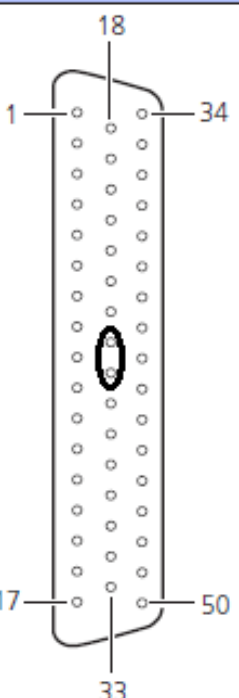
Connector P1B	Pin	Signal	Pin	Signal	Pin	Signal
	1	GND	18	GND	34	ADCH1
	2	ADCH3	19	ADCH5	35	GND
	3	GND	20	GND	36	ADCH7
	4	ADCH9	21	ADCH11	37	GND
	5	GND	22	GND	38	ADCH13
	6	ADCH15	23	ADCH17	39	GND
	7	GND	24	GND	40	ADCH19
	8	GND	25	DACH1	41	GND
	9	GND	26	GND	42	DACH3
	10	DACH5	27	DACH7	43	GND
	11	GND	28	GND	44	GND
	12	SADCH1	29	SADCH3	45	GND
	13	GND	30	GND	46	SADCH5
	14	SADCH7	31	SADCH9	47	GND
	15	GND	32	GND	48	SADCH11
	16	SADCH13	33	SADCH15	49	GND
	17	GND			50	SADCSOC

Figure 6.9. Connector P1B pins mapping.

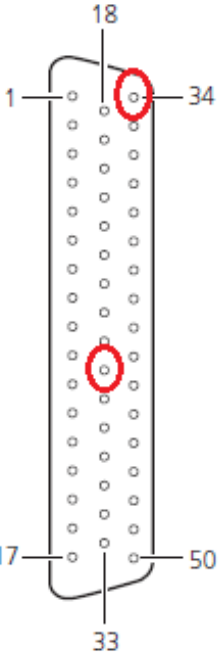
Connector P2A	Pin	Signal	Pin	Signal	Pin	Signal
	1	GND	18	IO1	34	GND
	2	IO3	19	IO5	35	GND
	3	IO7	20	IO9	36	GND
	4	IO11	21	IO13	37	GND
	5	IO15	22	IO17	38	GND
	6	IO19	23	IO21	39	GND
	7	IO23	24	IO25	40	GND
	8	IO27	25	IO29	41	GND
	9	IO31	26	STINT2	42	GND
	10	STMCLK	27	ST2PWM	43	GND
	11	SPDPINT	28	SPWM2	44	GND
	12	SPWM4	29	SPWM8	45	SPWM6
	13	GND	30	SCAP2	46	GND
	14	SCAP4	31	SBIO	47	GND
	15	SSTE	32	GND	48	SSOMI
	16	INT1	33	VCC1 (+ 5 V)	49	INT3
	17	VCC1 (+ 5 V)			50	GND

Figure 6.10. Connector P2A pins mapping.

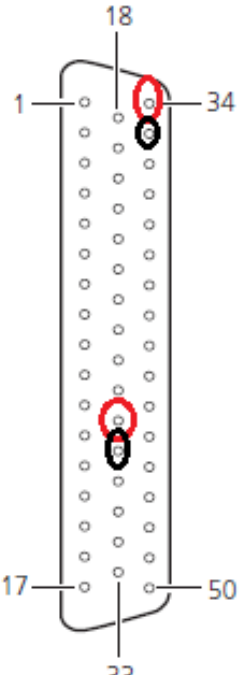
Connector P2B	Pin	Signal	Pin	Signal	Pin	Signal
	1	GND	18	IO0	34	GND
	2	IO2	19	IO4	35	GND
	3	IO6	20	IO8	36	GND
	4	IO10	21	IO12	37	GND
	5	IO14	22	IO16	38	GND
	6	IO18	23	IO20	39	GND
	7	IO22	24	IO24	40	GND
	8	IO26	25	IO28	41	GND
	9	IO30	26	STINT1	42	GND
	10	STMRDIR	27	ST1PWM	43	GND
	11	ST3PWM	28	SPWM1	44	GND
	12	SPWM3	29	SPWM7	45	SPWM5
	13	SPWM9	30	SCAP1	46	GND
	14	SCAP3	31	SXF	47	GND
	15	SSCLK	32	GND	48	SSIMO
	16	INT0	33	VCC1 (+ 5 V)	49	INT2
	17	VCC1 (+ 5 V)			50	GND

Figure 6.11. Connector P2B pins mapping.

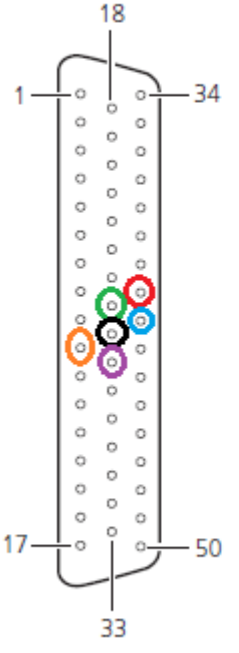
Connector P3A	Pin	Signal	Pin	Signal	Pin	Signal
	1	GND	18	DCD ($\overline{\text{RXD}}$)	34	Not used for RS232 ($\overline{\text{TXD}}$)
	2	DTR ($\overline{\text{RTS}}$)	19	GND	35	DSR ($\overline{\text{CTS}}$)
	3	$\overline{\text{STXD}}$	20	–	36	$\overline{\text{SRXD}}$
	4	–	21	–	37	–
	5	–	22	$\overline{\text{PHI0(7)}}$	38	GND
	6	$\overline{\text{PHI0(7)}}$	23	GND	39	$\overline{\text{IDX(7)}}$
	7	$\overline{\text{PHI0(6)}}$	24	$\overline{\text{IDX(6)}}$	40	$\overline{\text{PHI90(6)}}$
	8	GND	25	$\overline{\text{PHI90(1)}}$	41	$\overline{\text{PHI0(1)}}$
	9	$\overline{\text{IDX(1)}}$	26	$\overline{\text{PHI0(2)}}$	42	GND
	10	$\overline{\text{PHI90(2)}}$	27	GND	43	$\overline{\text{IDX(2)}}$
	11	$\overline{\text{PHI0(3)}}$	28	$\overline{\text{IDX(3)}}$	44	$\overline{\text{PHI90(3)}}$
	12	GND	29	$\overline{\text{PHI90(4)}}$	45	$\overline{\text{PHI0(4)}}$
	13	$\overline{\text{IDX(4)}}$	30	$\overline{\text{PHI0(5)}}$	46	GND
	14	$\overline{\text{PHI90(5)}}$	31	GND	47	$\overline{\text{IDX(5)}}$
	15	GND	32	GND	48	GND
	16	VCC2 (+ 5 V)	33	VCC3 (+ 5 V)	49	VCC2 (+ 5 V)
	17	VCC3 (+ 5 V)			50	GND

Figure 6.12. Connector P3A pins mapping.

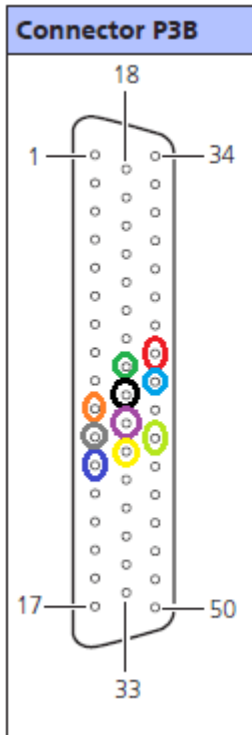
Connector P3B	Pin	Signal	Pin	Signal	Pin	Signal
	1	GND	18	RXD (RXD)	34	TXD (TXD)
	2	RTS (RTS)	19	RI (not used for RS422)	35	CTS (CTS)
	3	STXD	20	–	36	SRXD
	4	–	21	–	37	–
	5	–	22	PHI0(7)	38	GND
	6	PHI90(7)	23	GND	39	IDX(7)
	7	PHI0(6)	24	IDX(6)	40	PHI90(6)
	8	GND	25	PHI90(1)	41	PHI0(1)
	9	IDX(1)	26	PHI0(2)	42	GND
	10	PHI90(2)	27	GND	43	IDX(2)
	11	PHI0(3)	28	IDX(3)	44	PHI90(3)
	12	GND	29	PHI90(4)	45	PHI0(4)
	13	IDX(4)	30	PHI0(5)	46	GND
	14	PHI90(5)	31	GND	47	IDX(5)
	15	CANL	32	GND	48	CANH
	16	VCC2 (+ 5 V)	33	VCC3 (+ 5 V)	49	VCC2 (+ 5 V)
	17	VCC3 (+ 5 V)			50	GND

Figure 6.13. Connector P3B pins mapping.

For the DS1103 expansion box the connectors are required to be constructed, as presented in Figure 6.13. Their code name is 50 pin D-SUB male connector cables and pinouts. It should be advised that the order of soldering (from left to right and from the upper row to the lower one for example), depends whether the user is left handed or right handed.



Figure 6.14. The connectors of the DS1103 expansion box.

The power supply requirements for the setup are presented in the following table.

Table 6.7. Power requirements of the setup

Power Requirements	
Hardware	Power
FSR Sensors	+ 5 V and - 5 V
Slave Motor	13.5 - 24 V
Master Motors	4.5 V
L293d Quadruple Half-H Driver	+5 V
Encoders Supply	+5 V

6.2 Simulink Program

With the advent of the setup the preparation of the Simulink program used for the simulations arrived. After many trials and overbearing the tides of programming using blocks a final Simulink file was designed and it will be examined thoroughly in this section. It has to be noted that at the laboratory there are other versions provided as well with minor differences; however the main core of the program remains the same.

The objective of this stage was to implement the control schemes of Bidirectional Classic EPP and Bidirectional Biomechatronic EPP ^[4]. These schemes are presented in Figures 6.14 and 6.15. For the classic EPP the FSR force sensors must provide the input command to the slave motor. Depending of the difference of the output two sensors the direction of the motor must be variable the measured output is the position of the motor. Moreover, in the Biomechatronic EPP the output of the slave motor is the reference input of the master motors closed loop. This notion must be implemented in Simulink to be used in ControlDesk for the real time experiments. The structure of the program analysis will be separated divisions. At each one a specific aspect of the control scheme design will be presented.

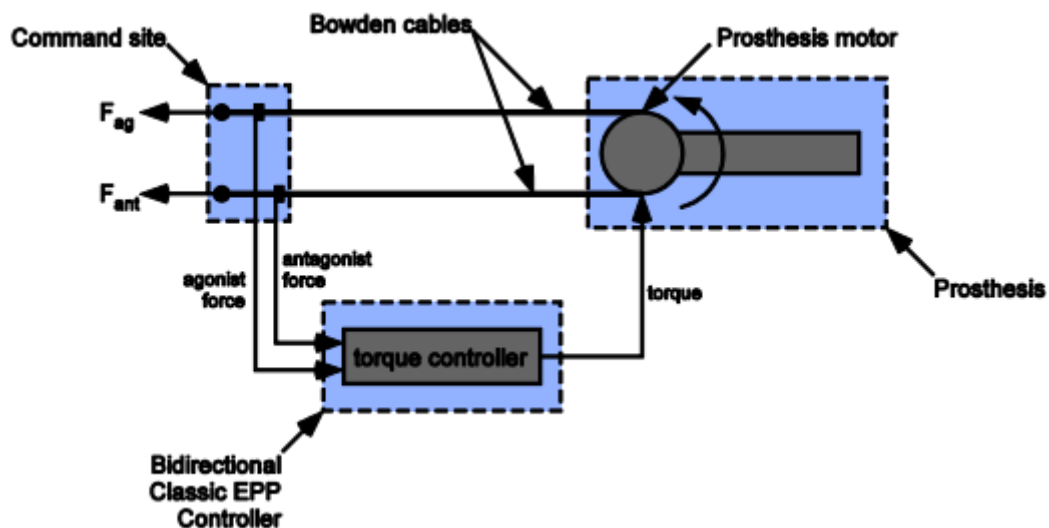


Figure 6.15. Bidirectional Classic EPP. Copied from [4]. ^[4]

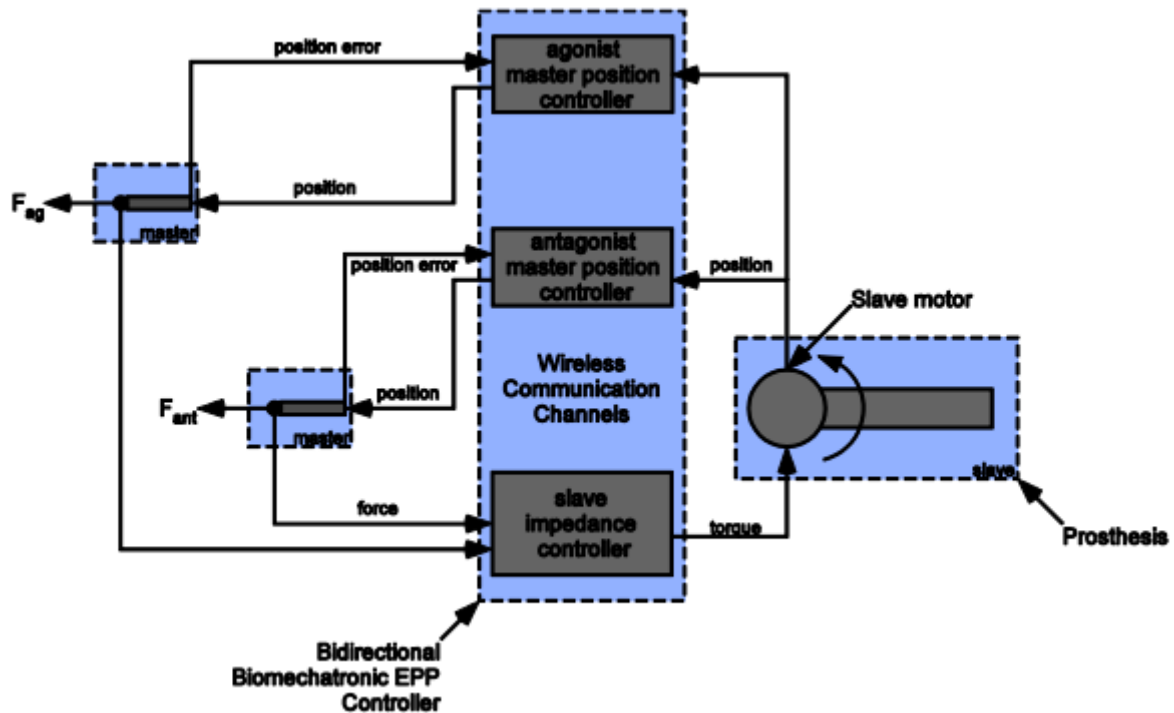


Figure 6.16. Bidirectional Biomechatronic EPP. Copied from [4].

6.3 Reading the FSR Sensors

In Chapter 3. Design and Implementation of the Reference Input the procedure to construct the FSR Sensors was presented thoroughly. However, reading the output of the integrated circuit of the sensors required processing. First, bounds for the output value must be set. Because the purpose of the control schemes is to imitate the upper limb prosthetics; some restrictions have to be taken into account. Low output values must not trigger the motion of the slave motor and after an upper bound is reached, the force must remain constant, as presented in Figure 6.16. These bounds must be variable during the real time experiment. Each user will apply a different range of load, minimum and maximum, ergo variable bounds are mandatory.

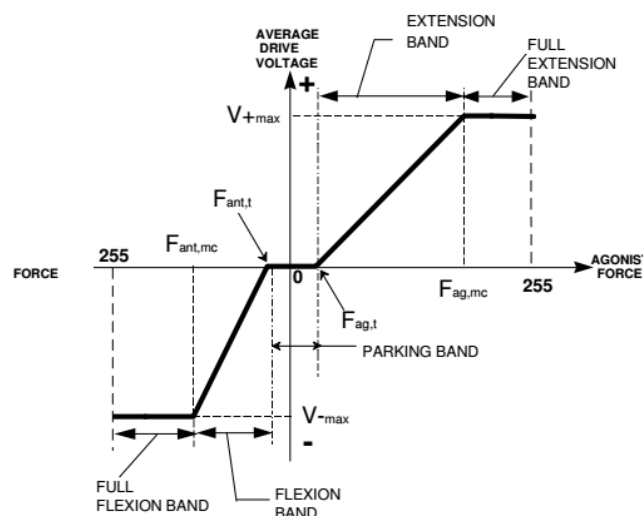


Figure 6.17. Upper and Lower Bounds of the FSR sensor Output. Copied from [1].

Furthermore, behind the advantage of the low price of the FSR sensors looms the drawback of residual stress. After continuous experiments, even without load, the output of the sensor is not zero. Thus, it's required to add an offset value that will set the output to zero and must also be variable, because the residual stress does not remain constant either. Finally, if the measurement of the sensor includes noise that renders the sensors intolerable for the user, then a filter must be added. However, the increase of the delay must be examined and if it is required by the user, so this demand is not absolute. In Figure 6.17 it is presented the required structure of the Simulink program.

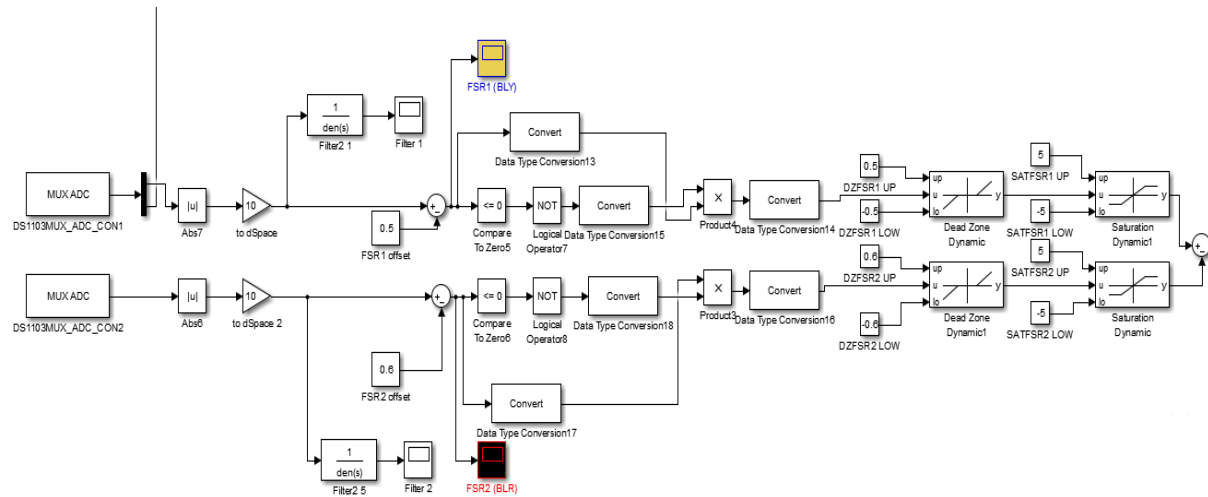


Figure 6.18. Measurement of the FSR sensor block diagram.

The A/D converter blocks read the value of the output value of the two sensors. The offset values are subtracted from the measured values. However, if the residual stress is less than the estimated one, then the result would be less than zero. In this case, the final value must be zero. This can be implemented using the logic operations blocks of Simulink. The value refined value is multiplied by a logic variable that is either 0, if the value is less than zero, or 1, if the value is greater than zero. To implement the diagram of Figure 6.16 the Dead Zone and Saturation blocks are used. Due to the desire to change the bounds of the two blocks real time, the dynamic ones are used because the bounds are inserted as inputs. Furthermore, the range of the position of the slave motor must be defined. Without setting limits to the position, the motor would rotate eternally until the power supply runs out. If a mechanical joint is connected to the motor, the danger of mechanical failure is imminent. To avoid these cases, a logic diagram must be inserted to the open loop control of the slave motor. For this mathematical model the logic variables x , y , z and w are defined. If ϕ is the position of the motor and ϕ_d is the boundary value and FSR_1 and FSR_2 the output values of the two sensors respectively, the values of the variables x , y , z and w are presented in the following table.

Table 6.8. Definition of the logic variables

Logic Variables Values		
Variable	Description	Value
x	$\varphi \geq \varphi_d$	1
\bar{x}	$\varphi < \varphi_d$	0
y	$FSR_1 \geq FSR_2$	1
\bar{y}	$FSR_1 \leq FSR_2$	0
z	$\varphi \leq -\varphi_d$	1
\bar{z}	$\varphi > -\varphi_d$	0
w	Rotation occurs	1
\bar{w}	The motor is stopped	0

If the FSR_1 rotates the slave motor clockwise (to the positive values of φ) and the FSR_2 rotates the slave motor counterclockwise (to the negative values of φ), then if the limit φ_d is reached and $FSR_1 \geq FSR_2$ the motor must stop. The result must be the same in case the limit $-\varphi_d$ is reached and $FSR_1 \leq FSR_2$. The verbal expression of the design demand reveals the structure of the logic circuit, presented in Figure 6.18. The case $FSR_1 = FSR_2$ seems contradicting, but it's lackadaisical due to the fact that in these circumstances the motor is halted.

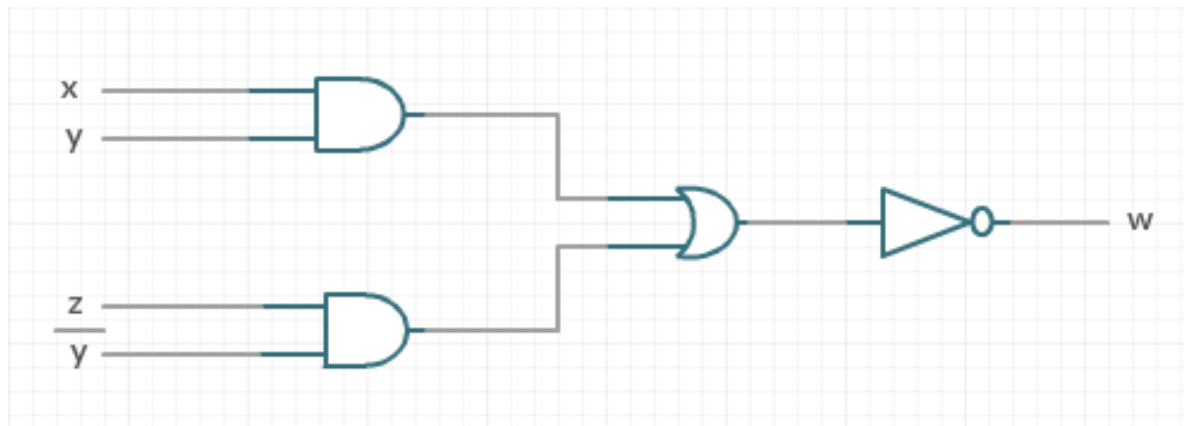


Figure 6.19. Logic gate circuit of the position - force control.

Using Boolean algebra the circuit is equivalent to the following equation:

$$w = \overline{(x \bullet y) + (\bar{y} \bullet z)} = (\bar{x} + \bar{y}) \bullet (y + \bar{z}) \quad (6.1)$$

Taking into account that the states $\varphi \geq \varphi_d$ ($x = 1$) and $\varphi \leq -\varphi_d$ ($z = 1$) cannot occur simultaneously, the valid states are two less from the 2^3 combinations, the truth table of equation (6.1) is the following.

Table 6.9. Truth table of the logic circuit.

Input			Output	Description
x	y	z	w	-
1	1	0	0	$\varphi \geq \varphi_d$ and $FSR_1 \geq FSR_2$ (Motor halted)
0	1	1	1	$\varphi \leq -\varphi_d$ and $FSR_1 \geq FSR_2$ (Rotation initiated cw)
0	1	0	1	$-\varphi_d \leq \varphi \leq \varphi_d$ and $FSR_1 \geq FSR_2$ (Rotation initiated cw)
1	0	0	1	$\varphi \geq \varphi_d$ and $FSR_1 \leq FSR_2$ (Rotation initiated ccw)
0	0	1	0	$\varphi \leq -\varphi_d$ and $FSR_1 \leq FSR_2$ (Motor halted)
0	0	0	1	$-\varphi_d \leq \varphi \leq \varphi_d$ and $FSR_1 \leq FSR_2$ (Rotation initiated ccw)

Thus, this specific logic circuit is the ideal one for the application. Multiplying the logic variable w by the difference of the outputs of the force sensors will result the desired outcome. The block diagram that was designed in Simulink is presented in Figure 6.20.

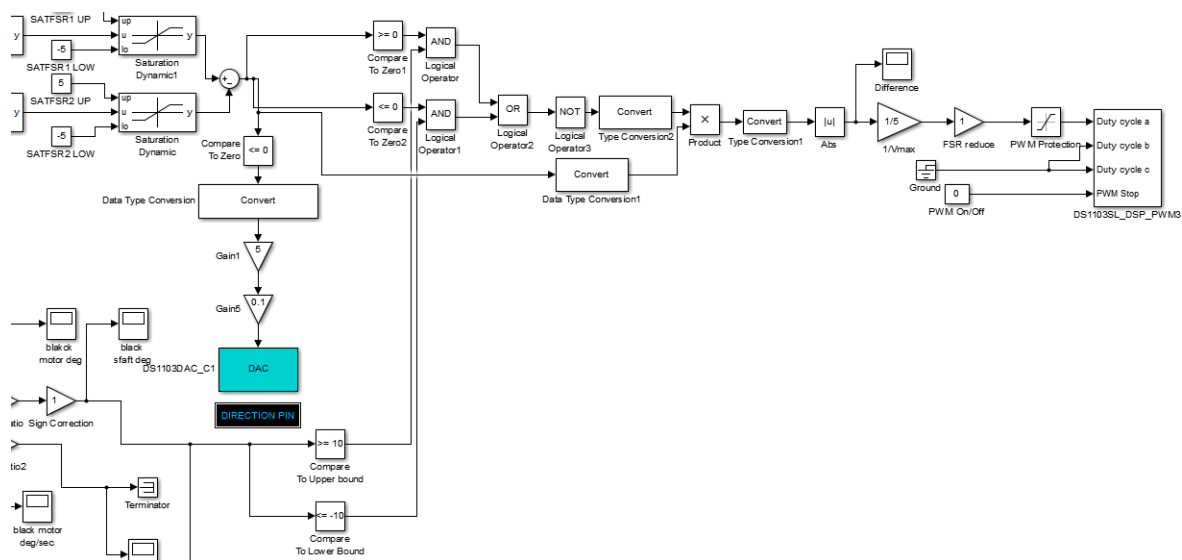


Figure 6.20. Defining the position limits and the normalization of the input to duty cycle.

Figure 6.20 also displays two more crucial parts of the open loop control of the slave motor. The first one is the direction change. Depending on the difference of the outputs of the force sensors, the D/A converter pin connected to the Analog Servo Drive AZBDC10A4 direction pin will be either HIGH or LOW, providing the ability to change direction. Moreover, even though the output of the drive is current, its input is PWM pulses. The magnitude of the current depends on the duty cycle of the PWM pulse. Thus, the input of the drive must be normalized to [0 1]. The maximum value of the difference of the two outputs is +5, while the minimum is 0. Ergo, to normalize it to the desired range the gain 1/5 can be used ($1/V_{max}$ in the Figure). However, if the range of the duty cycle is the [0 1], then even at pretty insignificant forces that will surpass the Dead Zone bound the duty cycle will reach the value

1 pretty easily. The resulting speed of the slave motor will reach the maximum value swiftly, presented in Figure 6.20, making the user unable to control the Force Sensors quickly enough. To reduce the range of the duty cycle to $[0 \ 0.1]$ for instance, the FSR reduce Gain was inserted, that can be changed real time during the experiments.

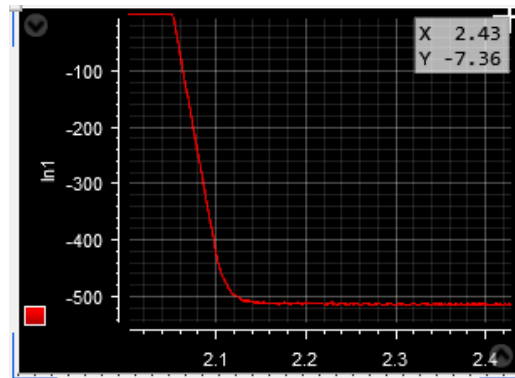


Figure 6.21. Motor Velocity Response with duty cycle 1 as being displayed at ControlDesk. x axis is time (s) and y axis is the velocity (deg/s).

With the FSR sensors connected to the Bowden Cables this division of the Simulink file can be used to conduct experiments for the Classic EPP configuration. The last thing that must be noted is the reading of the encoder, which is examined thoroughly in Appendix A BASICS ON dSPACE, and is presented in Figure 6.22.

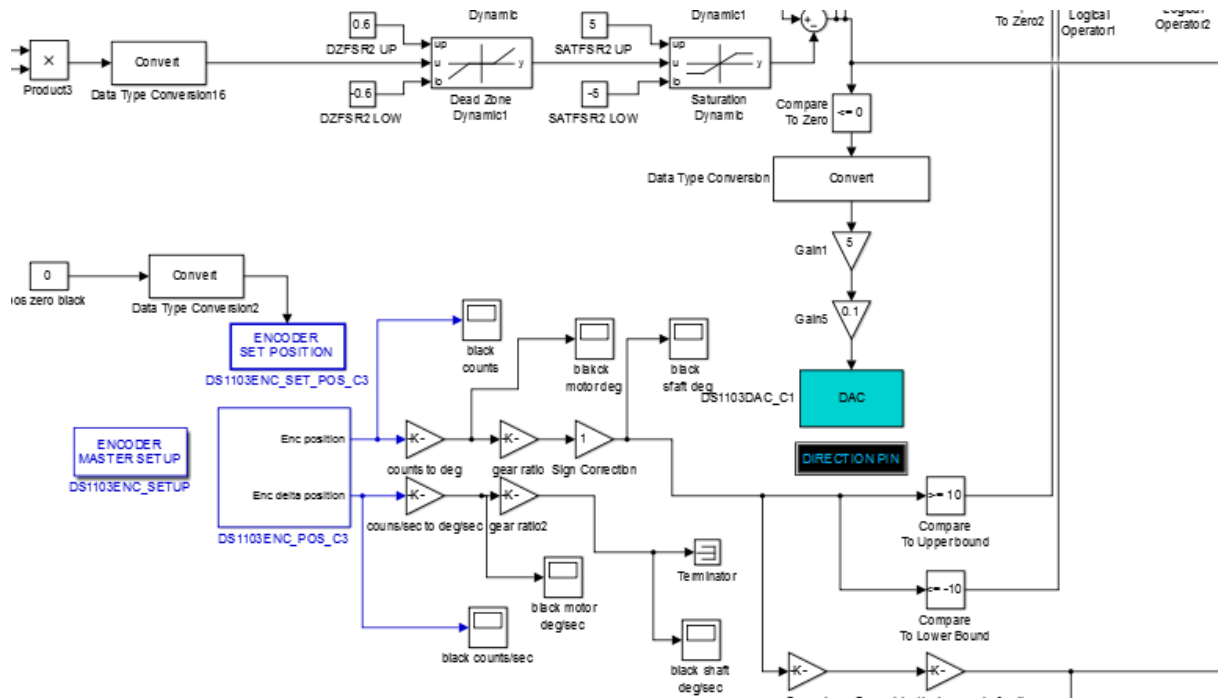


Figure 6.22. Reading of the encoder position and velocity.

Consequently, the Bidirectional Biomechatronic EPP of Figure 6.15 must be designed in the block diagram syntax of Simulink. To imitate the motion provided by the Bowden cables the Master motors must rotate on opposite directions. Furthermore, to follow the slave motor swiftly and with small error, a controller is required. In Chapter 5. Preliminary data

processing it was determined that a PD control is capable of satisfying these design demands. A block diagram structure of this notion is presented in Figure 6.23.

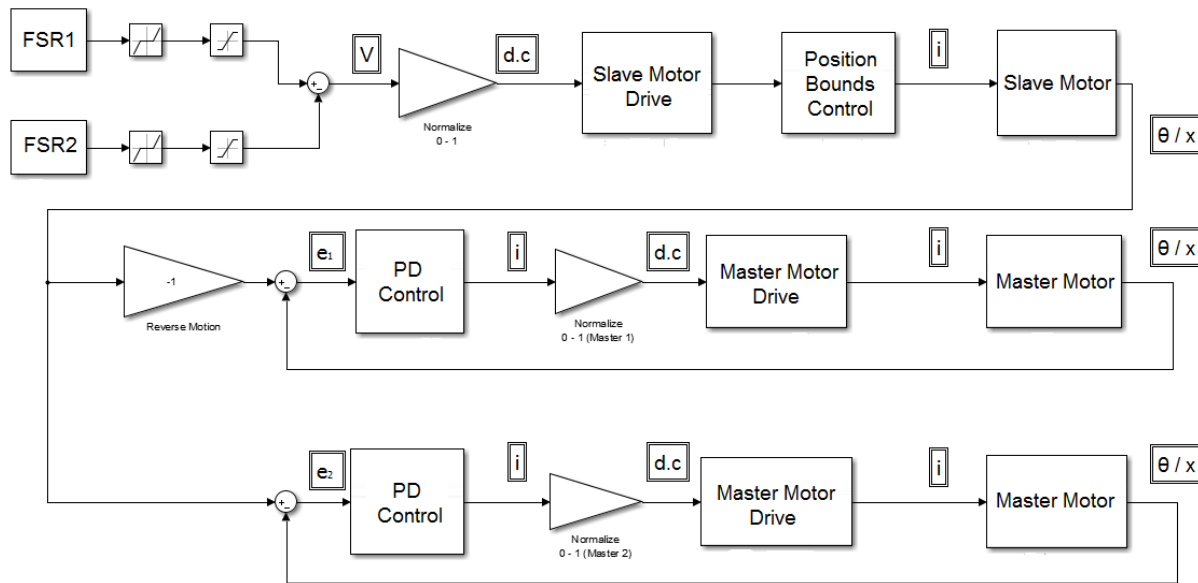


Figure 6.23. Biomechatronic EPP control scheme.

The open loop control of the slave motor is the same as in the Classic EPP configuration. However, the Master Motor closed loop control must be included in the Simulink program. The block diagram syntax that was used is presented in Figures 6.24, 6.25 and 6.26.

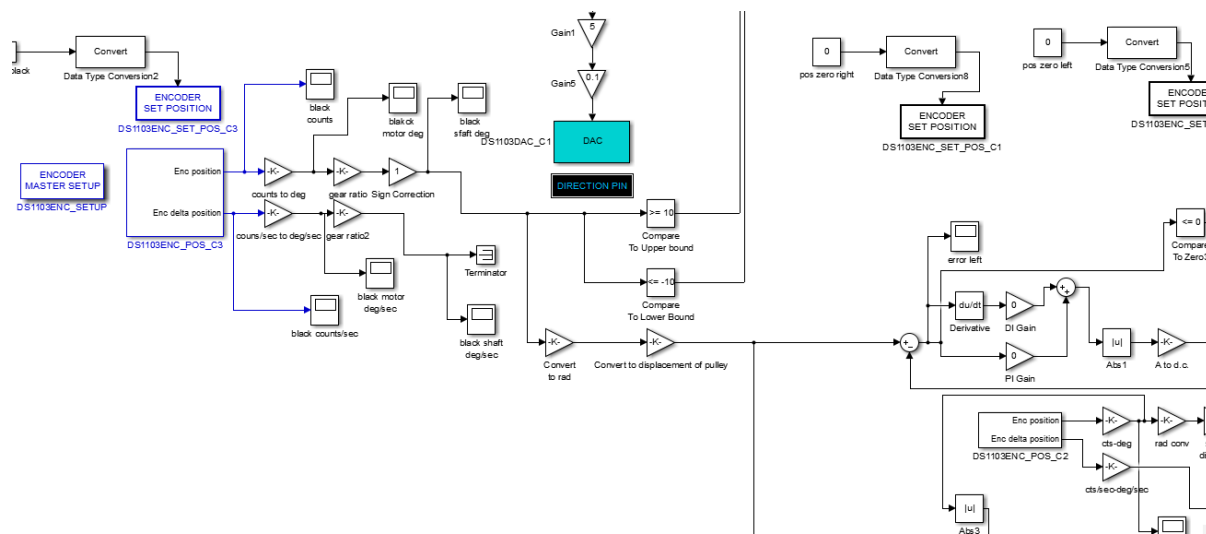


Figure 6.24. Biomechatronic EPP Simulink program for the Master Motors (Part 1).

It has to be underscored the fact that to control the motors properly, the direction of the motors must be determined according to the value of the error, as it is designed in the Simulink program. For instance, if the motor is rotating clockwise and the error is positive, then to reduce it the motor must change direction, rotating counterclockwise. If this requirement is not resolved, then the motor can rotate only in one direction, rendering the plant unstable. In contrast to the drive of the slave motor that has one direction pin, the corresponding drive of the master motors has two. That is the reason why two D/A converter



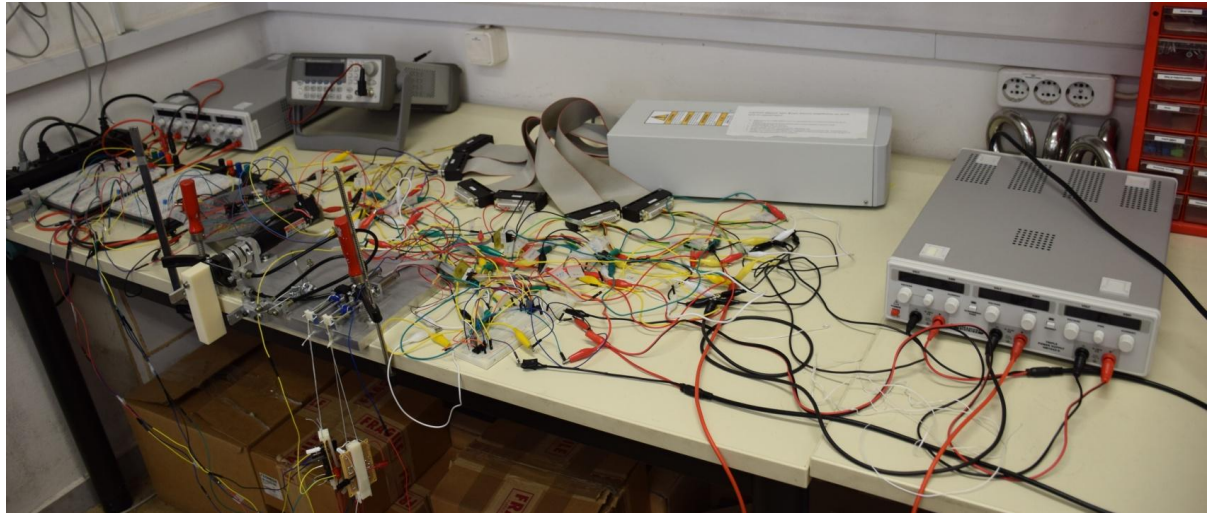


Figure 6.27. Side view of the setup.

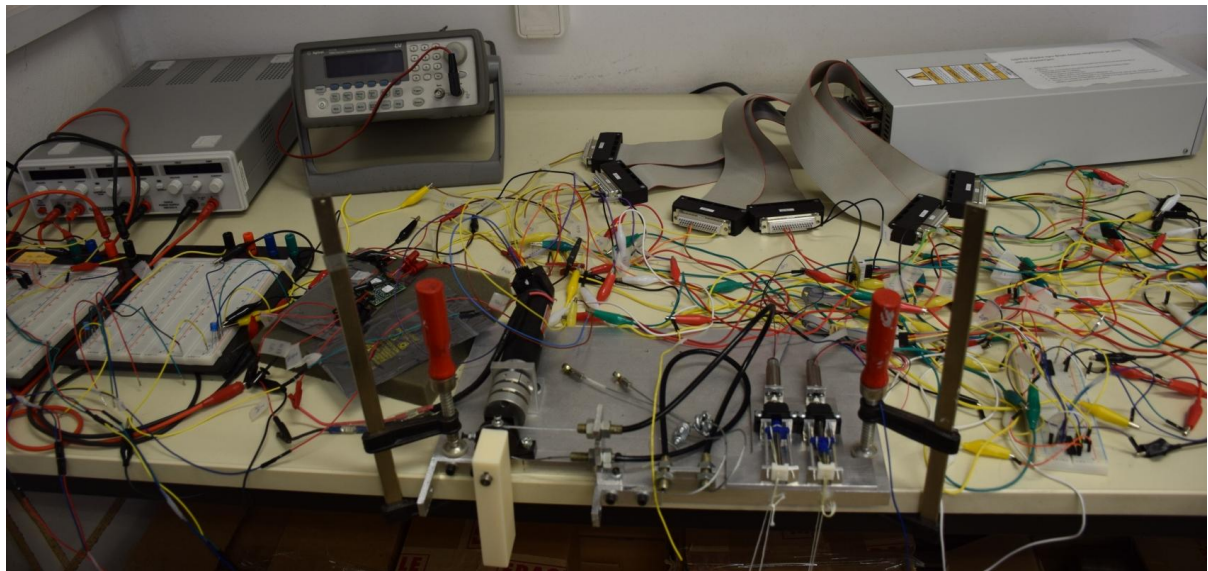


Figure 6.28. Front view of the setup.

That was the final stage for the preparation of the setup. With the fort of the setup conquered, the experimental stage of the thesis can be initialized and it will be presented in the next installment.

7 Experimental Verification

7.1 Experiment 1 Transparency – Equivalence

With the completion of the experimental setup and the Simulink – ContolDesk program the experimental stage came. As it is stated in the Introduction, three different experiments have to be conducted. The one that will be presented in this chapter is the Transparency – Equivalence experiment. The purpose of this experiment is to examine whether the responses from the Classic EPP and the Biomechatronic EPP would be similar. To clarify it, the data that have to be evaluated are the delays for both of the setups, the functionality of the control scheme of the Biomechatronic EPP and the responses of the FSR sensors in both cases^[4]. In case that the results would not be the desired ones, a new controller will be used.

The ControlDesk environment prepared for this specific experiment is presented in figure 7.1.

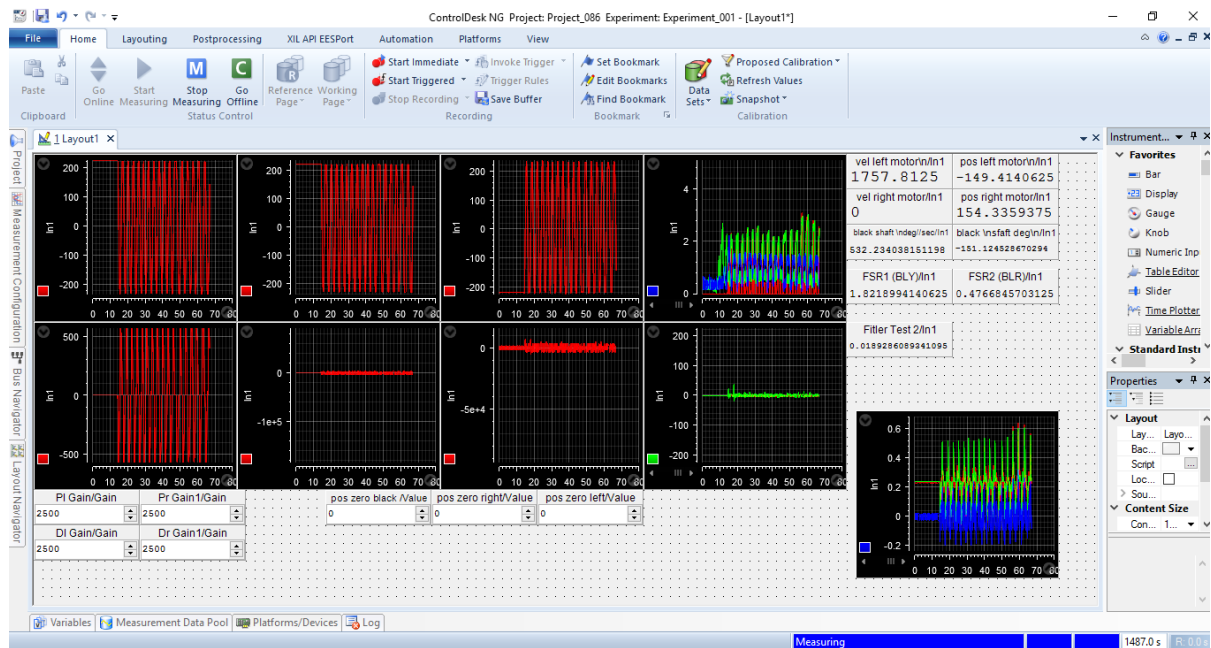


Figure 7.1. ControlDesk environment for the Transparency test.

The parameters that can be displayed during the real- time experiments are the position and the velocity of the motors, the current of the slave motor, the output of the FSR sensors and the closed loop error of the master motors. The gains of the PD controller can change real - time if variances in the responses are observed throughout the experiment. First, the results of the Biomechatronic EPP setup will be presented.

Classic EPP

For this specific setup the parameters that must be examined are the delays between the FSR Sensors and the Slave Motor. In figure 7.2 the response of the Slave Motor is presented applying load to the FSR sensors.

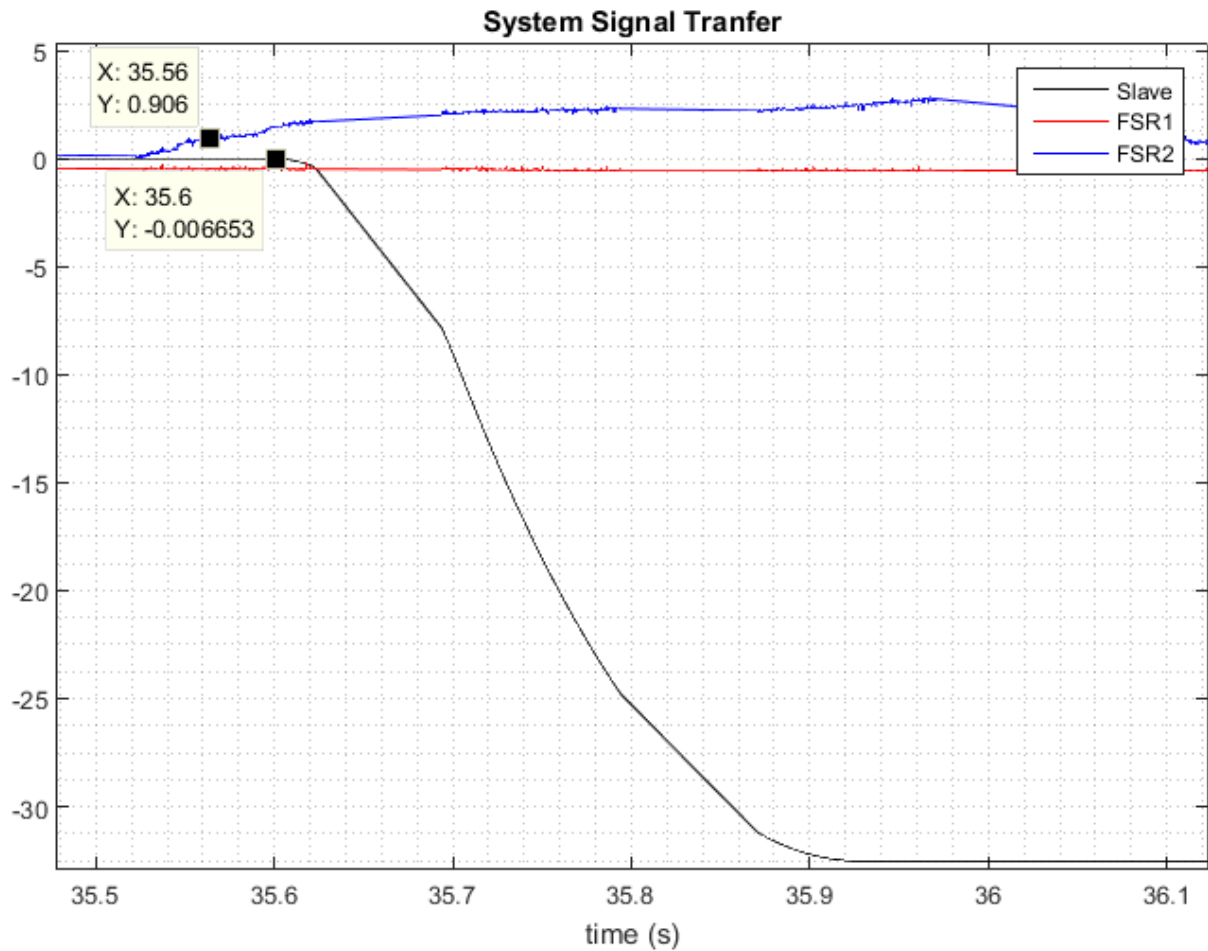


Figure 7.2. Delay Time between the FSR sensor and the slave motor.

It should be noted that the deadzone lower bound limit, as it was presented in the previous chapter is 0.9, thus, the input of the motor will be greater than zero when a load greater than 0.5 V is applied. Approximately the delay between the input command and the slave motor is 0.04 sec, a result that is considered accepted; taking into account that the sensors and the motor are bound together and the translation of the user is instant from the Bowden cables.

In the following figures the response of various parameters of the system are presented. Figures 7.4 and 7.5 reveal that the filtered response of the FSR sensors has significant delays over the unfiltered ones, making the choice to just present them and not to use them in the open loop control valid. Moreover the fact that the time constant of the current of the slave motor is at the range of $\pm 0.05A$, way below the maximum continuous current that is 3.44 A according to the datasheet of the motor.

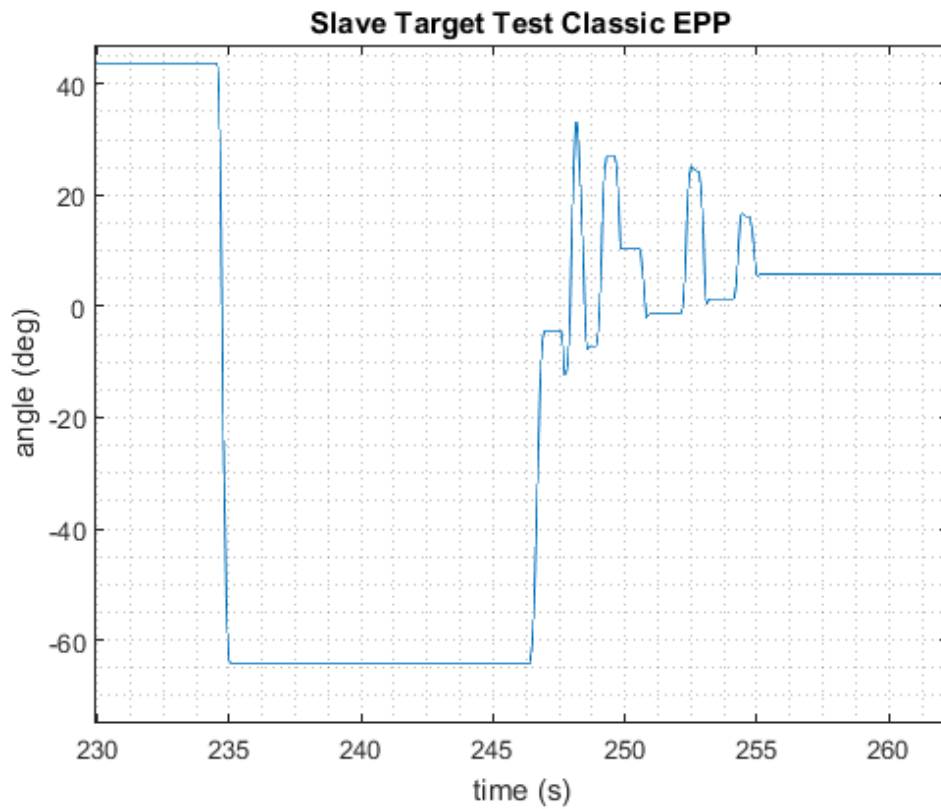


Figure 7.3. Response of the slave motor for a specific time range.

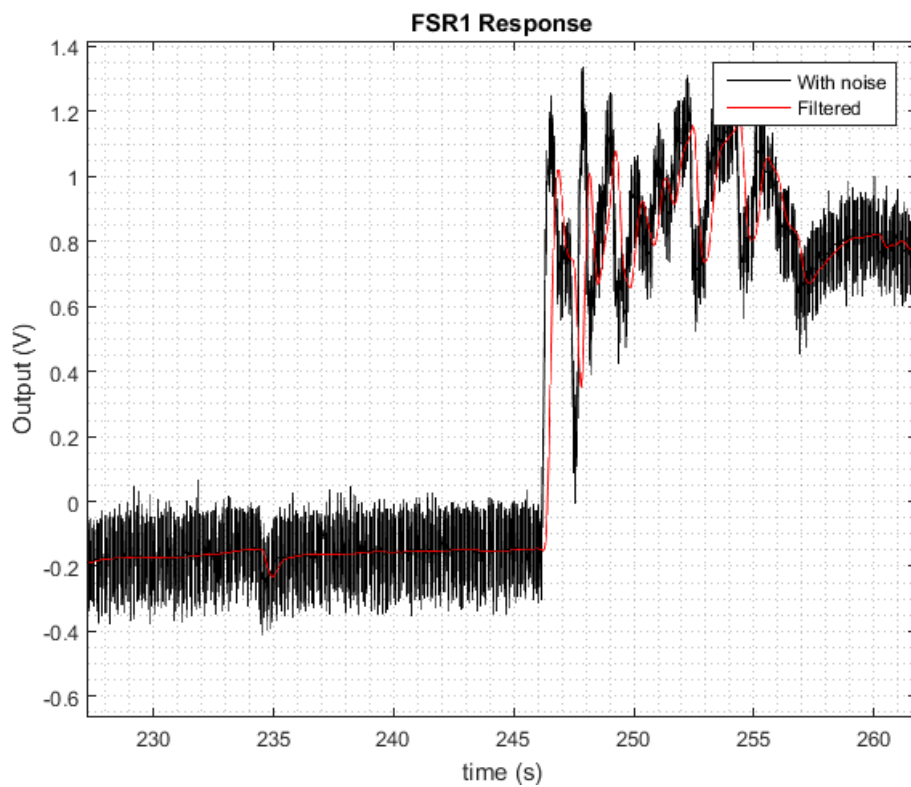


Figure 7.4. FSR 1 response for the same time range.

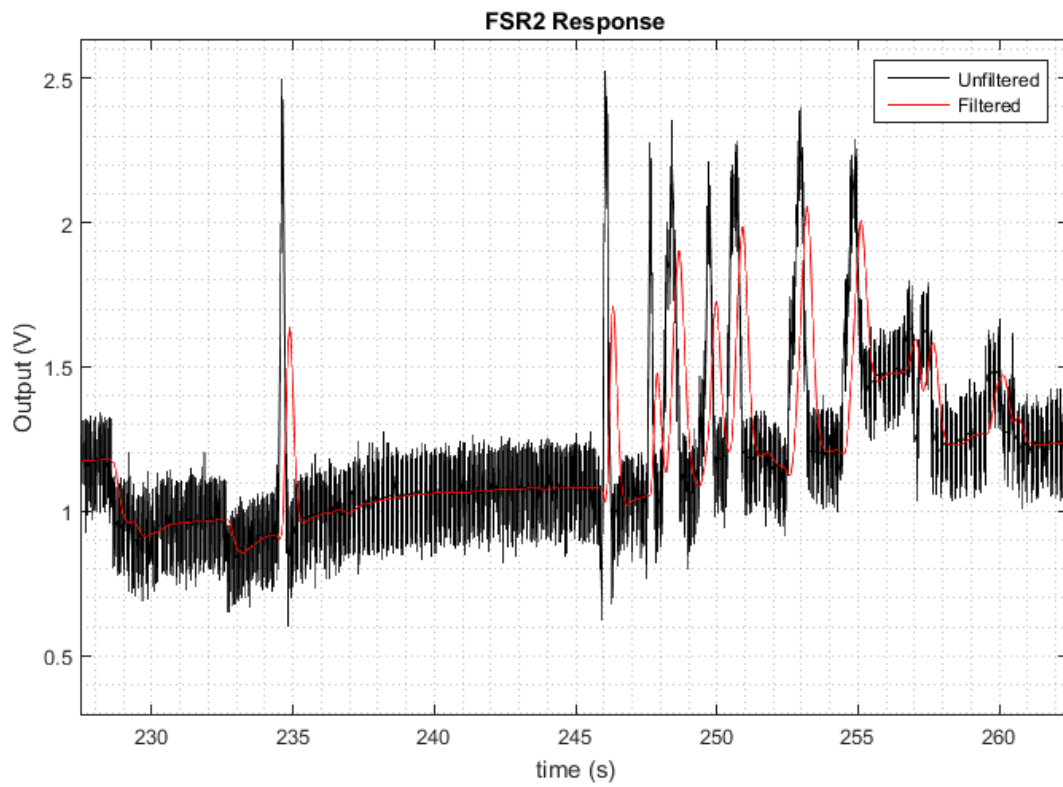


Figure 7.5. FSR 2 Response for the same time range.

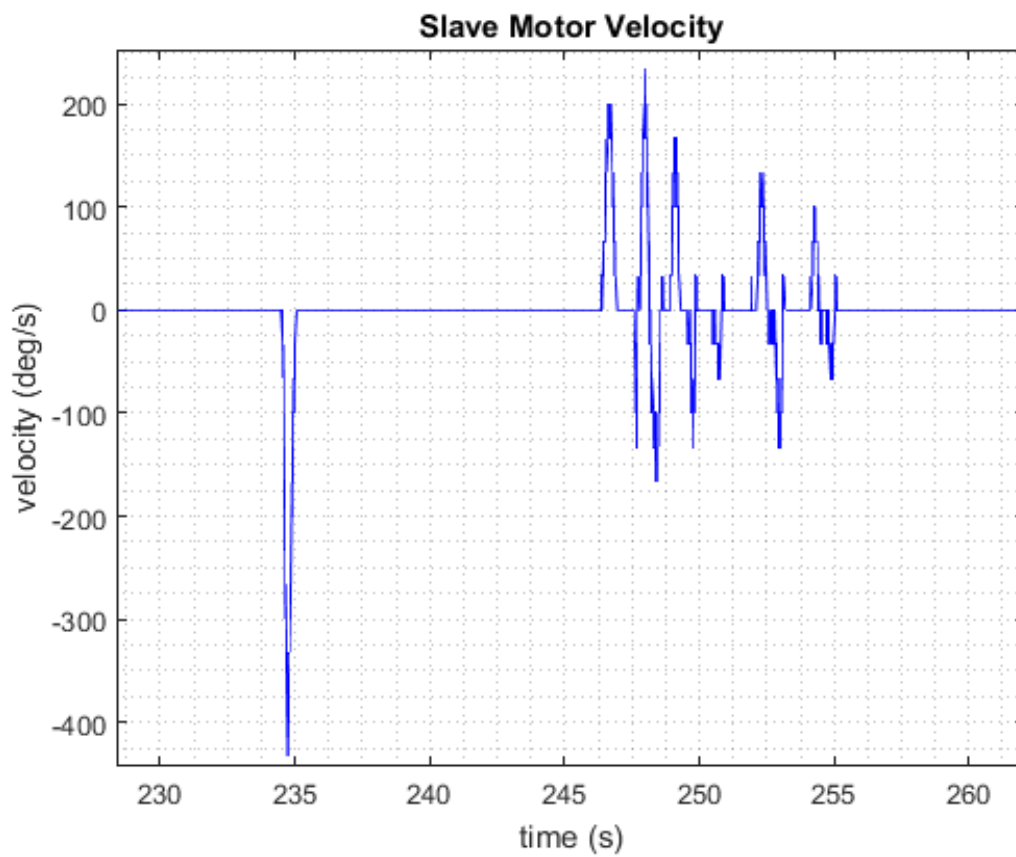


Figure 7.6. Slave motor velocity for the same time range.

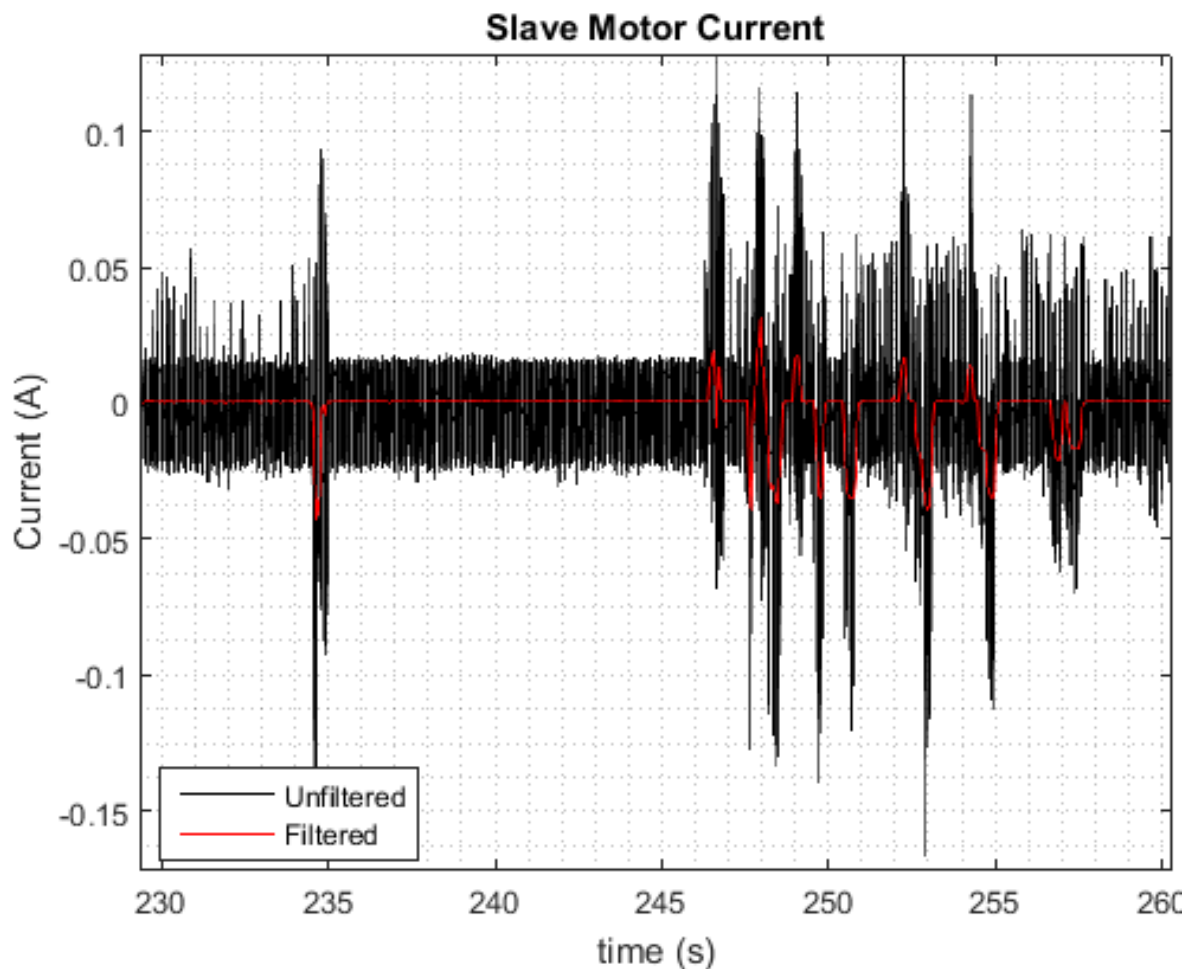


Figure 7.7. Slave motor Current for the same time range.

The immediate results that have to be evaluated are the ones of the Biomechatronic EPP and whether they are similar or not to the Classic EPP.

Biomechatronic EPP

At this stage the delay and the quality of the controller will be presented, compared to the results of the Classic EPP. Inserting at ControlDesk the value of $K_P = 5000$ and $K_D = 8000$, from equations (20) and (21) of the previous chapter the damping ratio of the system is 1.9080 and the natural frequency 6.5876 r/s, meaning that the overshoot will be zero.

In figure 7.8 the delay between the master and the slave motor is presented. It is observed that in comparison to the Classic EPP, the delays are far greater, approximately 0.2 – 0.5 sec, 10 times greater than the Classic EPP. Apart from the delay, as it is presented in figures 14 and 15 the controller of the Master Motor 1 works properly, leading to extremely low errors (tends to 0), however, the Master Motor 2 has more significant error. The reason might be the higher friction in this case.

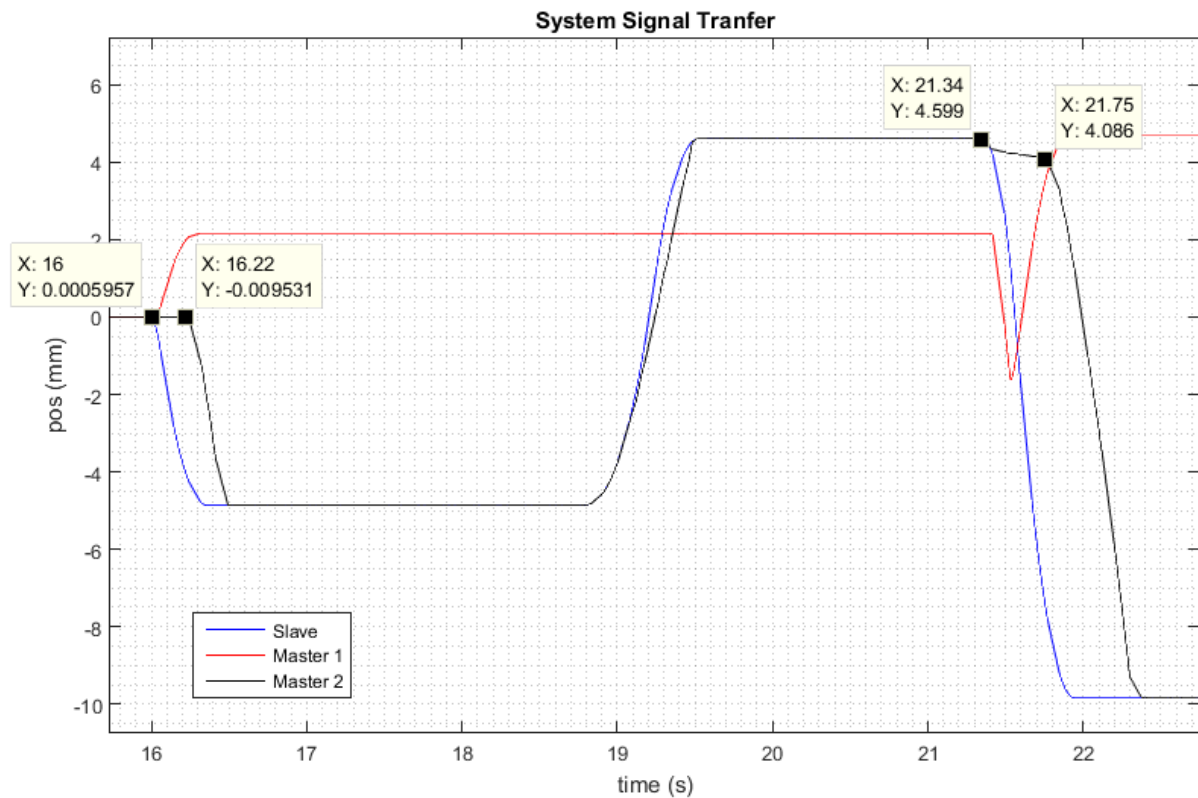


Figure 7.8. Delay between the slave motor and the master motor.

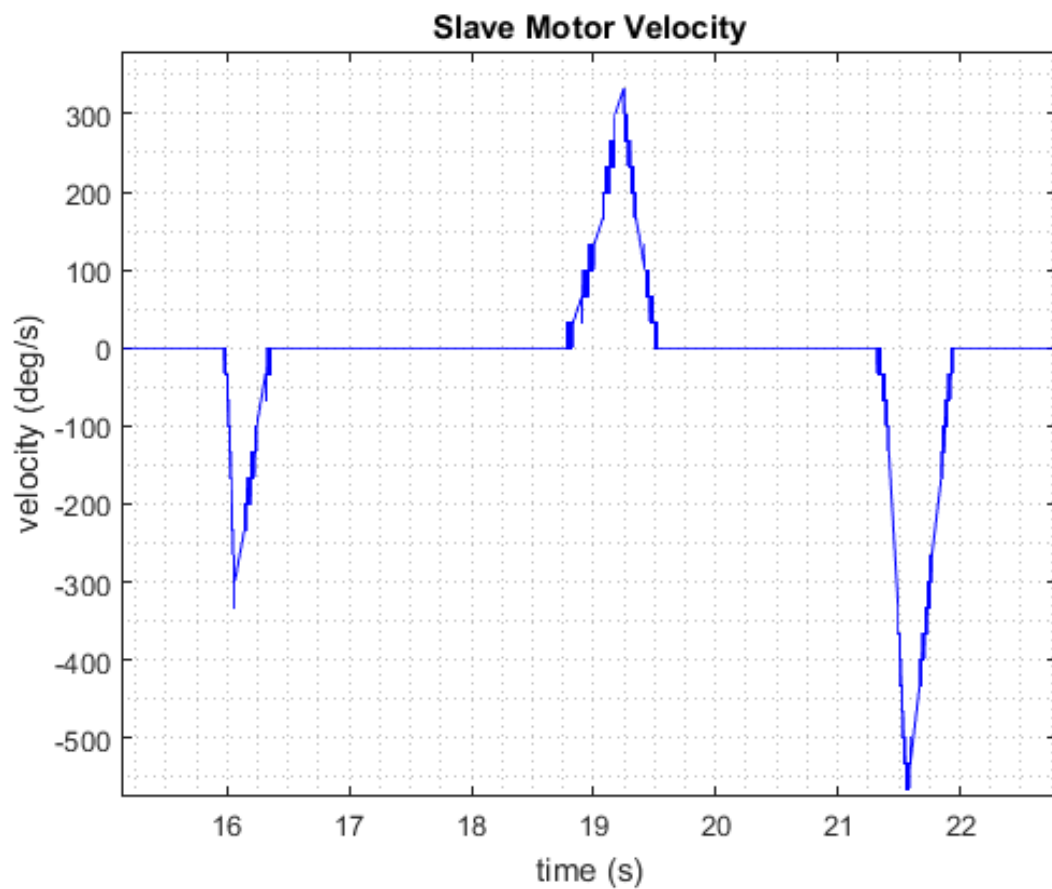


Figure 7.9. Velocity of the slave motor.

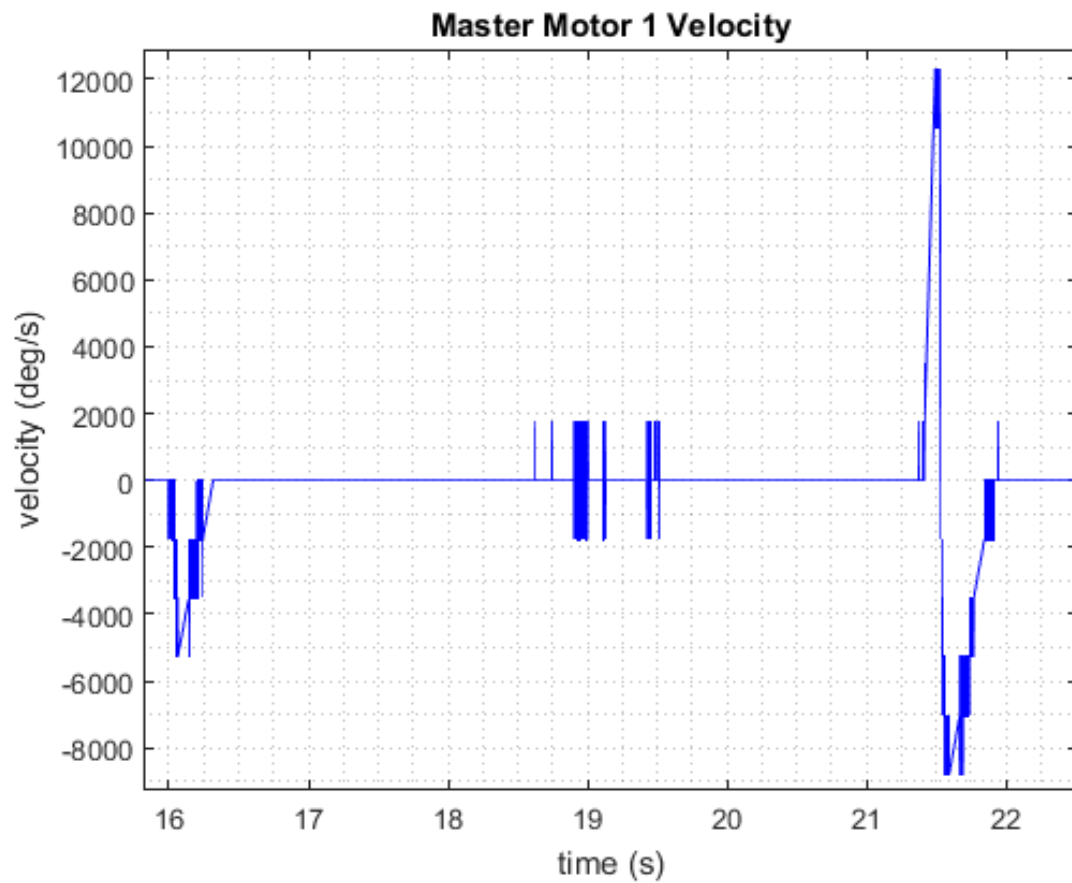


Figure 7.10. Velocity of the Master 1 motor.

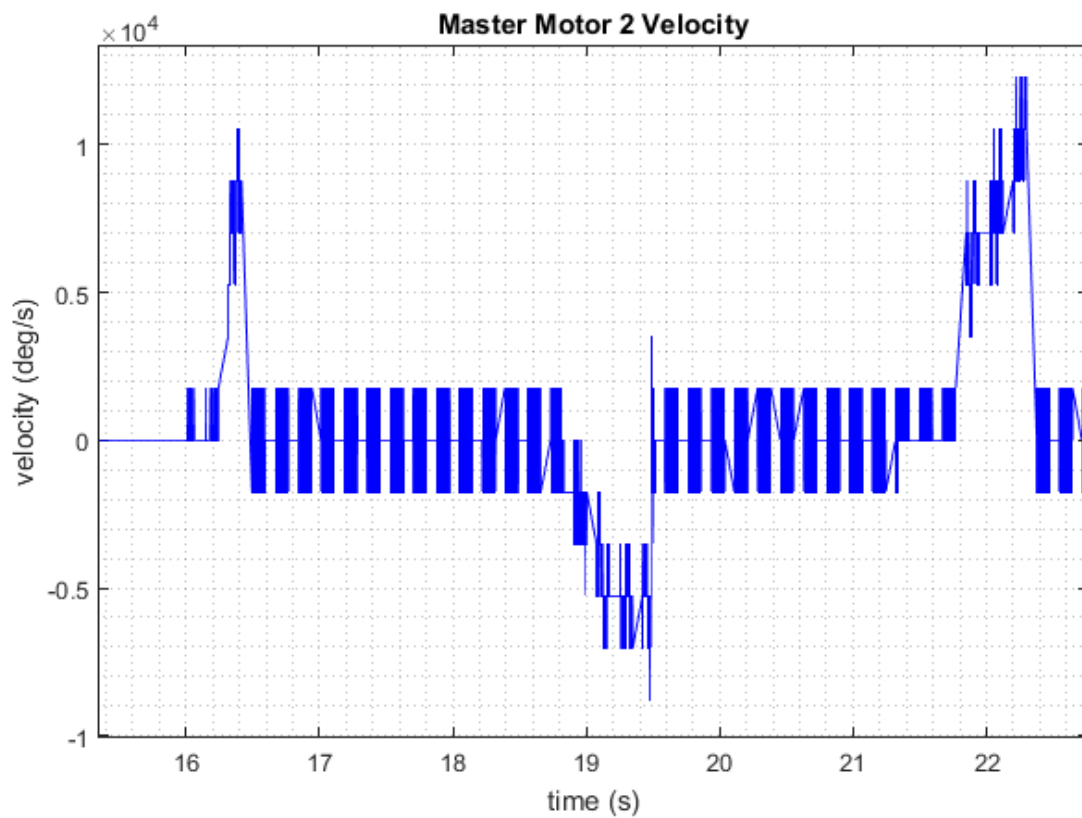


Figure 7.11. Velocity of the Master 2 motor.

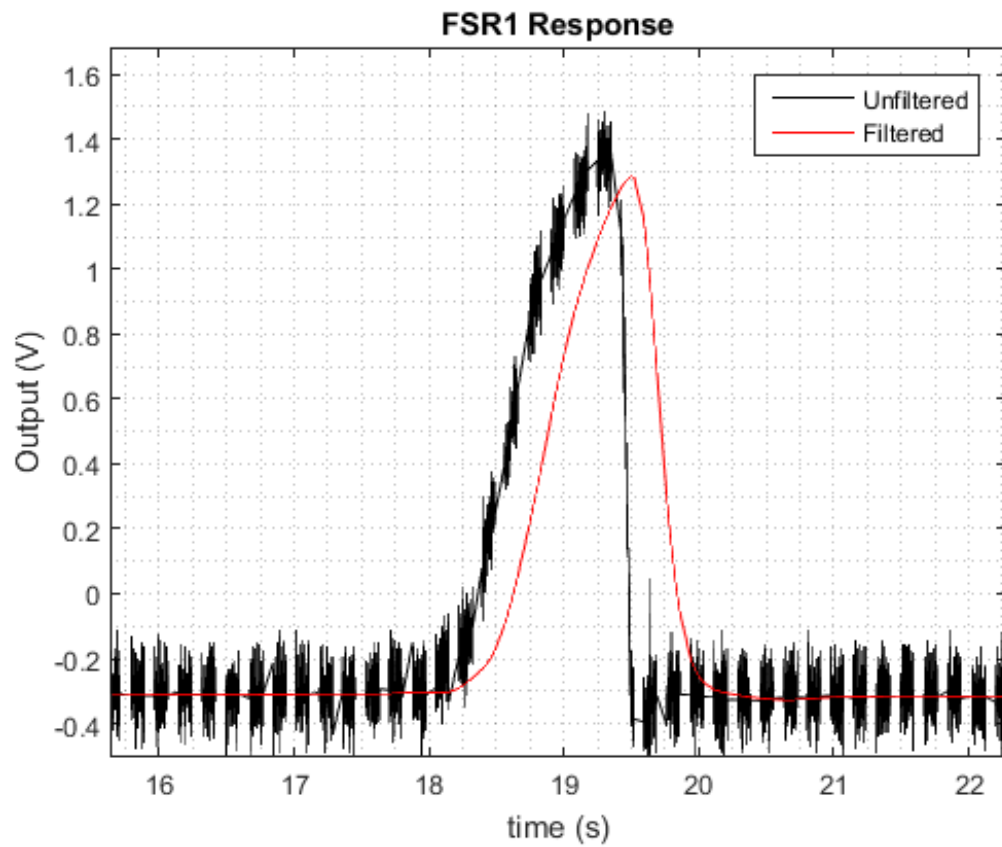


Figure 7.12. FSR 1 response.

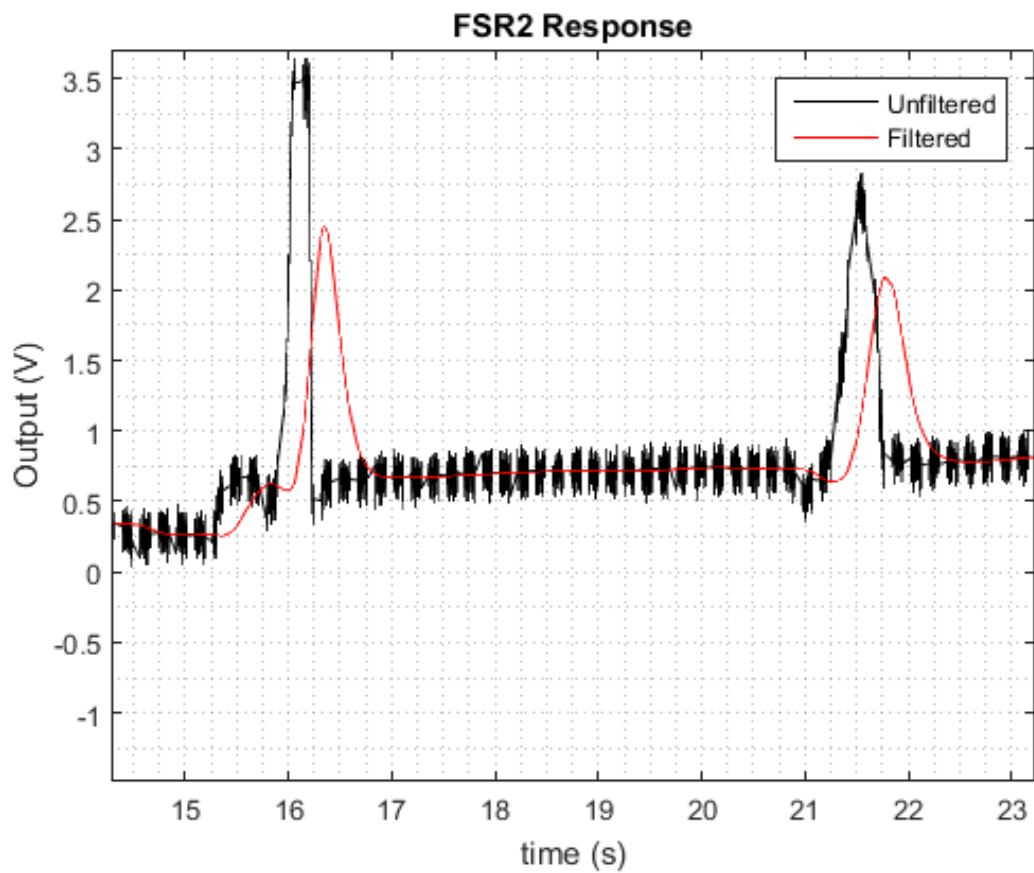


Figure 7.13. FSR 2 response.

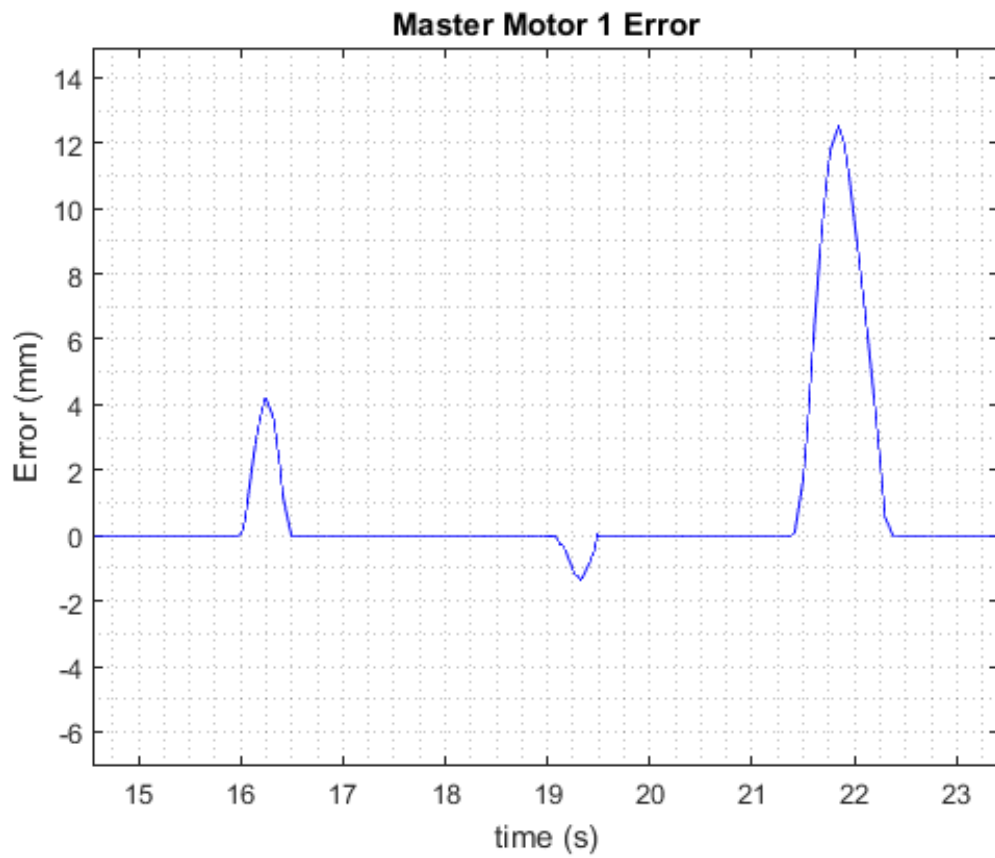


Figure 7.14. Master Motor 1 error.

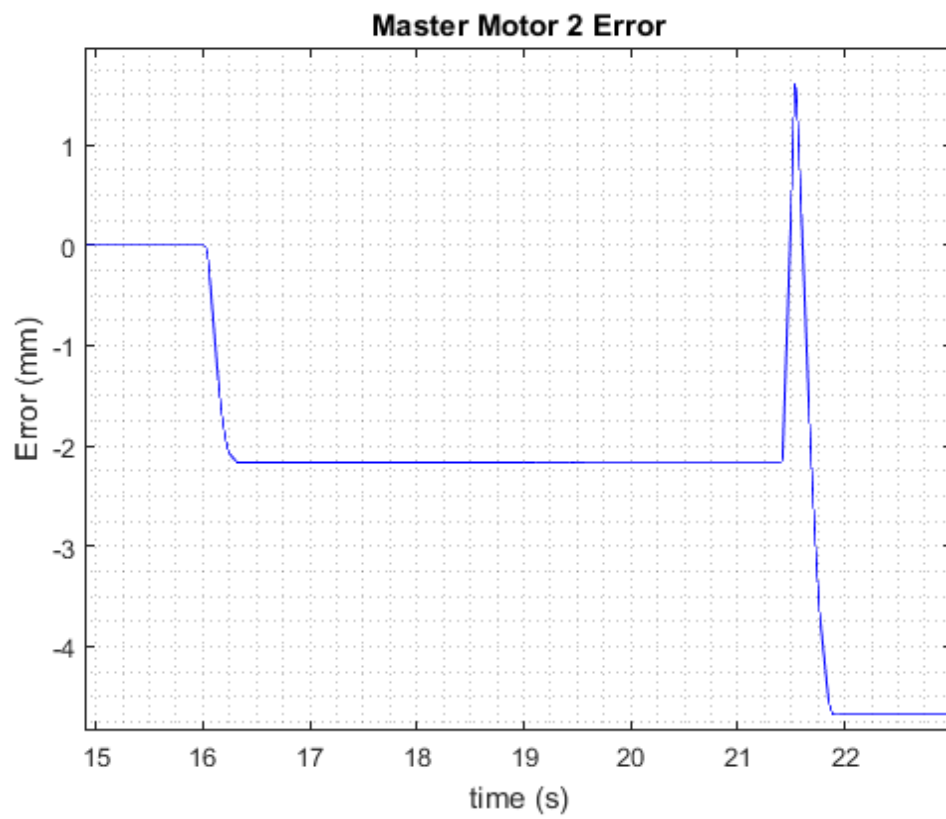


Figure 7.15. Master Motor 2 Error.

Taking into account these results, this controller proved incapable for this application. Thus, it was decided to use a new controller, reduce the annotations of the setup and use the Linear Lubricant APG-2G provided with the power screws to reduce the friction. In figure 7.16 it is presented the improvement of the assembly for more uniform friction throughout the motion.

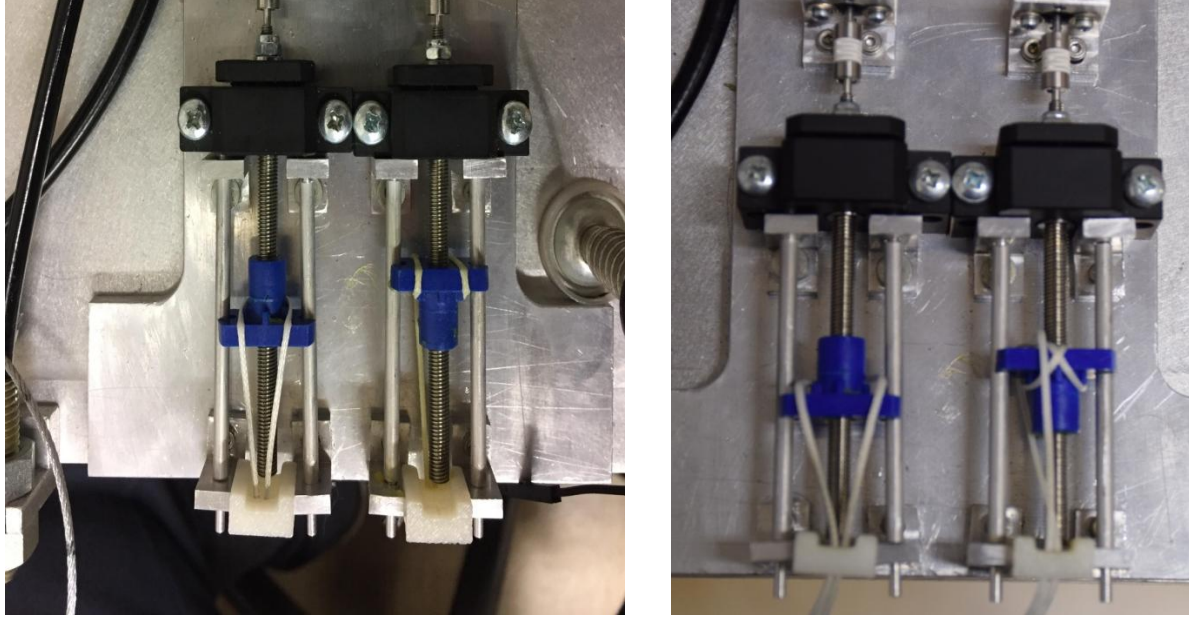


Figure 7.16. Power screws before (left) and after the improvement of the assembly.

Moreover, a new controller was selected. From equation (5.8) of chapter 5. Preliminary data processing taking into account the friction of the system with equivalent torque τ_f it can be deduced:

$$\frac{dv_m}{dt} m_{eq} + v_m B_{eq} = K_T \frac{2\pi}{h} i_s(t) - \frac{2\pi}{h} \tau_f \quad (7.1)$$

In this case the control law that will be used is the following ^[9]:

$$i_s = K_T^{-1} \frac{h}{2\pi} (K_p e_{x_m} + K_D \frac{de_{x_m}}{dt} + m_{est} \frac{d^2 x_{m_d}}{dt^2} + B_{est} \frac{dx_{m_d}}{dt}) + K_T^{-1} \tau_f \quad (7.2)$$

m_{est} and B_{est} are the estimated equivalent mass and damping constant of the system. Considering that the estimated properties are equal to the real ones, it can be obtained:

$$\frac{d^2 e_{x_m}}{dt^2} + \frac{B_{eq} + K_D}{m_{eq}} \frac{de_{x_m}}{dt} + \frac{K_p}{m_{eq}} e_{x_m} = 0 \quad (7.3)$$

Thus, the damping ratio and natural frequency if the system can be obtained by the following equations:

$$\omega_n = \sqrt{\frac{K_p}{m_{eq}}} \quad (7.4)$$

$$2\zeta\omega_n = \frac{B_{eq} + K_D}{m_{eq}} \xrightarrow{(7.4)}$$

$$\zeta = \frac{B_{eq} + K_D}{2m_{eq}} \sqrt{\frac{m_{eq}}{K_p}} \quad (7.5)$$

The equivalent mass and damping constants were calculated on chapter 5. Preliminary data processing. However, the equivalent friction torque is required to implement this control law. To do so, a precision resistance $1\text{ Ohm} \pm 1\%$ was connected in series to the motor and for small duty cycles its current was measured. At the duty cycle value that the motor started rotating, the required current to overrun the friction torque flows through the circuit. It was calculated that the friction current i_f is 0.0121 A and the friction torque can be obtained using the following equation:

$$\tau_f = K_T i_f \quad (7.6)$$

The change that has to be accomplished on the Simulink program is presented in figure 7.17.

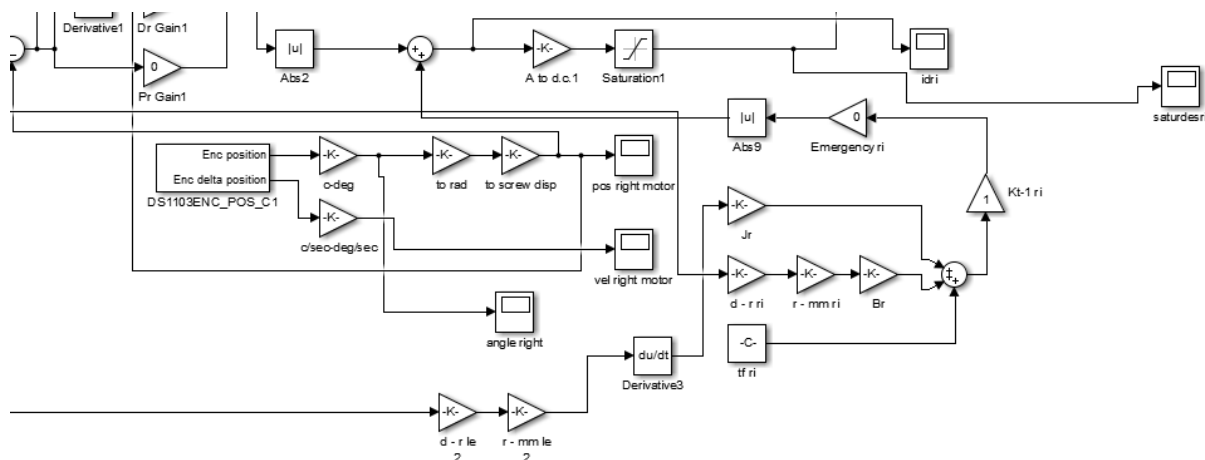


Figure 7.17. New Controller implementation on Simulink.

In this case apart from the results of the various outputs of the system, the input will be presented as well. The reason is whether or not the master motors can provide the necessary torque to the system or they are inept for the application. Furthermore, the results will be presented for steadily increased gain values to examine whether the response of the system will be improved. The results are presented in the following figures for each case.

Case 1 $K_D = 80000$ $K_P = 25000$

In comparison to the previous state the gains were increased to improve the response of the master motor 2. In figure 7.18 the delays of the master motors are presented. It is observed that depending on the position of the motors and the force applied by the user the delay can be from almost zero to 0.5 sec, as it is presented on figure 7.19 as well. When the position of the slave motor is reached, the error is almost zero as it is presented in figures 7.20 and 21. However, as it is presented in figures 7.22 and 23 the input reaches its upper bound and remains constant for a long period of time, indicating that the current provided by the controller reaches greater values, that it is not provided though. Thus, the motor will not produce the required torque to rotate the power screw.

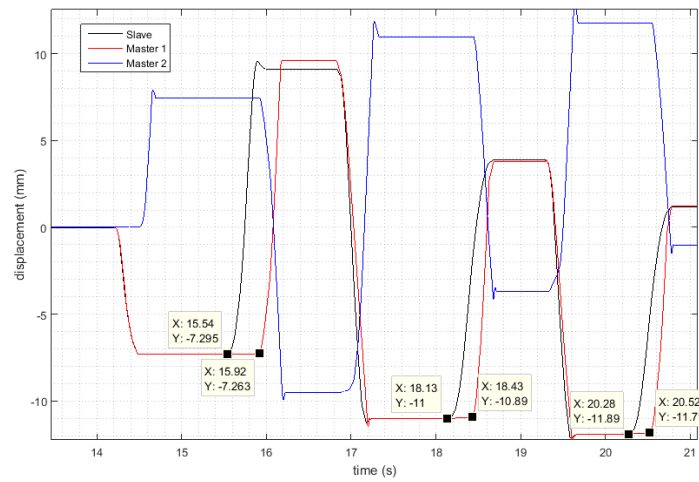


Figure 7.18. Delays between the master motors and the slave motor (case 1).

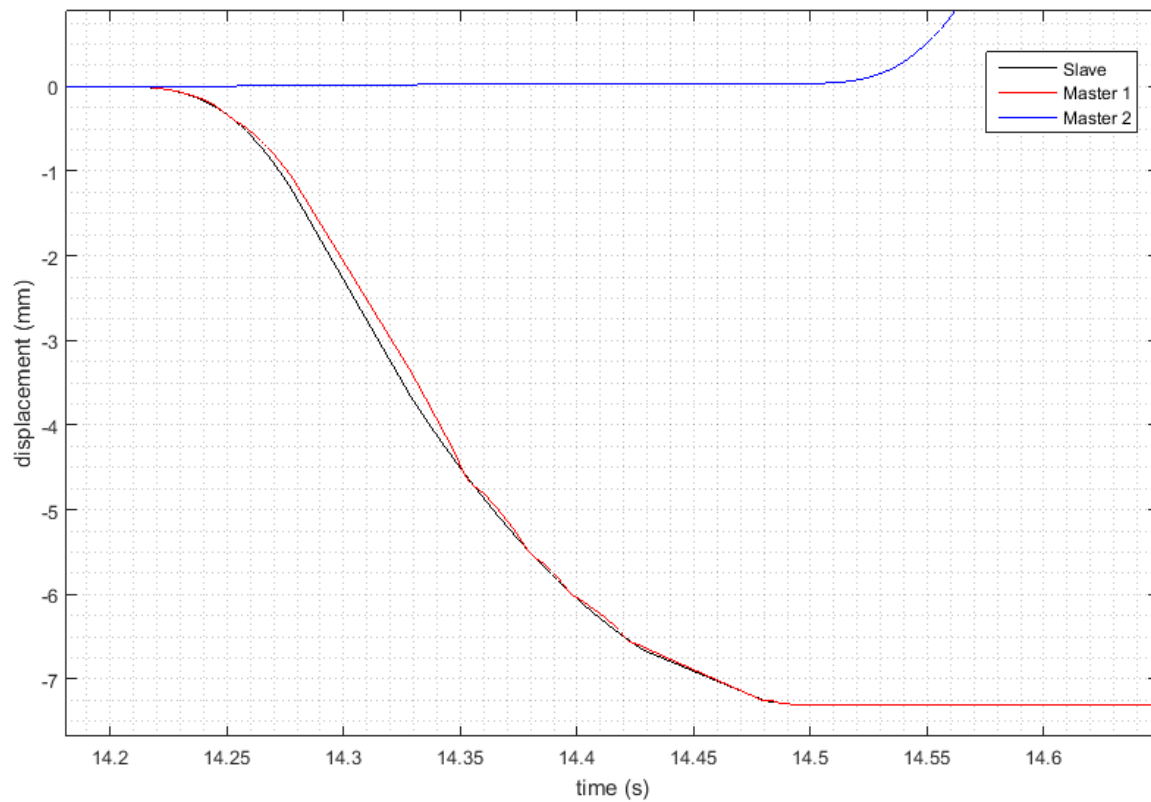


Figure 7.19. Zoom in to examine the range of the delays depending of the position of the motor (case 1).

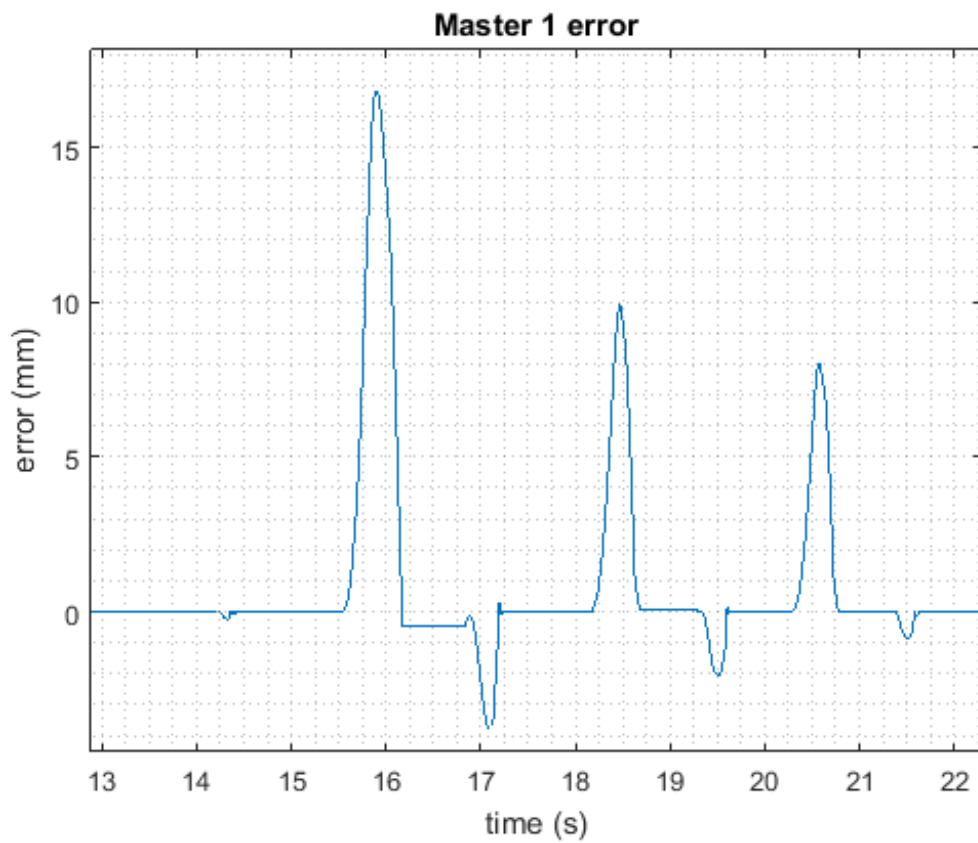


Figure 7.20. Master Motor 1 error (case 1).

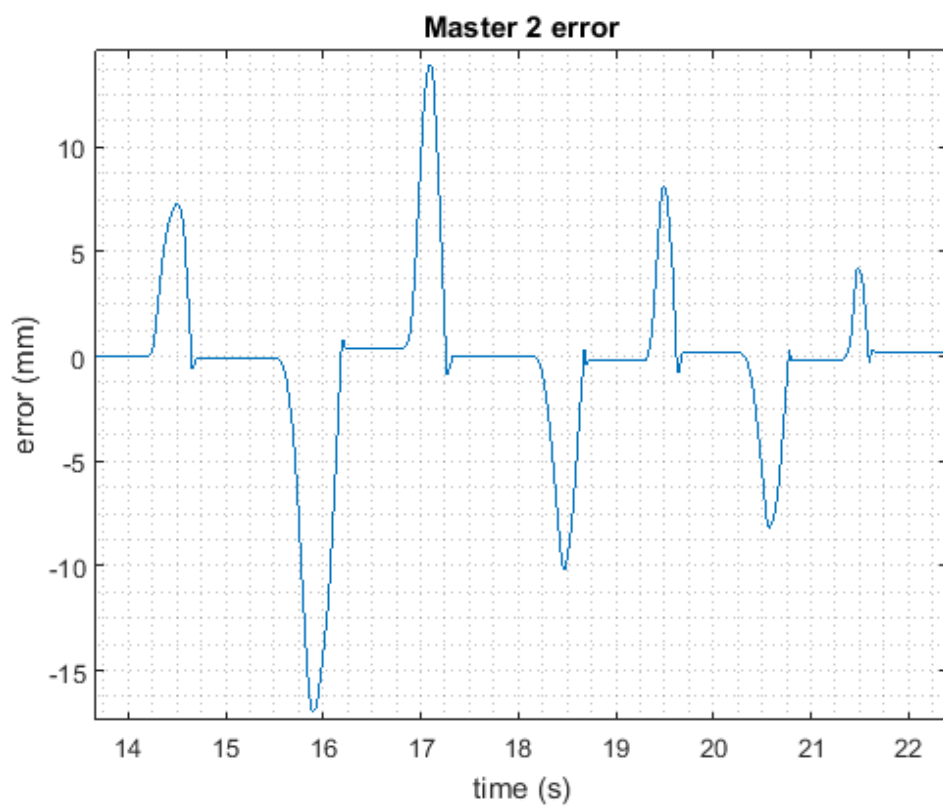


Figure 7.21. Master Motor 2 error (case 1).

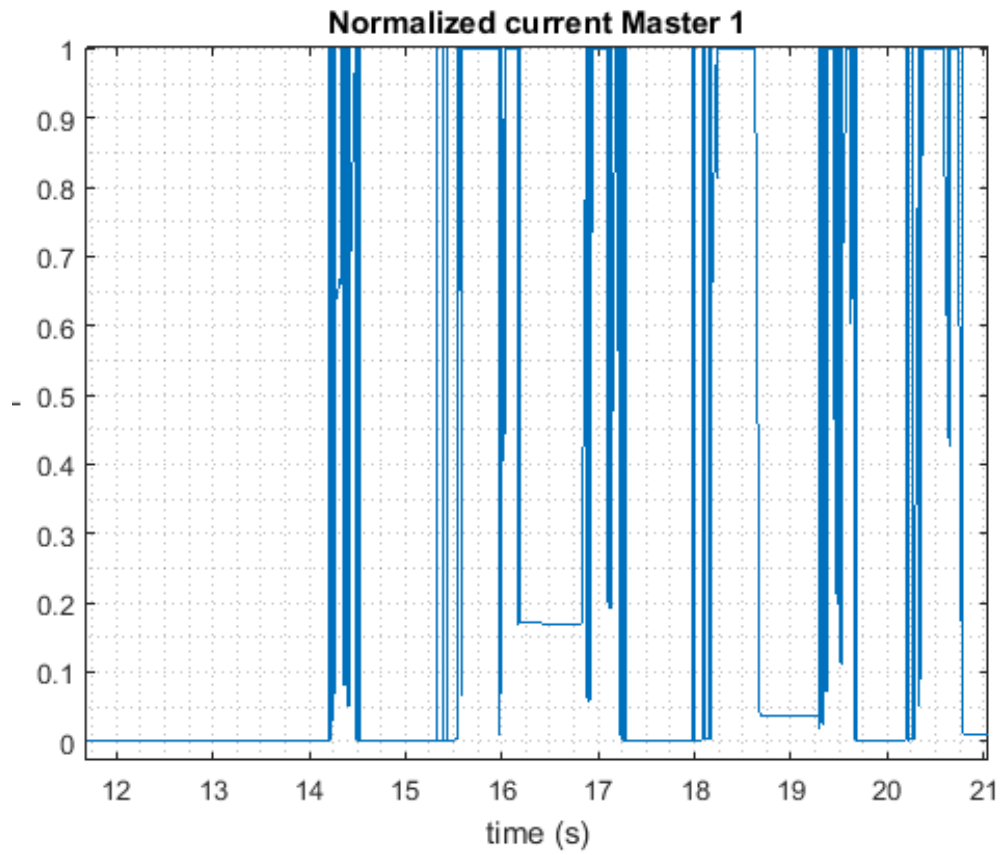


Figure 7.22. Master Motor 1 normalized current (converted to d.c.) (case 1).

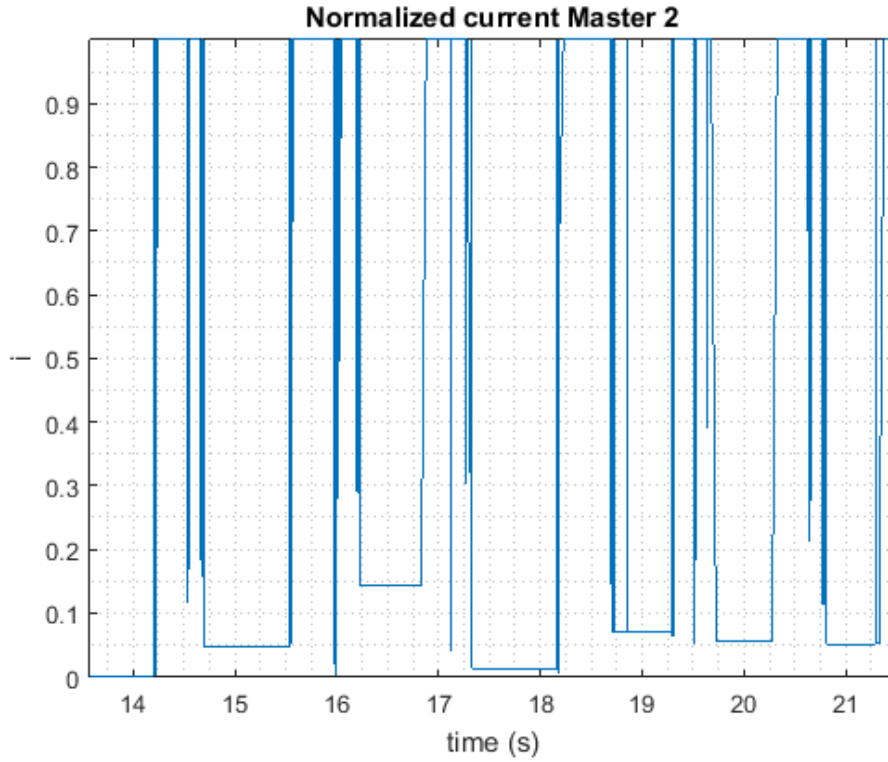


Figure 7.23. Master Motor 2 normalized current (converted to d.c.) (case 1).

Case 2 $K_D = 10^6$ $K_P = 5 \cdot 10^6$

In this case the gains were increased significantly to examine whether any improvement occurred. The results are presented in the following figures. From figures 7.24 and 7.25 it can be deduced that the situation did not improve and the delays are not reduced. Moreover, the fact that the motor is inept to provide the necessary torque remains.

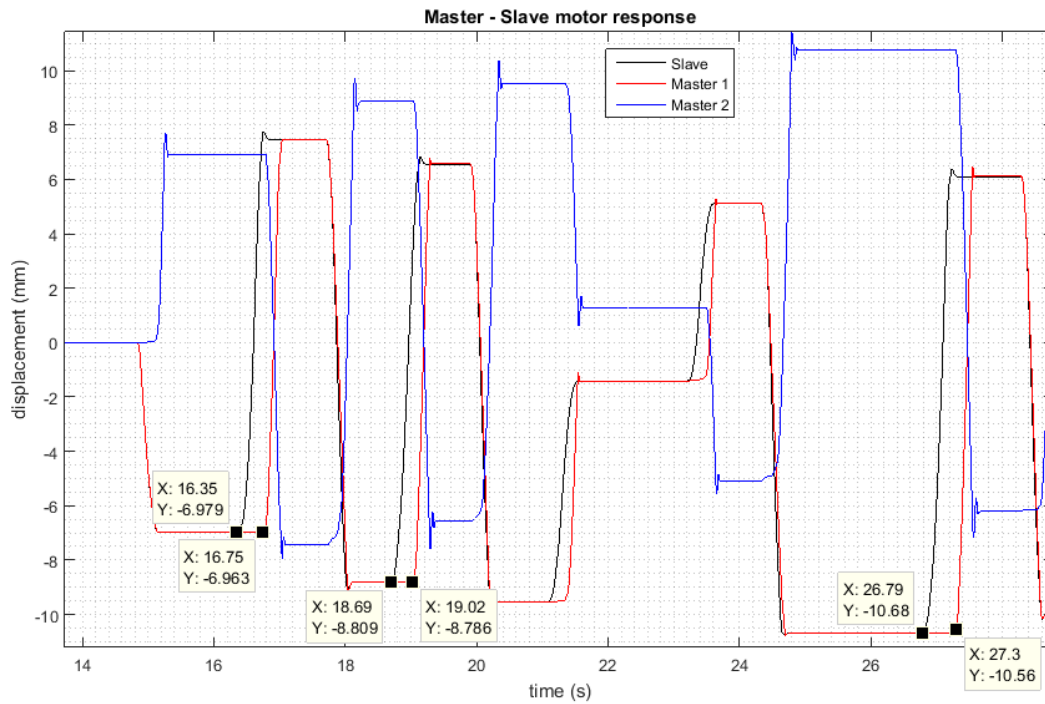


Figure 7.24. Delays between the master motors and the slave motor (case 2).

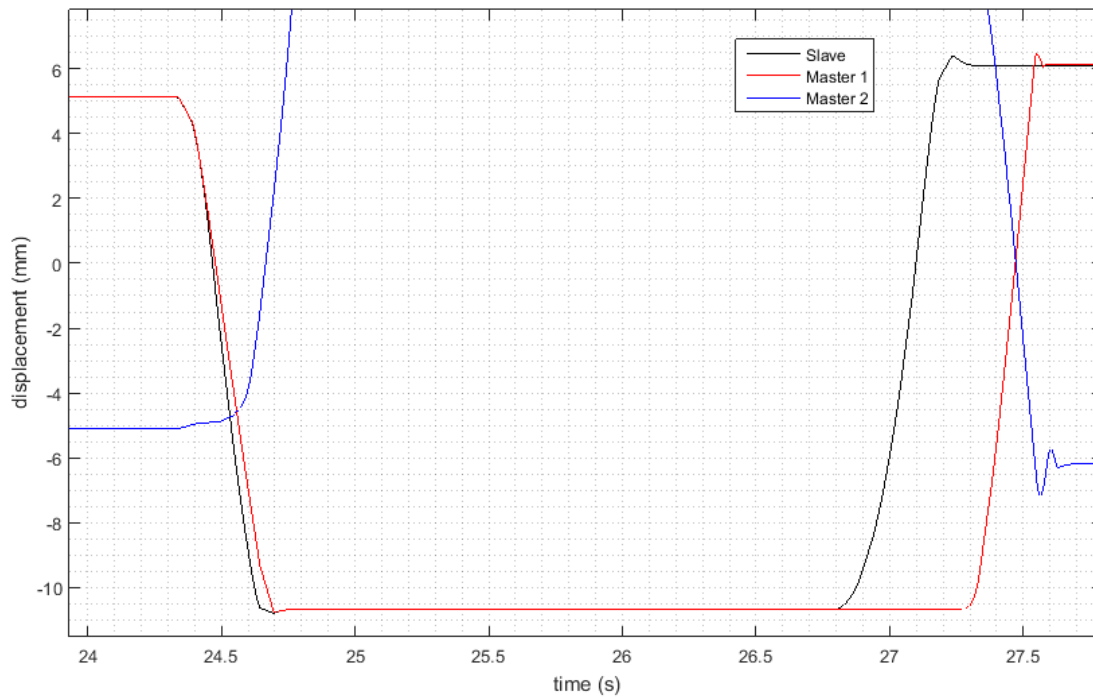


Figure 7.25. Zoom in to examine the range of the delays depending of the position of the motor (case 2).

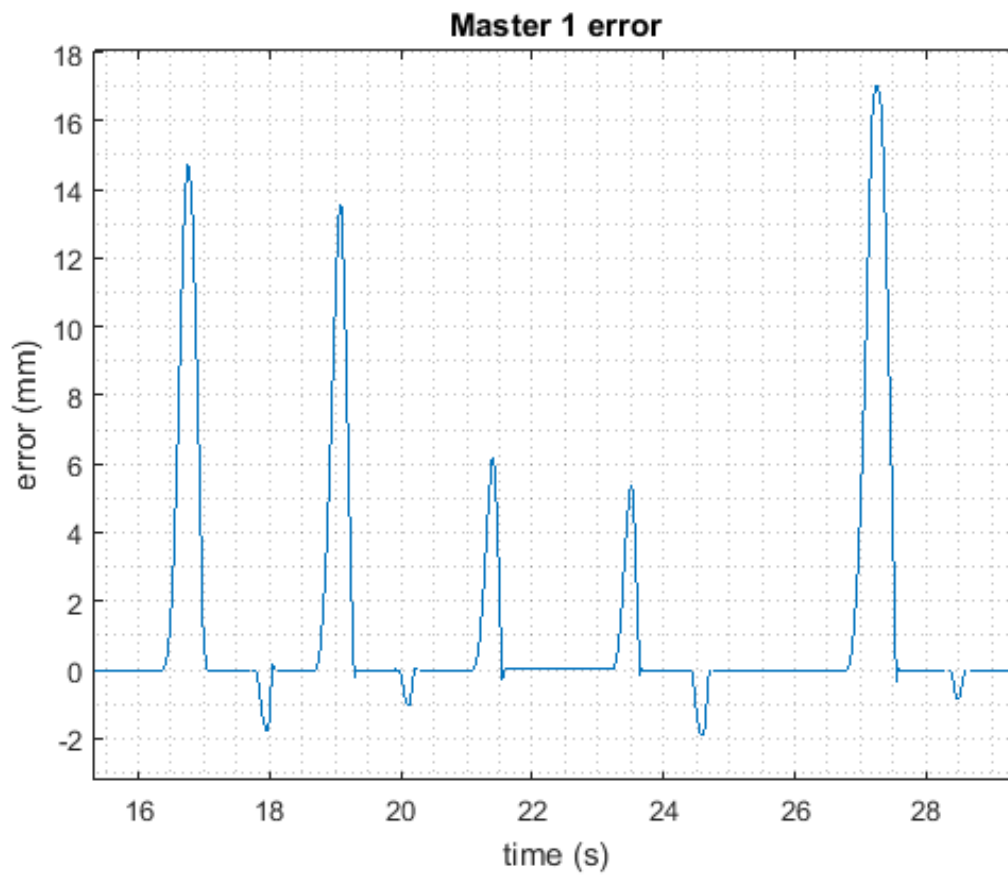


Figure 7.26. Master Motor 1 error (case 2).

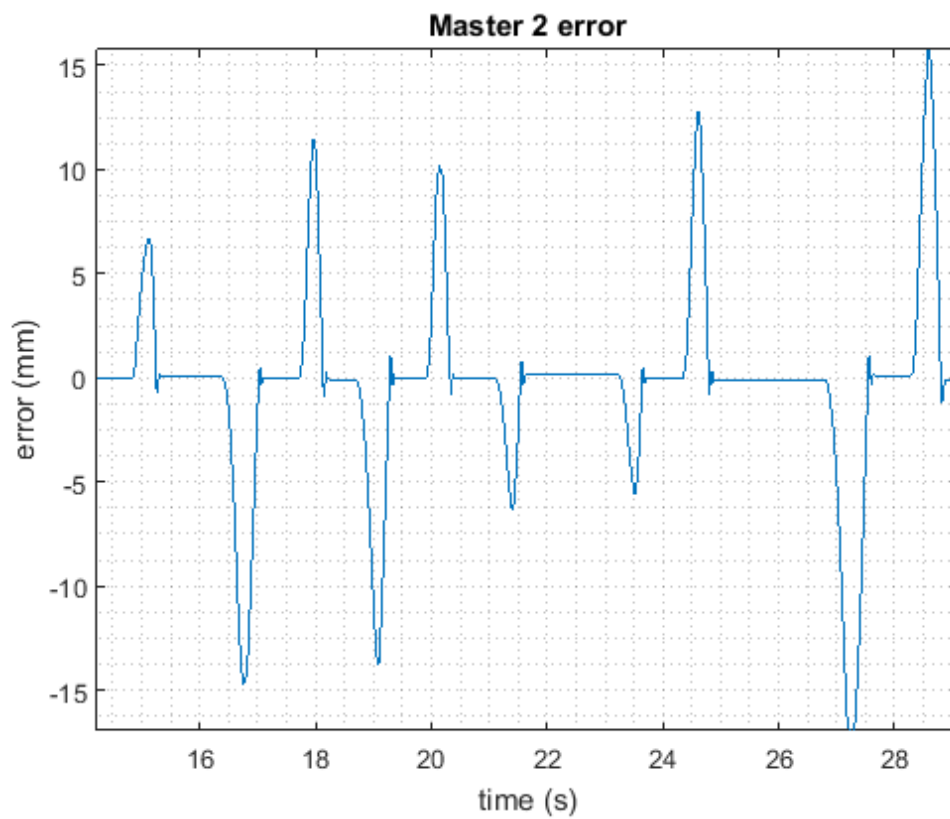


Figure 7.27. Master Motor 2 error (case 2).



Case 3 Increase in Supply voltage

Moreover, it was noticed that even though it was stated at the datasheet of the h-bridge that the maximum current is 600 mA, during all of the experiments the peak of the current at the voltage supply was 432 mA, therefore it was decided to increase the supply voltage from 4.5 V to 7 V. The results are presented in the following figures and reveal a dramatic improvement at the results.

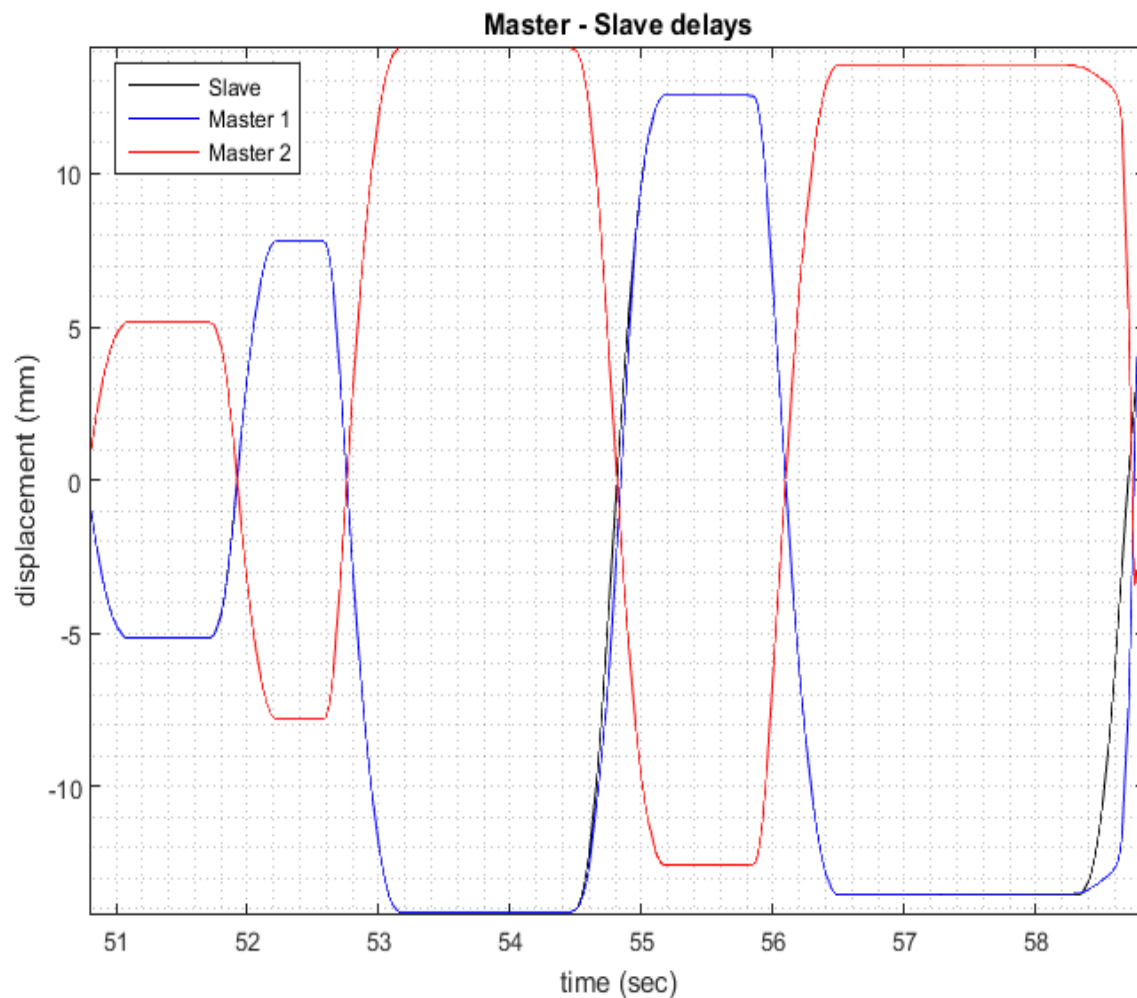


Figure 7.30 Response of the motors with increased supply voltage.

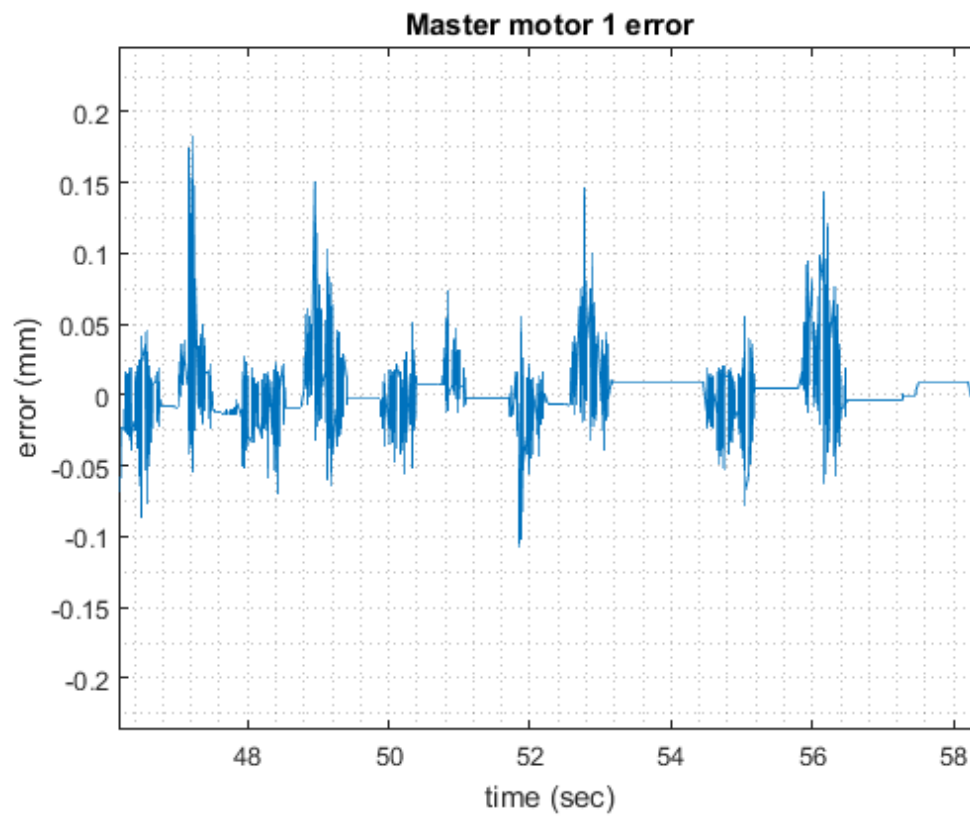


Figure 7.31. Master Motor 1 error.

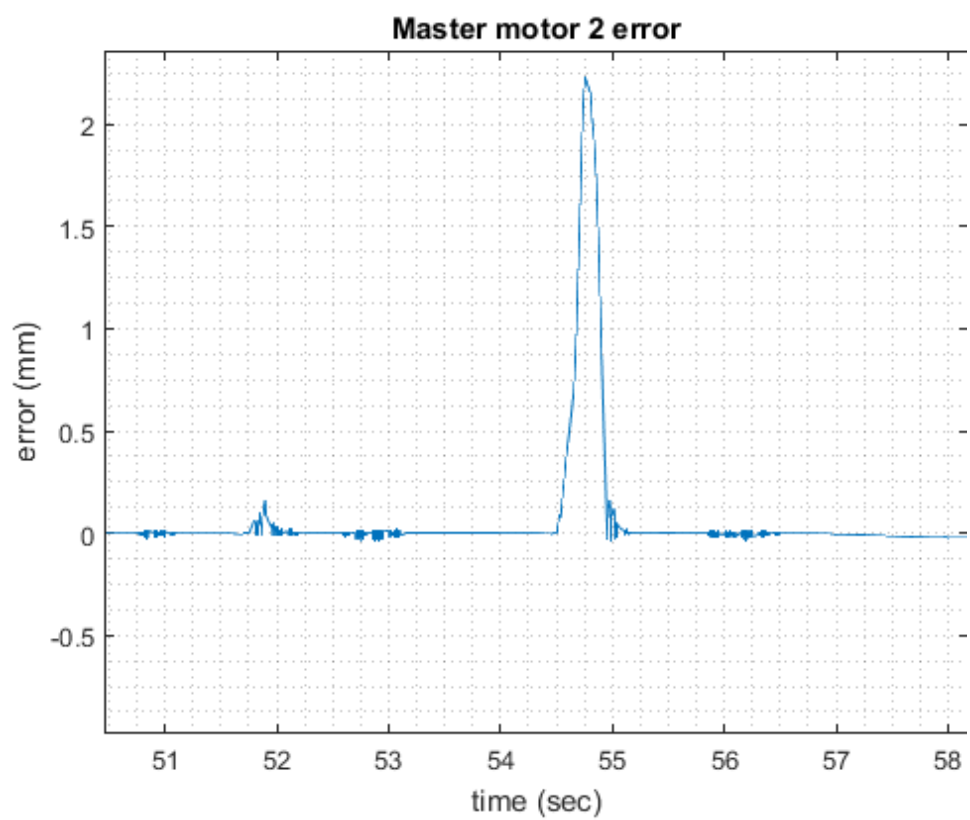


Figure 7.32. Master Motor 2 error.

The increase of the supply voltage proved to render the delays of the system zero. Thus the two control schemes seem to be equivalent to each other from this aspect (transparency is achieved). Nevertheless, more experiments of different nature have to be conducted to examine whether or not these two methods are equivalent. However, these experiments will be presented to the next installment.

7.2 Experiment 2 Target – Experiment

The purpose of this experiment is to inquire whether or not the user can reach specific targets using the Classic EPP and the Biomechatronic EPP. Moreover, it has to be tested whether the Biomechatronic EPP amends the Proprioception of the user compared to the Classic EPP. Before the experimental results will be presented, a protocol of the experimental procedure should be stated. The objective of this protocol is to render the experiment repeatable and the results less arduous to process. Thus, the protocol of the experiment will be presented^[16-23].

Target Experiment Protocol

For this experiment two people are required. The first one is the supervisor of the experiment and the second is the participant to the experiment.

The supervisor of the experiment will operate the ControlDesk environment, while the ControlDesk window will be recorded. The ControlDesk environment is presented on figure 7.33.

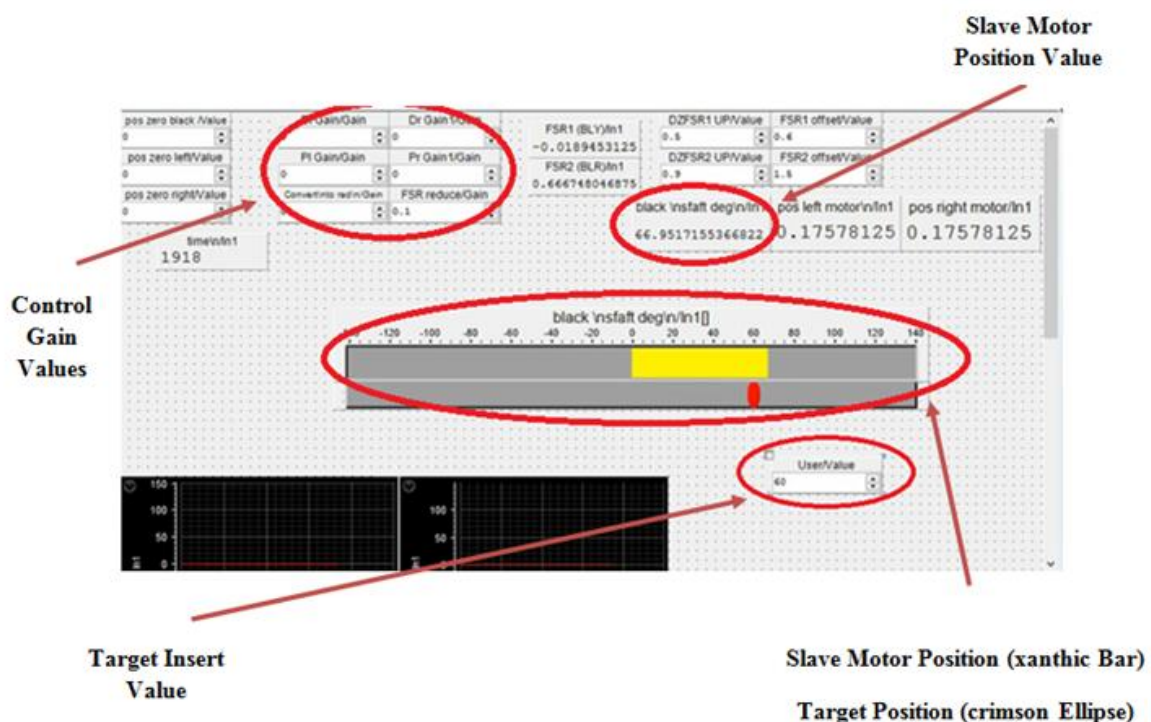


Figure 7.33. ControlDesk environment for the supervisor.

The supervisor of the experiment from the Target Insert Value can change the position of the target (crimson ellipse) and the participant has to apply the necessary force to the FSR sensors to rotate the slave motor to the desired target. The position of the motor is connected

to the bar instrument (xanthic bar), thus, the user is provided with visual feedback of the slave motor's position.

The experimental stages are the following.

Biomechatronic EPP

- The supervisor connects the DS1103 to the PC using the optical fiber and turns on the ControlDesk environment. Then the control gains of the system and various parameters of the system are adjusted from the environment real – time and finally the power supply is turned on.
- The supervisor makes a short test to reassure that everything works properly and lets the participant take the FSR sensors. Then he presses the record button as it is presented on figure 7.34.

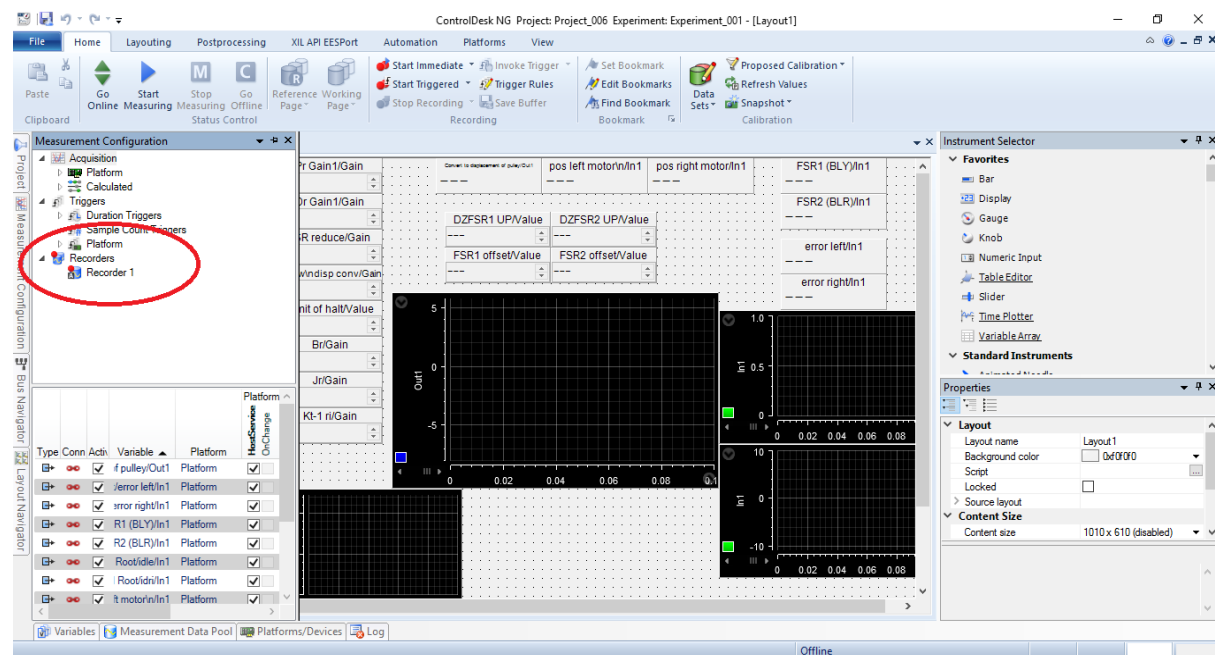


Figure 7.34. Record button on ControlDesk 5.6.

• Phase 1

The supervisor inserts a target value to the User/Value input box of ControlDesk while the participant tries to reach the target. During this phase the participant **has 20 seconds to reach the target**, otherwise his attempt is considered a failure and the target changes position. If the participant succeeds reaching the target, the supervisor waits whether the participant **is able to stay at least 5 seconds on the target**. If he/she is unable to keep absolutely still, his attempt is considered a failure and the target changes position. The same procedure is repeated for every single target position. The pattern of the targets is unknown to the user and it is up to the supervisor to define its route, so that the participant is not mentally prepared for the forces that must be applied and to which direction.

• Phase 2

The ellipse and the bar of the ControlDesk increase in size. The supervisor inserts a target value to the User/Value input box of ControlDesk while the participant tries to reach the target. During this phase the participant **has 15 seconds to reach the target**, otherwise his attempt is considered a failure and the target changes position. If the participant succeeds in reaching the target, the supervisor waits if the participant **is able to stay at least 8 seconds on the target**. If he/she is unable to keep absolutely still, his attempt is considered a failure and the target changes position. The same procedure is repeated for every single target position. The pattern of the targets is unknown to the user and it is up to the supervisor to define its route, so that the participant is not mentally prepared for the forces that must be applied and to which direction. The parameters that must be evaluated are the following [24-27].

- 2) Movement time to the target
- 3) Dwell time to the target
- 4) Number of successes and failures
- 5) Error rate of the final position reached from the actual target

Classic EPP

The supervisor connects the FSR sensors to the Bowden Cables of the setup (figure 3.17 chapter 3. Design and Implementation of the Reference Input).

- Then the supervisor sets the gains presented on figure 32 to zero that are related to the Biomechatronic EPP.

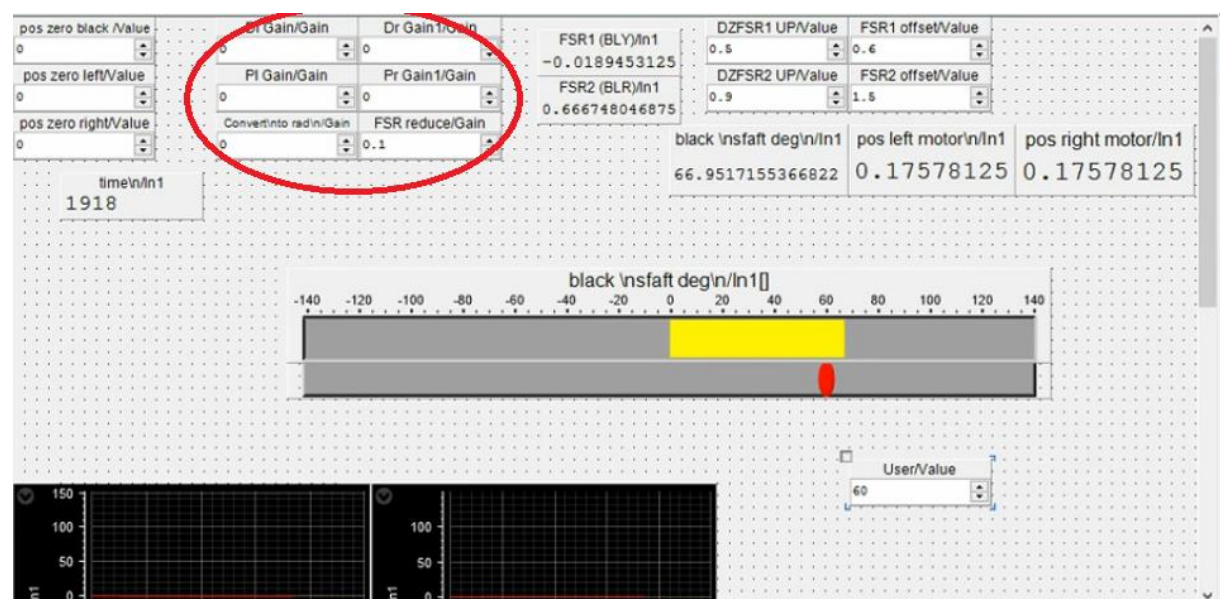


Figure 7.35. Setting the Control Gains of the Master Motors to zero for the Classic EPP target position experiment.

The phases of the test are the same with the Biomechatronic EPP. It has to be noted that the same target position pattern that was used for the previous stage of the experiment remains the same. Moreover, the parameters that must be evaluated remain the same as well.

With the protocol defined, an experiment will be presented along with the evaluation process of its results.

7.3 Case study Presentation – Pilot Test

During this case study the pattern of positions that the target reached are presented on the following table. Moreover, in this table is presented the index of difficulty of the experiment, which is a way to calculate the difficulty of the experiment ^[24-27]. The index of difficulty can be calculated using the following equation:

$$ID = \log_2\left(\frac{A}{W} + 1\right) \quad (7.7)$$

A is the value of the target, for instance if the target is positioned to 90 degrees, then A is equal to 90. W is the width of the target. For the environment of figure 7.33 the width of the target (crimson ellipse) is approximately 8 degrees. The final results are displayed on table 7.6. The desired ID range must be $2 \div 8$ ^[24].

Table 7.6 Case Study Target Positions

Target Positions		
s/n	Position [deg]	ID
1	90	3.792558
2	5	0.777608
3	25	2.192645
4	-95	3.86507
5	-40	2.747234
6	10	1.280108
7	-35	2.584963
8	65	3.36257
9	-50	3.025535
10	-40	2.747234
11	100	3.934112
12	-80	3.635589
13	70	3,459432
14	30	2.402098
15	-30	2.402098

The recordings of each phase of the test are included on the CD of this thesis. The results are displayed to the following figures for each phase of the case study. The more valuable data are presented on the target and slave motor position curves, because the route the participant followed is presented. Furthermore, the FSR sensor responses, the slave motor current, and the master motor closed loop error and response are presented. After the display of each case, the evaluation of the experimental results will be presented.

➤ **Biomechatronic EPP Phase 1**

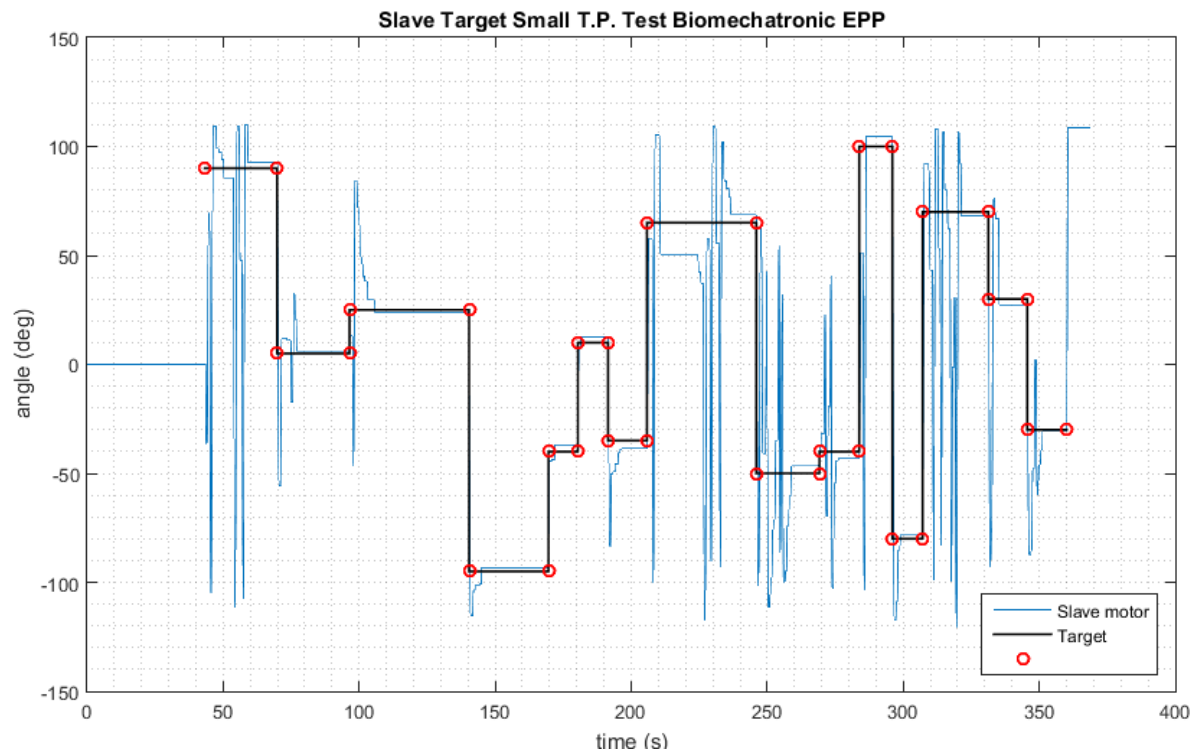


Figure 7.36. Slave motor path during the phase 1 of Biomechatronic EPP test.

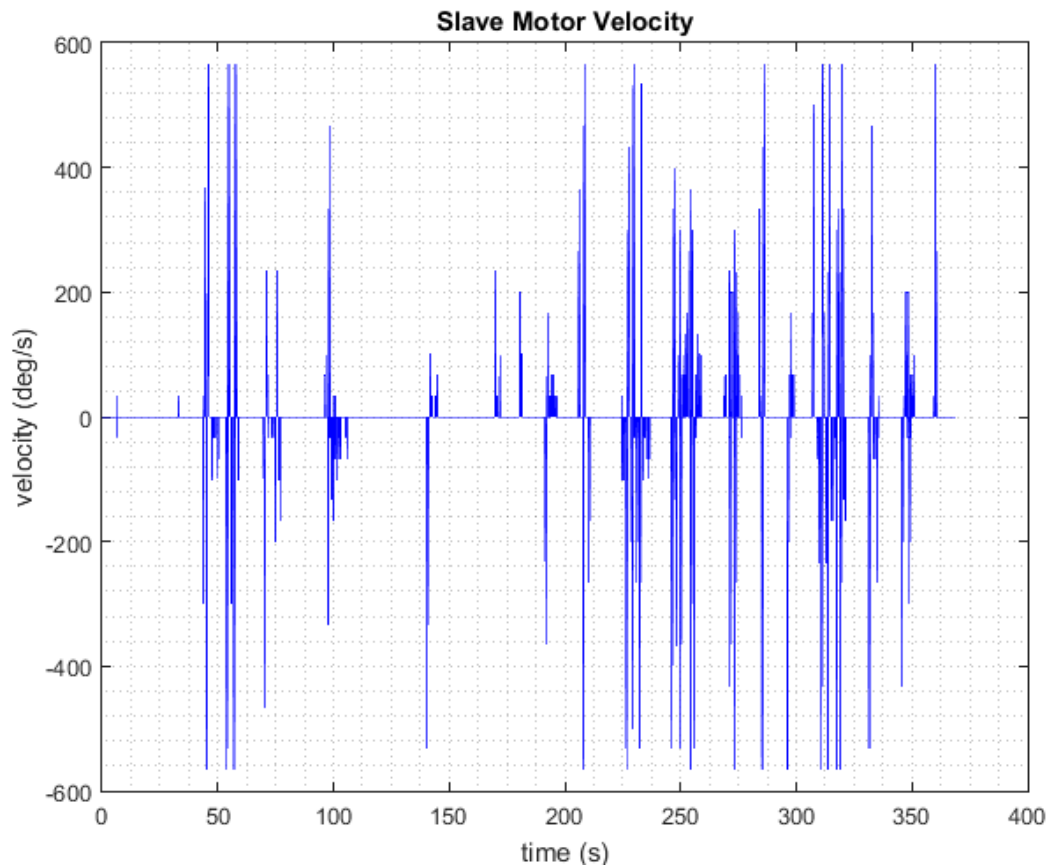


Figure 7.37. Slave motor velocity during the phase 1 of Biomechatronic EPP test.

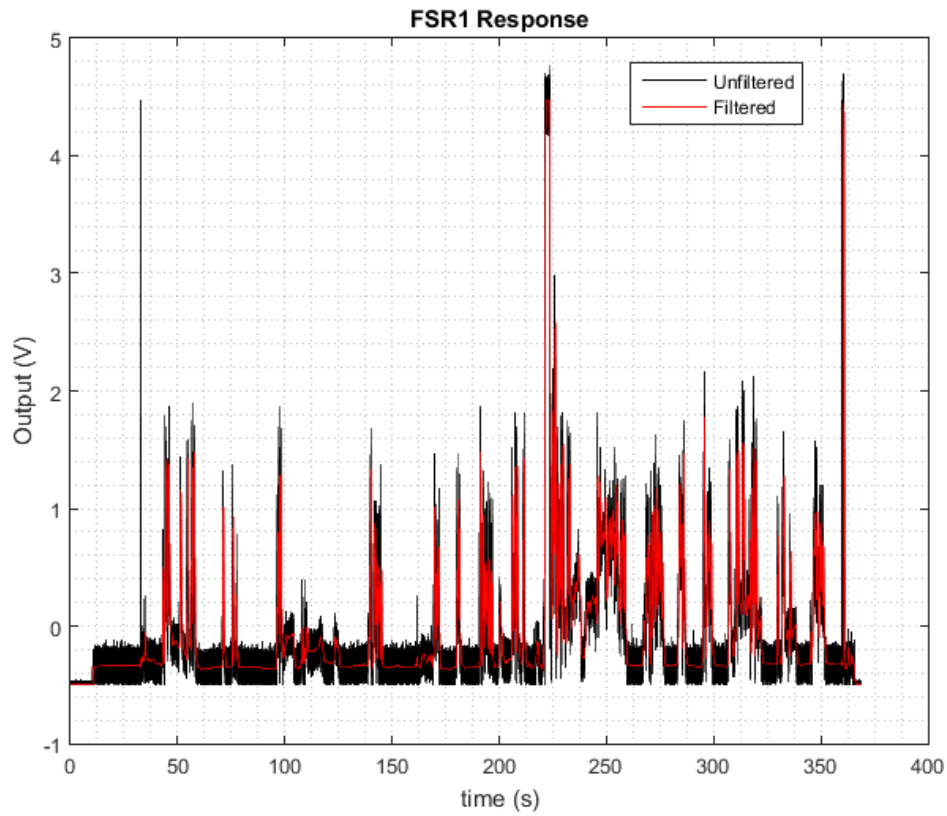


Figure 7.38. FSR 1 output during the phase 1 of Biomechatronic EPP test.

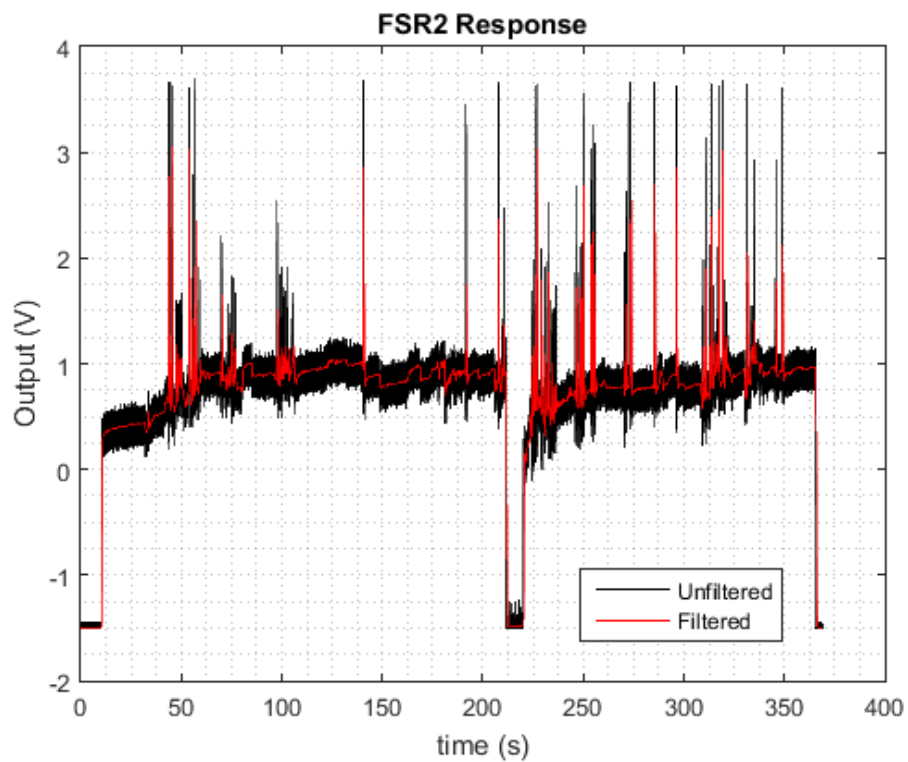


Figure 7.39. FSR 2 output during the phase 1 of Biomechatronic EPP test.

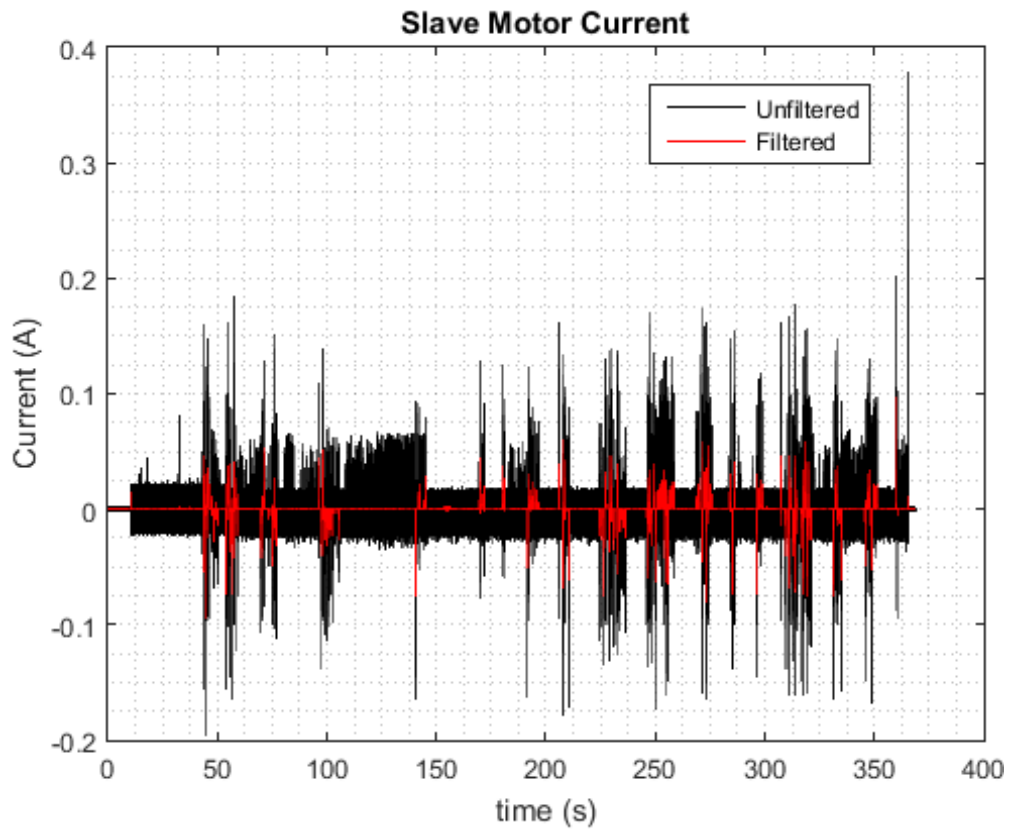


Figure 7.40. Slave motor current during the phase 1 of Biomechatronic EPP test.

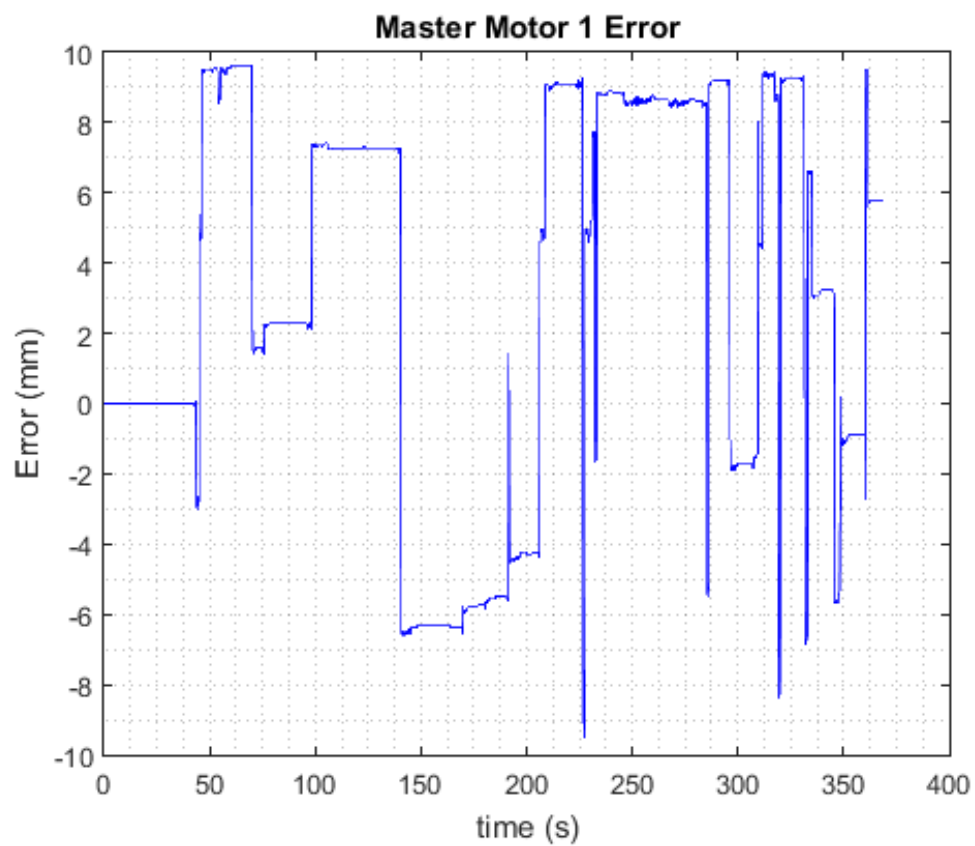


Figure 7.41. Master 1 Motor error during the phase 1 of Biomechatronic EPP test.

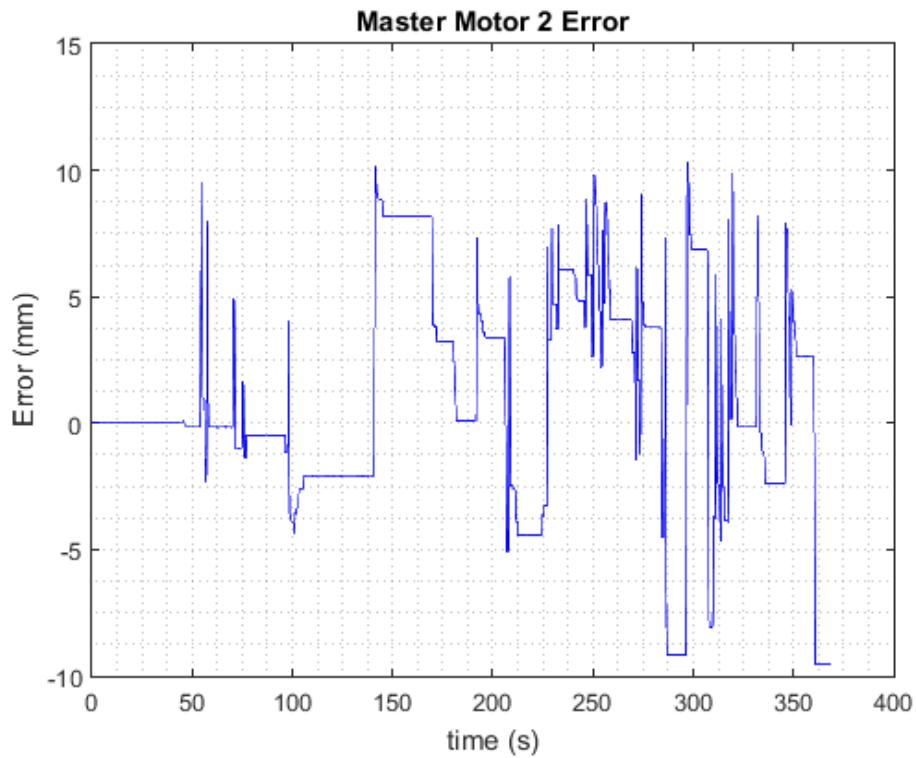


Figure 7.42. Master 2 Motor error during the phase 1 of Biomechatronic EPP test.

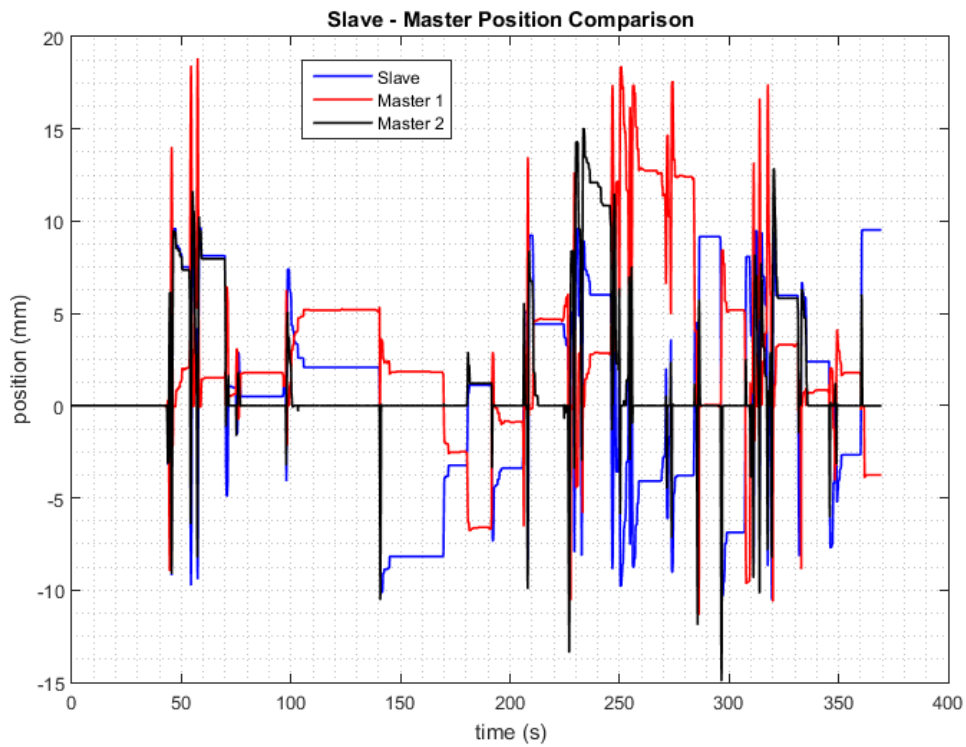


Figure 7.43. Slave - Master Motor positioning during the phase 1 of Biomechatronic EPP test.

➤ **Biomechatronic EPP Phase 2**

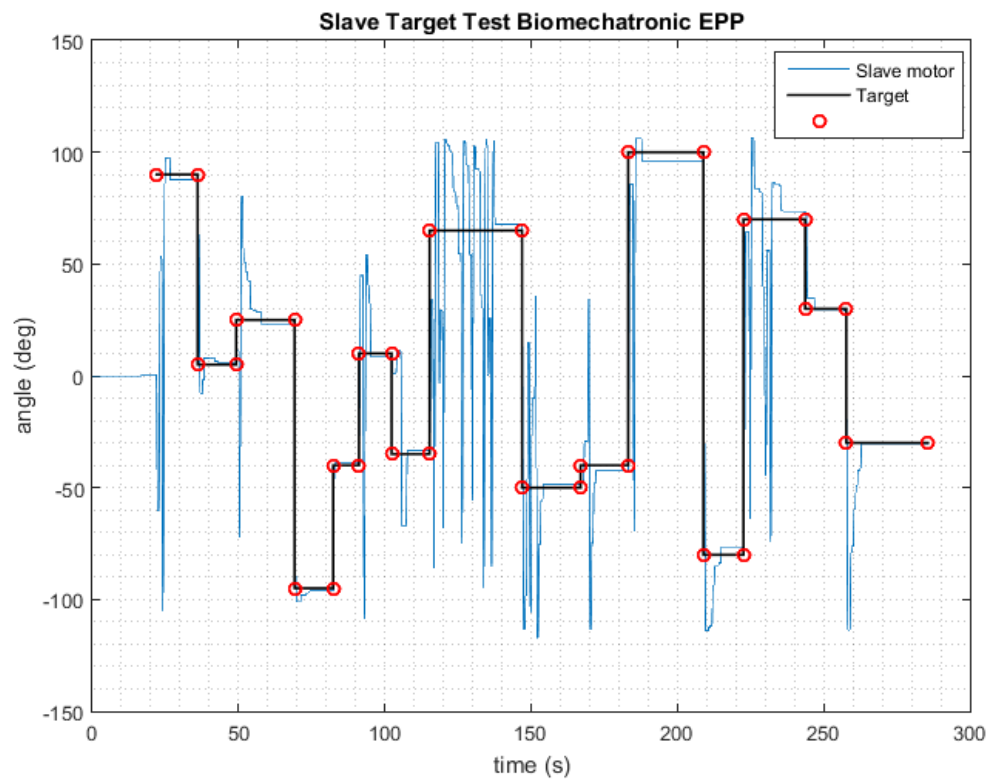


Figure 7.44. Slave motor path during the phase 2 of Biomechatronic EPP test.

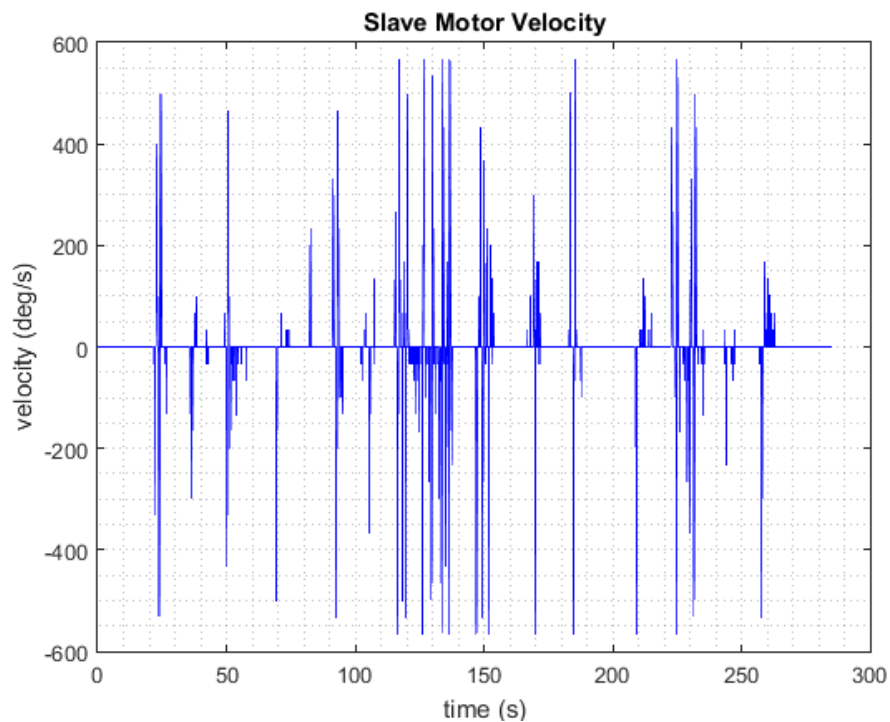


Figure 7.45. Slave motor velocity during the phase 2 of Biomechatronic EPP test.

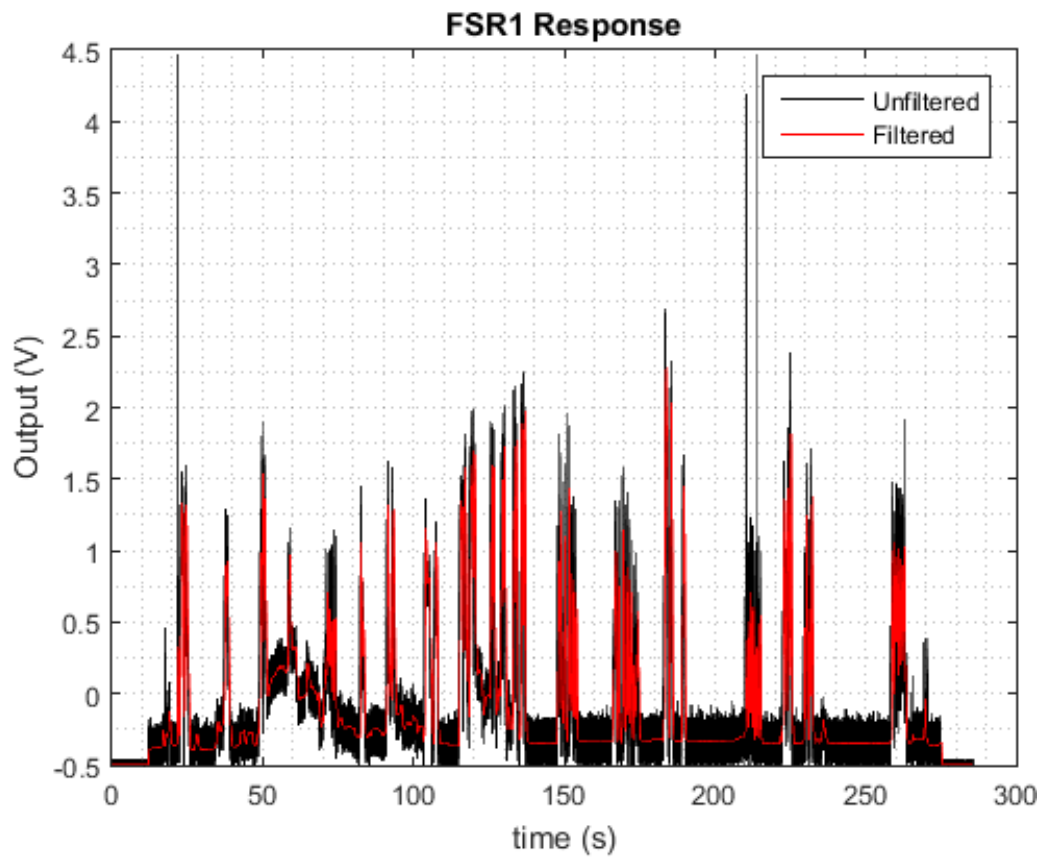


Figure 7.46. FSR 1 output during the phase 2 of Biomechatronic EPP test.

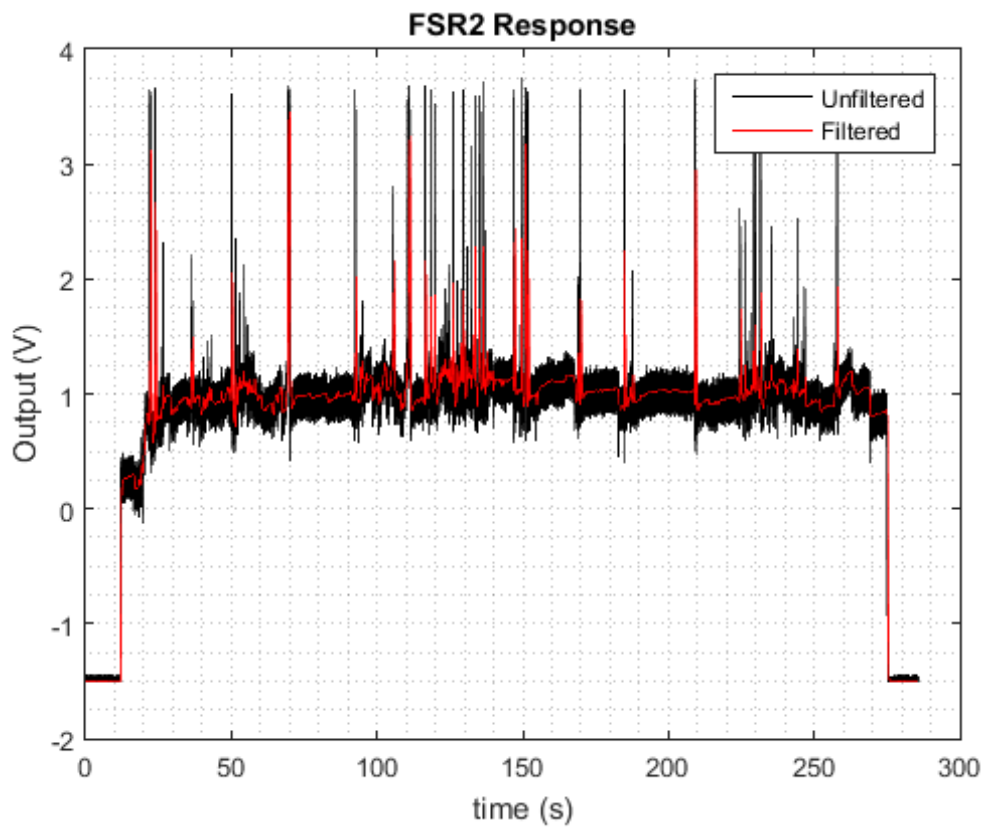


Figure 7.47. FSR 2 output during the phase 2 of Biomechatronic EPP test.

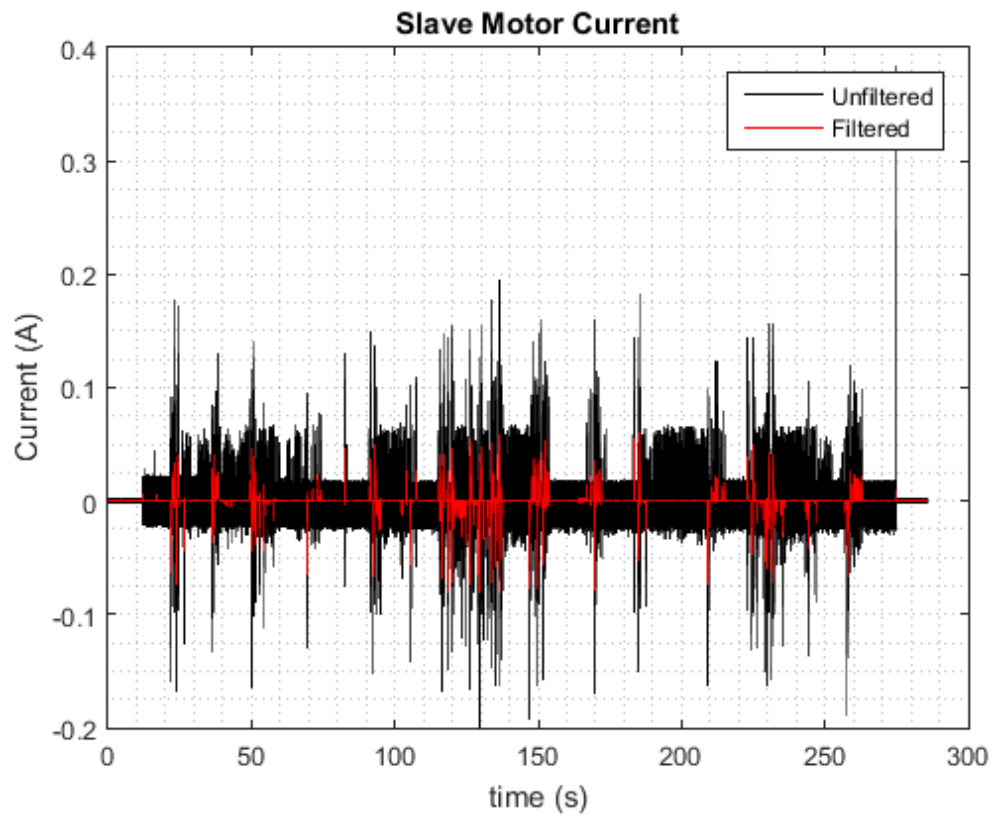


Figure 7.48. Slave motor current during the phase 2 of Biomechatronic EPP test.

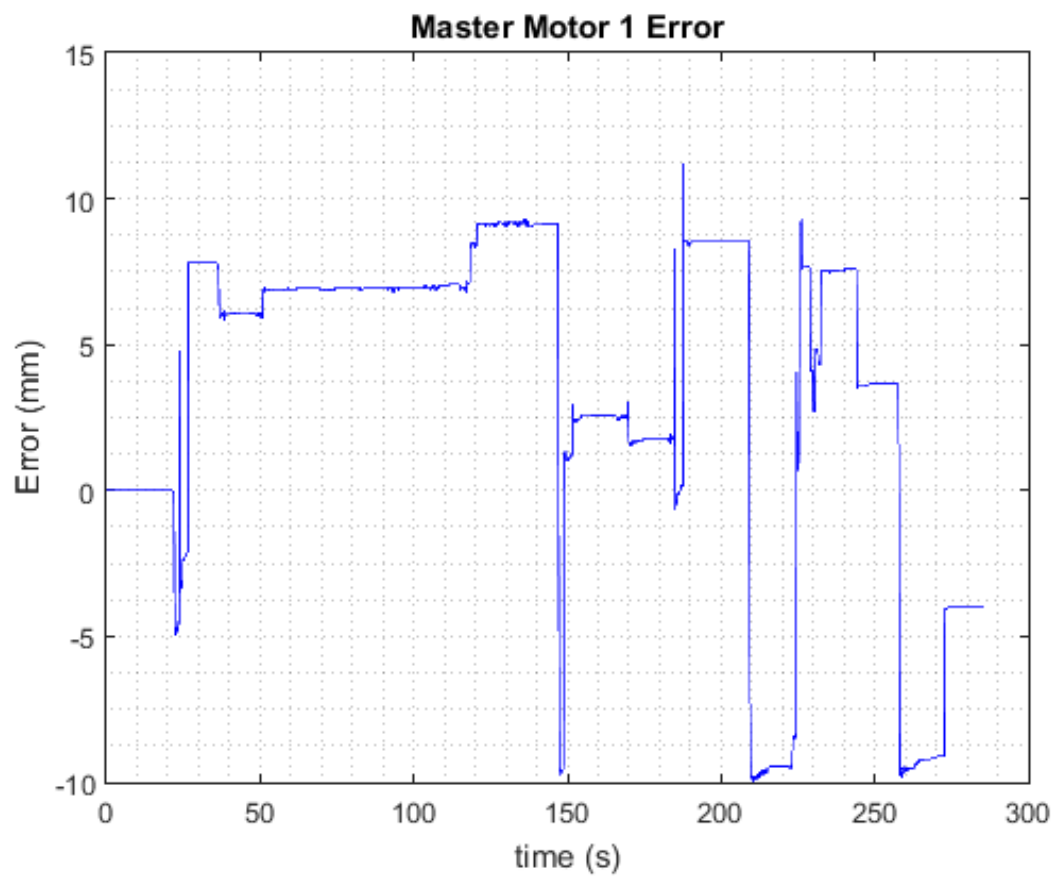


Figure 7.49. Master 2 Motor error during the phase 2 of Biomechatronic EPP test.

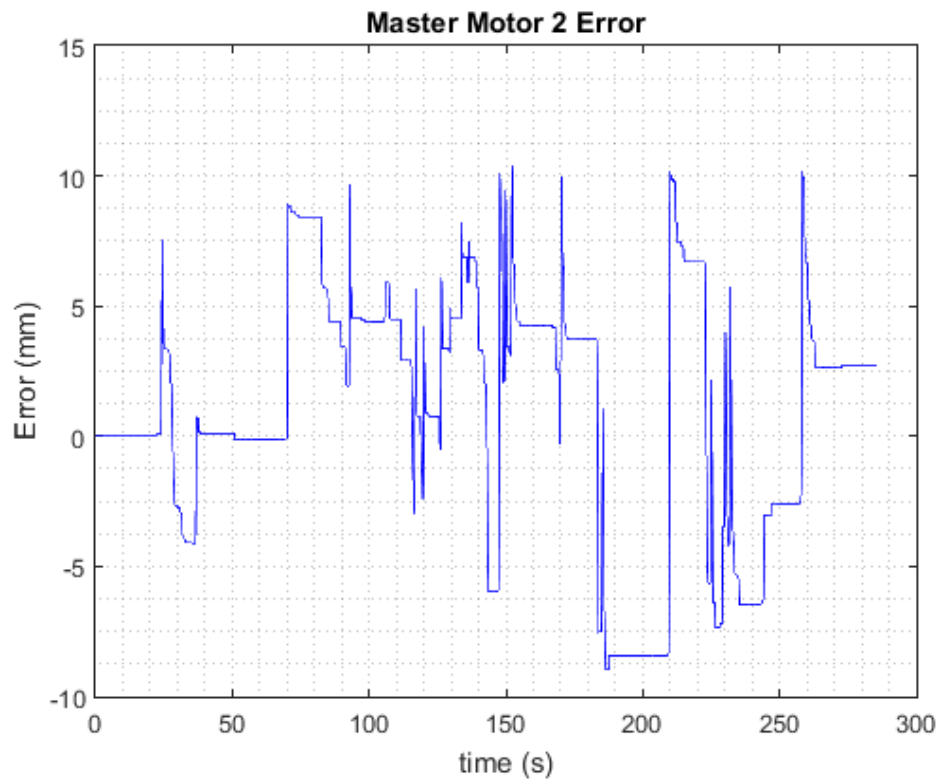


Figure 7.50. Master 1 Motor error during the phase 2 of Biomechatronic EPP test.

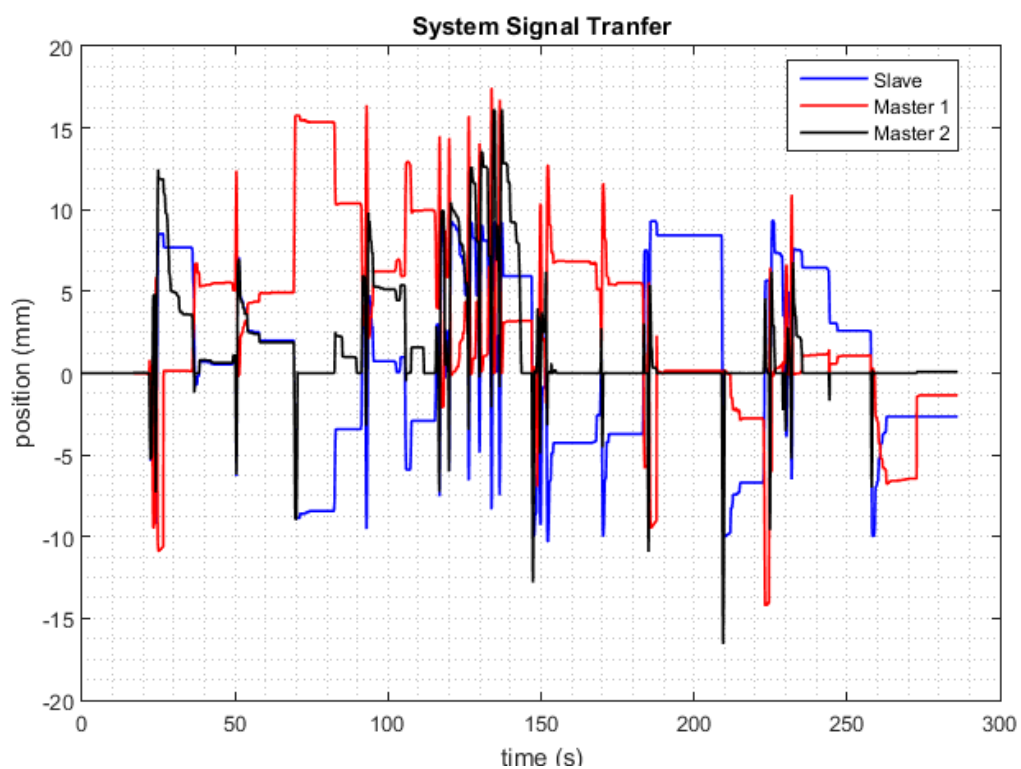


Figure 7.51. Slave - Master Motor positioning during the phase 2 of Biomechatronic EPP test.

➤ **Classic EPP Phase 1**

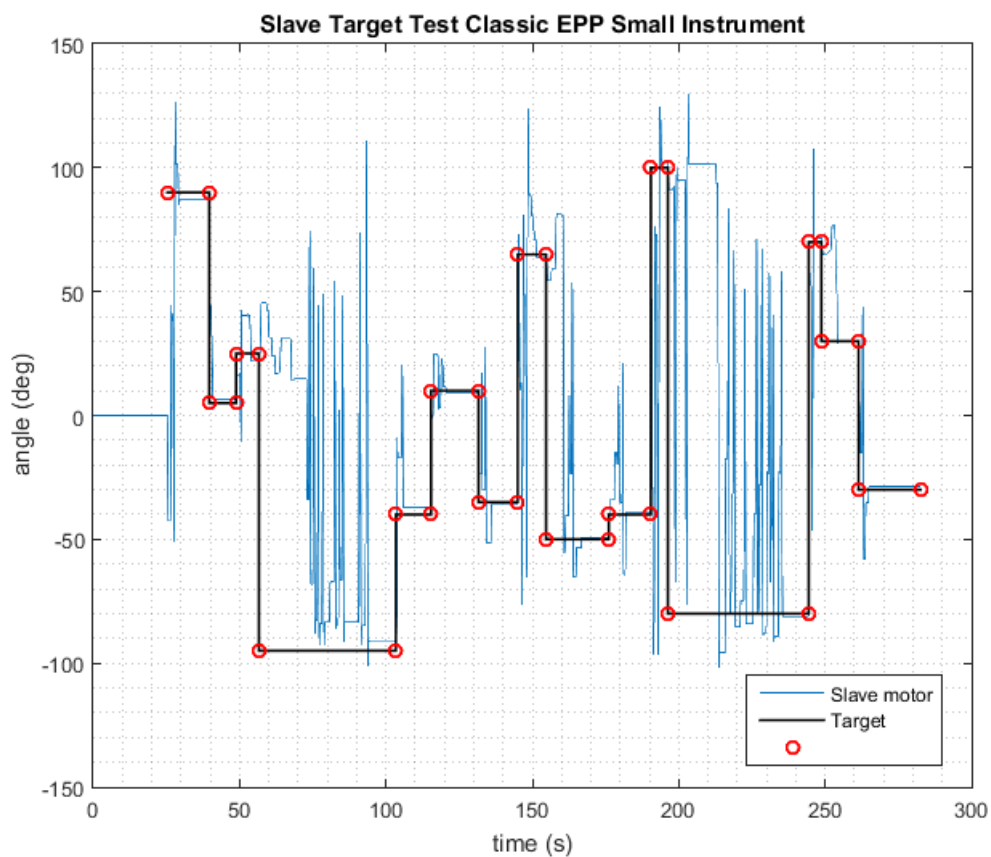


Figure 7.52. Slave motor path during the phase 1 of Classic EPP test.

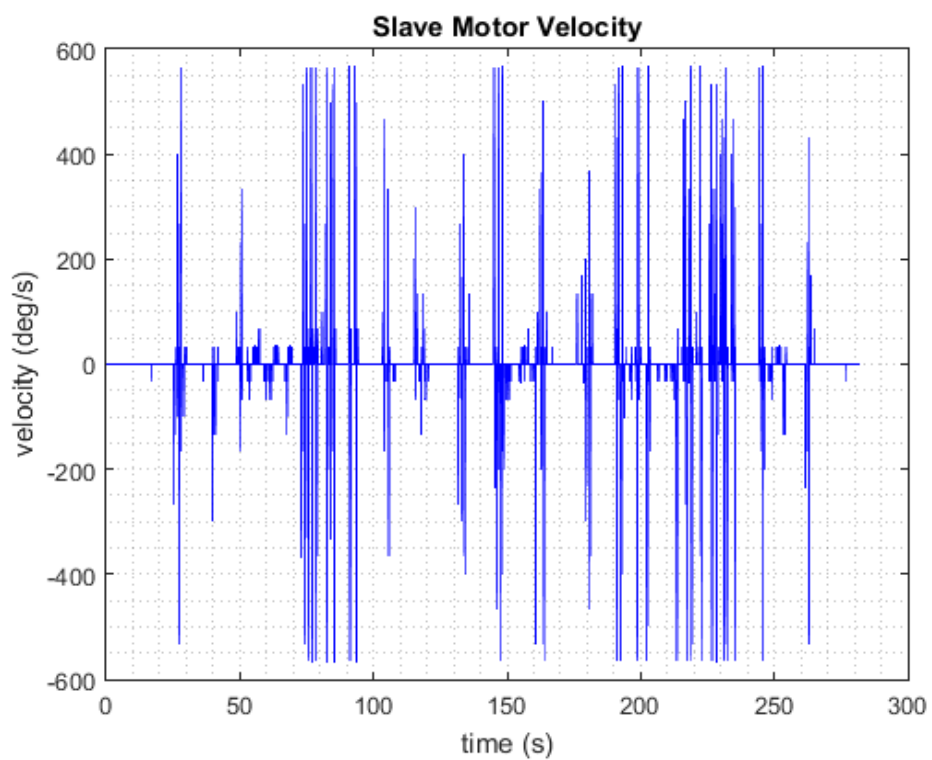


Figure 7.53. Slave motor velocity during the phase 1 of Classic EPP test.

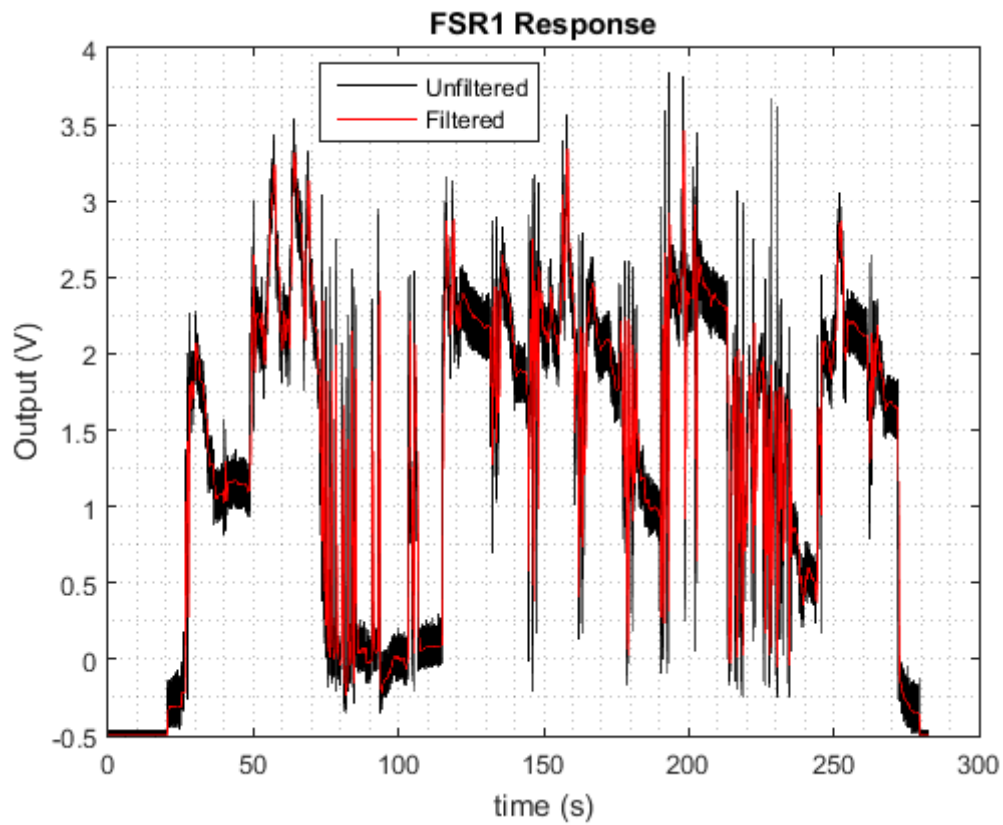


Figure 7.54. FSR 1 output during the phase 1 of Classic EPP test.

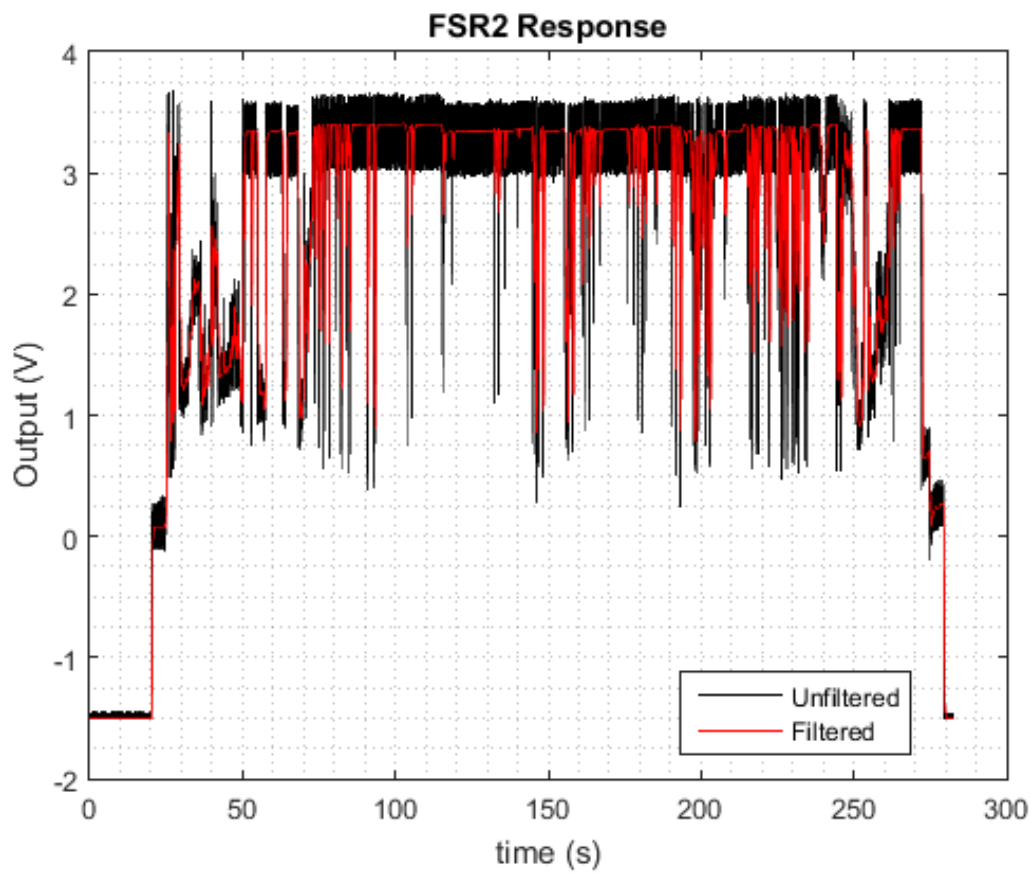


Figure 7.55. FSR 2 output during the phase 1 of Classic EPP test.

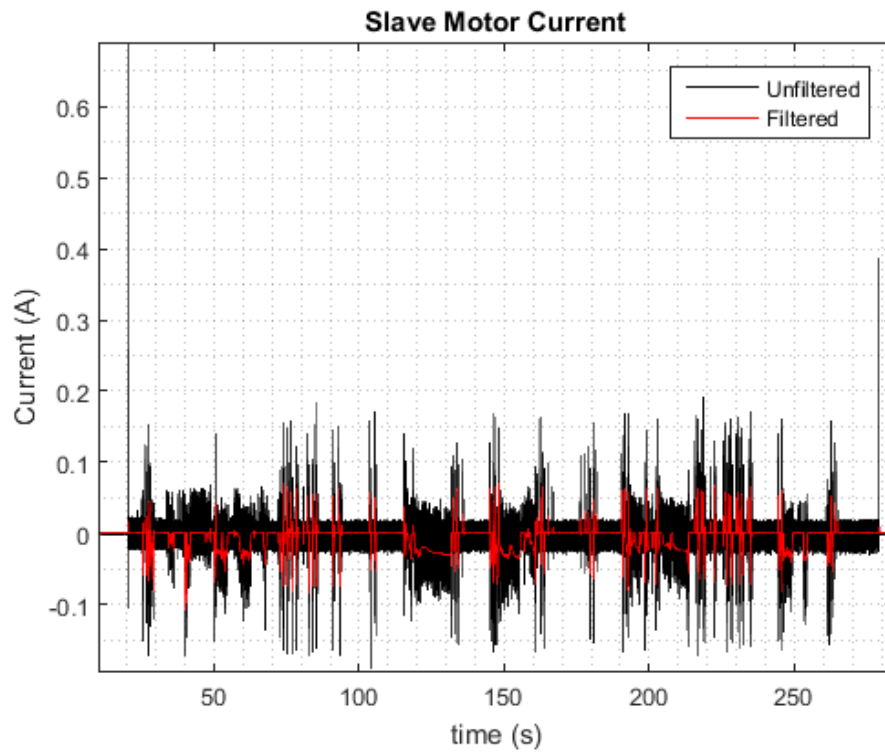


Figure 7.56. Slave motor current during the phase 1 of Classic EPP test.

➤ **Classic EPP Phase 2**

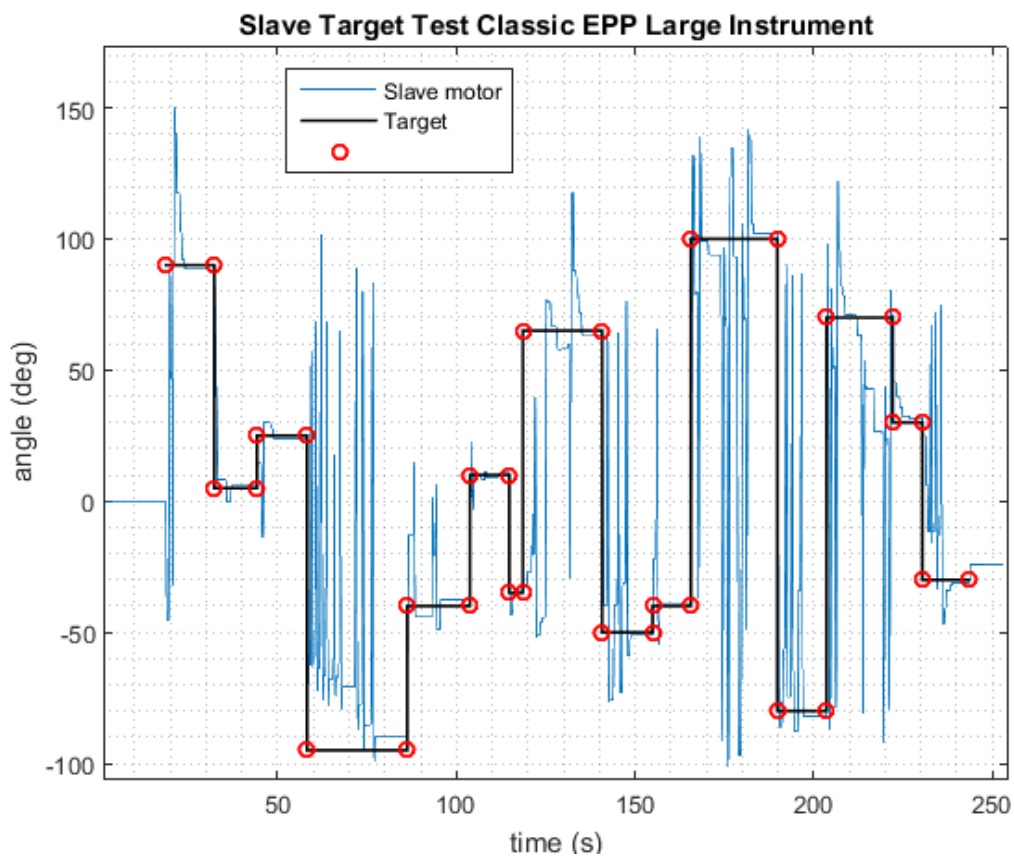


Figure 7.57. Slave motor path during the phase 2 of Classic EPP test.

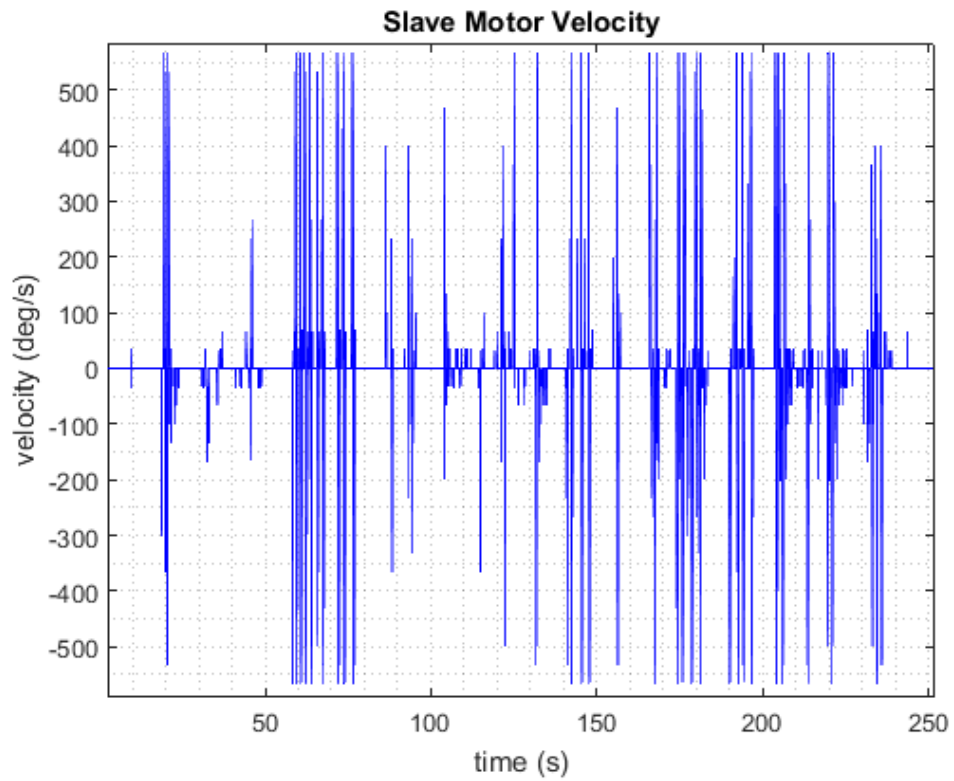


Figure 7.58. Slave motor velocity during the phase 2 of Classic EPP test.

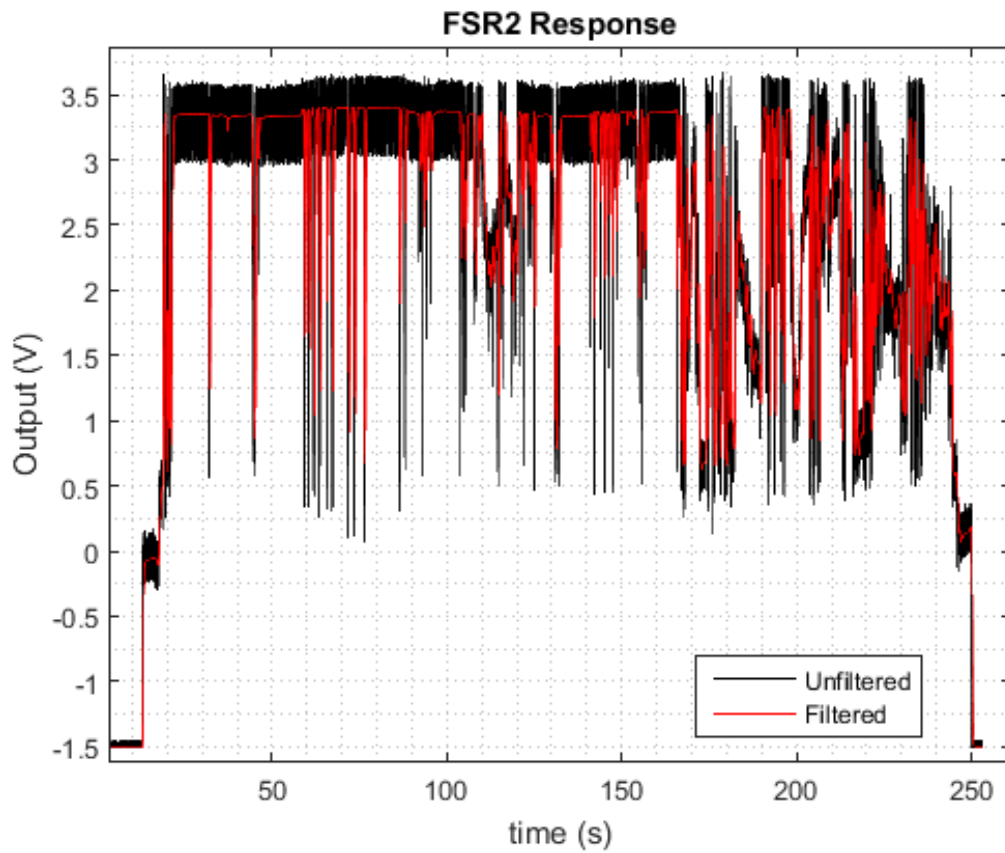


Figure 7.59. FSR 1 output during the phase 2 of Classic EPP test.

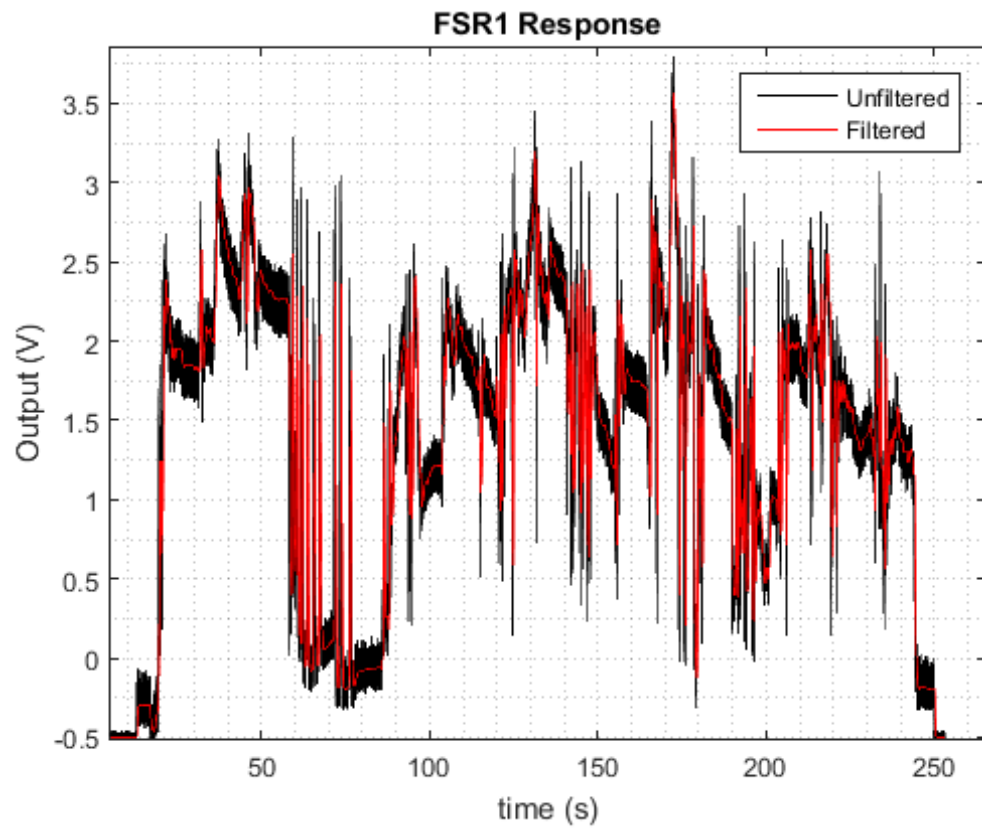


Figure 7.60. FSR 2 output during the phase 2 of Classic EPP test.

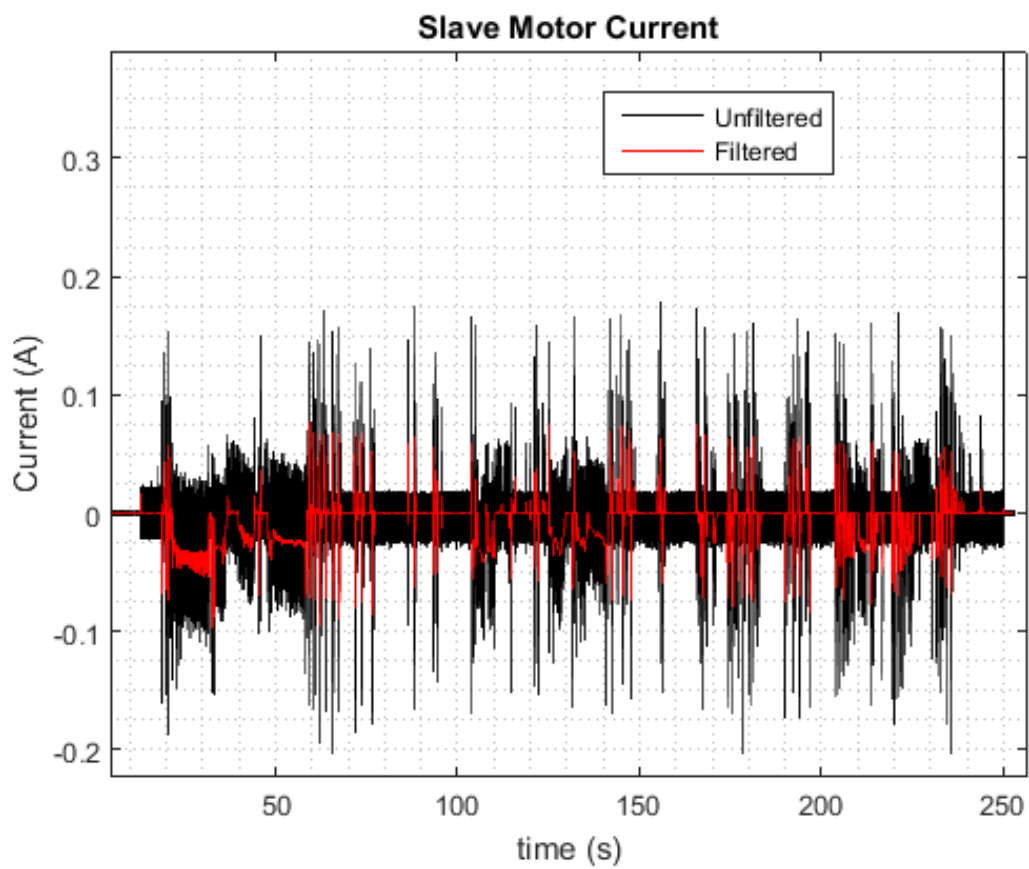


Figure 7.61. Slave motor current during the phase 2 of Classic EPP test

7.4 Experimental Data Evaluation

After the experimental results were obtained, then they were evaluated. The parameters that have to be evaluated are the movement time to the target, the time the participant is able to still inside the area of the target, the number of failures and the error between the final reached value and the actual target position. It is important to find a way to represent these data in a way that provides the widest amount of information for the experiment evaluation. Thus, it was decided that the best way to compare each phase is the one presented on the following figures. The independent variable is related to the Biomechatronic EPP experiment and the dependent variable is related to the Classic EPP experiment. The blue lines represent the constraints that were determined for each phase at the protocol. The black line ($y = x$) represents the case that the two experiments have data that match perfectly, meaning that the two control schemes are equivalent. For the movement time comparison, with the enumeration of the trigonometric circle, the points that are on the third quadrant are qualified as success for both schemes. If the points are on the second quadrant, then during the Classic EPP experiment the movement time constraint is breached and the Classic EPP attempt is considered a failure, while the Biomechatronic EPP attempt is considered a success. The opposite case is the fourth quadrant. If a point lies there, then during the Biomechatronic EPP experiment the movement time constraint is breached and the Biomechatronic EPP attempt is considered a failure, while the Classic EPP attempt is considered a success. If a point lies into the first quadrant, then both the Biomechatronic EPP attempt and the Classic EPP attempt are considered a failure. Finally, if a point lies below the black line, then the participant moved to the respective target faster during the Classic EPP time. Figure 7.62 renders pellucid that for the phase 1 the Classic EPP has slightly better results than the Biomechatronic EPP (more points below the black line). However at two occasions the participant failed to reach the target in time during the Classic EPP time, while in Biomechatronic EPP he or she failed only once. Moreover, figure 7.63 reveals that again the participant fails more often during the Classic EPP, while the number of successes is almost equal for both cases. In addition the points are near the black line, ergo the two schemes from the aspect of movement time could be considered equivalent.

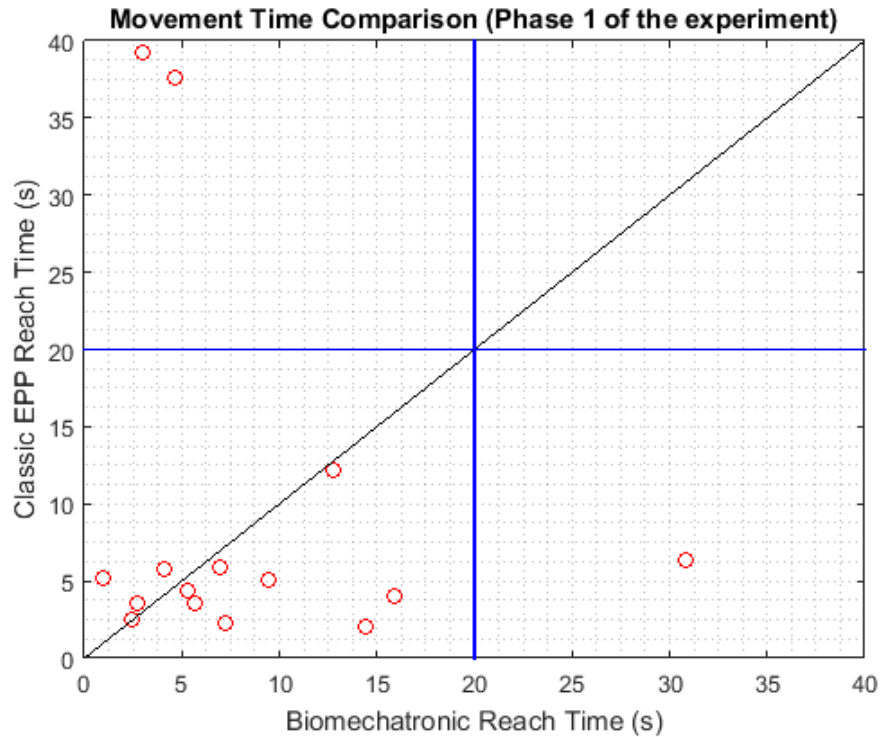


Figure 7.62. Movement time comparison curve (phase 1).

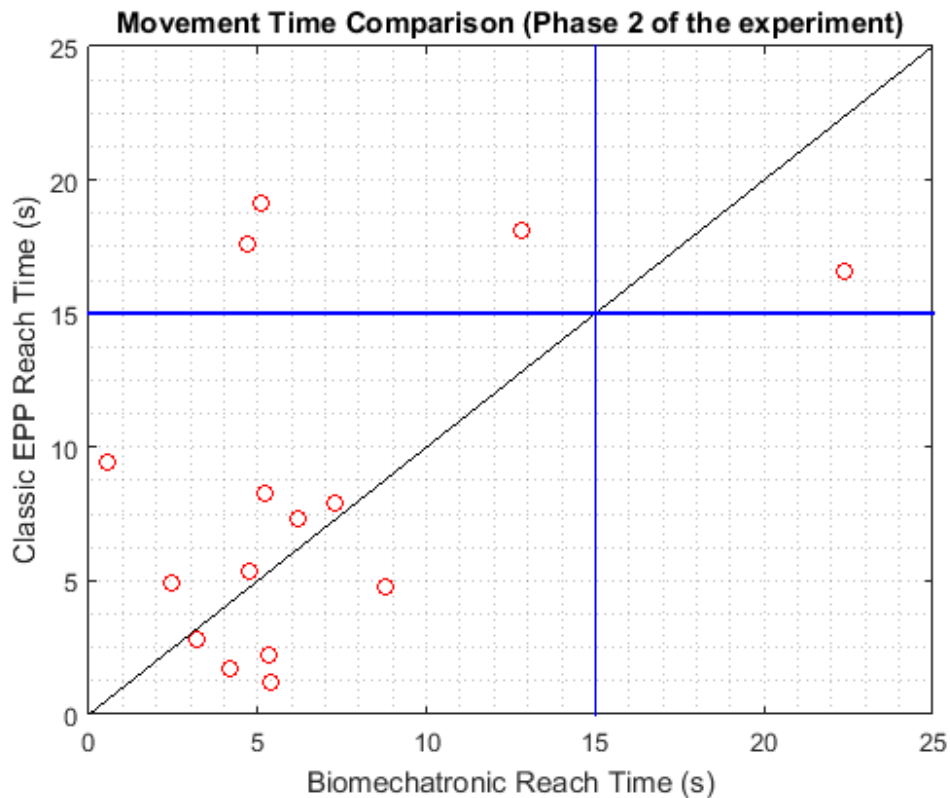


Figure 7.63. Movement time comparison curve (phase 2).

As for the duel time curves (figures 7.64 and 7.65), if the points are on the second quadrant, then during the Biomechatronic EPP experiment the duel time constraint is breached and the Biomechatronic EPP attempt is considered a failure, while the Classic EPP attempt is

considered a success. The opposite case is the fourth quadrant. If a point lies there, then during the Classic EPP experiment the duel time constraint is breached and the Classic EPP attempt is considered a failure, while the Biomechatronic EPP attempt is considered a success. If a point lies into the fourth quadrant, then both the Biomechatronic EPP attempt and the Classic EPP attempt are considered a failure while points on the first quadrant are considered a success in both cases. Finally, if a point lies below the black line, then the participant stayed to the respective target longer during the Classic EPP time. For the two phases the participant could stay longer on the target with the Biomechatronic EPP scheme. Moreover, the number of failures for the Classic EPP increased dramatically. Thus, the Biomechatronic EPP is proved to be better than the Classic EPP to stay on target. However this result should be connected to the lack of sense of the user during the experiment. Thus, the participant feels less resistance from the master motors and he/she is able to stay longer at the target effortlessly, while at the Classic EPP the participant has to balance the torque of the slave motor, which is much higher than the torque of the master motors. The error rate curves (which is the difference between the position reached and actual target when the yellow bar is within the width of the red ellipse which is the target) of figures 7.66 and 7.67 reveal that in both cases the error is insignificant, because the participant is able to rotate the slave motor to the desired position with very low errors in degrees. Thus, the open loop controller of the slave motor as it was designed is efficient.

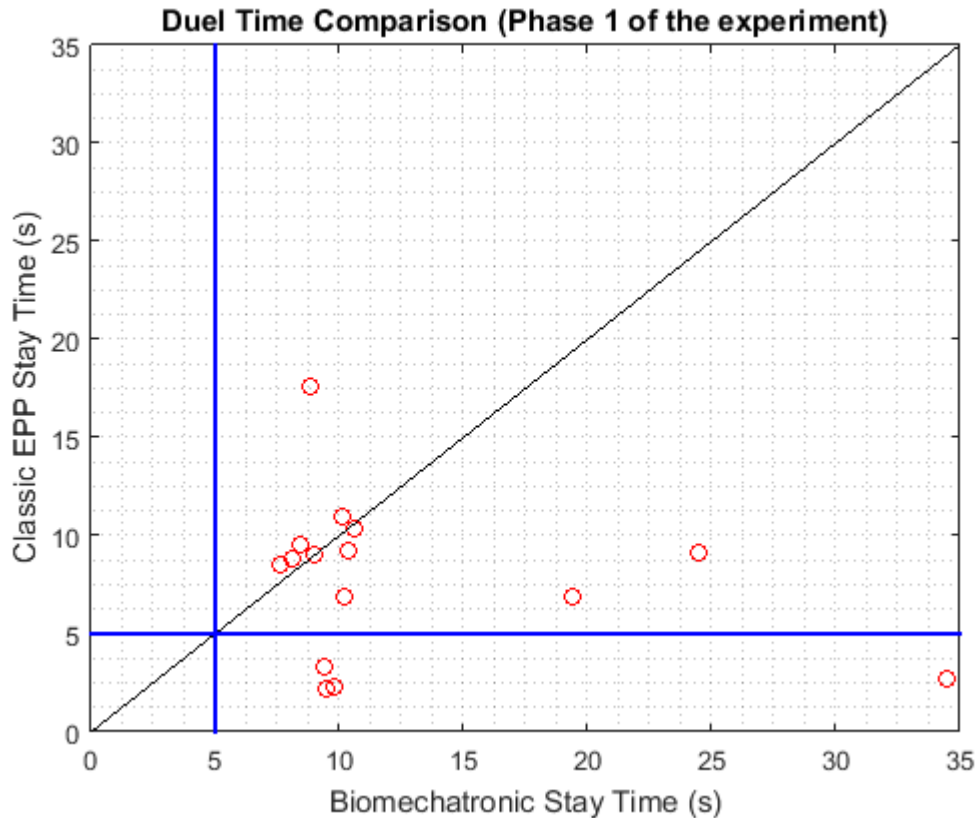


Figure 7.64. Duel time comparison curve (phase 1).

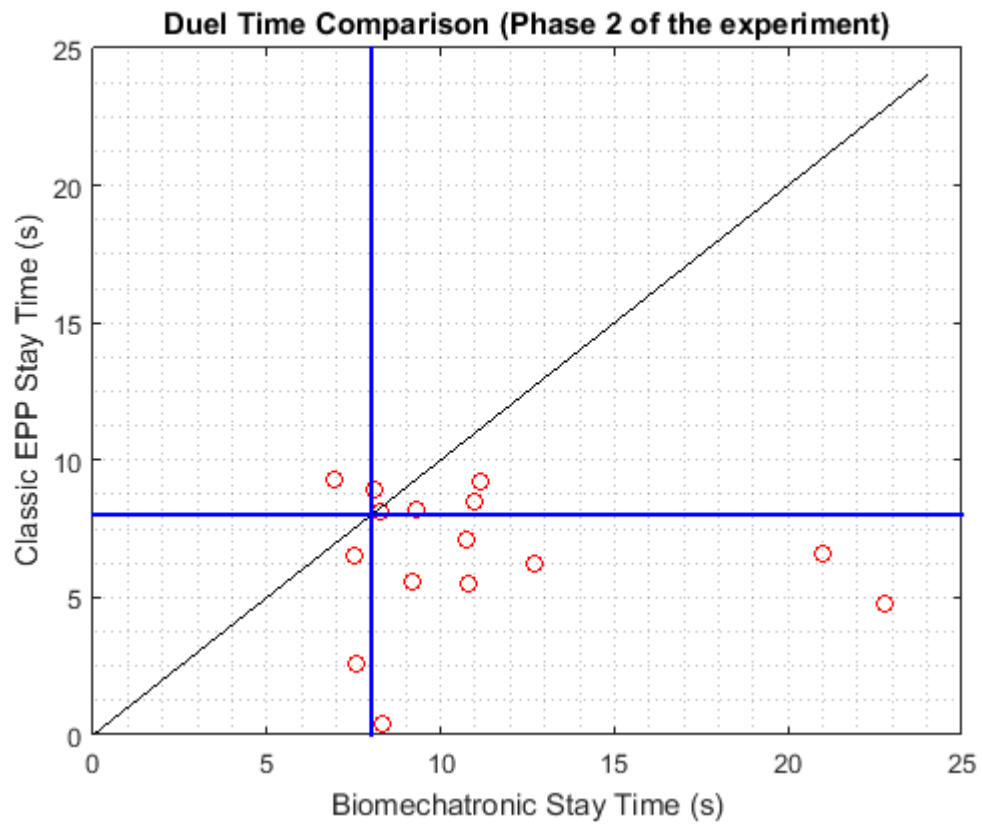


Figure 7.65. Duel time comparison curve (phase 2).

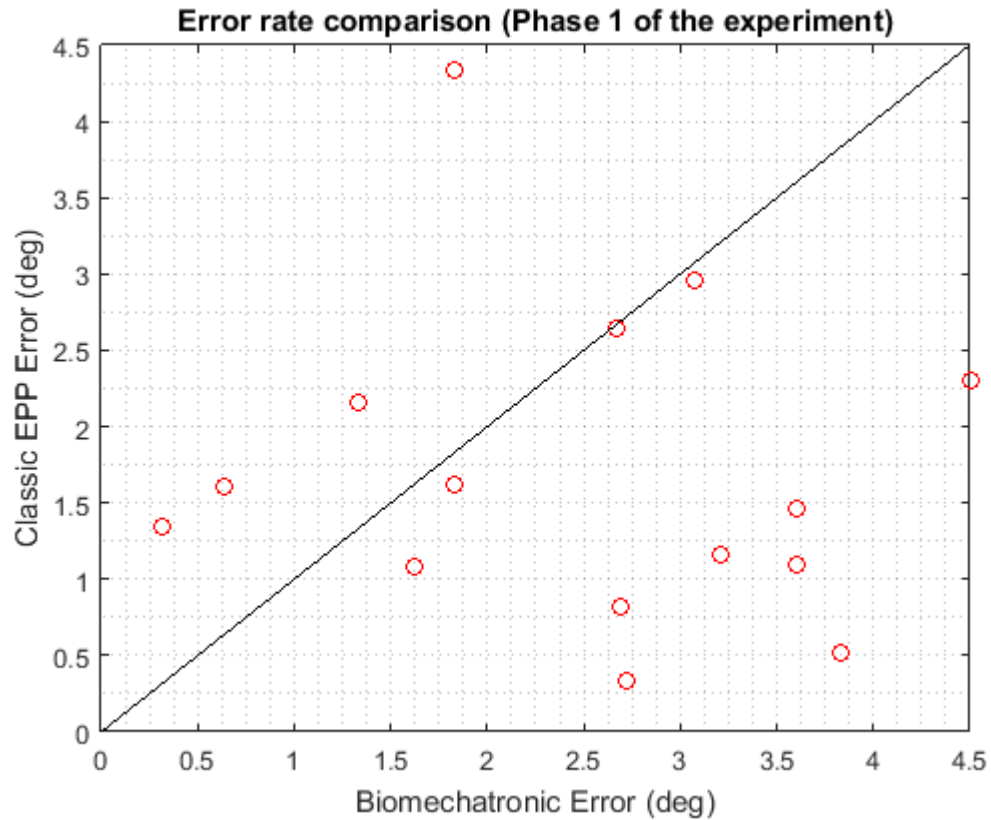


Figure 7.66. Reach target error (phase 1).



Figure 7.67. Reach target error (phase 2).

Moreover, it has to be delved into whether the two schemes have results that are statistically the same. The question whether the samples of the two experiments are statistically the same, is equivalent to the question whether the two samples belong to the same probabilistic set. Three conditions are required for a positive answer.

1. The two samples belong to the same distribution

To prove it, the Kolmogorov –Smirnov must be used [11]. If the variable of equation (7.8) is defined:

$$D_{n,m} = \sup |F_{1,n}(x) - F_{2,m}(x)| \quad (7.8)$$

With $F_{1,n}$, $F_{2,m}$ distribution functions of the first and second sample respectively (n , m the number of samples), then the null hypothesis and the alternative hypothesis are as follows:

$$H_o : D_{n,m} > c(a) \sqrt{\frac{n+m}{nm}} \quad (7.9)$$

$$H_1 : D_{n,m} \leq c(a) \sqrt{\frac{n+m}{nm}} \quad (7.10)$$

$$c(a) = \sqrt{-\frac{1}{2} \ln\left(\frac{a}{2}\right)} \quad (7.11)$$

a is the confidence level of the test. If the null hypothesis is rejected, then the two samples do not belong to the same distribution. For this test the Matlab command kstest2 will be used.

2. The two samples have the same standard deviation

For this test the null hypothesis and the alternative hypothesis are as follows ^[10]:

$$H_o : \sigma_1^2 - \sigma_2^2 = 0 \quad (7.12)$$

$$H_1 : \sigma_1^2 - \sigma_2^2 \neq 0 \quad (7.13)$$

To examine whether the confidence value bounds are breached the Snedecor's F distribution is used:

$$F_{o_{v_1, v_2}} = \frac{s_1^2}{s_2^2}, \quad v_1 = N_1 - 1, \quad v_2 = N_2 - 1 \quad (7.14)$$

3. The two samples have the same mean value

For this test the null hypothesis and the alternative hypothesis are as follows ^[10]:

$$H_o : \mu_1 - \mu_2 = 0 \quad (7.15)$$

$$H_1 : \mu_1 - \mu_2 \neq 0 \quad (7.16)$$

To examine whether the confidence value bounds are breached the Student distribution is used:

$$t_o = \frac{(\bar{x}_1 - \bar{x}_2) - d_o}{s \sqrt{\left(\frac{1}{N_1}\right) + \left(\frac{1}{N_2}\right)}} \quad (7.17)$$

$$s^2 = \frac{(N_1 - 1)s_1^2 + (N_2 - 1)s_2^2}{N_1 + N_2 - 2} \quad (7.18)$$

N_1 is the number of data of the first sample and N_2 the number of data of the second sample. In this pilot test the number of data is 15. The test requires a specific confidence level. In this case the test will be conducted for confidence level 5%. Moreover, the test is two sided for the standard deviation and for the mean value. The t-distribution is symmetric, however, for the Snedecor's F distribution to calculate the lower bound of the distribution the following equation is required.

$$F_{\frac{1-p}{2}} = \frac{1}{F_{1-\frac{1-p}{2}}} \quad (7.19)$$

The movement time depends on the position of the previous target, thus, there is no point inquiring data such as the mean value and the standard deviation. The reason is that they depend on the experimental pattern decided by the supervisor of the experiment. Nevertheless, the random variables: the error between the actual target position and the position reached and the time the participant is halted to the target have to be examined

whether they belong to the same probabilistic set regardless the scheme that is used is the Classic EPP or the Biomechatronic EPP. In this case these variables are independent from the decision of the supervisor – puppeteer who pulls the strings of the fate of the participant. The tests will be conducted for both the Phase 1 and Phase 2 data. In the following tables the results will be presented for each case.

Table 7.1. Results of statistical tests for Phase 1 duel time random variable.

Phase 1 duel time				
Classic EPP mean \bar{x}_1 (s)	EPP value	Classic EPP standard deviation s_1 (s)	Biomechatronic EPP mean value \bar{x}_2 (s)	Biomechatronic EPP standard deviation s_2 (s)
7.8233		4.0739	12.6827	7.5867
Condition		Results		Accepted/Rejected Null Hypothesis
Kolmogorov - Smirnov		0		Accepted
Mean value	$t_{2.5(28)}$	t_o	$t_{97.5(28)}$	Rejected
	-2.048	-2.1856	2.048	
Standard deviation	$F_{2.5_{14,14}}$	$F_{o_{14,14}}$	$F_{97.5_{14,14}}$	Rejected
	0.3495	0.2887	2.86	
Result			Negative	

Table 7.2. Results of statistical tests for Phase 2 duel time random variable.

Phase 2 duel time				
Classic EPP mean value \bar{x}_1 (s)	Classic EPP standard deviation s_1 (s)	Biomechatronic EPP mean value \bar{x}_2 (s)		Biomechatronic EPP standard deviation s_2 (s)
6.5013	2.5087	11.0267		4.7201
Condition	Results			Accepted/Rejected Null Hypothesis
Kolmogorov - Smirnov	1			Rejected
Mean value	$t_{2.5(28)}$	t_o	$t_{97.5(28)}$	Rejected
	-2.048	-3.2789	2.048	
Standard deviation	$F_{2.5_{14,14}}$	$F_{0_{14,14}}$	$F_{97.5_{14,14}}$	Rejected
	0.3495	0.2825	2.86	
Result		Negative		

Table 7.3. Results of statistical tests for Phase 1 error random variable.

Phase 1 error				
Classic EPP mean value \bar{x}_1 (deg)	Classic EPP standard deviation s_1 (deg)		Biomechatronic EPP mean value \bar{x}_2 (deg)	Biomechatronic EPP standard deviation s_2 (deg)
1.6957	1.0454		2.4975	1.2064
Condition	Results			Accepted/Rejected Null Hypothesis
Kolmogorov - Smirnov	0			Accepted
Mean value	$t_{2.5(28)}$	t_o	$t_{97.5(28)}$	Accepted
	-2.048	-0.8246	2.048	
Standard deviation	$F_{2.5_{14,14}}$	$F_{o_{14,14}}$	$F_{97.5_{14,14}}$	Accepted
	0.3495	1.0219	2.86	
Result		Positive		

Table 7.4. Results of statistical tests for Phase 2 error random variable.

Phase 2 error				
Classic EPP mean value \bar{x}_1 (deg)	Classic EPP standard deviation s_1 (deg)		Biomechatronic EPP mean value \bar{x}_2 (deg)	Biomechatronic EPP standard deviation s_2 (deg)
1.6981	1.1559		2.0443	1.1435
Condition	Results			Accepted/Rejected Null Hypothesis
Kolmogorov - Smirnov	0			Accepted
Mean value	$t_{2.5(28)}$	t_o	$t_{97.5(28)}$	Accepted
	-2.048	-1.9451	2.048	
Standard deviation	$F_{2.5_{14,14}}$	$F_{o_{14,14}}$	$F_{97.5_{14,14}}$	Accepted
	0.3495	0.7509	2.86	
Result		Positive		

The results of the statistical tests illuminate the umbral suspicions that the transparency test implied. The delays caused by the master motors render the user unable to have feedback from the Biomechatronic EPP setup. Thus, the user faces much higher resistance from the slave motor, being unable to stay for long period of time halted to the target. These results are congruent with the results of figures 7.64 and 7.65. The statistical test related to the error

reveals that the error of the participant is the same regardless the scheme that he or she uses. The reason is the same to the one that was concluded during the evaluation of figures 7.66 and 7.67. The open loop controller of the slave motor designed in Simulink is functional for both control schemes. However a second example will be held, with the increase in voltage supply of the master motors to examine whether the results are the same.

7.5 Target Experiment 2

During this test, only the first phase of the previous experiment was conducted. However, in this stage apart from the Classic EPP and the Biomechatronic EPP that the FSR sensors are connected to the rest of the setup, in this session the Classic EPP without coupling and the Biomechatronic EPP without connection with the power screws will be included. The pattern will be the same with the one of table 7.6. In the following figures the results of each setup will be presented.

➤ Biomechatronic EPP with connection

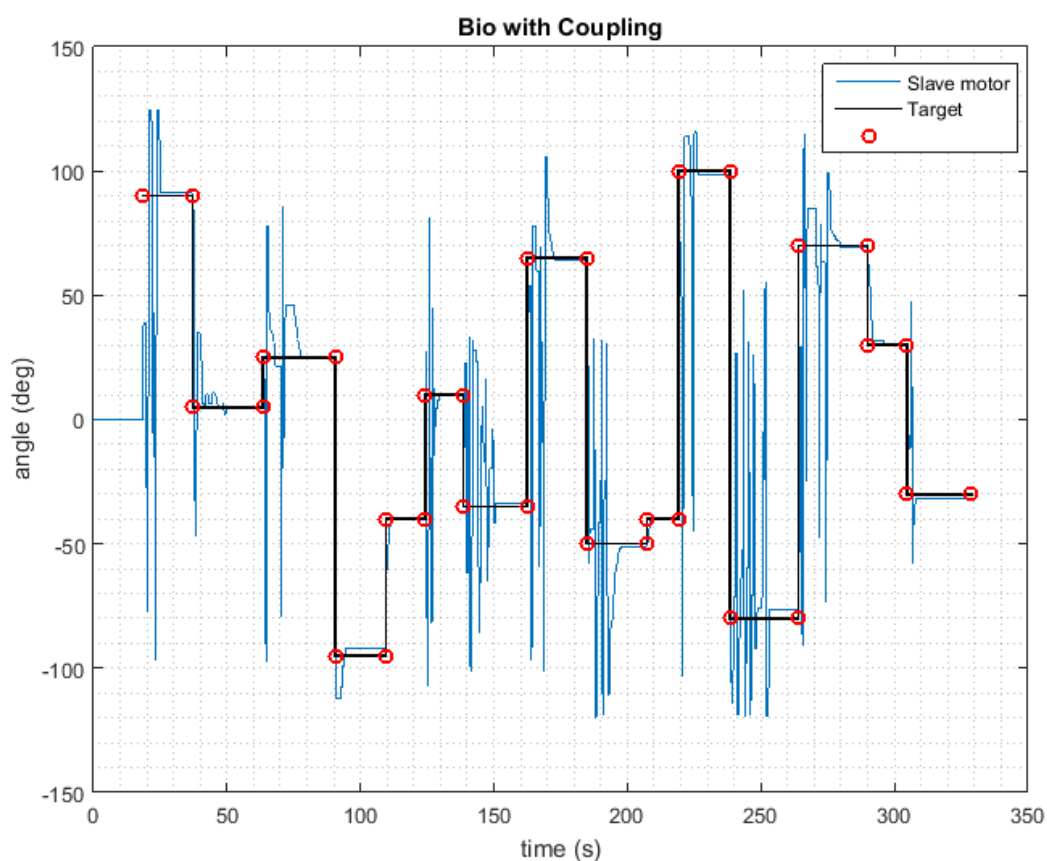


Figure 7.68. Biomechatronic EPP with connection slave - target position.

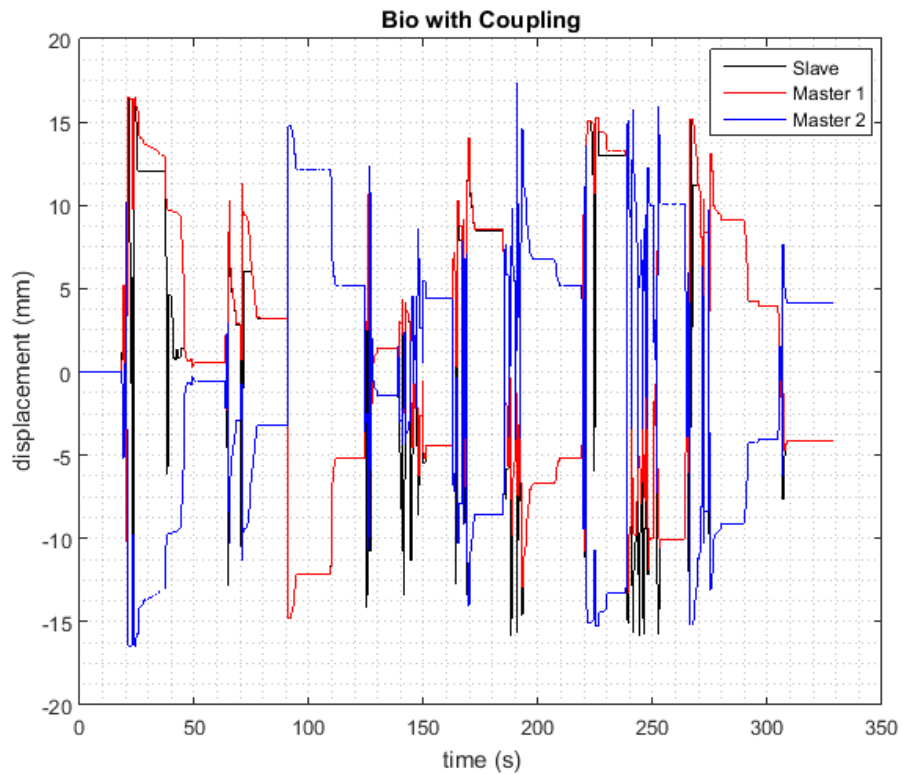


Figure 7.69. Biomechatronic EPP with connection master slave position.



Figure 7.69. Biomechatronic EPP with connection master motor 1 closed loop error.

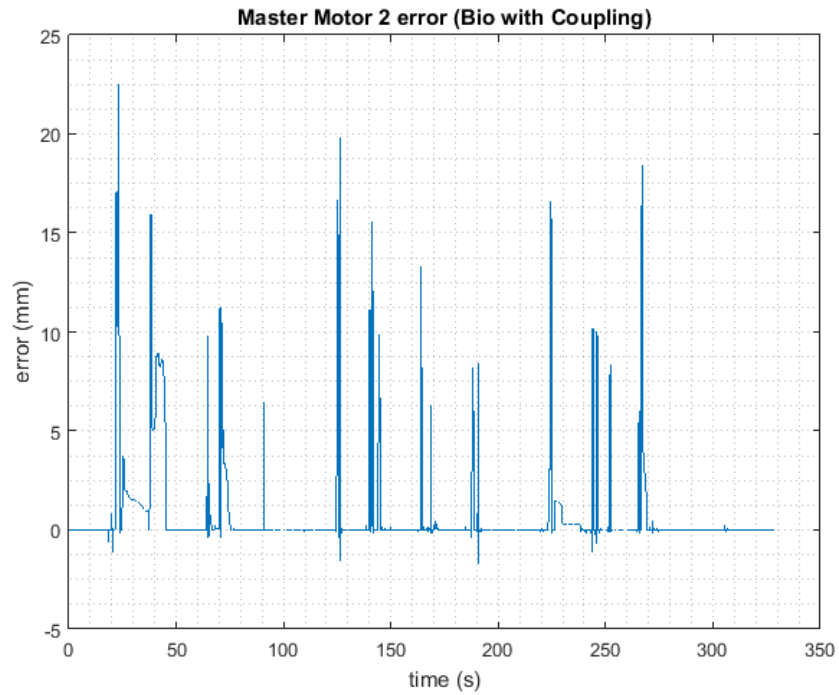


Figure 7.70. Biomechatronic EPP with connection master motor 1 closed loop error.

- **Biomechatronic EPP without connection (disconnected signal pathway from slave to master).**

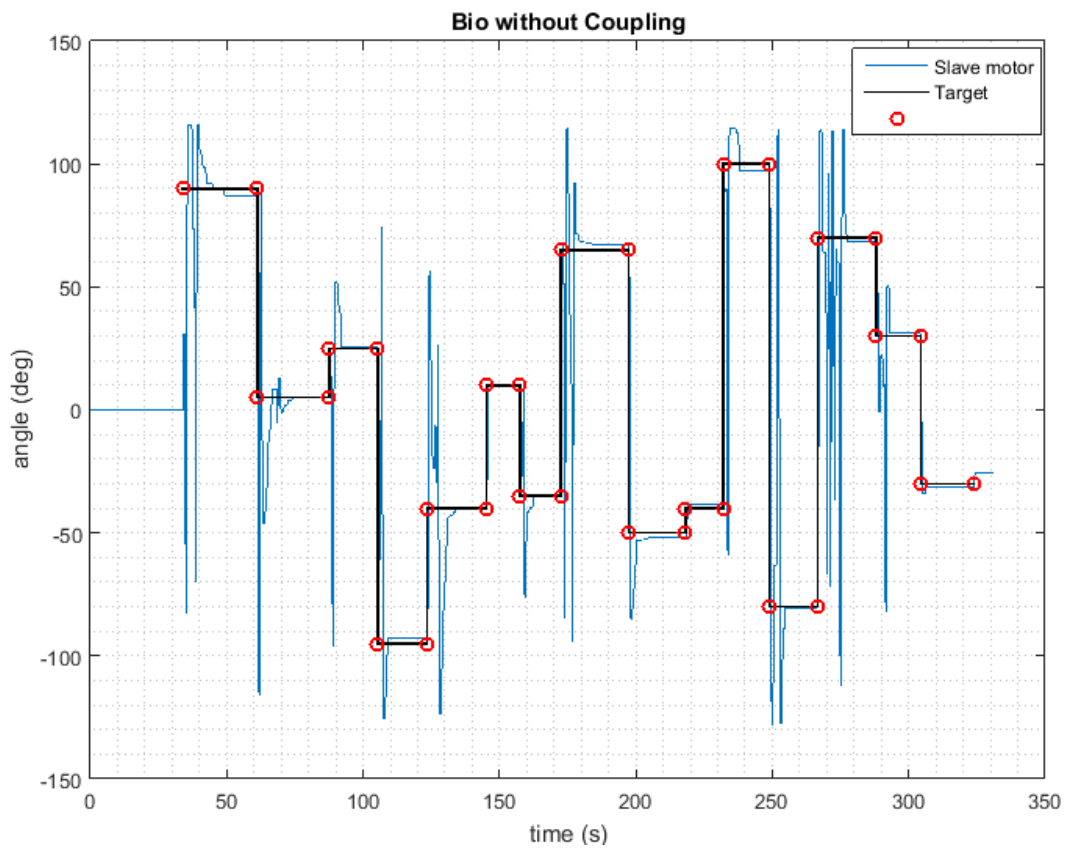


Figure 7.71. Biomechatronic EPP without connection slave - target position.

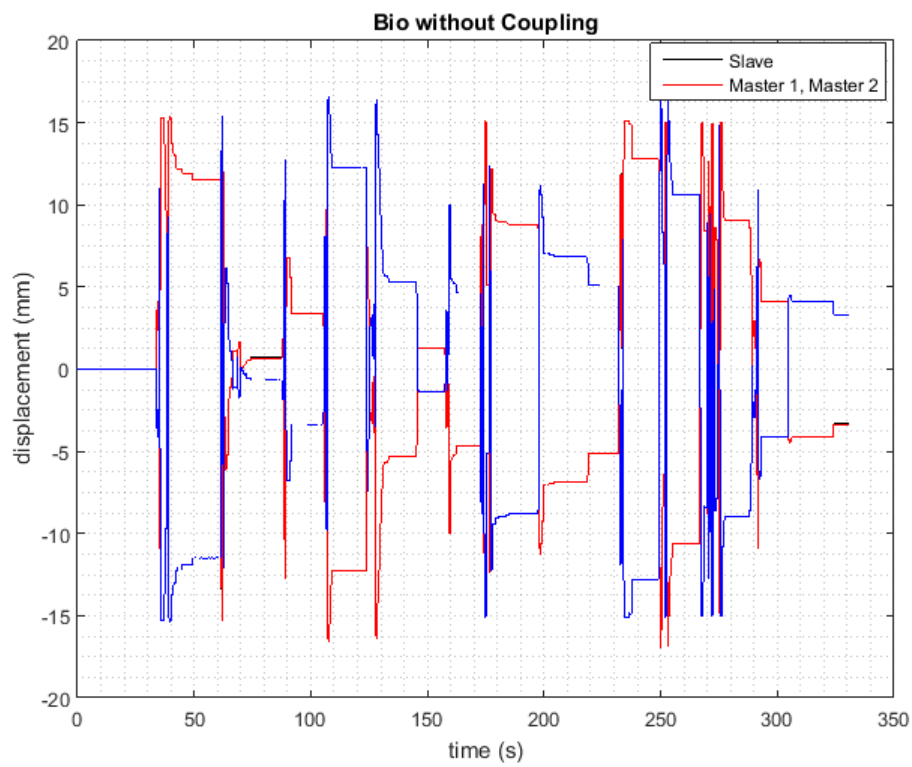


Figure 7.72. Biomechatronic EPP without connection master slave position.

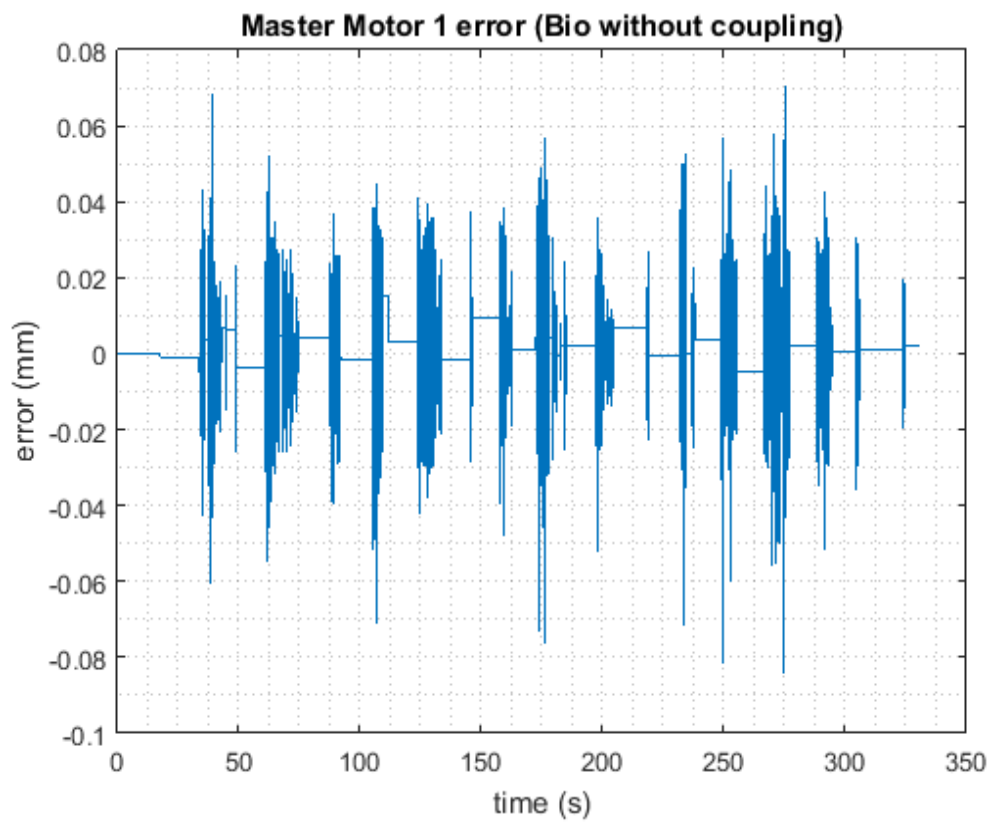


Figure 7.73. Biomechatronic EPP with connection master motor 1 closed loop error.

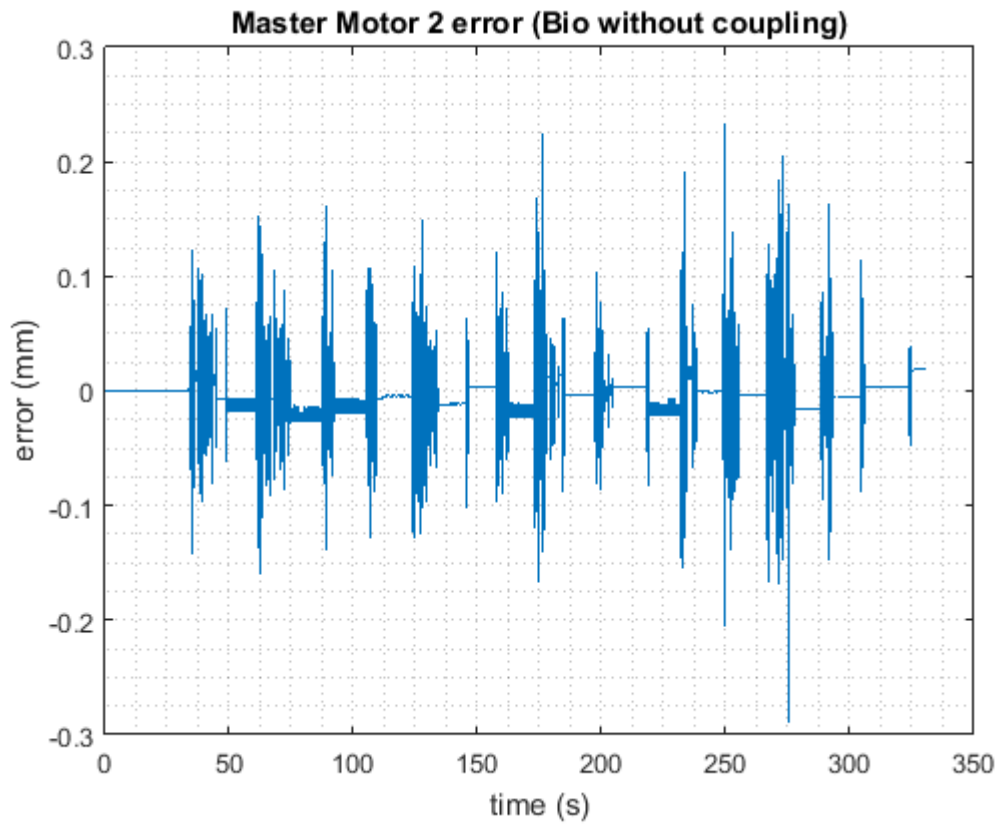


Figure 7.74. Biomechatronic EPP with connection master motor 2 closed loop error.

➤ **Classic EPP with coupling**

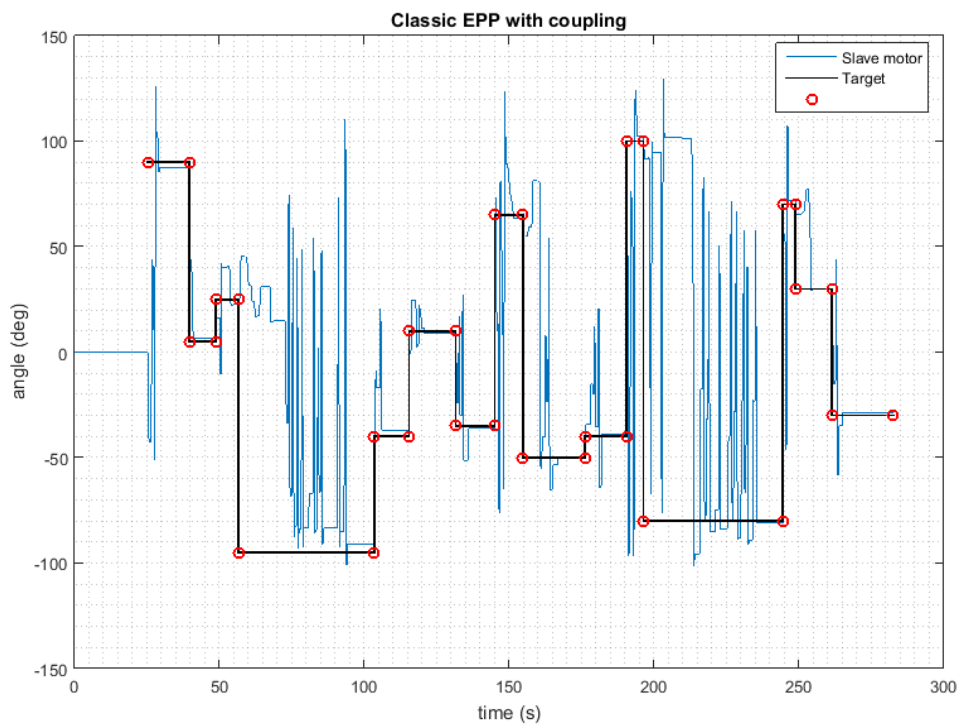


Figure 7.75. Classic EPP with connection slave - target position.

- **Classic EPP without coupling (disconnected Bowden cables from couple).**

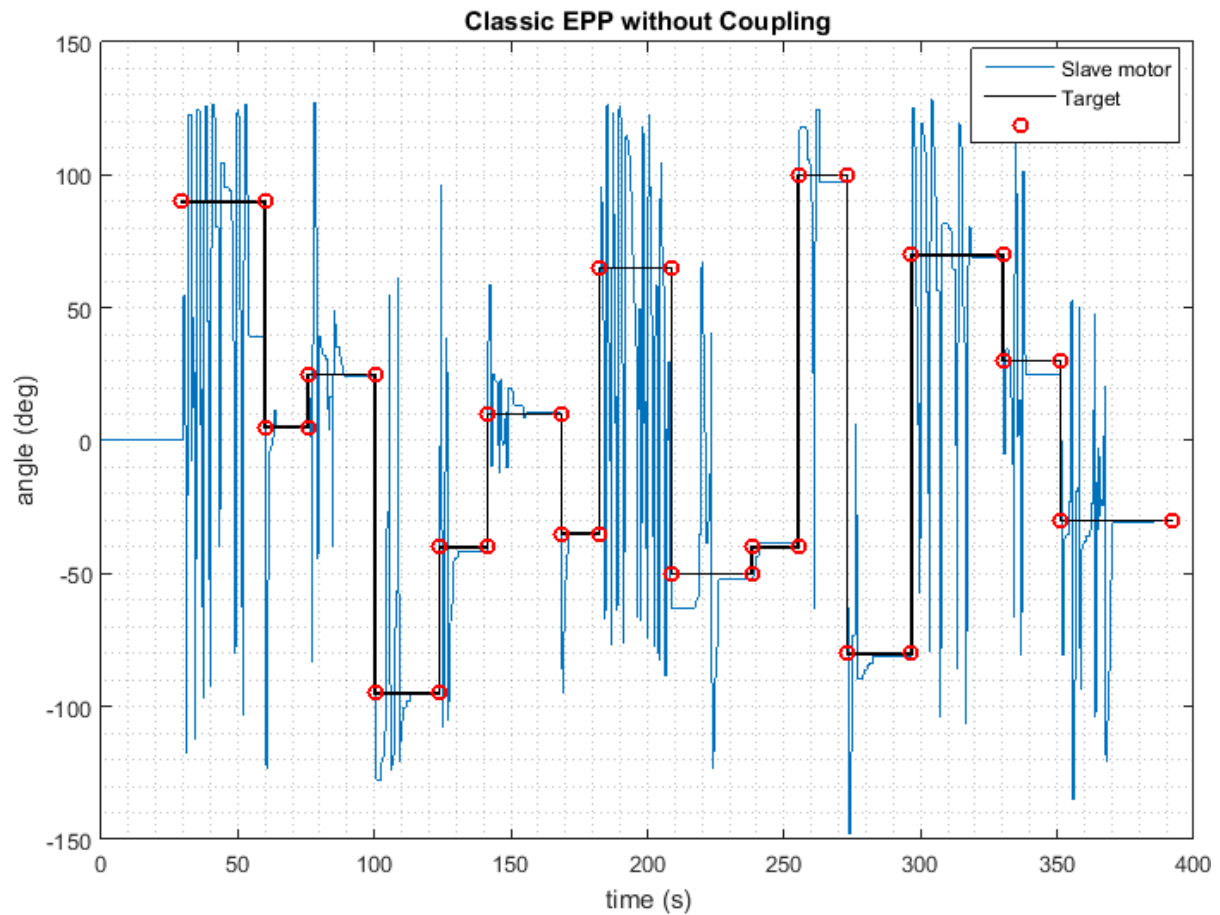


Figure 7.76. Classic EPP with connection slave - target position.

7.5 Experimental Data Evaluation vol. 2

In this section the parameters that will be compared will be the movement time, the duel time and the error again. However, one new parameter that will be included is the required time to finish the experiment. The data that will be compared for each setup are the mean time and the standard deviation. It has to be noted that the maximum current of the master motors was 0.55 A.

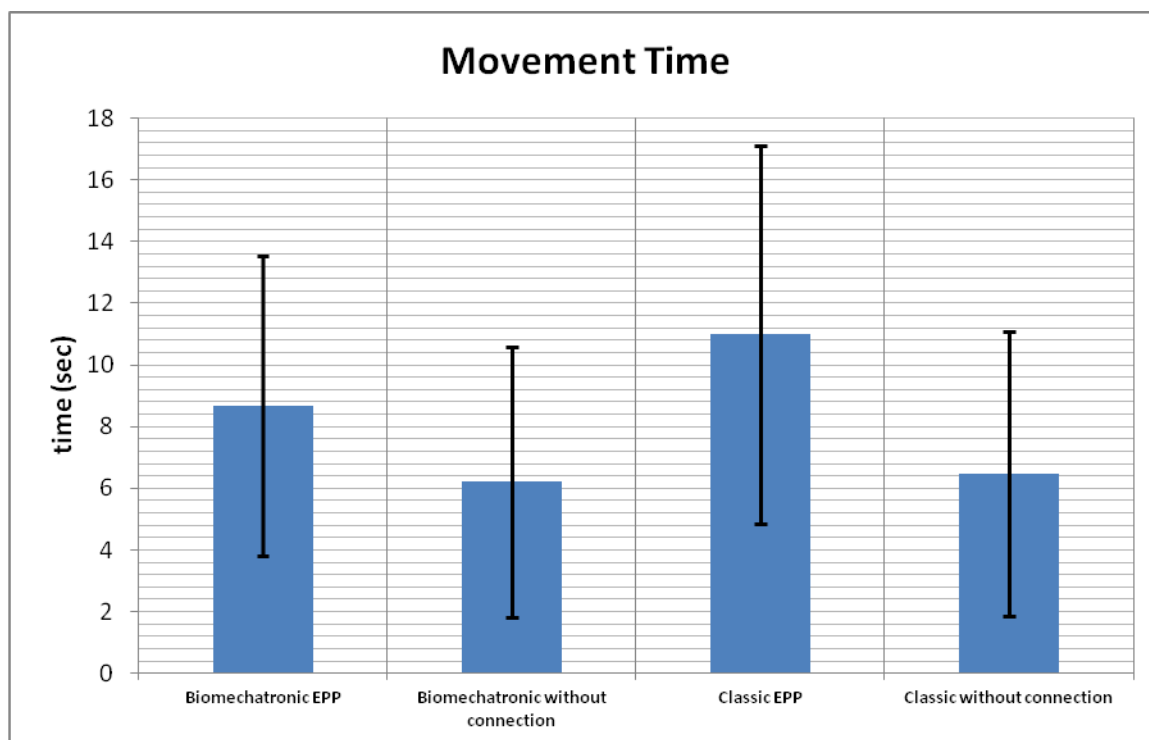


Figure 7.77. Movement time comparison.

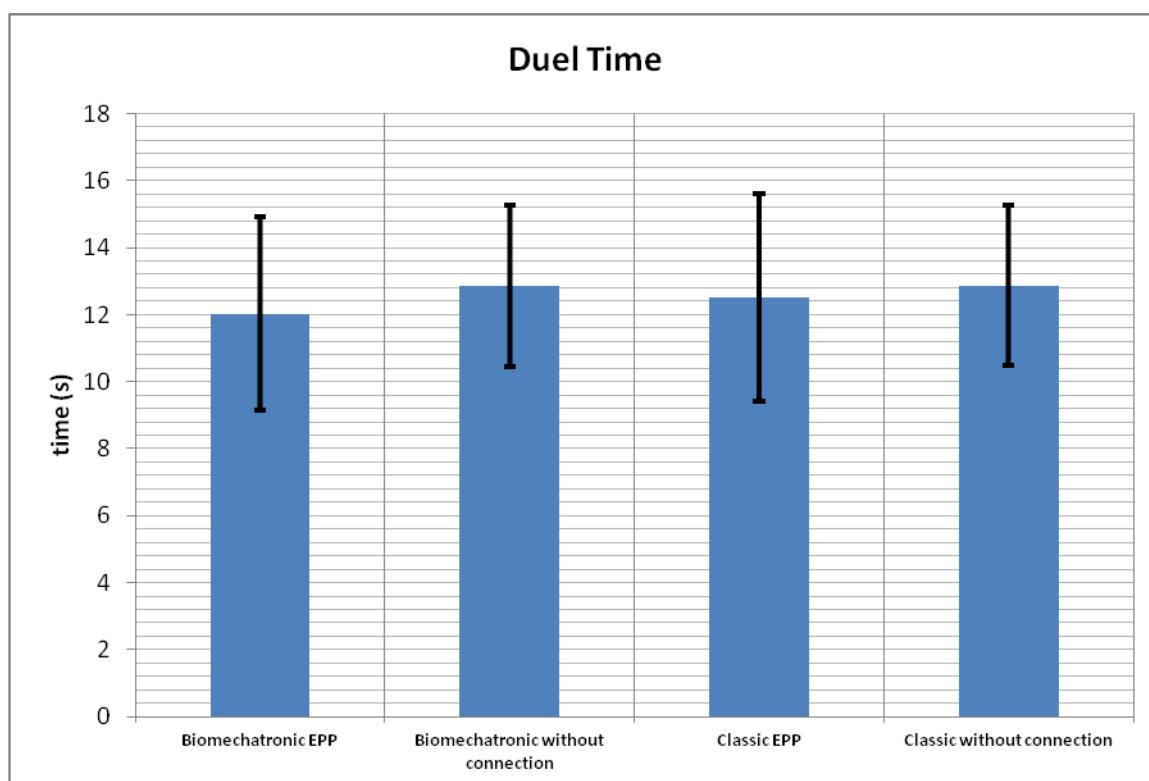


Figure 7.78. Duel time comparison.

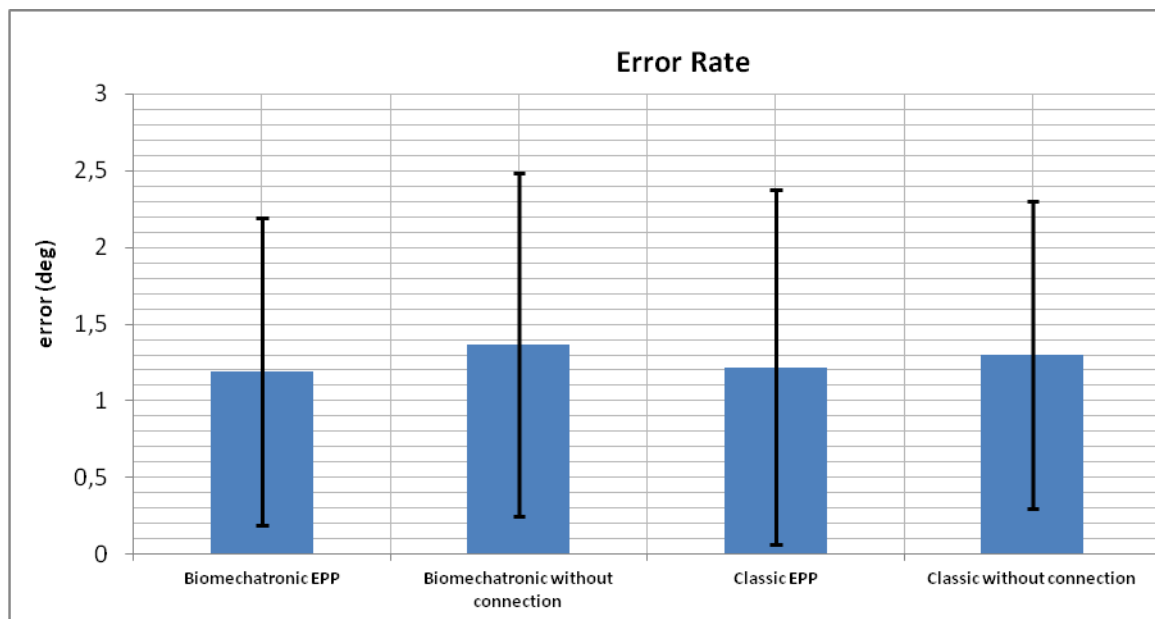


Figure 7.79. Error comparison.

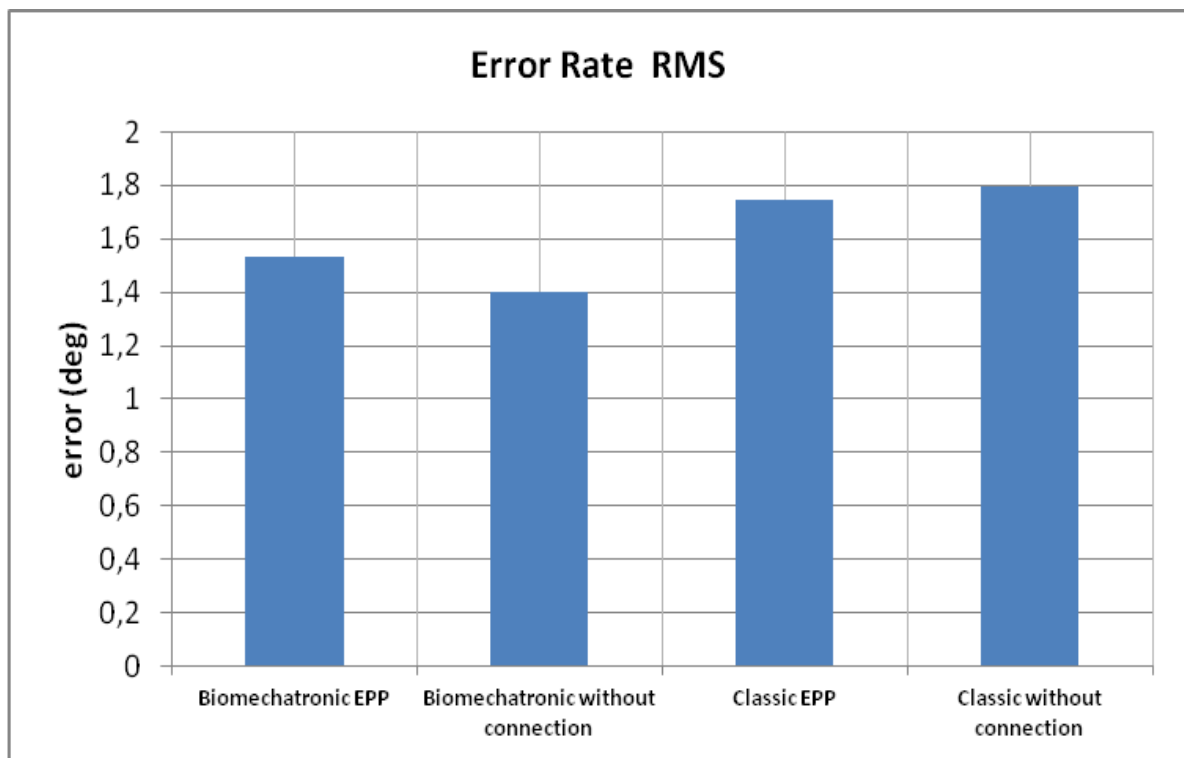


Figure 7.79. Error comparison (RMS).

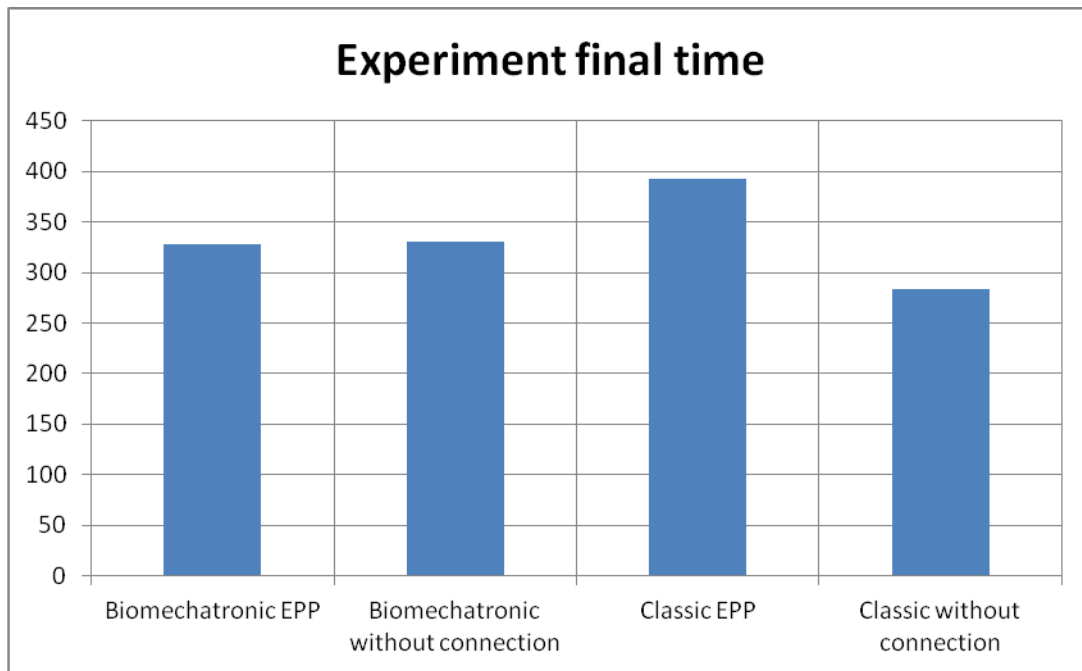


Figure 7.81. Experiment final time comparison.

It has to be noted that during the Classic setup without the coupler two failures occurred, while on the other three experiments no failure occurred. The reason that the Classic unconnected is has greater movement time than the other three setups is because the Bowden Cables in contrast to the ropes of the Biomechatronic setup have an elasticity that is distinguishable by the participant to the experiment. This renders the participant face difficulty reach the target. The same result can be observed to the duel time as well. For both the movement time and the duel time the Biomechatronic unconnected has the better results. The reason is that the participant has no force sense feed back from master motors and just with a little practice he/she can achieve to reach the target and stay on it by just applying the required force to the sensors and conduct the experiment without a hassle. The error rate between the actual target position and the final position reached is the same for the four setups. The reason is the fact that the open loop controller of the slave motor is the same and is independant of the rest of the setup. This topic will be discussed further after the statistical tests. However, it seems that this variable might be independent of the control method that is used. As for the duel time and the movement time of the Classic EPP and the Biomechatronic EPP, they seem to be almost identical on the aspect of the time range. This means that the desired equivalence might be accomplished. However, to inquire it, statistical tests have to be conducted that will be presented next. Finally, it has to be mentioned that the results of each parameter have slight variances depending of the order the setups were used. For instance, if the participant starts with the Classic EPP, he /she will have to learn at first how to use the setup, rendering the first attempts worse than the following ones. However, in the following experiments, the participant has learned how to use the setup and the amount of force that has to be applied to the sensors, improving his/her performance. For the record, the order the setups were used is the following: the Biomechatronic unconnected, the Biomechatronic EPP,

the Classic unconnected and finally the Classic EPP. With the experimental data obtained it has to be inquired whether or not the data belong to the same probabilistic set. Thus the same statistical test will be conducted. However, in this case the samples that will be compared are the Biomechatronic EPP and Classic EPP connected to the rest of the setup (with the ropes and the coupling respectively). The results are presented in the following tables.

Table 7. Statistical Tests for the duel time with the whole setup connected

Duel time - Connected setup				
Classic EPP mean value \bar{x}_1 (s)	Classic EPP standard deviation s_1 (s)		Biomechatronic EPP mean value \bar{x}_2 (s)	Biomechatronic EPP standard deviation s_2 (s)
12.86933	2.391397		12.02533	2.891131
Condition		Results		Accepted/Rejected Null Hypothesis
Kolmogorov - Smirnov		0		Accepted
Mean value	$t_{2.5(28)}$	t_o	$t_{97.5(28)}$	Accepted
	-2.048	-0,84168	2.048	
Standard deviation	$F_{2.5_{14,14}}$	$F_{o_{14,14}}$	$F_{97.5_{14,14}}$	Accepted
	0.3495	1,461614	2.86	
Result			Positive	

Table 8. Statistical Tests for the duel time with the whole setup unconnected

Duel time - Unconnected setup				
Classic EPP mean value \bar{x}_1 (s)	Classic EPP standard deviation s_1 (s)		Biomechatronic EPP mean value \bar{x}_2 (s)	Biomechatronic EPP standard deviation s_2 (s)
12.51769	3.087216		12.856	2.401903
Condition	Results			Accepted/Rejected Null Hypothesis
Kolmogorov - Smirnov	0			Accepted
Mean value	$t_{2.5(28)}$	t_o	$t_{97.5(28)}$	Accepted
	-2.048	0.33819	2.048	
Standard deviation	$F_{2.5_{14,14}}$	$F_{o_{14,14}}$	$F_{97.5_{14,14}}$	Accepted
	0.3495	0.605309	2.86	
Result			Positive	

Table 9. Statistical Tests for the error with the whole setup connected

Error - Connected setup				
Classic EPP mean value \bar{x}_1 (deg)	Classic EPP standard deviation s_1 (deg)		Biomechatronic EPP mean value \bar{x}_2 (deg)	Biomechatronic EPP standard deviation s_2 (deg)
1.369933	1.117659		1.1902	1.002717
Condition		Results		Accepted/Rejected Null Hypothesis
Kolmogorov - Smirnov		0		Accepted
Mean value	$t_{2.5(28)}$	t_o	$t_{97.5(28)}$	Accepted
	-2.048	-0.44787	2.048	
Standard deviation	$F_{2.5_{14,14}}$	$F_{o_{14,14}}$	$F_{97.5_{14,14}}$	Accepted
	0.3495	0.804893	2.86	
Result			Positive	

Table 10. Statistical Tests for the error with the whole setup unconnected

Error - Unconnected setup				
Classic EPP mean value \bar{x}_1 (deg)	Classic EPP standard deviation s_1 (deg)		Biomechatronic EPP mean value \bar{x}_2 (deg)	Biomechatronic EPP standard deviation s_2 (deg)
1.219462	1.373669		1.369933	1.117659
Condition		Results		Accepted/Rejected Null Hypothesis
Kolmogorov - Smirnov		0		Accepted
Mean value	$t_{2.5(28)}$	t_o	$t_{97.5(28)}$	Accepted
	-2.048	0.331685	2.048	
Standard deviation	$F_{2.5_{14,14}}$	$F_{o_{14,14}}$	$F_{97.5_{14,14}}$	Accepted
	0.3495	0.661995	2.86	
Result			Positive	

The results of the statistical comparison with the increase in voltage supply are much more positive, because in this case both of the setups (with the coupling and the ropes and not) are proved that are statistically the same. Thus the two setups for both the error and the duel time prove to be identical to each other, rendering the target experiments successful. Next is the

preparation of the setup for the force sense, however, it will be presented to the next installment.

7.6 Experiment 3 Force

In this test it has to be examined whether the user feels an increase in the load applied to the joint of the slave motor and is able to apply higher load to the FSR sensors to augment the current provided to the motor. The idea is to apply various loads to the shaft of the motor and delve into whether the user is able to feel the increase in force required to rotate the slave motor. The weight will be held from a fishing line wreathed in the pulley used for the Bowden cables. The only difference is that in its CAD a hole was included to pass the line through it and it was constructed with 3D printing. The final setup is presented to the following figures.

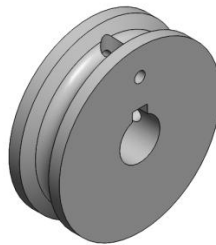


Figure 7.82. Redesigned CAD of the pulley with a hole to hold the fishing line.

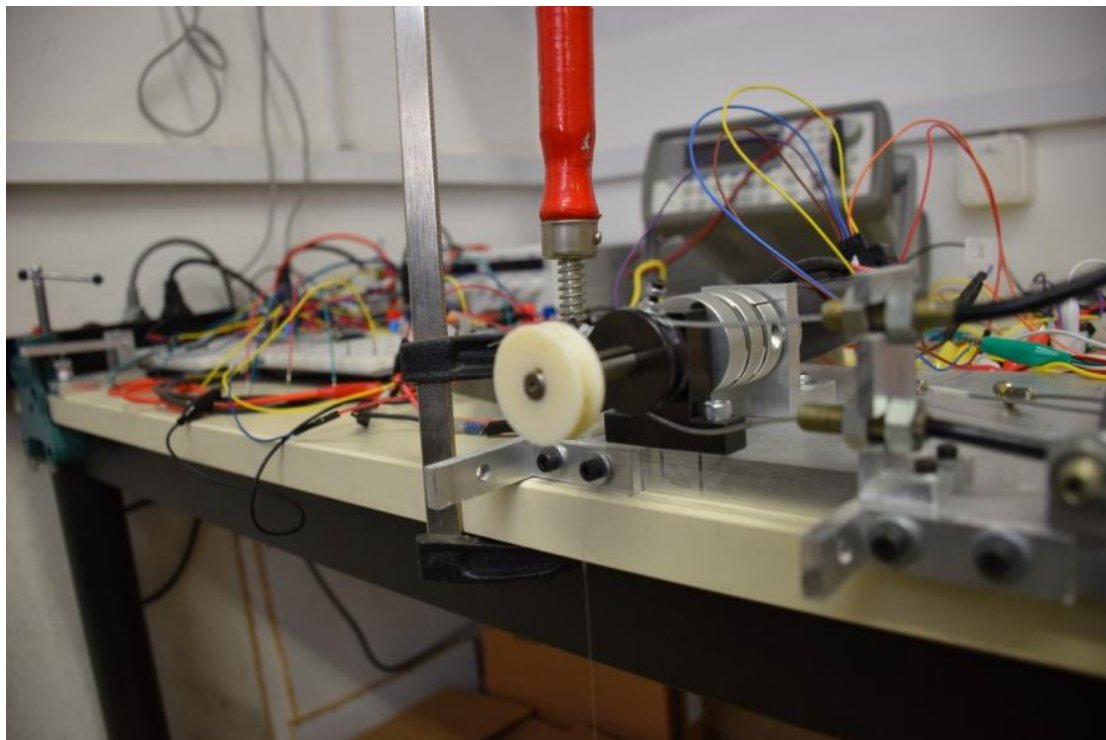


Figure 7.83. 3D printed pulley on the shaft of the setup.



Figure 7.84. Standard weight placed in a base connected to the 3D printed pulley.

Furthermore, a physical obstacle has to be placed to the shaft to examine whether the user is able to feel the Dirac – Impulse loadings. For this purpose a rectangular shaft was designed, as it is presented on figure 7.68. The shaft was constructed using the 3D printer of the laboratory and its assembly is presented on figure 7.69. To stop the shaft two flanges were adjusted to the setup, presented on figure 7.70.

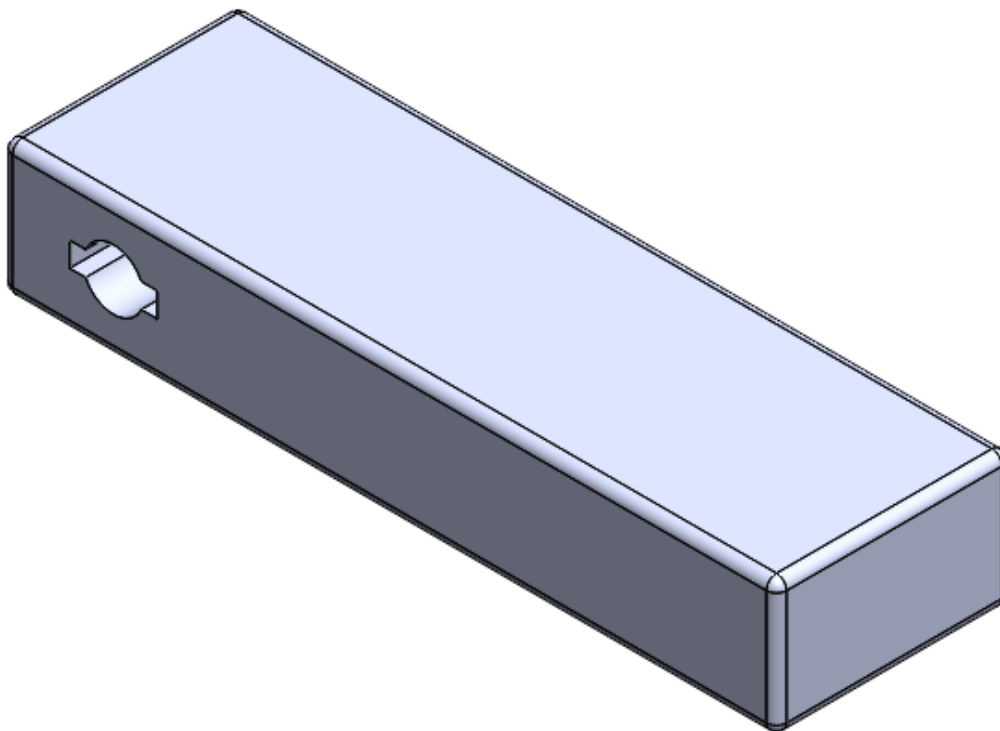


Figure 7.85. CAD of the rectangular shaft.

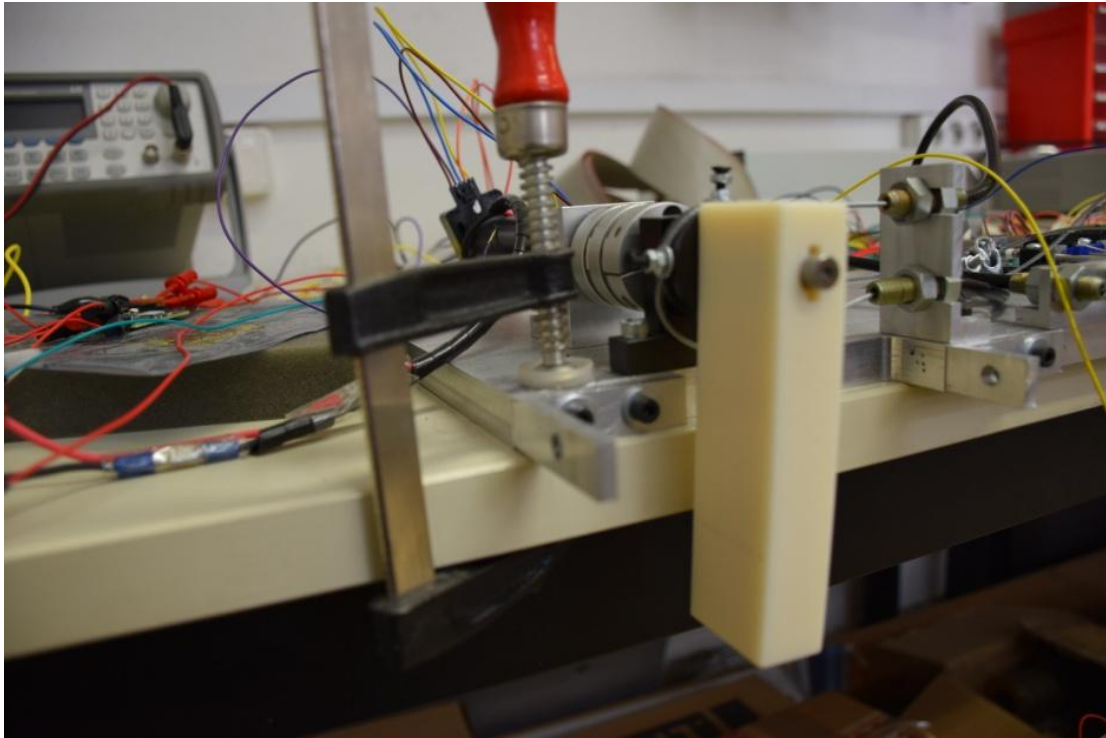


Figure 7.86. Assembly of the 3D printed shaft to the setup.

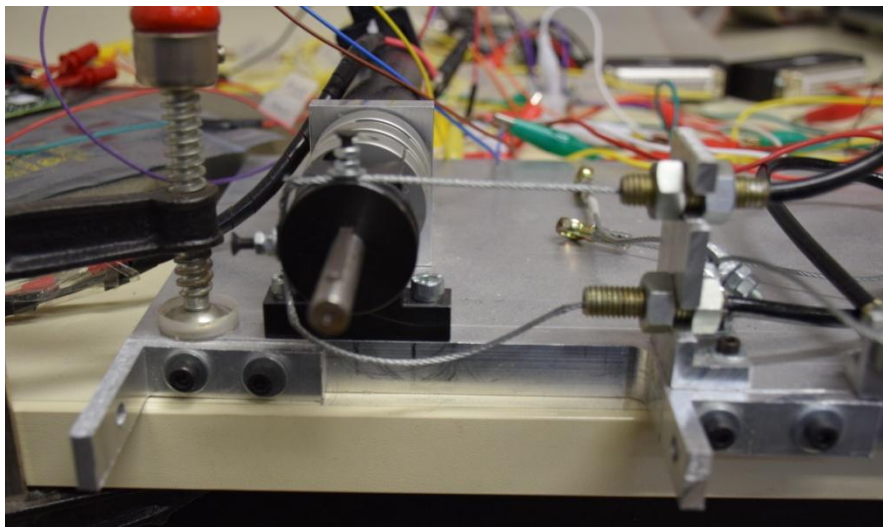


Figure 7.87. The flanges that are used as bounds for the shaft.

The results that must be compared are the FSR sensor curves for 1 kg of load and to no load for the Classic EPP setup and the Biomechatronic EPP setup. Then to inquire whether the two methods are equivalent the stochastic variable output of the FSR sensor for the Biomechatronic EPP and for the Classic EPP must belong to the same probabilistic set. Through an experiment the integral mean of the output that is the stochastic variable can be calculated by the following equation.

$$\bar{V} = \frac{1}{T} \int_0^T |V(t)| dt \quad (7.20)$$

Thus, the same tests have to be conducted with the target experiment. However, this would prove to be a squander because the answer can be obtained by just asking the participant if he or she felt any resistance from the Biomechatronic EPP. Unfortunately, the answer was negative. In comparison to the Classic EPP in which the resistance that the user felt was obvious, during the Biomechatronic EPP the user feels less resistance, because of the low torque provided by the master motors and the delays of the system. Thus, this must be recorded as a fault of the setup, which however is a sacrifice that must be taken because the master motors were chosen to be able to be implanted to the real upper limb prosthetic. With the experimental stage finished, the conclusions of this thesis will be discussed. Nevertheless, this will be presented to the next installment.

8 Conclusions and Continuation - Legacy

8.1 Conclusions

This chapter summarizes the findings of this thesis. The setup that was designed by another thesis ^[4] was assembled and was combined with the FSR sensors that were designed. Furthermore, the electromechanical parts were included in the setup and with this step the setup as a whole was completed. The next step of this thesis was to unravel the arcane traits of DS1103 and ControlDesk to set the stage for the Classic EPP and the Biomechatronic EPP control schemes and the preparation of the experiments that had to be conducted.

The theoretical simulations that were conducted prior to this thesis proved that the two control schemes are equivalent and fortunately for us at some points the experiments proved the same (see section 7.1).

The delays of the master motors displayed on the chapter 7 reached zero using a more efficient controller, rendering the Biomechatronic EPP pass the test of transparency. Furthermore, the open loop control system of the slave motor proved substantial for both the Classic EPP and the Biomechatronic EPP, which was proved by the results of the target experiment tests. In detail, the slave motor's performance was adequate when controlled from both topologies (dead zone, saturation, direction of motor as function of FSR values, upper value bounds of slave motor).

The target experiment statistical evaluation proved that both the control schemes are equivalent. However, the user of the Biomechatronic EPP did not feel a significant change in the loading of the slave motor, while with the Classic EPP the resistance that was felt was significant and the user felt changes in the loading. Ergo, the Biomechatronic EPP does not achieve the perfect sense of forces per se. The question that rises of course is the same with the homonymous song: who's to blame? The answer to this question must be provided to move forward (kotaeru as they say in Japanese). The fact that the torque provided by the master motors is lower than the slave motor seems to be a valid one. The user can sense the movement of the power nut, but not force that moves it. In contrast, at the Classic EPP the user sensed the force of the slave motor that moved him forward more intensively. Nevertheless, to become the devil's advocate, the selection of the master motors was mandatory for the design of the real upper limb prosthetic. And in this aspect, this insufficiency must be dealt with. Next, the continuation of this thesis will be presented. However, what will be done will be presented to the next installment.

The current target experiment setup did not prove any differences between the classic EPP and classic EPP without Bowden cables connected. A reason for this might be due to the sequence of experiments performed. The classic EPP was conducted first and the user might have learned how to use the system with a learning after effect even when Bowden cables were disconnected. Another reason might be that the index of Difficulty did not go to higher values. We propose to correct for both above reasons in our next round of target experiments. It is to be noted, that the user felt more resistance and feedback and force (resistance) from motor when Bowden cables were connected. When not connected, the user felt elasticity of Bowden cables which were not connected to motors. Visual feedback was also present during both experiment which we should avoid in the future tracking experiments.

The current target experiment setup between Biomechatronic EPP and disconnected sensors, did not prove any differences. A reason for this might be again visual feedback, which should be avoided in the future. As stated above the order of the experiments played a significant role (connected case first) and the user might have learned how the system works and then could almost achieve same performance. We also recommend to expand the Index of Difficulty of the next set of target experiments.

8.2 Continuation - Legacy

This thesis proved that even though the theoretical results obtained by a previous diploma thesis ^[4] rendered the two control methods equivalent, there was a lack of force sense at the Biomechatronic EPP. However, the experiments conducted proved that the new control scheme bears potential, because the responses during the target experiment were swift and the participant was able to reach the targets. Moreover, the delays of the system were on par with the Classic EPP, rendering the transparency test a success. One possible change that can be done is the design of sensors that can measure lower values of forces and do not face the never ending problem of the remaining stresses to the force sensitive resistances. Last but not least, this thesis resurrected the long forgotten DS1103 that lied on the lab tarrying to be used. The older updates of Simulink that were kept at the lab proved obsolete and it was required to study the hardware and the software from scratch. Now with the manual provided with this thesis on the appendix, everyone at the lab can effortlessly use the DS1103 for measurements, controller's prototyping and even more. Finally, it has to be noted that the experiments that were presented had the form of a proof of concept. If the transparency test shows satisfying results, a stricter protocol and environment should be stated. This specific duty is conducted simultaneously with this thesis by another diploma thesis candidate, thus there will be no spoilers about this topic. Let's hope that this thesis will not be the ending of a journey, but the beginning of a new one that will resolve the challenge of the equivalence

prove and will bring the DS1103 with ControlDesk at the vanguard of the research at the laboratory. To sum up, another set of experiments that can be conducted are the comparison of Biomechatronic EPP with the contemporary control method used, the myoelectric control, to validate which is superior, as well as experiments with more participants (14 subjects for instance).

9 REFERENCES

- [1] Yiorgos Andrea Bertos, May 1999, "A microprocessor - Based EPP position controller for electric - powered upper - limb prostheses", Master's Thesis, Northwestern University, Evanston, Illinois.
- [2] Norman S. Nise, 2011, "*Control Systems Engineering*", Sixth Edition, John Wiley & Sons, Inc., NJ 07030-5774, ISBN13 978-0470-54756-4.
- [3] Karl A. Seeler, 2014, "*System Dynamics, An introduction for Mechanical Engineers*", Springer New York, ISBN 978-1-4614-9151-4.
- [4] Ανέστης Μαμπλέκος - Αλεξίου, Αθήνα 2016, "Σχεδιασμός και Προσομοίωση συστήματος τηλεχειρισμού προσθετικού άκρου με ιδιοδεκτική αίσθηση", Διπλωματική Εργασία, Εθνικό Μετσόβιο Πολυτεχνείο, Σχολή Μηχανολόγων Μηχανικών, Τομέας Μ.Μ. και Α.Ε., Εργαστήριο Αυτομάτου Ελέγχου.
- [5] Scott, R. N., "Myoelectric Control of Prostheses a brief history", MEC 92, *Proceedings of the 1992 MyoElectric Controls/Powered Prosthetics Symposium*, Fredericton, New Brunswick, Canada, 1992.
- [6] Vanghetti, G., "Amputazioni, Disarticolazioni e protesi", Florence, Italy 1898.
- [7] Yokokohji, Y. and Yoshikawa, T., "Bilateral control of master-slave manipulators for ideal kinesthetic coupling-formulation and experiment," *IEEE Trans. on Robotics and Automation*, vol. 10, no. 5, pp. 605-620, 1994.
- [8] dSpace Embedded Success, Catalog 2017, dSpace GmbH • Rathenausstraße 26 • 33102 Paderborn • Germany • info@dspace.de • www.dspace.com.
- [9] John J. Craig, 1987, "*Adaptive Control of Mechanical Manipulators by John J. Craig (1987-09-03)*", Addison-Wesley Pub (Sd) (1890), ISBN13 979-0201104904.
- [10] Σ.Ε. Σιμόπουλος, "*Μετρήσεις Τεχνικών Μεγεθών*", Β' Έκδοση, Αθήνα 1989.
- [11] Massey, F. J., 1951 "The Kolmogorov-Smirnov Test for Goodness of Fit." *Journal of the American Statistical Association*. Vol. 46, No. 253, 1951.
- [12] Vanghetti, G., "Plastica dei Monconi a Scopo di Protesi Cinematica", *Arch. d. Ortop.*, Vol. 16, no. 5, 1899a, pp. 305-324.

- [13] Vanghetti, G., "Plastica dei Monconi a Scopo di Protesi Cinematica", *Arch. d. Ortop.*, Vol. 16, no. 6, 385-410 1899b.
- [14] Childress, D.S. (1992), "Control of Limb Prostheses", Chapter 6D, *Atlas of Limb Prosthetics, Surgical, Prosthetic, and Rehabilitation Principles*, 2nd ed., Bowker, J.H. & Michael, J. W. (eds.), Mosby-Year Book, Inc., St. Louis MO, 175-199.
- [15] Cho, H. C., Park, J. H., Kim, K. and J. O. Park, "Sliding-model-based impedance controller for bilateral teleoperation under varying time-delay," *Proc. of IEEE International Conference on Robotics and Automation*, pp. 1025-1030, May 2001.
- [16] Reva E. Johnson, IEEE Student Member, Konrad P. Kording, Levi J. Hargrove, IEEE Member, and Jonathon W. Sensinger, IEEE Member, "The effect of powered prosthesis control signals on trial-by-trial adaptation to visual perturbations", 978-1-4244-7929-0/14/\$26.00 ©2014 IEEE.
- [17] Alessandro Marco De Nunzio, Member, IEEE, Sabrina Lemling, Marko Markovic, Strahinja Dosen, Schweisfurth, Cornelia Hartmann, Bernhard Graimann, and Dario Farina, Senior Member, IEEE, "Learning an internal model of myoelectric prostheses to improve accuracy of grasping force: the importance of a vibrotactile feedback".
- [18] Lauren H. Smith, Student Member, IEEE, Todd A. Kuiken, Member, IEEE, and Levi J. Hargrove, Member, IEEE, "Real-time simultaneous myoelectric control by transradial amputees using linear and probability-weighted regression", 978-1-4244-9270-1/15/\$31.00 ©2015 IEEE.
- [19] James A. Doubler, Ph.D., Dudley S. Childress, Ph. D., "Design and Evaluation of a Prosthesis Control System Based on the Concept of Extended Physiological Proprioception", *Journal of Rehabilitation Research and Development*, Vol. 21, No. 1, BPR 10-39 pages 19-31, Prosthetics Research Laboratory Northwestern University 345 East Superior Street Chicago, Illinois 60611.
- [20] James A. Doubler, Ph.D., Dudley S. Childress, Ph.D. "An Analysis of Extended Physiological Proprioception as a Prosthesis-Control Technique", *Journal of Rehabilitation Research and Development*, Vol. 21, No. 1 BPR 10-39 pages 5-18, Northwestern University 345 East Superior Street Chicago, Illinois 60611.
- [21] Aaron J. Suminski, Dennis C. Tkach, Andrew H. Fagg, and Nicholas G. Hatsopoulos, "Incorporating Feedback from Multiple Sensory Modalities Enhances Brain-Machine

Interface Control", *The Journal of Neuroscience*, December 15, 2010 • 30(50):16777–16787 • 16777, Department of Organismal Biology and Anatomy, Committee on Computational Neuroscience, University of Chicago, Chicago, Illinois 60637.

- [22] Michal Eisenberg, Lior Shmuelof, Eilon Vaadia, and Ehud Zohary, "The Representation of Visual and Motor Aspects of Reaching Movements in the Human Motor Cortex", *The Journal of Neuroscience*, August 24, 2011 • 31(34):12377–12384 • 12377.
- [23] Erik J. Scheme, Student Member, IEEE, Kevin B. Englehart, Senior Member, IEEE, "Validation of a Selective Ensemble-Based Classification Scheme for Myoelectric Control Using a Three Dimensional Fitts' Law Test", *TNSRE-2012-00150*.
- [24] Fitts, P. M. (1954). "The information capacity of the human motor system in controlling the amplitude of movement". *Journal of Experimental Psychology*, 47(6), 381-391. doi:10.1037/h0055392.
- [25] MacKenzie, I. S., & Buxton, W. (1992). "Extending Fitts's law to two-dimensional tasks" *Proceedings of the SIGCHI conference on Human factors in computing systems* CHI 92, p, 219-226. ACM Press. doi:10.1145/142750.142794.
- [26] Soukoreff, R., & Mackenzie, I. (2004). "Towards a standard for pointing device evaluation, perspectives on 27 years of Fitts's law research in HCI." *International Journal of Human-Computer Studies*, 61(6), 751-789. Elsevier. doi:10.1016/j.ijhcs.2004.09.001.
- [27] Bootsma, R. J., Fernandez, L., & Mottet, D. (2004). "Behind Fitts's law: kinematic patterns in goal-directed movements". *International Journal of Human-Computer Studies*, 61(6), 811-821. doi:10.1016/j.ijhcs.2004.09.004.

10 APPENDIX A BASICS ON dSPACE

The purpose of this chapter is to present the most often required material to use dSPACE and more specifically DS1103 PPC Controller Board and ControlDesk 5.6. With this information the reader would be able to understand the basic concepts of using DS1103 and what should be avoided. For further and more thorough details it should be advised to read the manuals of dSPACE and ControlDesk provided by dSPACE. The reason this chapter is included in this thesis is that ControlDesk has faced rapid changes through the last couple of years, however its manuals are either obscure about some aspects or they are referring to older releases. Ergo it should be judicious to include this chapter in the thesis, so that everyone can use the DS1103 coherently without being forced to ask for support from dSPACE.

10.1 dSpace and Simulink - Basic Concepts

The DS1103 is an all-rounder in rapid control prototyping. You can mount the board in a dSPACE Expansion Box or dSPACE AutoBox to test your control functions in a laboratory or directly in a vehicle. Its processing power and fast I/O are vital for applications that involve numerous actuators and sensors. Used with Real-Time Interface, the controller board is fully programmable from the Simulink ® block diagram environment. All I/O graphically by using RTI can be configured. This is a quick and easy way to implement your control functions on the board. Implementing your model on dSPACE single-board hardware is easy with Simulink ® and dSPACE's Real-Time Interface. The on-board I/O modules can be initialized and configured graphically within the Simulink environment. Real-time code generation, compiling and downloading is reduced to a single mouse click. Programming your single-board hardware without Real-Time Interface is also possible with the included C software environment, together with a compiler and loader software. The control of electrical drives requires accurate recording and output of I/O values. It is possible to synchronize the A/D channels and D/A channels, and the position of the incremental encoder interface, with an internal PWM signal or an external trigger signal. Also, the serial interface (UART) is driven by a phase-locked loop to achieve absolutely accurate baud rate selection. Figure AA.1 provides an overview of the architecture and the functional units DS1103.

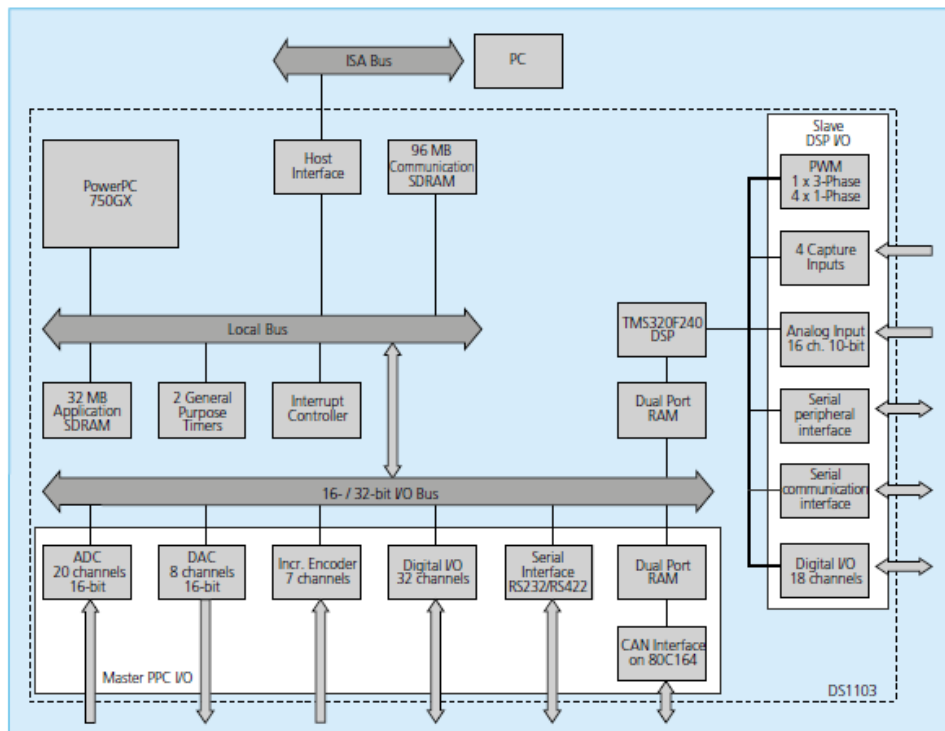


Figure AA.1Block diagram of the architecture of DS1103.

The core of prototyping with DS1103 is the creation of a Simulink block model. Next, the most significant blocks that can be used will be presented and the main options provided for the user.

- **A/D converter**

To read analog signals two blocks can be used, the DS1103MUX_ADC_CONx and the DS1103ADC_Cx, presented in figures AA.2 and AA.3.

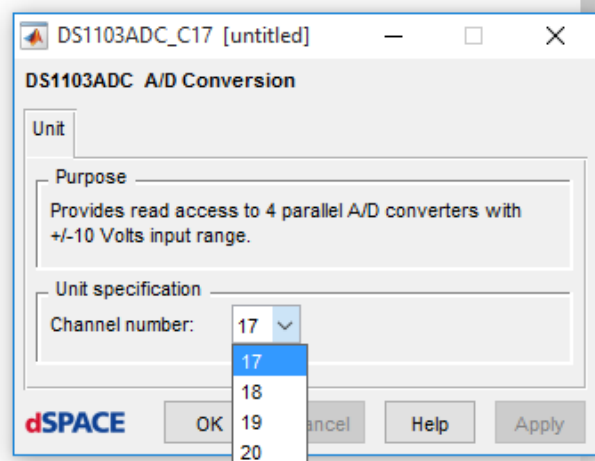
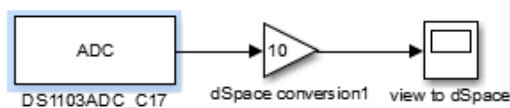


Figure AA.2. DS1103ADC_Cx.

This block can be used to read from a single channel of one of 4 parallel A/D converter channels. Scaling between the analog input voltage and the output of the block is:

Input Voltage Range	Simulink Output
-10 V ... +10 V	-1 ... +1 (double)

Thus, as presented in figure AA.2, to read the real value of the signal after the ADC block a gain of value 10 must be placed. Double - click on the block and 4 values can be chosen that portray the four different channels. The pins of these channels are presented in the following figures.

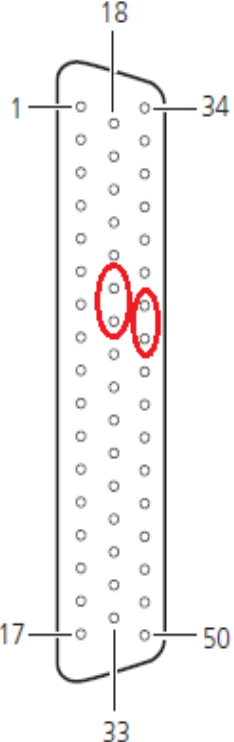
Connector P1A	Pin	Signal	Pin	Signal	Pin	Signal
	1	GND	18	GND	34	ADCH2
	2	ADCH4	19	ADCH6	35	GND
	3	GND	20	GND	36	ADCH8
	4	ADCH10	21	ADCH12	37	GND
	5	GND	22	GND	38	ADCH14
	6	ADCH16	23	ADCH18	39	GND
	7	GND	24	GND	40	ADCH20
	8	GND	25	DACH2	41	GND
	9	GND	26	GND	42	DACH4
	10	DACH6	27	DACH8	43	GND
	11	GND	28	GND	44	GND
	12	SADCH2	29	SADCH4	45	GND
	13	GND	30	GND	46	SADCH6
	14	SADCH8	31	SADCH10	47	GND
	15	GND	32	GND	48	SADCH12
	16	SADCH14	33	SADCH16	49	GND
	17	GND			50	GND

Figure AA.3. Channels 18 and 20 pins.

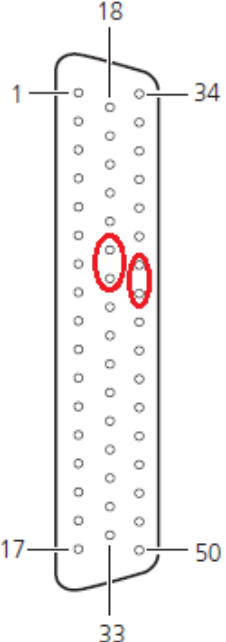
Connector P1B	Pin	Signal	Pin	Signal	Pin	Signal
	1	GND	18	GND	34	ADCH1
	2	ADCH3	19	ADCH5	35	GND
	3	GND	20	GND	36	ADCH7
	4	ADCH9	21	ADCH11	37	GND
	5	GND	22	GND	38	ADCH13
	6	ADCH15	23	ADCH17	39	GND
	7	GND	24	GND	40	ADCH19
	8	GND	25	DACH1	41	GND
	9	GND	26	GND	42	DACH3
	10	DACH5	27	DACH7	43	GND
	11	GND	28	GND	44	GND
	12	SADCH1	29	SADCH3	45	GND
	13	GND	30	GND	46	SADCH5
	14	SADCH7	31	SADCH9	47	GND
	15	GND	32	GND	48	SADCH11
	16	SADCH13	33	SADCH15	49	GND
	17	GND			50	SADCSOC

Figure AA.4. Channels 17 and 19 pins.

The value of channel can be measured correctly only under the condition that the other lead of the signal is connected to the ground. The next block is similar and it allows reading from up to 4 channels of one of the 4 parallel A/D converters that are multiplexed to 4 channels each.

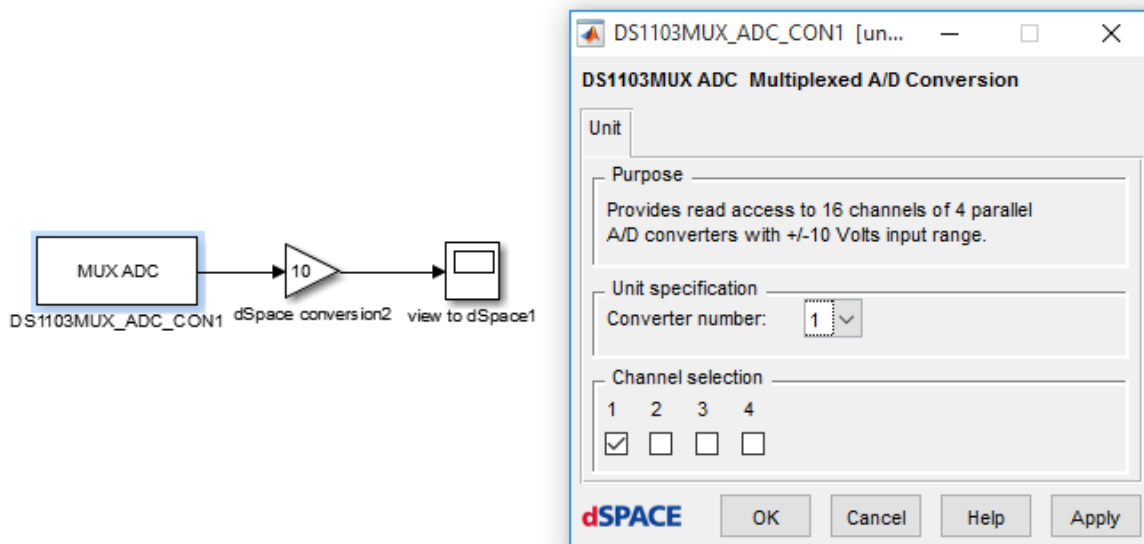


Figure AA.5. DS1103MUX_ADC_CONx block.

Scaling between the analog input voltage and the output of the block is the same as in the DS1103ADC_Cx. Thus, as presented in figure AA.5, to read the real value of the signal after the ADC block a gain of value 10 must be placed. Double - click on the block and you can use either the Converter number or the Channel Selection. Each block is related to one of 4 independent A/D converters. Therefore, you can access channel 1 ... 4 using the first converter, channel 5 ... 8 using the second, and so on. For optimized data conversion do not use more than one channel from one converter if possible. Using only one channel per converter leads to parallel conversion of the channels. Therefore, use the channels 1, 5, 9, and 13 if your application needs 4 input channels. The pins of these channels are presented in the following figures.

Connector P1A	Pin	Signal	Pin	Signal	Pin	Signal
	1	GND			34	ADCH2
	2	ADCH4	18	GND	35	GND
	3	GND	19	ADCH6	36	ADCH8
	4	ADCH10	20	GND	37	GND
	5	GND	21	ADCH12	38	ADCH14
	6	ADCH16	22	GND	39	GND
	7	GND	23	ADCH18	40	ADCH20
	8	GND	24	GND	41	GND
	9	GND	25	DACH2	42	DACH4
	10	DACH6	26	GND	43	GND
	11	GND	27	DACH8	44	GND
	12	SADCH2	28	GND	45	GND
	13	GND	29	SADCH4	46	SADCH6
	14	SADCH8	30	GND	47	GND
	15	GND	31	SADCH10	48	SADCH12
	16	SADCH14	32	GND	49	GND
	17	GND	33	SADCH16	50	GND

Figure AA.6. Correspondence of pins. Converter 1 (green), Converter 2 (red), Converter 3 (blue) and Converter 4 (orange).

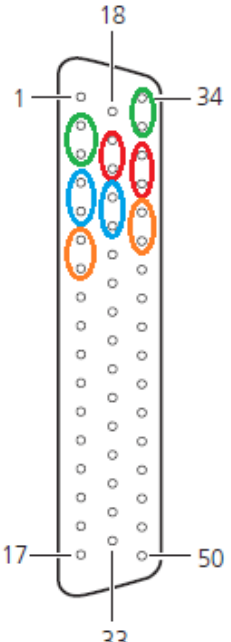
Connector P1B	Pin	Signal	Pin	Signal	Pin	Signal
	1	GND	18	GND	34	ADCH1
	2	ADCH3	19	ADCH5	35	GND
	3	GND	20	GND	36	ADCH7
	4	ADCH9	21	ADCH11	37	GND
	5	GND	22	GND	38	ADCH13
	6	ADCH15	23	ADCH17	39	GND
	7	GND	24	GND	40	ADCH19
	8	GND	25	DACH1	41	GND
	9	GND	26	GND	42	DACH3
	10	DACH5	27	DACH7	43	GND
	11	GND	28	GND	44	GND
	12	SADCH1	29	SADCH3	45	GND
	13	GND	30	GND	46	SADCH5
	14	SADCH7	31	SADCH9	47	GND
	15	GND	32	GND	48	SADCH11
	16	SADCH13	33	SADCH15	49	GND
	17	GND			50	SADCSOC

Figure AA.7. The pins on the connector. Converter 1 (green), Converter 2 (red), Converter 3 (blue) and Converter 4 (orange).

- **D/A converter**

To write to D/A converter channels, the block DS1103DAC_Cx can be used for one of the 8 parallel D/A converter channels provided, as presented in figure AA.8.

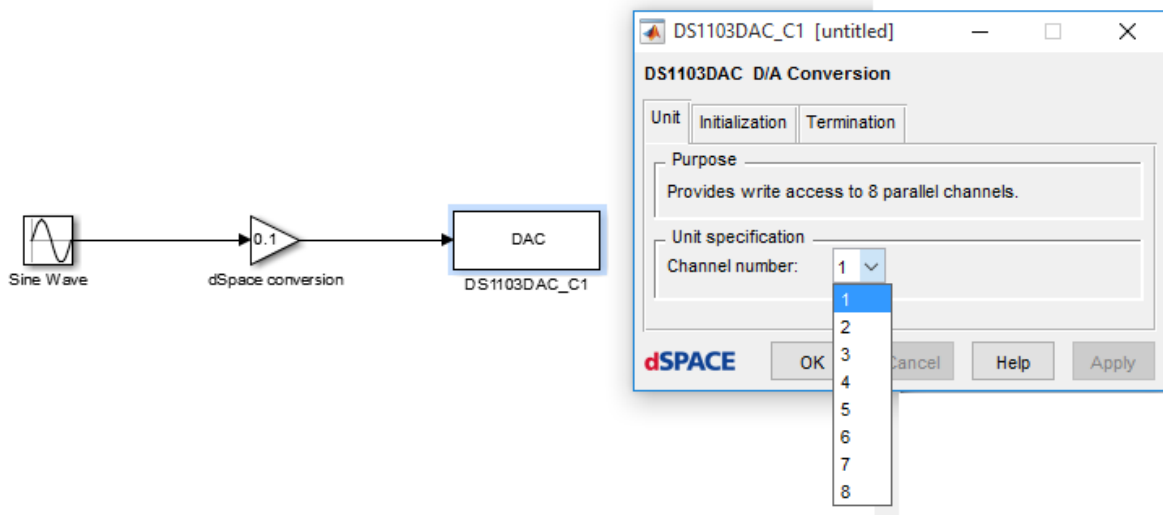


Figure AA.8. DS1103DAC_Cx block.

Scaling between the analog input voltage and the output of the block is:

Input Voltage Range	Simulink Output
-1 ... +1 (double)	-10 V ... +10 V

Thus, as presented in figure AA.8, to read the real value of the signal after the ADC block a gain of value 0.1 must be placed. Double - click on the block and 8 values can be chosen that portray the eight different channels. The pins of these channels are presented in the following figures.

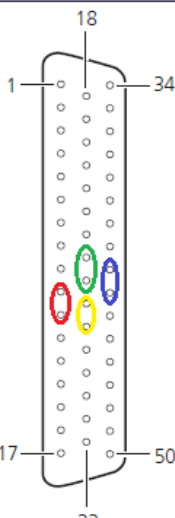
Connector P1A	Pin	Signal	Pin	Signal	Pin	Signal
	1	GND	18	GND	34	ADCH2
	2	ADCH4	19	ADCH6	35	GND
	3	GND	20	GND	36	ADCH8
	4	ADCH10	21	ADCH12	37	GND
	5	GND	22	GND	38	ADCH14
	6	ADCH16	23	ADCH18	39	GND
	7	GND	24	GND	40	ADCH20
	8	GND	25	DACH2	41	GND
	9	GND	26	GND	42	DACH4
	10	DACH6	27	DACH8	43	GND
	11	GND	28	GND	44	GND
	12	SADCH2	29	SADCH4	45	GND
	13	GND	30	GND	46	SADCH6
	14	SADCH8	31	SADCH10	47	GND
	15	GND	32	GND	48	SADCH12
	16	SADCH14	33	SADCH16	49	GND
	17	GND			50	GND

Figure AA.9. The pins on the connector. For instance, if Channel 2 is used, then the DACH2 must be connected.

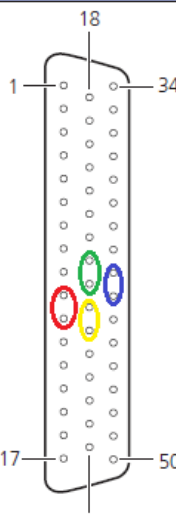
Connector P1B	Pin	Signal	Pin	Signal	Pin	Signal
	1	GND	18	GND	34	ADCH1
	2	ADCH3	19	ADCH5	35	GND
	3	GND	20	GND	36	ADCH7
	4	ADCH9	21	ADCH11	37	GND
	5	GND	22	GND	38	ADCH13
	6	ADCH15	23	ADCH17	39	GND
	7	GND	24	GND	40	ADCH19
	8	GND	25	DACH1	41	GND
	9	GND	26	GND	42	DACH3
	10	DACH5	27	DACH7	43	GND
	11	GND	28	GND	44	GND
	12	SADCH1	29	SADCH3	45	GND
	13	GND	30	GND	46	SADCH5
	14	SADCH7	31	SADCH9	47	GND
	15	GND	32	GND	48	SADCH11
	16	SADCH13	33	SADCH15	49	GND
	17	GND			50	SADCSOC

Figure AA.10. The pins on the connector.

- **PWM Signal Generation**

To generate PWM pulses two blocks can be used. The DS1103SL_DSP_PWM and the DS1103SL_DSP_PWM3, presented in figures AA.11 and AA.12.

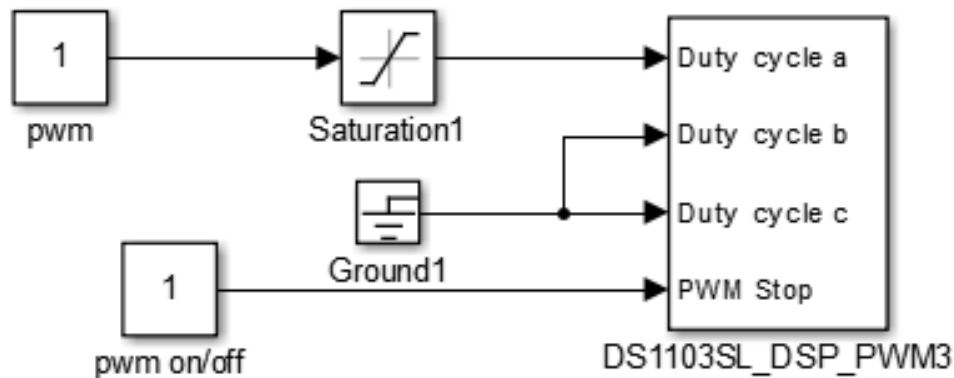


Figure AA.11. The DS1103SL_DSP_PWM3 block.

This block To generate 3-phase PWM signals with original and inverted outputs, variable duty cycles, and a variable deadband in symmetric PWM mode. Using the DS1103_DSP_PWM3 block, a PWM interrupt from the slave DSP to the master PPC is available. The interrupt can be triggered nearly over the whole period (interrupt alignment). The interrupt signal is provided via ST1PWM for user - specific purposes. To make the PWM interrupt available to your system, the DS1103SLAVE_PWMINT block must be used. The PWM interrupt can be used to synchronize the generation of the PWM signals on the slave DSP with, for example, the input of the A/D converters of the master PPC. The size of the deadband must be selected carefully to avoid effects caused by a deadband which is too big for the chosen PWM period. The following table shows the available block ports related to the Simulink data types:

Simulink Inport	Value	Data Type	Meaning
Duty cycle a, b, c	0 ... 1	Double	Duty cycle of the PWM signal for channel a, b, c.
Stop PWM	0 / 1	Boolean	Enables PWM stop for channel pairs a/ \bar{a} , b/ \bar{b} and c/ \bar{c} : <ul style="list-style-type: none"> Value 1 stops PWM generation Value 0 resumes PWM generation

- **Warnings**

- PWM stop suspends the output of the PWM signal. Internally the signal is still generated. If you resume PWM signal generation the currently calculated value is output and not the initialization or termination value.
- If you specified *Deadband* = 0 and *PWM Stop* = TTL low (termination value), and you resume the PWM signal generation, all signals are momentarily on high level. To avoid this misbehavior of the slave DSP, use always a deadband greater than 0.

- PWM stop has no influence on interrupt generation activated by the DS1103SLAVE_PWMINT block.
- If the inverse channels are not required, set *Deadband* = 0, because for low duty cycles the original signal will be zero. For motor control this trait can make the controller dysfunctional.

Double click on the block and the window presented in figure AA.12 appears.

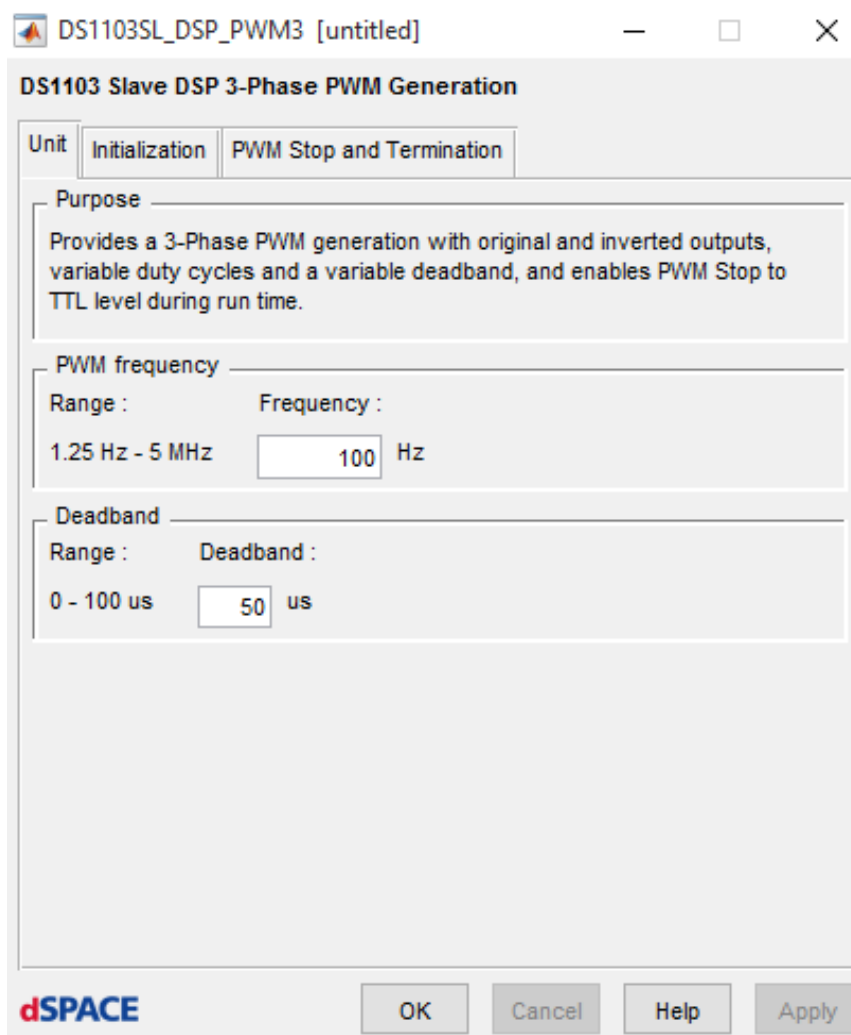


Figure AA.12. Options window for the DS1103SL_DSP_PWM3 block.

Its purpose is to set the following:

- **PWM frequency** Lets you specify the PWM frequency within the range 1.25 Hz ... 5 MHz.
- **Deadband** Lets you specify the deadband between the original and the inverted output signals. The maximum value is 100 μ s and nevertheless it should correspond to the PWM period, so it should not exceed 50% of the PWM period.

The next block is similar and it allows To generate standard PWM signals with variable duty cycles and enable PWM stop during run time, as presented in figure AA.13.

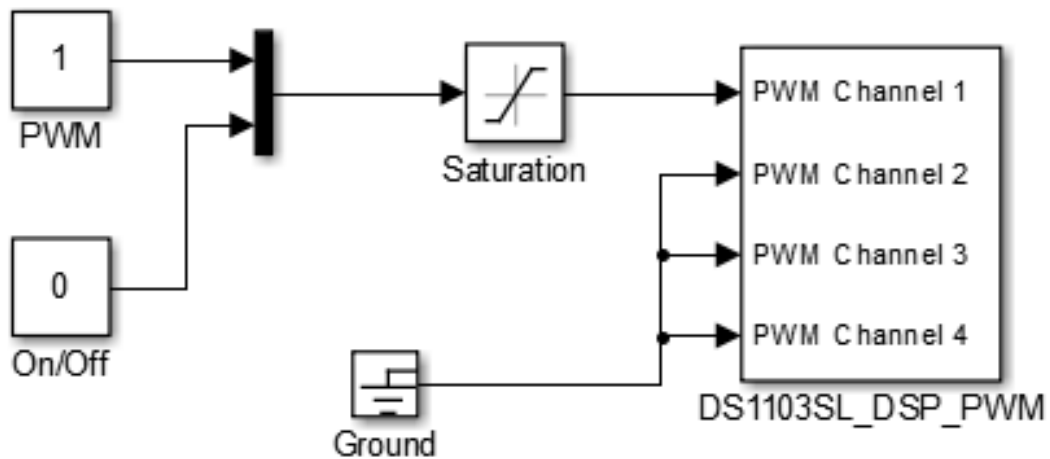


Figure AA.13. The DS1103SL_DSP_PWM block.

For 1-phase PWM generation, a PWM stop can be specified to suspend PWM signal output during run time. The outputs of the channels are set to a defined TTL level. The dimensions of the inports are set to 2, which allow entering two values over the same port. This can be done via a Simulink MUX block, for instance as shown in figure AA.13. Value 1 specifies the duty cycle and value 2 the PWM stop behavior. If value 2 is to “0” a PWM signal is generated, “1” suspends signal generation and sets the output to the specified TTL level. If the PWM stop is disabled for a channel only the duty cycle can be input. Although the PWM stop feature can be disabled for each channel during run time, it can be specified whether it is desired to set the PWM output to a specified TTL level or to generate a signal during the initialization phase. The following table shows the available block ports related to the Simulink data types.

Simulink Inport	Input	Value	Data Type	Meaning
PWM Channel 1 ... 4	Duty cycle 1 ... 4	0 ... 1	Double	Duty cycle of the PWM signal for channel 1 ... 4.
	PWM Stop 1 ... 4	0 / 1	Boolean	Enables PWM stop for channel 1 ... 4: <ul style="list-style-type: none"> Value 1 stops PWM generation Value 0 resumes PWM generation

Double - click on the block and the window presented in figure AA.14 appears.

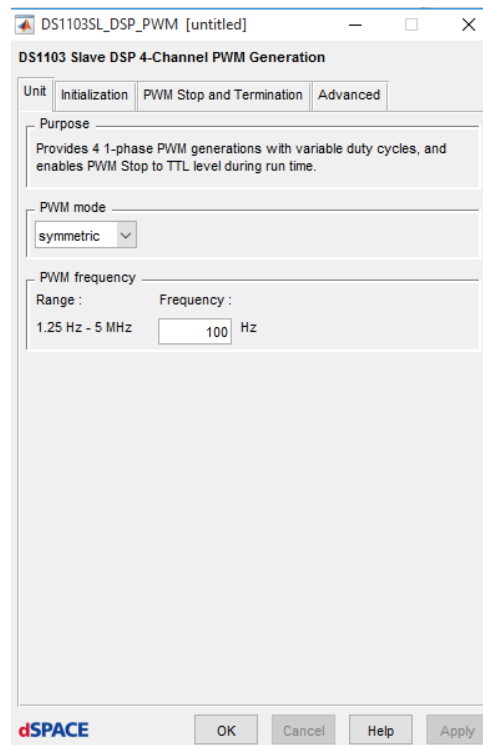


Figure AA.14. Options window for the DS1103SL_DSP_PWM block.

Its purpose is to set the following:

- **PWM mode** Lets you select "asymmetric" to start the pulse at the beginning of the PWM period, or "symmetric" to generate mid - symmetric PWM waveforms.
- **PWM frequency** Lets you select the PWM frequency. The frequency ranges correspond to the specified PWM mode:

PWM Mode	PWM Frequency
Asymmetric	2.5 Hz ... 5 MHz
Symmetric	1.25 Hz ... 5 MHz

For both blocks the correlation between the channel and its respective pin unfortunately requires deciphering, thus in the following tables the mapping between the RTI block and RTLib functions and the corresponding pins used to provide PWM signals is displayed.

Related RTI Block	Related RTLib Functions	Phase	Conn. Pin	Sub-D Pin	Pin on CP/CLP	Signal
DS1103SL_DSP_PWM3	See <i>Slave DSP PWM3 Generation</i>	Phase 1	P2 65	P2B 28	CP31 7	SPWM1
		Phase 2	P2 67	P2B 12	CP31 8	SPWM3
		Phase 3	P2 69	P2B 45	CP31 9	SPWM5
		Phase 1 (inverted)	P2 66	P2A 28	CP31 26	SPWM2
		Phase 2 (inverted)	P2 68	P2A 12	CP31 27	SPWM4
		Phase 3 (inverted)	P2 70	P2A 45	CP31 28	SPWM6

Related RTI Block	Related RTLib Functions	Channel	Conn. Pin	Sub-D Pin	Pin on CP/CLP	Signal
DS1103SL_DSP_PWM	See <i>Slave DSP PWM Generation</i>	Ch 1	P2 60	P2A 27	CP31 5	ST2PWM
		Ch 2	P2 71	P2B 29	CP31 10	SPWM7
		Ch 3	P2 72	P2A 29	CP31 29	SPWM8
		Ch 4	P2 73	P2B 13	CP31 11	SPWM9

The pins of these channels are presented in the following figures.

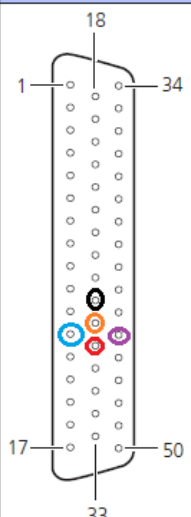
Connector P2A	Pin	Signal	Pin	Signal	Pin	Signal
	1	GND	18	IO1	34	GND
	2	IO3	19	IO5	35	GND
	3	IO7	20	IO9	36	GND
	4	IO11	21	IO13	37	GND
	5	IO15	22	IO17	38	GND
	6	IO19	23	IO21	39	GND
	7	IO23	24	IO25	40	GND
	8	IO27	25	IO29	41	GND
	9	IO31	26	STINT2	42	GND
	10	STMCLK	27	ST2PWM	43	GND
	11	SPDPINT	28	SPWM2	44	GND
	12	SPWM4	29	SPWM8	45	SPWM6
	13	GND	30	SCAP2	46	GND
	14	SCAP4	31	SBIO	47	GND
	15	SSTE	32	GND	48	SSOMI
	16	INT1	33	VCC1 (+ 5 V)	49	INT3
	17	VCC1 (+ 5 V)			50	GND

Figure AA.15. The PWM pins on the connector.

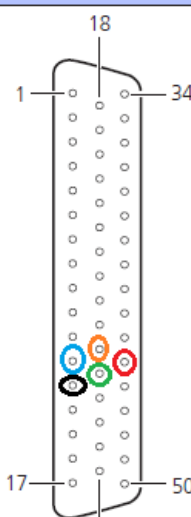
Connector P2B	Pin	Signal	Pin	Signal	Pin	Signal
	1	GND	18	IO0	34	GND
	2	IO2	19	IO4	35	GND
	3	IO6	20	IO8	36	GND
	4	IO10	21	IO12	37	GND
	5	IO14	22	IO16	38	GND
	6	IO18	23	IO20	39	GND
	7	IO22	24	IO24	40	GND
	8	IO26	25	IO28	41	GND
	9	IO30	26	STINT1	42	GND
	10	STMRDIR	27	ST1PWM	43	GND
	11	ST3PWM	28	SPWM1	44	GND
	12	SPWM3	29	SPWM7	45	SPWM5
	13	SPWM9	30	SCAP1	46	GND
	14	SCAP3	31	SXF	47	GND
	15	SSCLK	32	GND	48	SSIMO
	16	INT0	33	VCC1 (+ 5 V)	49	INT2
	17	VCC1 (+ 5 V)			50	GND

Figure AA.16. The PWM pins on the connector.

As usual the ground should be connected as well to generate the PWM signal.

- **Reading Encoders**

For the control prototyping one of the most important factors is the feedback of the control scheme. Usual outputs are the position and the velocity of the actuators of the system. Moreover, to find the parameters of a system, the velocity and the position responses are required to define them. Thus the main encoder blocks will be presented and some examples to unravel some details that are significant to use these blocks efficiently.

The first block is presented in figure AA.17 and it is the DS1103ENC_SETUP. Its purpose is to set the global parameters for the encoder channels. Double - click on the block and the setting window appears, allowing changing the following:

- **Encoder signal type** Differential (RS422) or single-ended (TTL) can be chosen for channels 1 ... 6. The encoder signal type for channel 7 can be selected as “Voltage” or “Current”.

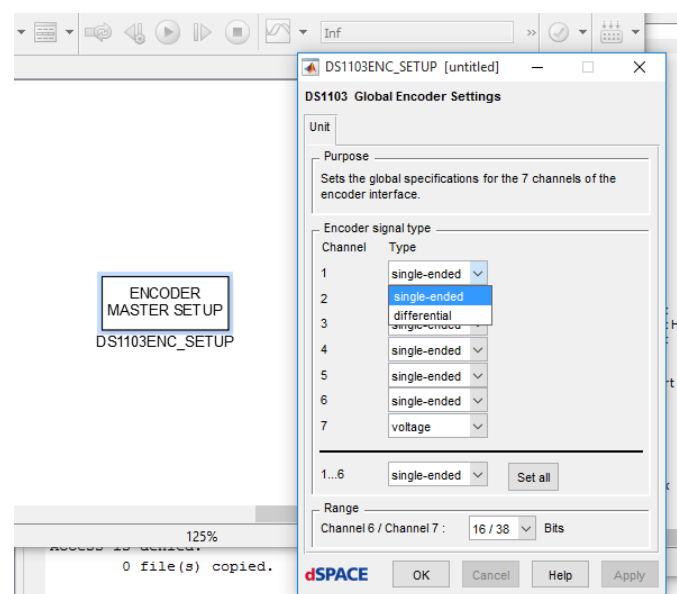


Figure AA.17. The DS1103ENC_SETUP block.

Without this block all of the other encoder related blocks cannot be used. Next, in figure AA.18 the DS1103ENC_POS_Cx block is presented.

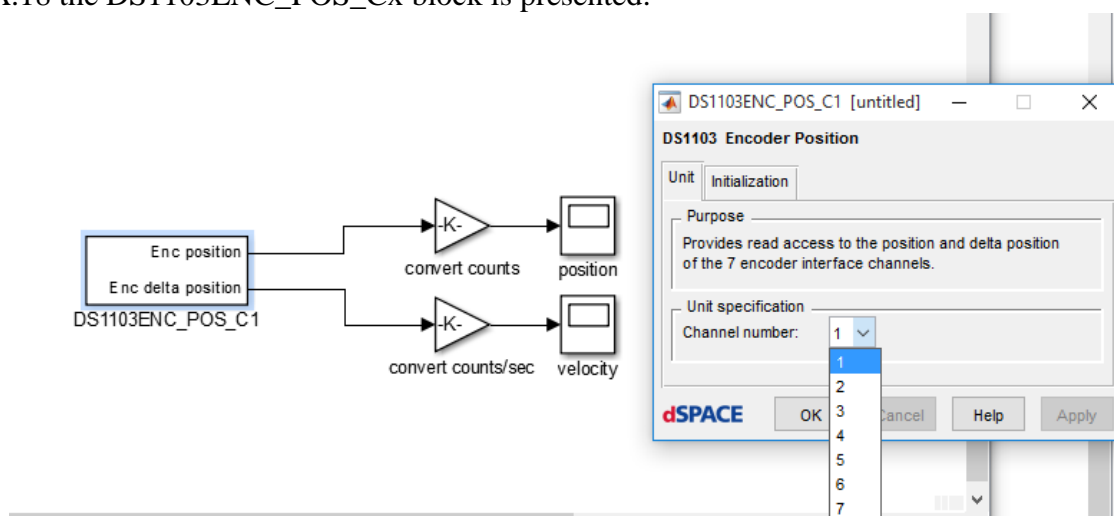


Figure AA.18. The DS1103ENC_POS_Cx block.

Its purpose is to read the position and delta position of one of the 7 encoder channels. By double clicking on the block the channel that is used can be selected. To measure the position in degrees the user must use the gain block with the value $(360/\# \text{ of counts per revolution})$. The counts per revolution are provided in the datasheet of the motor. To measure the velocity use a gain block as well, but this time apart from the term $(360/\# \text{ of counts per revolution})$, the inverse of the sample rate. For instance, if the sampling rate is 0.001 sec, then to measure the value in deg/s the gain block must have the value $(0.001)^{-1} * (360/\# \text{ of counts per revolution})$. Thus the following equations must be used:

$$\theta[\text{deg}] = \text{EncPosition} \frac{360}{\text{countsperrevolution}} \quad (\text{AA.1})$$

$$\frac{d\theta}{dt} \left[\frac{\text{deg}}{\text{sec}} \right] = \text{EncDeltaPosition} (\text{samplingrate})^{-1} \frac{360}{\text{countsperrevolution}} \quad (\text{AA.2})$$

The following block that is presented in figure AA.19 is the DS1103ENC_SET_POS_Cx block.

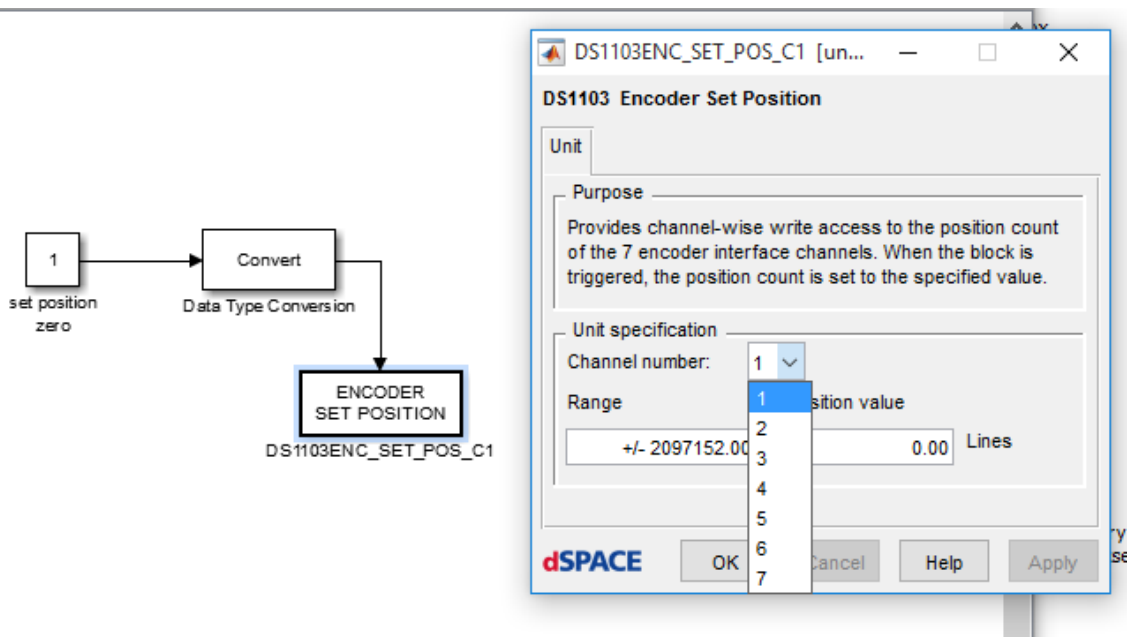


Figure AA.19. The DS1103ENC_SET_POS_Cx block.

Its purpose is to write to the position counter of one of 7 encoder channels. When the block is triggered during simulation by a rising edge signal, the counter of the specified channel is set to the adjusted position value, which must be given in lines. This block is ideal to set the values of the encoders to zero, so that the control plant will not have any initial values and to begin potential experiments again.

The upcoming block that is presented in figure AA.20 is the DS1103ENC_SW_INDEX_Cx block. Its purpose is to poll the encoder index of the channel selected and optionally to set the position counter by software.

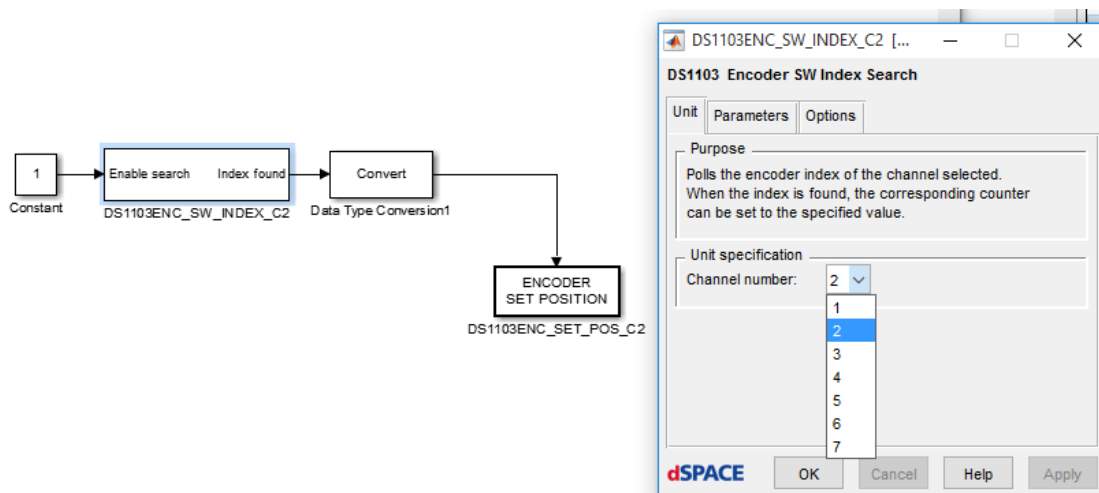


Figure AA.20. The DS1103ENC_SW_INDEX_Cx block.

This block can be used to display when the encoder has measured one complete revolution. An input value greater than zero, for example from a Simulink Constant input block, enables an index search for the selected interface channel. The block output depends on the selected search mode (Type of index search). By default, the index is searched twice (the Search index twice for speed-up checkbox is selected). If “Search index twice for speed-up” is cleared:

State	Simulink Output	
	Without Data Typing	With Data Typing
Index has not been found yet.	0 (double)	0 (int8)
Index has been found. Search is finished.	1 (double)	1 (int8)

If “Search index twice for speed-up” is selected:

State	Simulink Output	
	Without Data Typing	With Data Typing
Index has not been found yet.	-1 (double)	-1 (int8)
Index has been found once.	0 (double)	0 (int8)
Index has been found for the second time. Search is finished.	1 (double)	1 (int8)

The following figure shows the block output depending on the selected search options.

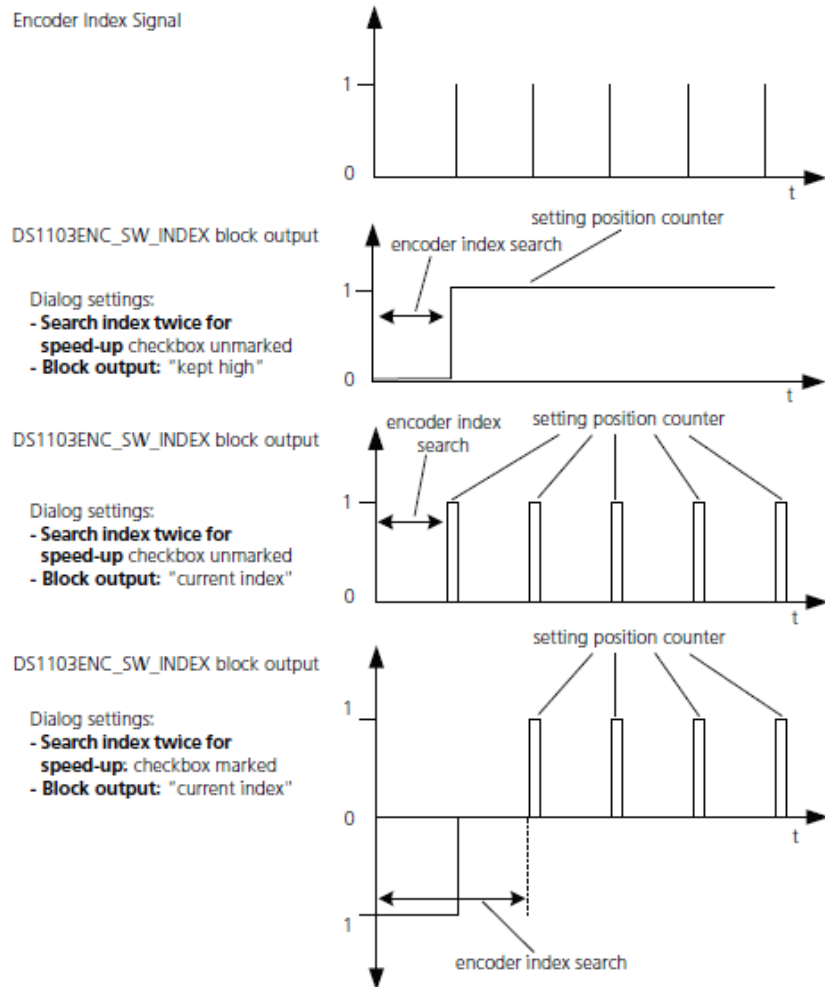


Figure AA.21. The DS1103ENC_SW_INDEX_Cx block output.

This block can be used with the the DS1103ENC_SET_POS_Cx block to measure the real value of counts that are corresponding to one revolution, to increase the precision of the measurements as displayed in figure AA.20. In the following figures the mapping of the pins for the first two encoder channels will be presented.

Connector P3A	Pin	Signal	Pin	Signal	Pin	Signal
	1	GND	18	DCD (RXD)	34	Not used for RS232 (TXD)
	2	DTR (RTS)	19	GND	35	DSR (CTS)
	3	STXD	20	—	36	SRXD
	4	—	21	—	37	—
	5	—	22	PHI0(7)	38	GND
	6	PHI90(7)	23	GND	39	IDX(7)
	7	PHI0(6)	24	IDX(6)	40	PHI90(6)
	8	GND	25	PHI90(1)	41	PHI0(1)
	9	IDX(1)	26	PHI0(2)	42	GND
	10	PHI90(2)	27	GND	43	IDX(2)
	11	PHI0(3)	28	IDX(3)	44	PHI90(3)
	12	GND	29	PHI90(4)	45	PHI0(4)
	13	IDX(4)	30	PHI0(5)	46	GND
	14	PHI90(5)	31	GND	47	IDX(5)
	15	GND	32	GND	48	GND
	16	VCC2 (+ 5 V)	33	VCC3 (+ 5 V)	49	VCC2 (+ 5 V)
	17	VCC3 (+ 5 V)			50	GND

Figure AA.22. The mapping for the inverse channels of the first two channels.

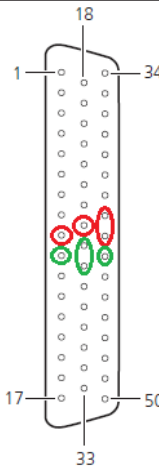
Connector P3B	Pin	Signal	Pin	Signal	Pin	Signal
	1	GND	18	RXD (RXD)	34	TXD (TXD)
	2	RTS (RTS)	19	RI (not used for RS422)	35	CTS (CTS)
	3	STXD	20	—	36	SRXD
	4	—	21	—	37	—
	5	—	22	PHI0(7)	38	GND
	6	PHI90(7)	23	GND	39	IDX(7)
	7	PHI0(6)	24	IDX(6)	40	PHI90(6)
	8	GND	25	PHI90(1)	41	PHI0(1)
	9	IDX(1)	26	PHI0(2)	42	GND
	10	PHI90(2)	27	GND	43	IDX(2)
	11	PHI0(3)	28	IDX(3)	44	PHI90(3)
	12	GND	29	PHI90(4)	45	PHI0(4)
	13	IDX(4)	30	PHI0(5)	46	GND
	14	PHI90(5)	31	GND	47	IDX(5)
	15	CANL	32	GND	48	CANH
	16	VCC2 (+ 5 V)	33	VCC3 (+ 5 V)	49	VCC2 (+ 5 V)
	17	VCC3 (+ 5 V)			50	GND

Figure AA.23. The mapping for the original channels of the first two channels.

- **Incremental Encoder Interface**

Next it will be presented the proper connection of the encoder with the connectors of the expansion box, depending on the encoder (single - ended or differential). Also some general instructions will be presented.

If your encoder provides differential signals (RS422, 1 Vpp, or 11 μ App signals), connect:

- The encoder output signals to the PHI0, PHI90 and IDX pins of the corresponding input channel.
- The inverted signals to the PHI0, PHI90 and IDX pins of the corresponding input channel.

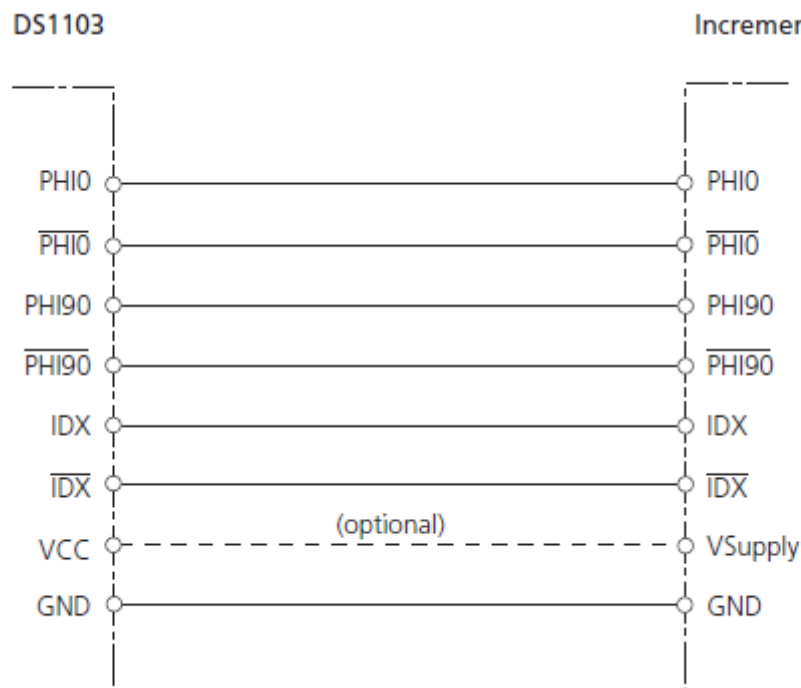


Figure AA.24. Encoder with differential signals connection.

If your encoder provides single - ended TTL signals, the inverted pins (PHI90, PHI0 and IDX) must be left unconnected.

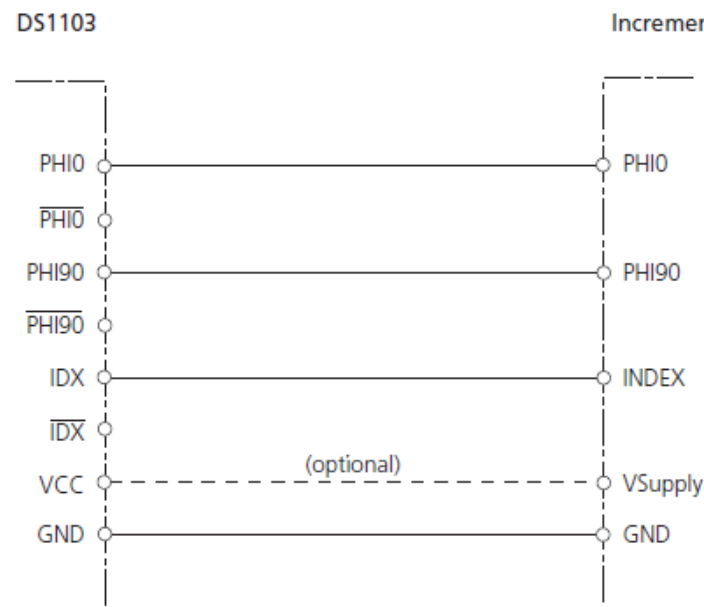


Figure AA.25. Encoder with single - ended signals connection.

For single - ended 1 Vpp signals, the connection depends on the value of the mean voltage (VCM) of the corresponding signals:

- If the mean voltage of the encoder signals is 0 V, you can connect pins PHI0, PHI90 and IDX to the GND pin
- If the mean voltage is not 0 V ($0\text{ V} < V_{CM} < 2.5\text{ V}$), you have to provide this voltage in the range 0 ... 2.5 V yourself

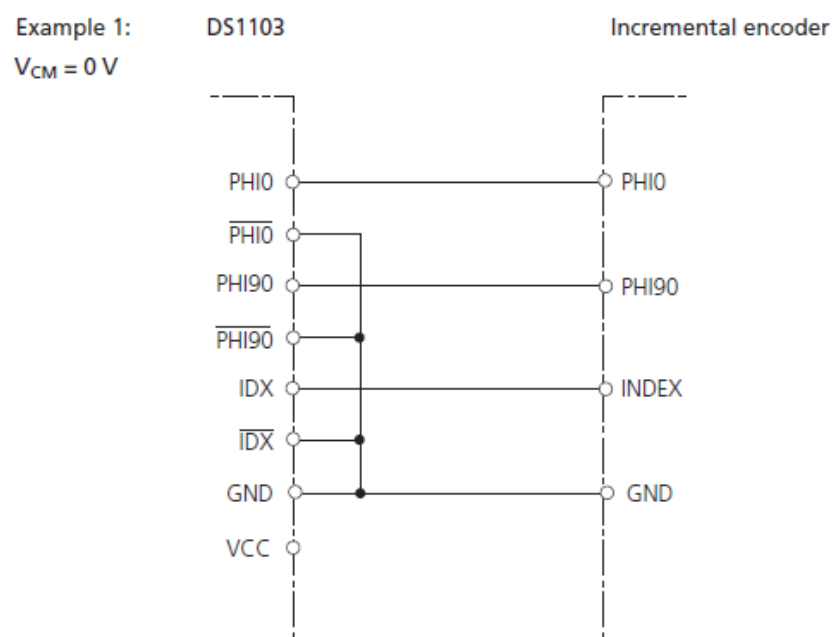


Figure AA.26. Single - ended 1 Vpp signals connection, case 1.

Example 2:
 $0\text{ V} < V_{CM} < 2.5\text{ V}$

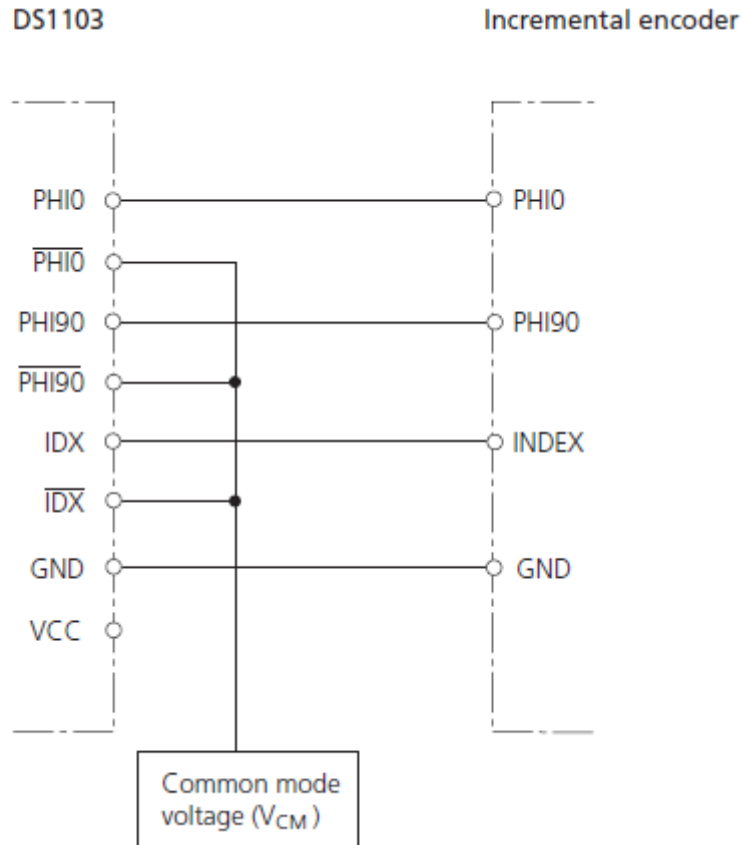


Figure AA.27. Single - ended 1 Vpp signals connection, case 2.

- **Supplying Power to Encoders**

The DS1103 offers three power supply outputs (VCC pins). You should use these supply voltages for all connected incremental encoders. All VCC pins must be connected so that the current is shared evenly by all pins. Use wires of sufficient diameter to avoid voltage drops. This does not apply if the connector panels are used to connect the encoder(s) to the board since the VCC pins are internally connected at the connector panels.

If the encoder's supply requirements cannot be met by the DS1103, an external supply voltage must be used. In this case:

- You have to guarantee that no input voltages are fed to the DS1103 while it is switched off
- You have to connect the encoder's ground line to a ground pin of the board, as presented in the following figure.

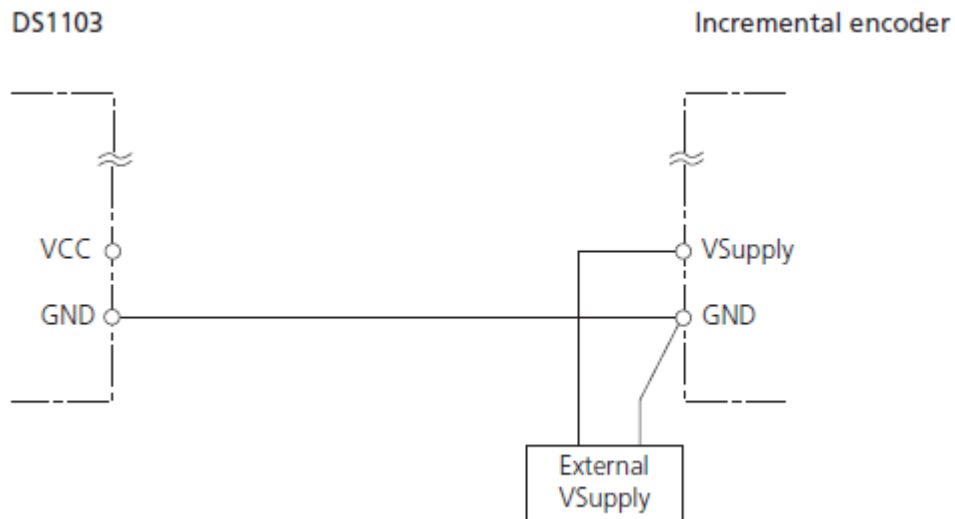


Figure AA.28. Connection of the encoder using external supply.

Connection Setup

For the DS1103 expansion box the connectors are required to be constructed, as presented in figure AA.29. If these connectors need to be purchased, their code name is 50 pin D-SUB male connector cables and pinouts.



Figure AA.29. Connectors of the expansion box.

- **Using typical Simulink blocks in dSpace**

In the code generation procedure it will be common to use blocks from other libraries of Simulink, however, if these blocks are not connected correctly, then at the code generation step an error will be displayed. Because the error explanations are almost always murky, in the following examples it will be displayed the correct way to connect the blocks.

1. Use of blocks the parameters of which are inserted as inputs

Apart from the Constant block and the Gain block, during the real time simulations, the parameters of the other blocks cannot change real - time. Thus, it is advised to use blocks that have as inputs their parameters, inserted with the constant block. An example is presented in figure AA.30 where the Dynamic Saturation and Dynamic Dead Zone are used. Moreover, if the integrator block is used, to change the initial condition real - time in the options of the block the initial condition must be changed from internal to external.

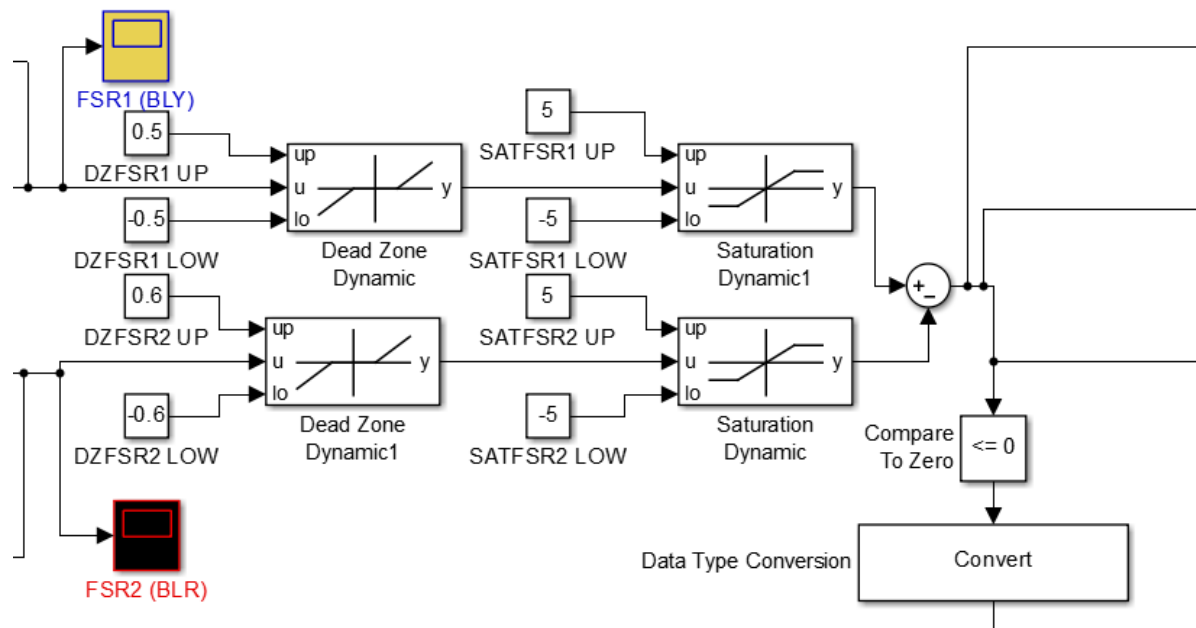


Figure AA.30. Use of Dynamic Dead Zone and Dynamic Saturation block.

2. Be wary using math and logic operators

To use the math and logic operators to make operation between signals, it is mandatory to use the Convert block to make the signals the same type. An example is presented in figure AA.31.

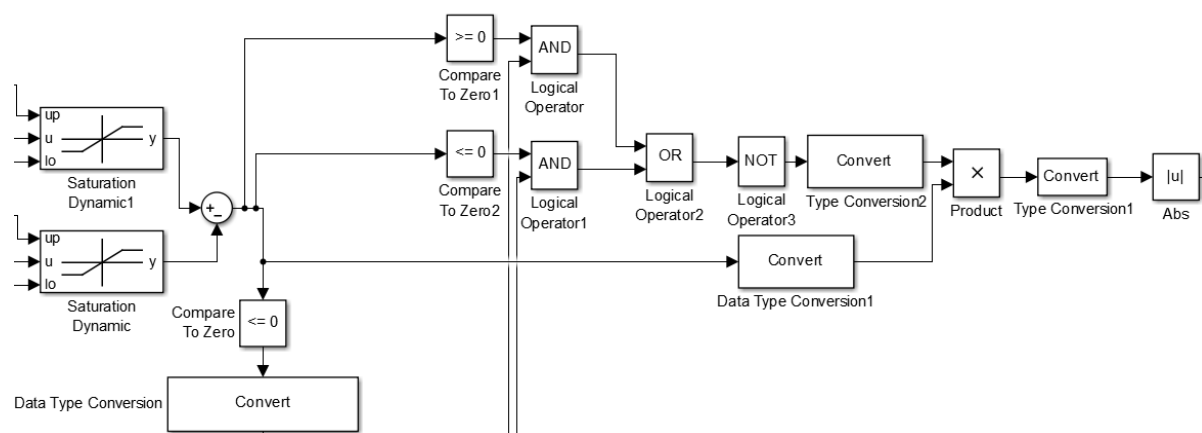


Figure AA.31. Example of using math and logic operations with the Convert block.

3. An illustration of a closed loop scheme

In figure AA.32 a closed loop scheme is presented. It must be noted that the input of the driver of the hbridge or the driver is a PWM pulse. However, the most important is the way that the direction is changed. Typically the drivers have one or two pins related with the direction of the motor. In this example, depending on the value of the error, to change the direction of the motor a logic input of either +5V or 0V is provided to the two pins of the driver. For the record the specific hbridge is the same as in the Biomechatronic EPP configuration (A3959 DMOS Full-Bridge PWM Motor Driver). If during the first experiments the motor does not change direction, then the two D/A converter channels must be switched.

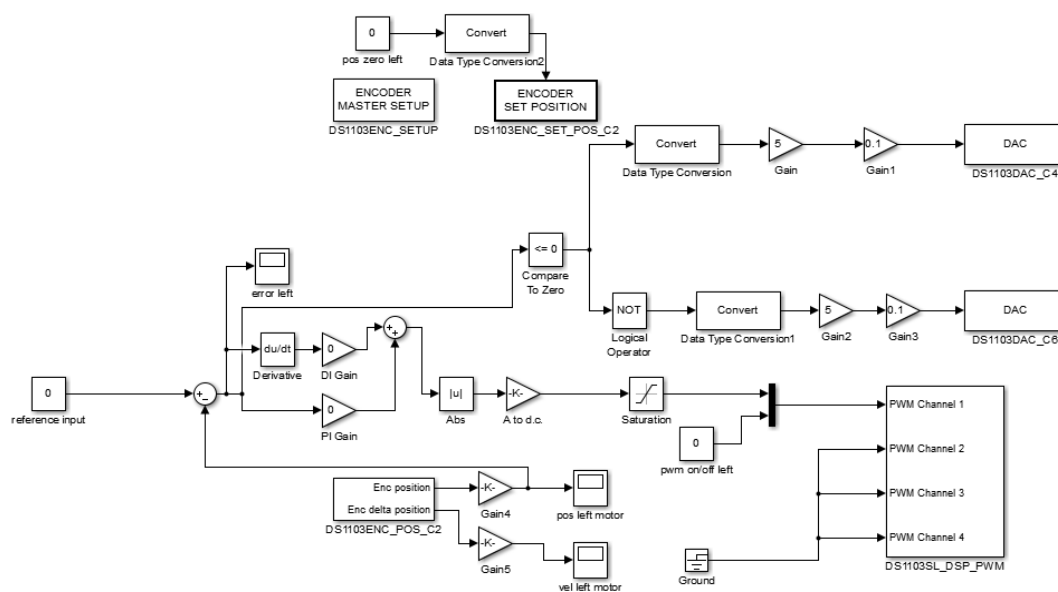


Figure AA.32. Closed loop scheme.

- **Basics using ControlDesk**

Before executing any program the DS1103 must be registered. To achieve this, press "Register Platforms" and select DS1103 PPC Controller Board and Press Register, as presented in figure AA.33.

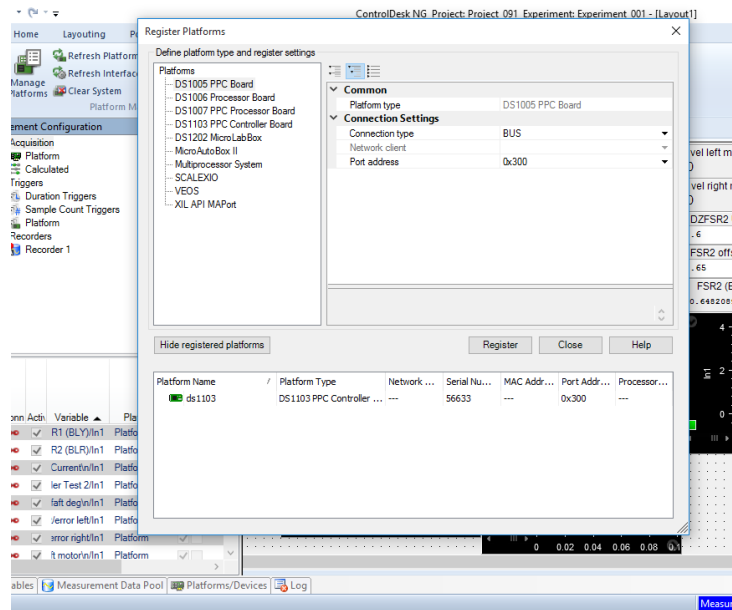


Figure AA.33. The register platform window.

After the creation of the Simulink file to create the code that is used by ControlDesk press Ctrl + B. If there are no errors, in figure AA.34 the following message will appear on the screen.

```

### Creating project marker file: rtw_proj.tmw
.
### Processing Template Makefile: C:\Program Files\dspace RCPHIL 2016-A\MATLAB\RTI\RTI1103\RTI\rti1103.tmf
### Creating test.mk from C:\Program Files\dspace RCPHIL 2016-A\MATLAB\RTI\RTI1103\RTI\rti1103.tmf
### Building test: "%SPACE_ROOT%\Exe\dsmake.exe" -f test.mk EXTMODE_STATIC_ALLOC=0 TMW_EXTMODE_TESTING=0 EXTMODE_STATIC_ALLOC_SIZE=1000000 EXTMODE_TRANSPORT=0 MAT_FILE=0
ISPROTECTINGMODEL=NOTPROTECTING
BUILDING APPLICATION "test" (Single Timer Task Mode)

WORK DIRECTORY "C:\dspace_test2\BigTest2\test14"
BUILD DIRECTORY "C:\dspace_test2\BigTest2\test14\test_rti1103"
TARGET COMPILER "C:\Program Files\dspace RCPHIL 2016-A\Compiler\PPCTools"

COMPILING "test.c"
COMPILING "rtGetInf.c"
COMPILING "rtGetNaN.c"
COMPILING "rt_nonfinite.c"
COMPILING "rt_zfcn.c"
COMPILING "test_data.c"
COMPILING "test_trc_ptr.c"
COMPILING "C:\Program Files\dspace RCPHIL 2016-A\MATLAB\RTI\RTI1103\RTI\rti_sim_engine.c"
COMPILING "C:\Program Files\dspace RCPHIL 2016-A\MATLAB\RTI\RTI1103\RTI\rti_init_c.c"
COMPILING "C:\PROGRAM-1\MATLAB\MATLAB-1\R2015a\rtw\c\src\rt_sim.c"
COMPILING "C:\Program Files\dspace RCPHIL 2016-A\MATLAB\RTI\RTI1103\RTI\rti_assert.c"
COMPILING "C:\Program Files\dspace RCPHIL 2016-A\MATLAB\RTI\RTI1103\RTI\rti_slv1103.c"
LINKING APPLICATION ...
LINKING FINISHED

MAKE PROCESS SUCCEEDED
LOADING APPLICATION "test.sdf" ...
PLATFORM: ds1103
[1] ds1103 - RILIB: DS1103 serial number: 56633 (0)
[3] ds1103 - RTI: Initializing ... (720)
[2] ds1103 - RILIB: Application UUID: 4F290D1C-E49F-40E7-B177-4B97BF5177F0 (0)
[4] ds1103 - RILIB SLVDSP: dSPACE firmware rev. 3.4 detected. (500)
[5] ds1103 - RTI: Initialization completed (721)
[6] ds1103 - RTI: Simulation state: RUN (700)
LOADING FINISHED
### Successful completion of Simulink Coder build procedure for model: test
*** Finished RTI build procedure for model test

```

Build process completed successfully

Figure AA.34 Creating the code from Simulink.

Opening the ControlDesk and selecting File > New and choosing the .sdf file (figure AA.35) created by the code - generation procedure the program will start to be executed.

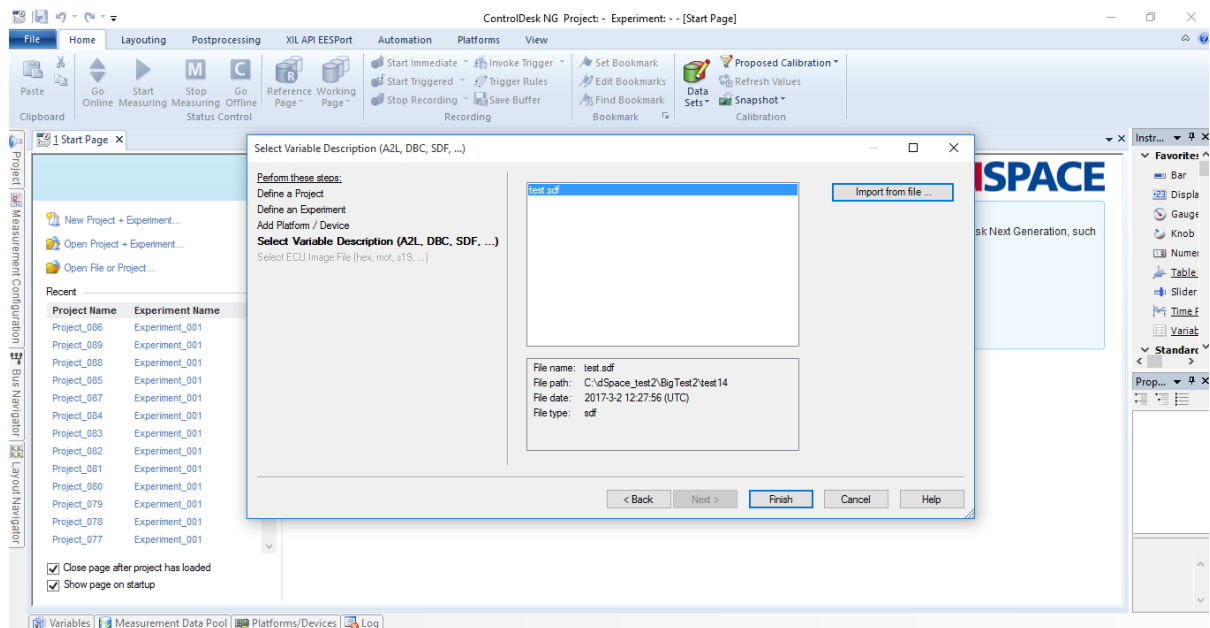


Figure AA.35. Choosing the .sdf file to execute the program.

The environment of ControlDesk allows changing the values of the Constant and Gain Blocks with numeric input, displaying the values of signals with display and time plot, as presented in figure AA.36.

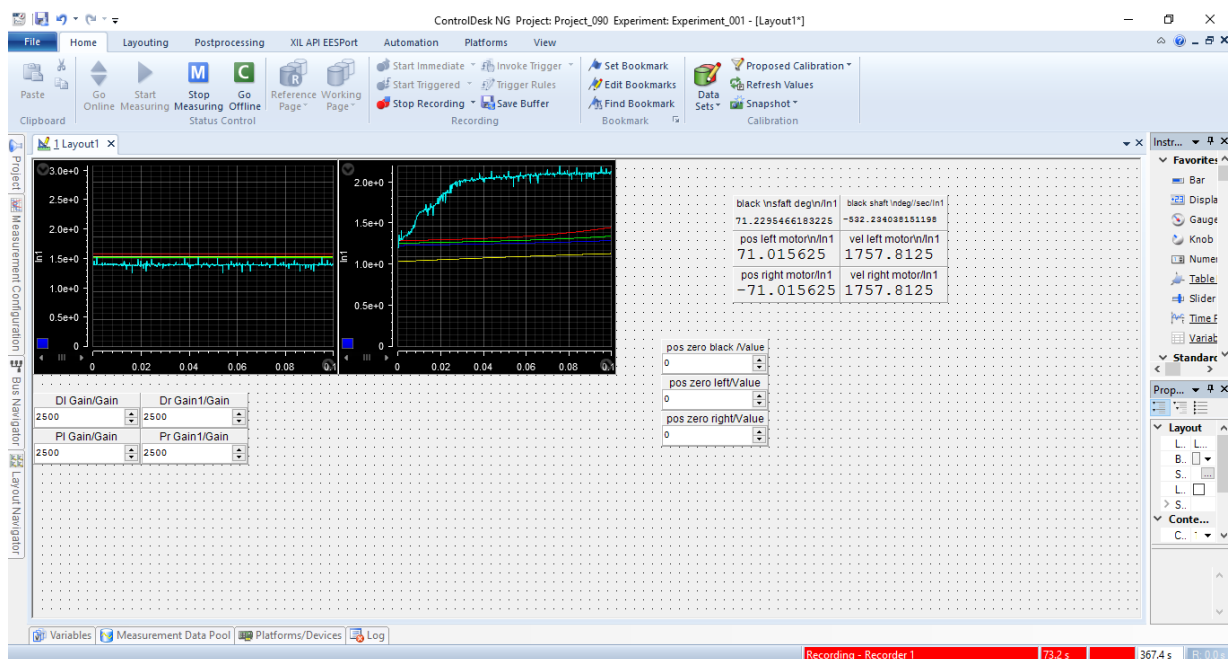


Figure AA.36. The ControlDesk environment.

To record the values of the measurements on the left of the window and selecting Measurement Configuration and selecting on recorder 1 "Start Immediate" the measurements are recorded as presented in figure AA.37.

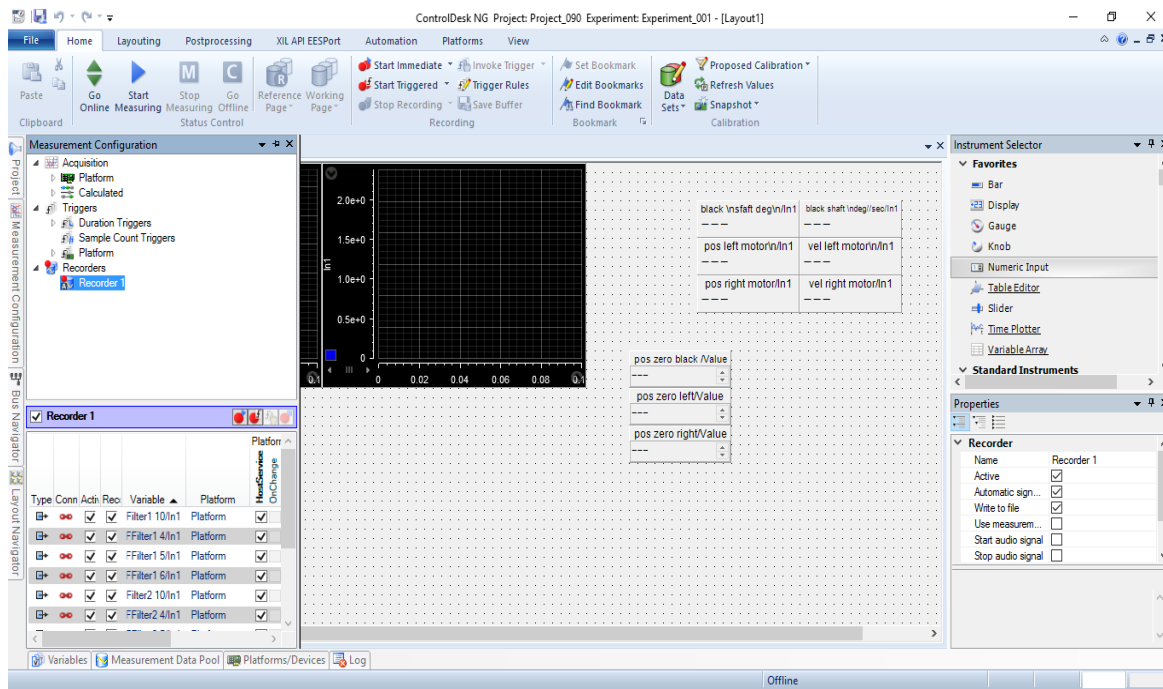


Figure AA.37. Record option.

To change the duration of the displayed signals in time plots the Measurement Configuration must be selected and selecting "Duration Trigger 1" the Duration can be changed, as presented in figure AA.38. However, it must be noted that if many signals are displayed then for high duration values the lagging increases significantly.

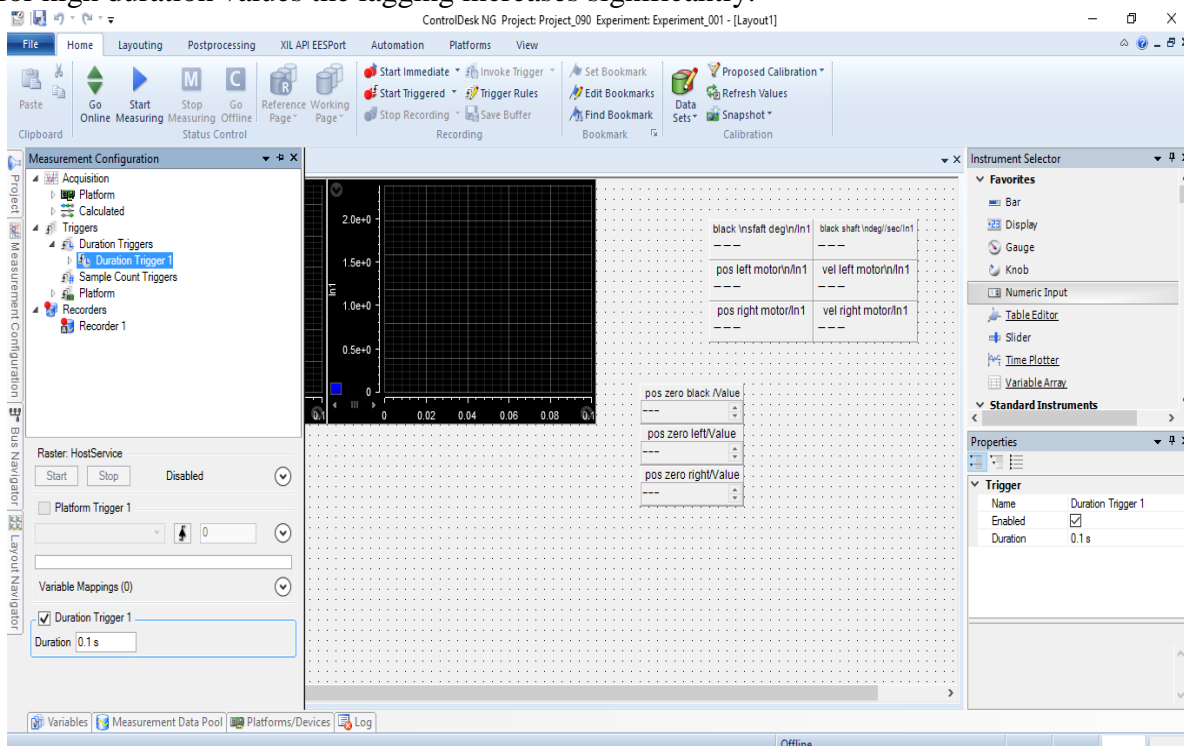


Figure AA.38. Changing the duration of the displayed signals.

The processing of the data after the recording can be achieved using Matlab. However, the measurements must be converted to a .mat file. This can be achieved selecting Project and then Measurement Data. Right - click on the .mf4 file and by selecting Export (figure AA.39) it can be converted to .mat file.

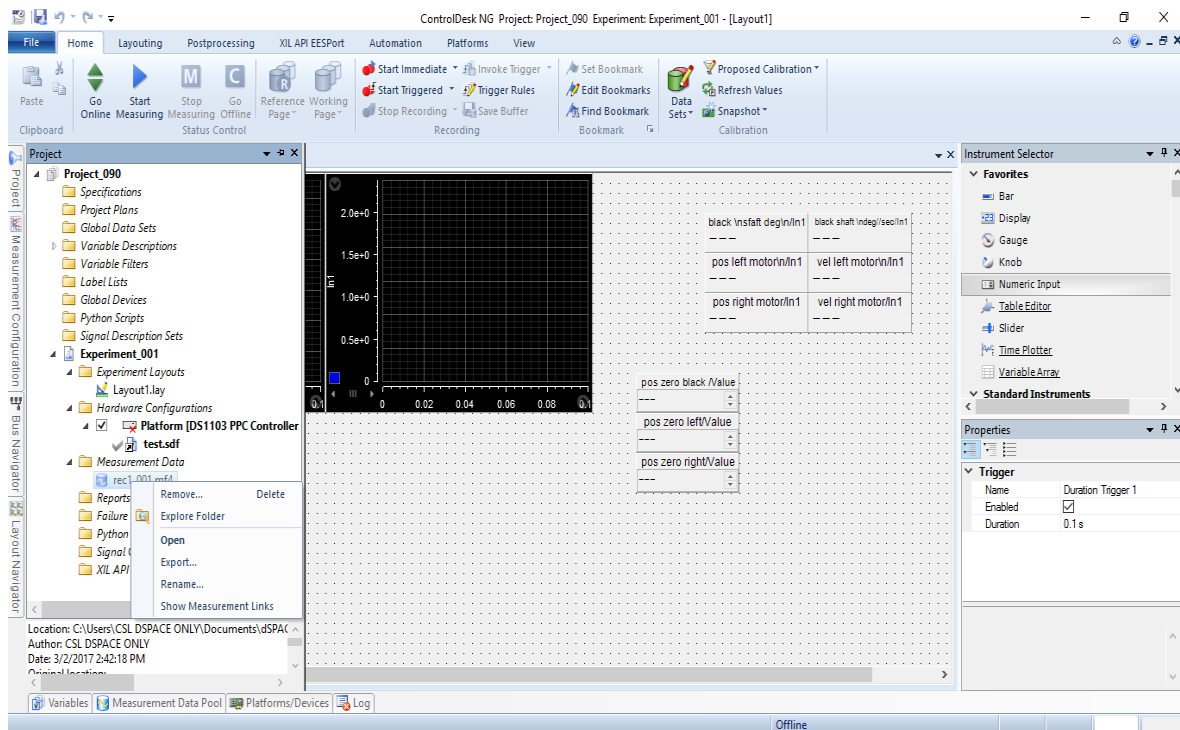


Figure AA.39. Exporting data.

ControlDesk 5.6 also allows the user to change the properties of the instruments. On the right of the screen when the user selects the instrument the properties window appears, as it is presented in figure AA.40. The user can change the color, the style, the range of the instrument and even more.

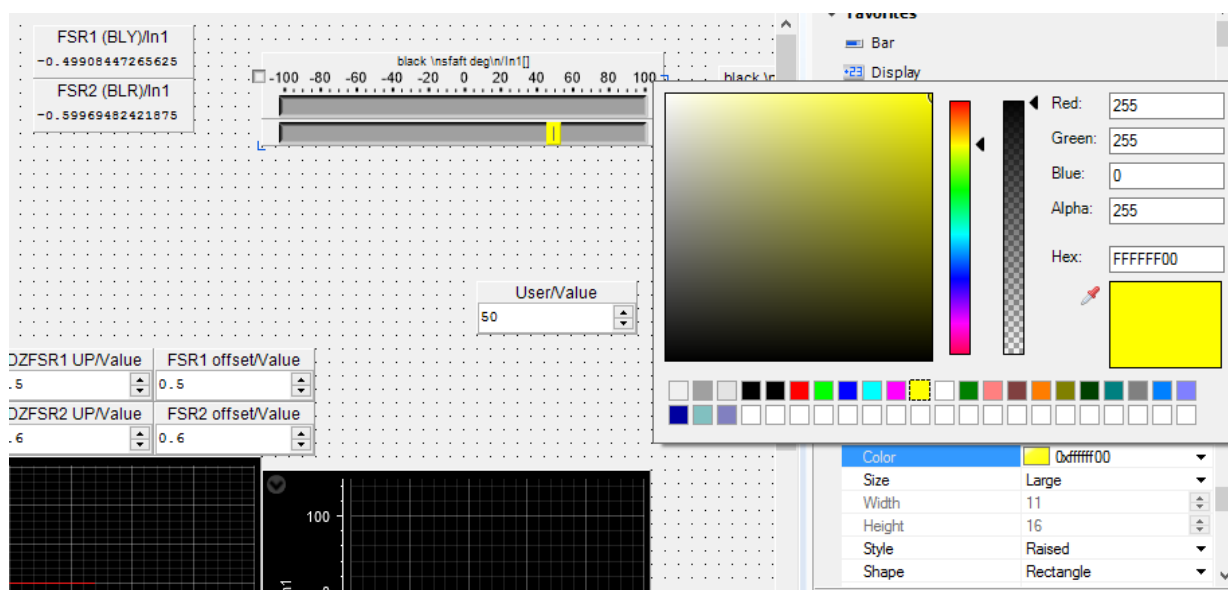


Figure AA.40. Changing the properties of the slider instrument.

11 APPENDIX B DATASHEETS

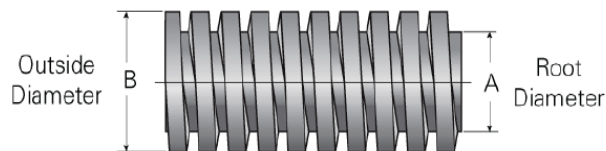
11.1 Biomechatronic Power Screw



Product Specification Sheet

Metric Lead Screw 4 mm x 1.22 mm Stainless Steel

Call 855-HELIXLT or visit us online at www.helixlinear.com to configure and order your Metric Lead Screw 4 mm x 1.22 mm Stainless Steel today!

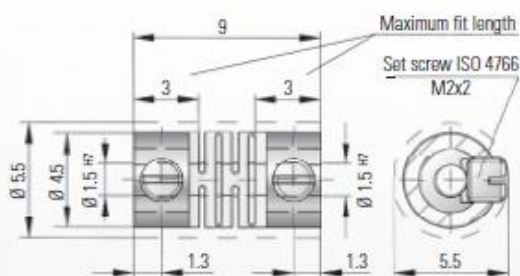


Product Info	
Part Number	016048S
Thread Direction	RH/LH
Screw Material	Stainless Steel
Details	
Lead [mm]	1.22
Starts	2
Pitch [mm]	0.6
Diameter [mm]	4
End Code for Types 1,2,3,5 [* Journals may show tracings of the thread]	2
End Code for Type 4 [* Journals may show tracings of the thread]	1
Diameter Code	016
Lead Code	048
Dimensions	
A [mm]	2.34
B [mm]	3.84
Performance Specifications	
Efficiency [%]	37-53
Lead Accuracy +/- [in/in]	0.0003

11.2 Master Motor Coupling

MODEL FK1 001/9

MICROFLEX-COUPPLINGS



Order example

FK1 / 001 / 9 / 1,5 / 1,5 / XX

Model	
Series / Nm	
Overall length	
Ø D H7	
Ø D H7	
Non standard	

Technical information

Nominal torque capacity:	1 Ncm
Maximum peak torque capacity:	2 Ncm
Weight:	0.47 g
Moment of inertia:	5.30 g/mm ²
Torsional stiffness:	23 Ncm/rad
Max. lateral misalignment:	0.1 mm
Max. angular misalignment:	1.5°
Max. axial misalignment:	0.2 mm

Material:

Coupling material: Polyamid
Hub material: stainless steel

Bore diameter: 1.5 mm
Radial clamping is achieved by using a
ISO 4766 M2 x 2 set screw.

Temperature range:

-50 to +120° C

Backlash:

Absolutely backlash-free

Brief overloads:

Acceptable up to 1.5 times the value specified.

Service life:

These couplings are maintenance-free if the
technical limits are not exceeded.

Speed range:

Up to 10.000 U/min

The extended diameter can be reduced by
using a flattened shaft.

A further reduction of the s to 4.5 mm can
be reached by using a M2x1.5 set screw
(Additional Charge)

The information mentioned in this document is based on our present
knowledge and experience and does not include the manufacturer's
own substantial testing of the equipment. So this is no obligatory
assurance even with regard to production rights of Third Parties. The
sale of our products is subject to our General Conditions of Sale
and Delivery.

R+W
COUPLING TECHNOLOGY

Experience and
Know-how for your
special requirements.

R+W Antriebs Elemente GmbH
Alexander-Wiegand-Straße 8 D-63911 Klingenberg/Germany
Tel. +49-(0)9372 - 9864-0 · Fax +49-(0)9372 - 9864-20
info@rw-kupplungen.de · www.rwcouplings.com

365/1104/2003

11.3 Slave Motor Coupling

Disc Couplings "Servo-Fine" High Rigidity Clamping / High Positioning Accuracy Clamping / Keywayed Bore For Servo Motors

For Servo Motors (High Rigidity)

Double Disc Type **SCPW**

Single Disc Type **SCPS**

*Applied hole for clamp screw might go through for some shafts.

① Measure hole diameter before fitting.
② The clamp screw must be inserted in its own hole.
③ The clamp screw must be inserted in its own hole.
④ For the installation and operation, see the PMS.

ROHS

Part Number	Type	No.	d1	d2	d3	Selection (d1/d2)	Unit Price
SCPW	Double Disc Type	15	15	15	15	15	15
SCPS	Single Disc Type	15	15	15	15	15	15

Part Number	Type	No.	d1	d2	d3	Selection (d1/d2)	Unit Price
SCPW	Double Disc Type	15	15	15	15	15	15
SCPS	Single Disc Type	15	15	15	15	15	15

① Measure hole diameter before fitting.
② The clamp screw must be inserted in its own hole.
③ The clamp screw must be inserted in its own hole.
④ For the installation and operation, see the PMS.

For Servo Motors High Positioning Accuracy

Double Disc Type **SCXW**

Single Disc Type **SCXS**

*Applied hole for clamp screw might go through for some shafts.

① Measure hole diameter before fitting.
② The clamp screw must be inserted in its own hole.
③ The clamp screw must be inserted in its own hole.
④ For the installation and operation, see the PMS.

ROHS

Part Number	Type	No.	d1	d2	d3	Selection (d1/d2)	Unit Price
SCXW	Double Disc Type	15	15	15	15	15	15
SCXS	Single Disc Type	15	15	15	15	15	15

Part Number	Type	No.	d1	d2	d3	Selection (d1/d2)	Unit Price
SCXW	Double Disc Type	15	15	15	15	15	15
SCXS	Single Disc Type	15	15	15	15	15	15

Keyway Dimension

① Measure hole diameter before fitting.
② The clamp screw must be inserted in its own hole.
③ The clamp screw must be inserted in its own hole.
④ For the installation and operation, see the PMS.

ROHS

Disc Couplings Clamping

Double Disc Type **CPDW**

Single Disc Type **CPDT**

*Applied hole for clamp screw might go through for some shafts.

① Measure hole diameter before fitting.
② The clamp screw must be inserted in its own hole.
③ The clamp screw must be inserted in its own hole.
④ For the installation and operation, see the PMS.

ROHS

Part Number	Type	No.	d1	d2	d3	Selection (d1/d2)	Unit Price
CPDW	Double Disc Type	15	15	15	15	15	15
CPDT	Single Disc Type	15	15	15	15	15	15

Part Number	Type	No.	d1	d2	d3	Selection (d1/d2)	Unit Price
CPDW	Double Disc Type	15	15	15	15	15	15
CPDT	Single Disc Type	15	15	15	15	15	15

① Measure hole diameter before fitting.
② The clamp screw must be inserted in its own hole.
③ The clamp screw must be inserted in its own hole.
④ For the installation and operation, see the PMS.

For Servo Motors

Double Disc Type **CPXW**

Single Disc Type **CPXS**

*Applied hole for clamp screw might go through for some shafts.

① Measure hole diameter before fitting.
② The clamp screw must be inserted in its own hole.
③ The clamp screw must be inserted in its own hole.
④ For the installation and operation, see the PMS.

ROHS

Part Number	Type	No.	d1	d2	d3	Selection (d1/d2)	Unit Price
CPXW	Double Disc Type	15	15	15	15	15	15
CPXS	Single Disc Type	15	15	15	15	15	15

Part Number	Type	No.	d1	d2	d3	Selection (d1/d2)	Unit Price
CPXW	Double Disc Type	15	15	15	15	15	15
CPXS	Single Disc Type	15	15	15	15	15	15

Keyway Dimension

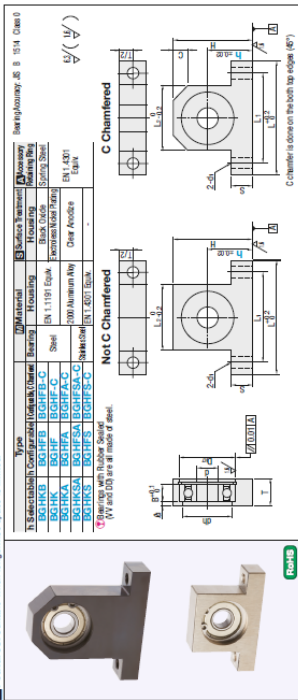
① Measure hole diameter before fitting.
② The clamp screw must be inserted in its own hole.
③ The clamp screw must be inserted in its own hole.
④ For the installation and operation, see the PMS.

ROHS

11.4 Slave Motor Bearing

Bearings with Housings T-Shaped

■ Features: Single when lengthwise space is limited.



Type	Part Number	Bearing No.	Seal	h	d	Dr	dh	B	h1	H	L	L1	L2	T	S	C	d1
h Selectable BGHKB BGHKS BGHKA BGHSA BGHSC	ZZ	620		15 20 25	10-30	3 10	10mm	7 4	h9	38 26 16	5						
		624				4 13		9	h11	38 26 16	10						4.5
		626				5 16	+0.018	12	h13	40 30 20							
		628				6 17		13	h13	42 32 21							
		630				8 19	0	15	h14	49 37 25	12						
		632				10 22	+0.021	18	h15	56 44 32	15						
		634				12 25	0	20	h15	56 44 32	15						
		636				14 28	+0.021	22	h16	63 51 39	18						
		638				16 31	0	24	h16	63 51 39	18						
		640				18 34	+0.021	26	h17	70 58 46	21						5.5
h Configurable BGHFB BGHFC BGHFA BGHFS	ZZ	620		20 30 40	20-40	12 25	0	24	h15	50 48 36	15						
		624				15 32	+0.021	21	h16	56 44 32	15						
		626				16 33	+0.025	22	h16	56 44 32	15						
		628				18 36	0	26	h17	63 51 39	18						
		630				20 39	0	29	h18	72 58 44	18						
		632				22 42	0	32	h19	84 52 38	21						
		634				24 45	+0.025	35	h20	96 60 48	24						
		636				26 48	0	38	h21	108 72 60	27						
		638				28 51	+0.025	41	h22	120 84 72	30						
		640				30 54	0	44	h23	132 96 84	33						6.5
h Configurable BGHFB-C BGHFC-C BGHFA-C BGHFS-C	ZZ	620		40 50 60	30-60	20 37	0	38	h18	68 53 40	18						
		624				22 40	+0.025	41	h19	76 60 48	21						
		626				24 43	0	44	h20	84 68 56	24						
		628				26 46	+0.025	47	h21	96 80 64	27						
		630				28 49	0	50	h22	108 96 80	30						
		632				30 52	+0.025	53	h23	120 104 88	33						
		634				32 55	0	56	h24	132 112 96	36						
		636				34 58	+0.025	59	h25	144 128 112	39						
		638				36 61	0	62	h26	160 144 128	42						
		640				38 64	+0.025	65	h27	176 160 144	45						
h Configurable BGHFB-C BGHFC-C BGHFA-C BGHFS-C	ZZ	620		50 60 80	40-80	25 47	0	48	h20	80 64 52	20						
		624				28 50	+0.025	51	h21	88 72 60	23						
		626				30 53	0	54	h22	96 80 64	26						
		628				32 56	+0.025	57	h23	108 96 80	29						
		630				34 59	0	60	h24	120 104 88	32						
		632				36 62	+0.025	63	h25	132 112 96	35						
		634				38 65	0	66	h26	144 128 112	38						
		636				40 68	+0.025	69	h27	160 144 128	41						
		638				42 71	0	72	h28	176 160 144	44						
		640				44 74	+0.025	75	h29	192 176 160	47						

Check for available sizes in the price list.

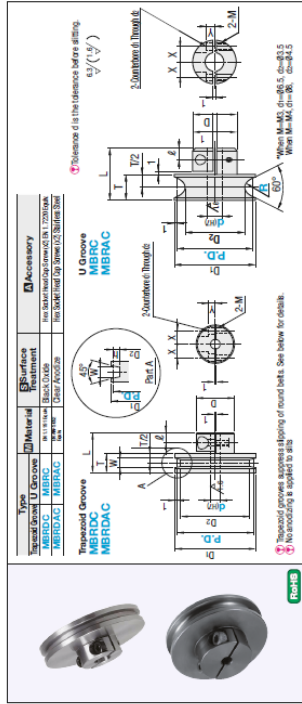
For details of Bearing Standards, see P589, 591, 593, 596, 1003 and 1004.

Ordering	Part Number	h
Example	BGHR 6000 ZZ	30
	BGHR 6001 W	30

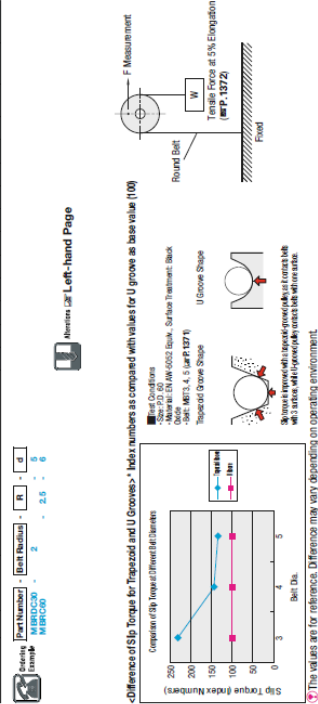
Bearing No.	Seal	h Selectable				h Configurable				Unit Price				h Configurable, C Chamfered			
		BOUB	BOBK	BOHKA	BOUKA	BOBK3	BOHKB	BOUKB	BOHKB	BOUB3	BOHKB	BOUKB	BOHKB	BOUB3	BOHKB	BOUKB	BOHKB
623																	
624																	
625																	
626																	
627																	
628																	
629																	
630																	
631																	
632																	
633																	
634																	
635																	
636																	
637																	
638																	
639																	
640																	
641																	
642																	
643																	
644																	
645																	
646																	
647																	
648																	
649																	
650																	
651																	
652																	
653																	
654																	
655																	
656																	
657																	
658																	
659																	
660																	
661																	
662																	
663																	
664																	
665																	
666																	
667																	
668																	
669																	
670																	
671																	
672																	
673																	
674																	
675																	
676																	
677																	
678																	
679																	
680																	
681																	
682																	
683																	
684																	
685																	
686																	
687																	
688																	
689																	
690																	
691																	
692																	
693																	
694																	
695																	
696																	
697																	
698																	
699																	
700																	
701																	
702																	
703																	
704																	
705																	
706																	
707																	
708																	
709																	
710																	
711																	
712																	
713																	
714																	
715																	
716																	
717																	
718																	
719																	
720																	
721																	
722																	
723																	
724																	
725																	
726																	
727																	
728																	
729																	
730																	
731																	
732																	
733																	
734																	
735																	
736																	
737																	
738																	
739																	
740																	
741																	
742																	
743																	
744																	
745																	
746																	
747																	
748																	
749																	
750																	
751																	
752																	
753																	
754																	
755																	
756																	
757																	
758																	
759																	
760																	
761																	
762																	
763																	
764																	
765																	
766																	
767																	
768																	
769																	
770																	
771																	
772																	
773																	
774																	
775																	

11.5 Slave Motor Pulley

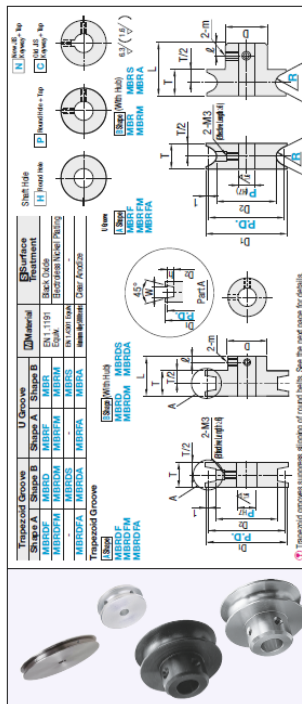
Pulleys for Round Belts Clamping Type



Part Number	P.D.	R	d	Material	Surface Treatment	Accessories	Unit Price																																																																																									
Type																																																																																																
MBRAC	1	4	5	6	8	10	11	12	13	14	15	16	17	18	19	20	21	22	23	24	25	26	27	28	29	30	31	32	33	34	35	36	37	38	39	40	41	42	43	44	45	46	47	48	49	50	51	52	53	54	55	56	57	58	59	60	61	62	63	64	65	66	67	68	69	70	71	72	73	74	75	76	77	78	79	80	81	82	83	84	85	86	87	88	89	90	91	92	93	94	95	96	97	98	99	100
MBRAC	1	4	5	6	8	10	11	12	13	14	15	16	17	18	19	20	21	22	23	24	25	26	27	28	29	30	31	32	33	34	35	36	37	38	39	40	41	42	43	44	45	46	47	48	49	50	51	52	53	54	55	56	57	58	59	60	61	62	63	64	65	66	67	68	69	70	71	72	73	74	75	76	77	78	79	80	81	82	83	84	85	86	87	88	89	90	91	92	93	94	95	96	97	98	99	100



Pulleys for Round Belts Set Screw Type



Unit Price									
MBRAC									
MBRAC									
MBRAC									
MBRAC									
MBRAC									
MBRAC									
MBRAC									
MBRAC									
MBRAC									
MBRAC									
MBRAC									
MBRAC									
MBRAC									
MBRAC									
MBRAC									
MBRAC									
MBRAC									
MBRAC									
MBRAC									
MBRAC									
MBRAC									
MBRAC									
MBRAC									
MBRAC									
MBRAC									
MBRAC									
MBRAC									
MBRAC									
MBRAC									
MBRAC									
MBRAC									
MBRAC									
MBRAC									
MBRAC									
MBRAC									
MBRAC									
MBRAC									
MBRAC									
MBRAC									
MBRAC									
MBRAC									
MBRAC									
MBRAC									
MBRAC									
MBRAC									
MBRAC									
MBRAC									
MBRAC									
MBRAC									
MBRAC									
MBRAC									
MBRAC									
MBRAC									
MBRAC									
MBRAC									
MBRAC									
MBRAC									
MBRAC									
MBRAC									
MBRAC									
MBRAC									
MBRAC									
MBRAC									
MBRAC									
MBRAC									
MBRAC									
MBRAC									
MBRAC									
MBRAC									
MBRAC									
MBRAC									
MBRAC									
MBRAC									
MBRAC									
MBRAC									
MBRAC									
MBRAC									
MBRAC									
MBRAC									
MBRAC									
MBRAC									
MBRAC									
MBRAC									
MBRAC									
MBRAC									
MBRAC									
MBRAC									
MBRAC									
MBRAC									
MBRAC									
MBRAC									
MBRAC									
MBRAC									
MBRAC									
MBRAC									
MBRAC									
MBRAC									
MBRAC									
MBRAC									
MBRAC									
MBRAC									
MBRAC									
MBRAC									
MBRAC									
MBRAC									
MBRAC									
MBRAC									
MBRAC									
MBRAC									
MBRAC									
MBRAC									
MBRAC									
MBRAC									
MBRAC									
MBRAC									
MBRAC									
MBRAC									
MBRAC									
MBRAC									
MBRAC									
MBRAC									
MBRAC									
MBRAC									
MBRAC									
MBRAC									
MBRAC									
MBRAC									
MBRAC									
MBRAC									
MBRAC									
MBRAC									
MBRAC									
MBRAC									
MBRAC									
MBRAC									
MBRAC									
MBRAC									
MBRAC									
MBRAC									
MBRAC									
MBRAC									
MBRAC									
MBRAC									
MBRAC									
MBRAC									
MBRAC									
MBRAC									
MBRAC									
MBRAC									
MBRAC									
MBRAC									
MBRAC									
MBRAC									
MBRAC									
MBRAC									
MBRAC									
MBRAC									
MBRAC									
MBRAC									
MBRAC									
MBRAC									
MBRAC									
MBRAC									
MBRAC									
MBRAC									
MBRAC									
MBRAC									
MBRAC									
MBRAC									
MBRAC									
MBRAC									
MBRAC									
MBRAC									
MBRAC									
MBRAC									
MBRAC									
MBRAC									
MBRAC									
MBRAC									
MBRAC									
MBRAC									
MBRAC									
MBRAC									
MBRAC									
MBRAC									
MBRAC									
MBRAC									
MBRAC									
MBRAC									
MBRAC									
MBRAC									
MBRAC									
MBRAC									
MBRAC									
MBRAC									
MBRAC									
MBRAC									
MBRAC									
MBRAC									
MBRAC									
MBRAC									
MBRAC									
MBRAC									
MBRAC									
MBRAC									
MBRAC									
MBRAC									
MBRAC									
MBRAC									
MBRAC									
MBRAC									
MBRAC									
MBRAC									
MBRAC									
MBRAC									
MBRAC									
MBRAC									
MBRAC									
MBRAC									
MBRAC									
MBRAC									
MBRAC									
MBRAC									
MBRAC									
MBRAC									
MBRAC									
MBRAC									
MBRAC									
MBRAC									
MBRAC									
MBRAC									
MBRAC									
MBRAC									
MBRAC									
MBRAC									
MBRAC									
MBRAC									
MBRAC									
MBRAC									
MBRAC									
MBRAC									
MBRAC									
MBRAC									
MBRAC									
MBRAC									
MBRAC									
MBRAC									
MBRAC									
MBRAC									
MBRAC									
MBRAC									
MBRAC									
MBRAC									
MBRAC									
MBRAC									
MBRAC									
MBRAC									
MBRAC									
MBRAC									
MBRAC									
MBRAC									
MBRAC									
MBRAC									
MBRAC									
MBRAC									
MBRAC									
MBRAC									
MBRAC									
MBRAC									
MBRAC									
MBRAC									
MBRAC									
MBRAC									
MBRAC									
MBRAC									
MBRAC									
MBRAC									
MBRAC									
MBRAC									
MBRAC									
MBRAC									
MBRAC									
MBRAC									
MBRAC									
MBRAC									
MBRAC									
MBRAC									
MBRAC									
MBRAC									
MBRAC									
MBRAC									
MBRAC									
MBRAC									
MBRAC									
MBRAC									
MBRAC									
MBRAC									
MBRAC									
MBRAC									
MBRAC									
MBRAC									
MBRAC									
MBRAC									
MBRAC									
MBRAC									
MBRAC									
MBRAC									
MBRAC									
MBRAC									
MBRAC									
MBRAC									
MBRAC									
MBRAC									
MBRAC									
MBRAC									
MBRAC									
MBRAC									
MBRAC									
MBRAC									
MBRAC									
MBRAC									
MBRAC									
MBRAC									
MBRAC									
MBRAC									
MBRAC									
MBRAC									
MBRAC									
MBRAC									
MBRAC									
MBRAC									
MBRAC									
MBRAC									
MBRAC									
MBRAC									
MBRAC									
MBRAC									
MBRAC									
MBRAC									
MBRAC									
MBRAC									
MBRAC									
MBRAC									
MBRAC									
MBRAC									
MBRAC									
MBRAC									
MBRAC									
MBRAC									
MBRAC									
MBRAC									
MBRAC									
MBRAC									
MBRAC									
MBRAC									
MBRAC									
MBRAC									
MBRAC									
MBRAC									
MBRAC									
MBRAC									
MBRAC									
MBRAC									
MBRAC									
MBRAC									
MBRAC									
MBRAC									
MBRAC									
MBRAC									
MBRAC									
MBRAC									
MBRAC									
MBRAC									
MBRAC									
MBRAC									
MBRAC									
MBRAC									
MBRAC									
MBRAC									
MBRAC									
MBRAC									
MBRAC									
MBRAC									
MBRAC									
MBRAC									
MBRAC									
MBRAC									
MBRAC									
MBRAC									
MBRAC									
MBRAC									
MBRAC									
MBRAC									
MBRAC									
MBRAC									
MBRAC									
MBRAC									
MBRAC									
MBRAC									
MBRAC									
MBRAC									
MBRAC									
MBRAC									
MBRAC									
MBRAC									
MBRAC									
MBRAC									
MBRAC									
MBRAC									
MBRAC									
MBRAC									
MBRAC									
MBRAC									
MBRAC									
MBRAC									
MBRAC									
MBRAC									
MBRAC									
MBRAC									
MBRAC									
MBRAC									
MBRAC									
MBRAC									
MBRAC									
MBRAC									
MBRAC									
MBRAC									
MBRAC									
MBRAC									
MBRAC									
MBRAC									
MBRAC									
MBRAC									
MBRAC									
MBRAC									
MBRAC									
MBRAC									
MBRAC									
MBRAC									
MBRAC									
MBRAC									
MBRAC									
MBRAC									
MBRAC									
MBRAC									
MBRAC									



11.6 Slave Motor Drive



Analog Servo Drive

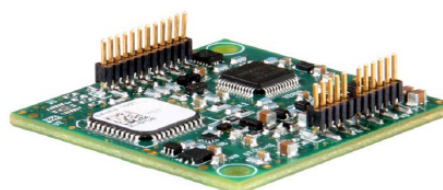
AZBDC10A4

Description	Power Range
<p>The AZBDC10A4 PWM servo drive is designed to drive brushless and brushed DC motors at a high switching frequency. To increase system reliability and to reduce cabling costs, the drive is designed for direct integration into your PCB. The AZBDC10A4 is fully protected against over-voltage, under-voltage, over-current, over-heating, and short-circuits. A single digital output indicates operating status. The drive interfaces with digital controllers that have digital PWM output. The PWM IN duty cycle determines the output current and DIR input determines the direction of rotation. This servo drive requires only a single unregulated isolated DC power supply, and is fully RoHS (Reduction of Hazardous Substances) compliant.</p> <p>See Part Numbering Information on last page of datasheet for additional ordering options.</p>	Peak Current
	Continuous Current
	Supply Voltage

10 A

5 A

10 - 36 VDC



Features

- ▲ Four Quadrant Regenerative Operation
- ▲ Direct Board-to-Board Integration
- ▲ Lightweight
- ▲ High Switching Frequency
- ▲ Wide Temperature Range
- ▲ Differential Input Command
- ▲ Digital Fault Output Monitor
- ▲ Current Monitor Output
- ▲ Single Supply Operation
- ▲ Compact Size
- ▲ High Power Density
- ▲ 12VDC Operation

HARDWARE PROTECTION

- Over-Voltage
- Under-Voltage
- Over-Current
- Over-Temperature
- Short-circuit (phase-phase)
- Short-circuit (phase-ground)

INPUTS/OUTPUTS

- Digital Fault Output
- Digital Inhibit Input
- Analog Current Monitor
- Analog Command Input

FEEDBACK SUPPORTED

- Hall Sensors

MODES OF OPERATION

- Current

COMMUTATION

- Trapezoidal

MOTORS SUPPORTED

- Three Phase (Brushless)
- Single Phase (Brushed, Voice Coil, Inductive Load)

COMMAND SOURCE

- PWM

COMPLIANCES & AGENCY APPROVALS

- RoHS
- UL/cUL Pending
- CE Pending

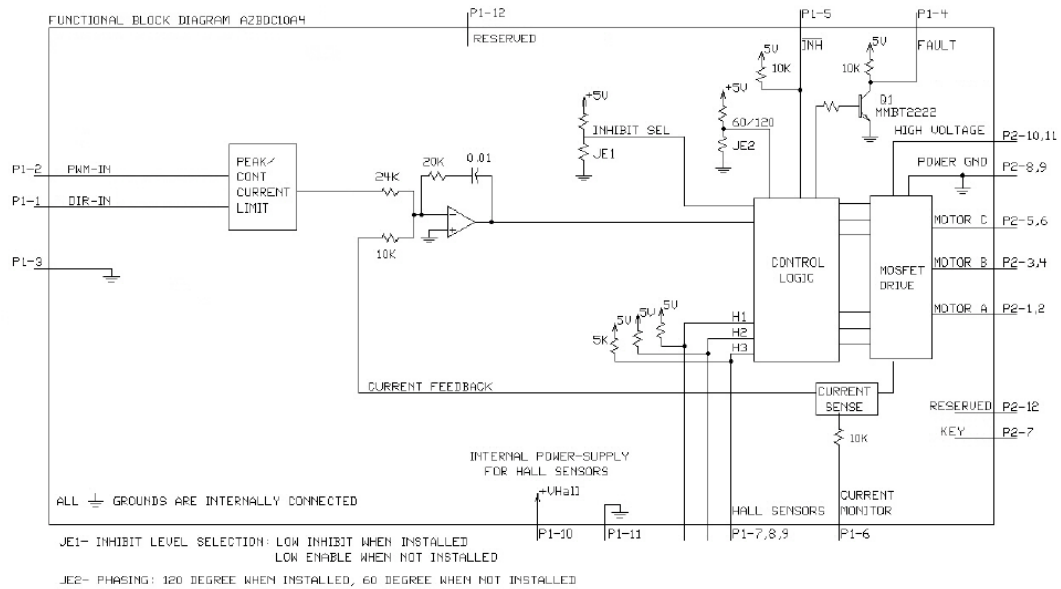
Release Date:
4/10/2015

Status:
Active

ADVANCED Motion Controls · 3805 Calle Tecate, Camarillo, CA, 93012
ph# 805-389-1935 · fx# 805-389-1165 · www.a-m-c.com

Page 1 of 7

BLOCK DIAGRAM



Information on Approvals and Compliances



RoHS (Reduction of Hazardous Substances) is intended to prevent hazardous substances such as lead from being manufactured in electrical and electronic equipment.

SPECIFICATIONS

Power Specifications		
Description	Units	Value
DC Supply Voltage Range	VDC	10 - 36
DC Bus Under Voltage Limit	VDC	8
DC Bus Over Voltage Limit	VDC	40
Maximum Peak Output Current ¹	A	10
Maximum Continuous Output Current	A	5
Maximum Continuous Output Power	W	171
Maximum Power Dissipation at Continuous Current	W	9
Minimum Load Inductance (Line-To-Line) ²	μH	100
Internal Bus Capacitance ³	μF	23.5
Low Voltage Supply Outputs	-	+5 VDC (30 mA)
Switching Frequency	kHz	40
Control Specifications		
Description	Units	Value
Command Sources	-	PWM
PWM Input Frequency Range	-	10 - 25
Feedback Supported	-	Halls
Commutation Methods	-	Trapezoidal
Modes of Operation	-	Current
Motors Supported	-	Three Phase (Brushless), Single Phase (Brushed, Voice Coil, Inductive Load)
Hardware Protection	-	Invalid Commutation Feedback, Over Current, Over Temperature, Over Voltage, Under Voltage, Short Circuit (Phase-Phase & Phase-Ground)
Mechanical Specifications		
Description	Units	Value
Agency Approvals	-	RoHS, UL/cUL Pending, CE Pending
Size (H x W x D)	mm (in)	38.1 x 38.1 x 7.34 (1.50 x 1.50 x 0.29)
Weight	g (oz)	8.5 (0.3)
Operating Temperature Range ⁴	°C (°F)	0 - 85 (32 - 185)
Storage Temperature Range	°C (°F)	-40 - 85 (-40 - 185)
Relative Humidity	-	0 - 90% Non-Condensing
Form Factor	-	PCB Mounted
P1 Connector	-	12-pin, 1.27 mm spaced header
P2 Connector	-	12-pin, 1.27 mm spaced header

Notes

1. Maximum duration of peak current is ~2 seconds. Peak RMS value must not exceed continuous current rating of the drive.
2. Lower inductance is acceptable for bus voltages well below maximum. Use external inductance to meet requirements.
3. Requires a minimum of 47 μF external bus capacitance between the DC Supply and Power Ground.
4. Additional cooling and/or heatsink may be required to achieve rated performance.

PIN FUNCTIONS

P1 - Signal Connector			
Pin	Name	Description / Notes	I/O
1	DIRECTION	Direction Input (+5V)	I
2	PWM / IN	10 – 25 kHz pulse width modulated digital input command (+5V). Input duty cycle commands the output current.	I
3	SIGNAL GND	Signal Ground (Common With Power Ground).	GND
4	FAULT OUT	TTL level (+5 V) output becomes high when power devices are disabled due to at least one of the following conditions: inhibit, invalid Hall state, output short circuit, over voltage, over temperature, power-up reset.	O
5	INHIBIT IN	TTL level (+5 V) inhibit/enable input. Leave open to enable drive. Pull to ground to inhibit drive. Inhibit turns off all power devices.	I
6	CURRENT MONITOR	Current Monitor. Analog output signal proportional to the actual current output. Scaling is 2 A/V. Measure relative to signal ground.	O
7	HALL 3	Single-ended Hall/Commutation Sensor Inputs (+5 V logic level)	I
8	HALL 2*		I
9	HALL 1		I
10	+V HALL OUT	Low Power Supply For Hall Sensors (+5 V @ 30 mA). Referenced to signal ground. Short circuit protected.	O
11	SIGNAL GND	Signal Ground (Common With Power Ground).	GND
12	RESERVED	Reserved	-

P2 - Power Connector			
Pin	Name	Description / Notes	I/O
1	MOTOR A	Motor Phase Outputs. Current output distributed equally across 2 pins per motor phase, 3A continuous current carrying capacity per pin.	O
2	MOTOR A		O
3	MOTOR B		O
4	MOTOR B		O
5	MOTOR C		O
6	MOTOR C		O
7	NC (KEY)	No Connection. Keyed pin.	-
8	PWR GND	Power Ground (Common With Signal Ground). 3A Continuous Current Rating Per Pin	GND
9	PWR GND		GND
10	HV IN	DC Power Input. 3A Continuous Current Rating Per Pin. Requires a minimum of 47 µF external capacitance between HV IN and PWR GND pins.	I
11	HV IN		I
12	RESERVED	Reserved	-

*For use with Single Phase (Brushed) motors, ground Hall 2 and only connect motor leads to Motor A and Motor B.

Note: P1 and P2 are identical 12-pin headers. To avoid damage to the drive, be sure when plugging or soldering the drive into a PCB or interface card that the drive orientation is correct. P1 and P2 are labeled on the PCB silkscreen. Pin 7 on P2 is keyed to differentiate it from P1. Consult the mounting dimension drawing on page 6 of this datasheet for an illustration of the locations of P1 and P2.

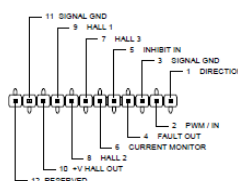
HARDWARE SETTINGS

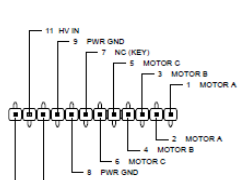
Jumper Settings

Jumpers are SMT, 0 ohm resistors located on the underside of the drive PCB. By default, the drive is configured with the jumpers installed. Typical drive operation will not require the jumpers to be removed. Please contact the factory before jumper removal.

Jumper	Description	Configuration	
		Not Installed	Installed
JE1	Inhibit logic. Sets the logic level of inhibit pins. Labeled JE1 on the PCB of the drive.	Low Enable	Low Inhibit
JE2	Hall sensor phasing. Selects 120 or 60 degree commutation phasing. Labeled JE2 on the PCB of the drive.	60 degree	120 degree

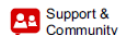
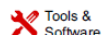
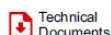
MECHANICAL INFORMATION

P1 - Signal Connector		
Connector Information	12-pin, 1.27 mm spaced header	
Mating Connector	Details	Samtec: RSM-112-02-L-S
	Included with Drive	No
		

P2 - Power Connector		
Connector Information	12-pin, 1.27 mm spaced header	
Mating Connector	Details	Samtec: RSM-112-02-L-S
	Included with Drive	No
		

[illegible]

11.7 Master Motor h - bridge



L293, L293D

SLRS008D – SEPTEMBER 1986 – REVISED JANUARY 2016

L293x Quadruple Half-H Drivers

1 Features

- Wide Supply-Voltage Range: 4.5 V to 36 V
- Separate Input-Logic Supply
- Internal ESD Protection
- High-Noise-Immunity Inputs
- Output Current 1 A Per Channel (600 mA for L293D)
- Peak Output Current 2 A Per Channel (1.2 A for L293D)
- Output Clamp Diodes for Inductive Transient Suppression (L293D)

2 Applications

- Stepper Motor Drivers
- DC Motor Drivers
- Latching Relay Drivers

3 Description

The L293 and L293D devices are quadruple high-current half-H drivers. The L293 is designed to provide bidirectional drive currents of up to 1 A at voltages from 4.5 V to 36 V. The L293D is designed to provide bidirectional drive currents of up to 600-mA at voltages from 4.5 V to 36 V. Both devices are designed to drive inductive loads such as relays, solenoids, DC and bipolar stepping motors, as well as other high-current/high-voltage loads in positive-supply applications.

Each output is a complete totem-pole drive circuit, with a Darlington transistor sink and a pseudo-Darlington source. Drivers are enabled in pairs, with drivers 1 and 2 enabled by 1,2EN and drivers 3 and 4 enabled by 3,4EN.

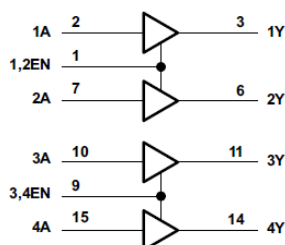
The L293 and L293D are characterized for operation from 0°C to 70°C.

Device Information⁽¹⁾

PART NUMBER	PACKAGE	BODY SIZE (NOM)
L293NE	PDIP (16)	19.80 mm x 6.35 mm
L293DNE	PDIP (16)	19.80 mm x 6.35 mm

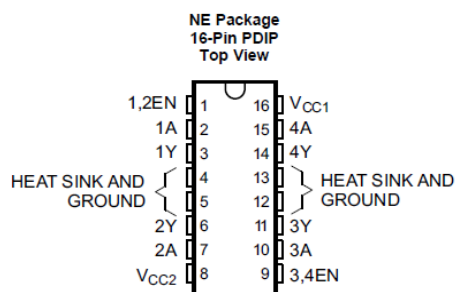
(1) For all available packages, see the orderable addendum at the end of the data sheet.

Logic Diagram



An IMPORTANT NOTICE at the end of this data sheet addresses availability, warranty, changes, use in safety-critical applications, intellectual property matters and other important disclaimers. PRODUCTION DATA.

5 Pin Configuration and Functions



Pin Functions

PIN		TYPE	DESCRIPTION
NAME	NO.		
1,2EN	1	I	Enable driver channels 1 and 2 (active high input)
<1:4>A	2, 7, 10, 15	I	Driver inputs, noninverting
<1:4>Y	3, 6, 11, 14	O	Driver outputs
3,4EN	9	I	Enable driver channels 3 and 4 (active high input)
GROUND	4, 5, 12, 13	—	Device ground and heat sink pin. Connect to printed-circuit-board ground plane with multiple solid vias
V _{CC1}	16	—	5-V supply for internal logic translation
V _{CC2}	8	—	Power VCC for drivers 4.5 V to 36 V

L293, L293D

SLRS008D – SEPTEMBER 1986 – REVISED JANUARY 2016

www.ti.com

6 Specifications

6.1 Absolute Maximum Ratings

 over operating free-air temperature range (unless otherwise noted)⁽¹⁾

	MIN	MAX	UNIT
Supply voltage, V_{CC1} ⁽²⁾		36	V
Output supply voltage, V_{CC2}		36	V
Input voltage, V_I		7	V
Output voltage, V_O	–3	$V_{CC2} + 3$	V
Peak output current, I_O (nonrepetitive, $t \leq 5$ ms): L293	–2	2	A
Peak output current, I_O (nonrepetitive, $t \leq 100$ μ s): L293D	–1.2	1.2	A
Continuous output current, I_O : L293	–1	1	A
Continuous output current, I_O : L293D	–600	600	mA
Maximum junction temperature, T_J		150	°C
Storage temperature, T_{stg}	–65	150	°C

- (1) Stresses beyond those listed under *Absolute Maximum Ratings* may cause permanent damage to the device. These are stress ratings only, which do not imply functional operation of the device at these or any other conditions beyond those indicated under *Recommended Operating Conditions*. Exposure to absolute-maximum-rated conditions for extended periods may affect device reliability.
- (2) All voltage values are with respect to the network ground terminal.

6.2 ESD Ratings

		VALUE	UNIT
$V_{(ESD)}$	Electrostatic discharge	Human-body model (HBM), per ANSI/ESDA/JEDEC JS-001 ⁽¹⁾	± 2000
		Charged-device model (CDM), per JEDEC specification JESD22-C101 ⁽²⁾	± 1000

- (1) JEDEC document JEP155 states that 500-V HBM allows safe manufacturing with a standard ESD control process.
- (2) JEDEC document JEP157 states that 250-V CDM allows safe manufacturing with a standard ESD control process.

6.3 Recommended Operating Conditions

over operating free-air temperature range (unless otherwise noted)

		MIN	NOM	MAX	UNIT
Supply voltage	V_{CC1}	4.5		7	V
	V_{CC2}	V_{CC1}		36	
V_{IH}	High-level input voltage	$V_{CC1} \leq 7$ V	2.3	V_{CC1}	V
		$V_{CC1} \geq 7$ V	2.3	7	V
V_{IL}	Low-level output voltage	–0.3 ⁽¹⁾		1.5	V
T_A	Operating free-air temperature	0		70	°C

- (1) The algebraic convention, in which the least positive (most negative) designated minimum, is used in this data sheet for logic voltage levels.

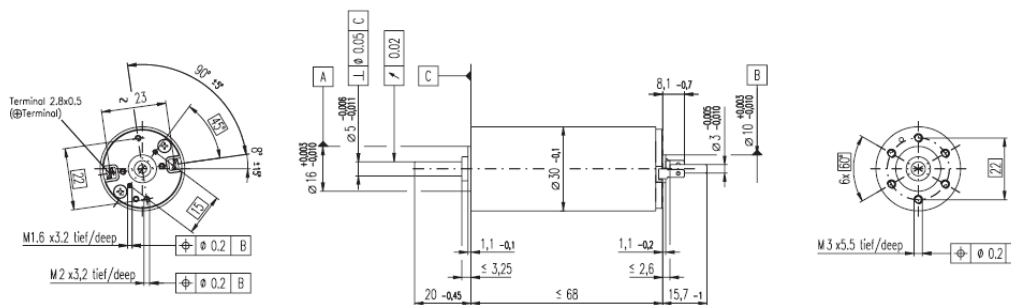
6.4 Thermal Information

THERMAL METRIC ⁽¹⁾		L293, L293D	UNIT
		NE (PDIP)	
		16 PINS	
$R_{\theta JA}$	Junction-to-ambient thermal resistance ⁽²⁾	36.4	°C/W
$R_{\theta JC(top)}$	Junction-to-case (top) thermal resistance	22.5	°C/W
$R_{\theta JB}$	Junction-to-board thermal resistance	16.5	°C/W
Ψ_{JT}	Junction-to-top characterization parameter	7.1	°C/W
Ψ_{JB}	Junction-to-board characterization parameter	16.3	°C/W

- (1) For more information about traditional and new thermal metrics, see the *Semiconductor and IC Package Thermal Metrics* application report, [SPRA953](#).
- (2) The package thermal impedance is calculated in accordance with JESD 51-7.

11.8 Slave Motor

RE 30 Ø30 mm, Graphite Brushes, 60 Watt



maxon DC motor

M 1:2

- Stock program
- Standard program
- Special program (on request)

according to dimensional drawing
shaft length 15.7 shortened to 8.7 mm

Order Number

310005	310006	310007	310008	310009
268193	268213	268214	268215	268216

Motor Data

Values at nominal voltage						
1	Nominal voltage	V	12.0	18.0	24.0	36.0
2	No load speed	rpm	8170	8590	8810	8590
3	No load current	mA	300	212	164	106
4	Nominal speed	rpm	7630	7900	8050	7810
5	Nominal torque (max. continuous torque)	mNm	51.7	75.5	85.0	83.4
6	Nominal current (max. continuous current)	A	4.00	4.00	3.44	2.20
7	Stall torque	mNm	844	991	1020	936
8	Starting current	A	60.5	49.8	39.3	23.5
9	Max. efficiency	%	86	87	87	88
Characteristics						
10	Terminal resistance	Ω	0.198	0.362	0.611	1.53
11	Terminal inductance	mH	0.0345	0.0703	0.119	0.281
12	Torque constant	mNm / A	13.9	19.9	25.9	39.8
13	Speed constant	rpm / V	685	479	369	240
14	Speed / torque gradient	rpm / mNm	9.74	8.71	8.69	9.22
15	Mechanical time constant	ms	3.42	3.25	3.03	3.17
16	Rotor inertia	gcm ²	33.5	35.7	33.3	32.9

Specifications

- 17 Thermal resistance housing-ambient 6.0 K / W
- 18 Thermal resistance winding-housing 1.7 K / W
- 19 Thermal time constant winding 16.2 s
- 20 Thermal time constant motor 714 s
- 21 Ambient temperature -30 ... +100°C
- 22 Max. permissible winding temperature +125°C

Mechanical data (ball bearings)

- 23 Max. permissible speed 12000 rpm
- 24 Axial play 0.05 - 0.15 mm
- 25 Radial play 0.025 mm
- 26 Max. axial load (dynamic) 5.6 N
- 27 Max. force for press fits (static) 110 N
- 28 Max. radial loading, 5 mm from flange 1200 N

Other specifications

- 29 Number of pole pairs 1
- 30 Number of commutator segments 13
- 31 Weight of motor 238 g

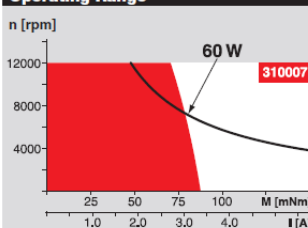
Values listed in the table are nominal.
Explanation of the figures on page 49.

Δ Tolerances may vary from the standard specification.

Option

Preloaded ball bearings

Operating Range



Comments

Continuous operation
In observation of above listed thermal resistance (lines 17 and 18) the maximum permissible winding temperature will be reached during continuous operation at 25°C ambient.
= Thermal limit.

Short term operation
The motor may be briefly overloaded (recurring).

— Assigned power rating

maxon Modular System

Overview on page 16 - 21

Planetary Gearhead

Ø32 mm

0.75 - 4.5 Nm

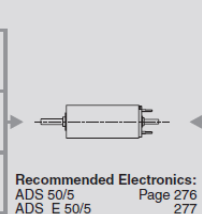
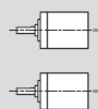
Page 239

Planetary Gearhead

Ø32 mm

1.0 - 6.0 Nm

Page 240



Recommended Electronics:
ADS 50/5 Page 276
ADS_E 50/5 277
EPOS 24/5 294
EPOS2 50/5 295
EPOS P 24/5 297
Notes 18

Encoder MR

256 - 1024 CPT

3 channels

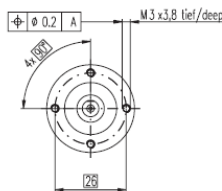
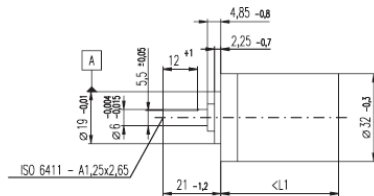
Page 259

11.9 Slave Motor Gearhead

Planetary Gearhead GP 32 C Ø32 mm, 1.0 - 6.0 Nm

Ceramic Version

maxon gear



M 1:2

Technical Data

Planetary Gearhead	straight teeth
Output shaft	stainless steel
Shaft diameter as option	8 mm
Bearing at output	ball bearing
Radial play, 5 mm from flange	max. 0.14 mm
Axial play	max. 0.4 mm
Max. radial load, 10 mm from flange	140 N
Max. permissible axial load	120 N
Max. permissible force for press fits	120 N
Sense of rotation, drive to output	=
Recommended input speed	< 8000 rpm
Recommended temperature range	-20 ... +100°C
Extended area as option	-35 ... +100°C

- Stock program
- Standard program
- Special program (on request)

Order Number

	166930	166933	166938	166939	166944	166949	166954	166959	166962	166967	166972	166977
1 Reduction	3.7 : 1	14 : 1	33 : 1	51 : 1	111 : 1	246 : 1	492 : 1	762 : 1	1181 : 1	1972 : 1	2829 : 1	4380 : 1
2 Reduction absolute	26/7	676/49	529/16	17576/343	13824/125	421824/1715	86112/175	19044/25	10123776/4075	8628176/4375	495144/175	109503/25
3 Max. motor shaft diameter	mm	6	6	6	4	4	4	3	4	4	3	3
Order Number	166931	166934	166940	166945	166950	166955	166960	166963	166968	166973	166978	
1 Reduction	4.8 : 1	18 : 1		66 : 1	123 : 1	295 : 1	531 : 1	913 : 1	1414 : 1	2189 : 1	3052 : 1	5247 : 1
2 Reduction absolute	24/5	624/35		16224/245	68771/56	101062/343	931776/625	36501/40	2425488/1715	5364096/245	1907712/625	839523/160
3 Max. motor shaft diameter	mm	4	4	4	3	3	3	3	3	3	3	3
Order Number	166932	166935		166941	166946	166951	166956	166961	166964	166969	166974	166979
1 Reduction	5.8 : 1	21 : 1		79 : 1	132 : 1	318 : 1	589 : 1	1093 : 1	1526 : 1	2362 : 1	3389 : 1	6285 : 1
2 Reduction absolute	23/4	299/14		3887/49	3312/25	389376/1225	20631/25	279841/256	9345024/6125	2066688/675	474513/140	6430343/1024
3 Max. motor shaft diameter	mm	3	3	3	3	4	3	3	4	3	3	3
Order Number		166936		166942	166947	166952	166957		166965	166970	166975	
1 Reduction		23 : 1		86 : 1	159 : 1	411 : 1	636 : 1		1694 : 1	2548 : 1	3656 : 1	
2 Reduction absolute		576/25		14976/175	1587/10	359424/675	79488/125		1162213/996	7962624/2125	457056/125	
3 Max. motor shaft diameter		mm		4	4	3	4		3	4	3	
Order Number		166937		166943	166948	166953	166958		166966	166971	166976	
1 Reduction		28 : 1		103 : 1	190 : 1	456 : 1	706 : 1		1828 : 1	2623 : 1	4060 : 1	
2 Reduction absolute		138/5		3588/35	12167/64	89401/196	158171/224		2238912/225	2056222/794	3637933/996	
3 Max. motor shaft diameter		mm		3	3	3	3		3	3	3	
4 Number of stages		1	2	2	3	3	4	4	4	5	5	5
5 Max. continuous torque	Nm	1	3	3	6	6	6	6	6	6	6	6
6 Intermittently permissible torque at gear output	Nm	1.25	3.75	3.75	7.5	7.5	7.5	7.5	7.5	7.5	7.5	7.5
7 Max. efficiency	%	80	75	75	70	70	60	60	60	50	50	50
8 Weight	g	118	162	162	194	194	226	226	258	258	258	258
9 Average backlash no load	°	0.7	0.8	0.8	1.0	1.0	1.0	1.0	1.0	1.0	1.0	1.0
10 Mass inertia	gcm ²	1.5	0.8	0.8	0.7	0.7	0.7	0.7	0.7	0.7	0.7	0.7
11 Gearhead length L1	mm	26.4	36.3	36.3	43.0	43.0	49.7	49.7	56.4	56.4	56.4	56.4



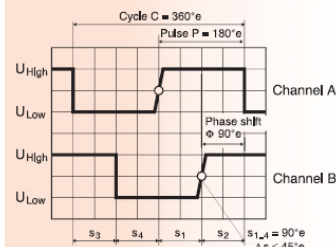
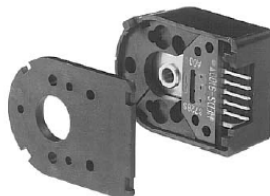
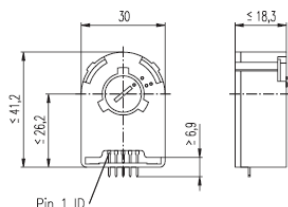
Combination

+ Motor	Page	+ Tacho / Brake	Page	Overall length [mm]	= Motor length + gearhead length + (tacho / brake) + assembly parts									
RE 25, 10 W	77			81.0	90.9	90.9	97.6	97.6	104.3	104.3	104.3	111.0	111.0	111.0
RE 25, 10 W	77	MR	258	92.0	101.9	101.9	108.6	108.6	115.3	115.3	115.3	122.0	122.0	122.0
RE 25, 10 W	77	Enc 22	260	95.1	105.0	105.0	111.7	111.7	118.4	118.4	118.4	125.1	125.1	125.1
RE 25, 10 W	77	HED_5540	262/264	101.8	111.7	111.7	118.4	118.4	125.1	125.1	125.1	131.8	131.8	131.8
RE 25, 10 W	77	DCT 22	271	103.3	113.2	113.2	119.9	119.9	126.6	126.6	126.6	133.3	133.3	133.3
RE 25, 20 W	78			69.5	79.4	79.4	86.1	86.1	92.8	92.8	92.8	99.5	99.5	99.5
RE 25, 20 W	79			81.0	90.9	90.9	97.6	97.6	104.3	104.3	104.3	111.0	111.0	111.0
RE 25, 20 W	79	MR	258	92.0	101.9	101.9	108.6	108.6	115.3	115.3	115.3	122.0	122.0	122.0
RE 25, 20 W	79	Enc 22	260	95.1	105.0	105.0	111.7	111.7	118.4	118.4	118.4	125.1	125.1	125.1
RE 25, 20 W	79	HED_5540	262/264	101.8	111.7	111.7	118.4	118.4	125.1	125.1	125.1	131.8	131.8	131.8
RE 25, 20 W	79	DCT 22	271	103.3	113.2	113.2	119.9	119.9	126.6	126.6	126.6	133.3	133.3	133.3
RE 25, 20 W	79	HED_5540 / AB 28	308	132.2	142.1	142.1	148.8	148.8	155.5	155.5	155.5	162.2	162.2	162.2
RE 26, 18 W	80			85.3	95.2	95.2	101.9	101.9	108.6	108.6	108.6	115.3	115.3	115.3
RE 26, 18 W	80	MR	258	96.3	106.2	106.2	112.9	112.9	119.6	119.6	119.6	126.3	126.3	126.3
RE 26, 18 W	80	Enc 22	260	102.7	112.6	112.6	119.3	119.3	126.0	126.0	126.0	132.7	132.7	132.7
RE 26, 18 W	80	HED_5540	262/264	103.7	113.6	113.6	120.3	120.3	127.0	127.0	127.0	133.7	133.7	133.7
RE 26, 18 W	80	DCT 22	271	106.3	116.2	116.2	122.9	122.9	129.6	129.6	129.6	136.3	136.3	136.3
RE 30, 60 W	81			94.5	104.4	104.4	111.1	111.1	117.8	117.8	117.8	124.5	124.5	124.5
RE 30, 60 W	81	MR	259	105.9	115.8	115.8	122.5	122.5	129.2	129.2	129.2	135.9	135.9	135.9
RE 35, 90 W	82			97.4	107.3	107.3	114.0	114.0	120.7	120.7	120.7	127.4	127.4	127.4
RE 35, 90 W	82	MR	259	108.8	118.7	118.7	125.4	125.4	132.1	132.1	132.1	138.8	138.8	138.8
RE 35, 90 W	82	HED_5540	262/264	118.4	128.3	128.3	135.0	135.0	141.7	141.7	141.7	148.4	148.4	148.4
RE 35, 90 W	82	DCT 22	271	115.5	125.4	125.4	132.1	132.1	138.8	138.8	138.8	145.5	145.5	145.5
RE 35, 90 W	82	AB 28	308	133.5	143.4	143.4	150.1	150.1	156.8	156.8	156.8	163.5	163.5	163.5
RE 35, 90 W	82	HEDS 5540 / AB 28	262/308	150.6	160.5	160.5	167.2	167.2	173.9	173.9	173.9	180.6	180.6	180.6
RE 36, 70 W	83			97.7	107.6	107.6	114.3	114.3	121.0	121.0	121.0	127.7	127.7	127.7
RE 36, 70 W	83	MR	259	109.1	119.0	119.0	125.7	125.7	132.4	132.4	132.4	139.1	139.1	139.1
RE 36, 70 W	83	HED_5540	262/264	118.7	128.6	128.6	135.3	135.3	142.0	142.0	142.0	148.7	148.7	148.7
RE 36, 70 W	83	DCT 22	271	115.8	125.7	125.7	132.4	132.4	139.1	139.1	139.1	145.8	145.8	145.8

11.10 Slave Motor Encoder

Encoder HEDS 5540, 500 Counts per turn, 3 Channels

maxon tachometer



- ☒ Stock program
- ☐ Standard program
- ☐ Special program (on request)

Order Number

110511 110513 110515

Type	500	500	500
Counts per turn	500	500	500
Number of channels	3	3	3
Max. operating frequency (kHz)	100	100	100
Shaft diameter (mm)	3	4	6



Combination	Page	+ Gearhead	Page	+ Brake	Page	Overall length [mm] / see: + Gearhead
RE 25, 10 W	77					75.3
RE 25, 10 W	77	GP 26, 0.5 - 2.0 Nm	235			•
RE 25, 10 W	77	GP 32, 0.4 - 2.0 Nm	237			•
RE 25, 10 W	77	GP 32, 0.75 - 6.0 Nm	238/240			•
RE 25, 20 W	79					75.3
RE 25, 20 W	79	GP 26, 0.5 - 2.0 Nm	235			•
RE 25, 20 W	79	GP 32, 0.4 - 2.0 Nm	237			•
RE 25, 20 W	79	GP 32, 0.75 - 6.0 Nm	238/240			•
RE 25, 20 W	79			AB 28	308	105.7
RE 25, 20 W	79	GP 26, 0.5 - 2.0 Nm	235	AB 28	308	•
RE 25, 20 W	79	GP 32, 0.4 - 2.0 Nm	237	AB 28	308	•
RE 25, 20 W	79	GP 32, 0.75 - 6.0 Nm	238/240	AB 28	308	•
RE 26, 18 W	80					77.2
RE 26, 18 W	80	GP 26, 0.5 - 2.0 Nm	235			•
RE 26, 18 W	80	GP 32, 0.4 - 2.0 Nm	237			•
RE 26, 18 W	80	GP 32, 0.75 - 6.0 Nm	238/240			•
RE 35, 90 W	82					91.9
RE 35, 90 W	82	GP 32, 0.75 - 6.0 Nm	239/240			•
RE 35, 90 W	82	GP 32, 8 Nm	242			•
RE 35, 90 W	82	GP 42, 3.0 - 15 Nm	244			•
RE 35, 90 W	82			AB 28	308	124.1
RE 35, 90 W	82	GP 32, 0.75 - 6.0 Nm	239/240	AB 28	308	•
RE 35, 90 W	82	GP 42, 3.0 - 15 Nm	244	AB 28	308	•
RE 36, 70 W	83					92.2
RE 36, 70 W	83	GP 32, 0.4 - 2.0 Nm	237			•
RE 36, 70 W	83	GP 32, 0.75 - 6.0 Nm	239/240			•
RE 36, 70 W	83	GP 42, 3.0 - 15 Nm	244			•
RE 40, 150 W	84					91.7
RE 40, 150 W	84	GP 42, 3.0 - 15 Nm	244			•
RE 40, 150 W	84	GP 52, 4.0 - 30 Nm	247			•
RE 40, 150 W	84			AB 28	308	124.2
RE 40, 150 W	84	GP 42, 3.0 - 15 Nm	244	AB 28	308	•
RE 40, 150 W	84	GP 52, 4.0 - 30 Nm	247	AB 28	308	•

Technical Data	Pin Allocation	Connection example
Supply voltage 5 V ± 10 %	Encoder	Channel A
Output signal TTL compatible	Pin 5	Channel B
Phase shift F (nominal) 90°e ± 45°e	Pin 4	Channel I
Signal rise time (typical at C _L = 25 pF, R _L = 2.7 kΩ, 25°C) 180 ns	Pin 3	V _{CC}
Signal fall time (typical at C _L = 25 pF, R _L = 2.7 kΩ, 25°C) 40 ns	Pin 2	Channel A
Index pulse width (nominal) 90°e	Pin 1	Channel I
Operating temperature range -40 ... +100°C		GND
Moment of inertia of code wheel ≤ 0.6 gcm ²		
Max. angular acceleration 250 000 rad s ⁻²		
Output current per channel min. -1 mA, max. 5 mA		

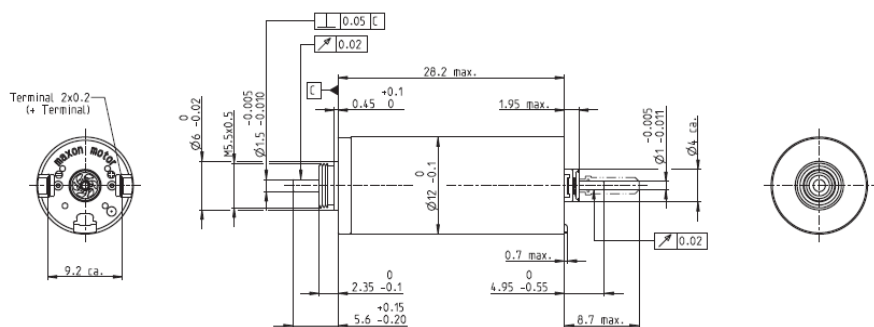
11.11 Master Motor

DCX 12 L Precious Metal Brushes DC motor Ø12 mm

2.5/4.8 W 4.2 mNm 12000 rpm



maxon X drives



M 3:2

Motor Data								
1_	Nominal voltage	V	3	4.5	6	9	12	18
2_	No load speed	rpm	8800	8810	8810	8820	8810	8800
3_	No load current	mA	34.5	23	17.2	11.5	8.62	5.75
4_	Nominal speed	rpm	6360	5710	5600	5800	5600	5590
5_	Nominal torque (max. continuous torque)	mNm	2.88	4.07	3.92	4.16	3.92	3.89
6_	Nominal current (max. continuous current)	A	0.924	0.861	0.622	0.441	0.311	0.206
7_	Stall torque	mNm	10.4	11.6	10.8	12.2	10.8	10.7
8_	Stall current	A	3.24	2.4	1.68	1.26	0.842	0.554
9_	Max. efficiency	%	81	82	81	82	81	81
10_	Terminal resistance	Ω	0.927	1.87	3.58	7.12	14.3	32.5
11_	Terminal inductance	mH	0.031	0.071	0.125	0.282	0.502	1.13
12_	Torque constant	mNm/A	3.22	4.83	6.44	9.66	12.9	19.3
13_	Speed constant	rpm/V	2970	1980	1480	989	741	494
14_	Speed/torque gradient	rpm/mNm	854	766	823	729	821	831
15_	Mechanical time constant	ms	4.32	4.27	4.28	4.27	4.28	4.3
16_	Rotor inertia	gcm²	0.484	0.533	0.496	0.559	0.498	0.495
Thermal data				Operating Range				
17_	Thermal resistance housing-ambient	K/W	31	n [rpm] Winding 4.5 V				
18_	Thermal resistance winding-housing	K/W	10.3					
19_	Thermal time constant winding	s	10.1					
20_	Thermal time constant motor	s	194					
21_	Ambient temperature ball bearings	°C	-40...+85					
21_	Ambient temperature sleeve bearings	°C	-30...+85					
22_	Max. winding temperature	°C	100					
Mechanical data ball bearings								
23_	Max. speed	rpm	12000					
24_	Axial play	mm	0...0.1					
	Preload	N	0.5					
25_	Radial play	mm	0.015					
26_	Max. axial load (dynamic)	N	0.5					
27_	Max. force for press fits (static)	N	8.8					
	(static, shaft supported)	N	120					
28_	Max. radial load [mm from flange]	N	1.5 [5]					
Mechanical data sleeve bearings				maxon Modular System				
23_	Max. speed	rpm	12000	maxon gear	Stages	maxon sensor	maxon motor control	
24_	Axial play	mm	0...0.15	116_GPX 12 A/C	1-4	146_ENX 10 EASY	416_ESCON Module 24/2	
	Preload	N	0	117_GPX 12 LN/LZ	1-4	146_ENX 10 QUAD	416_ESCON 36/2 DC	
25_	Radial play	mm	0.015	118_GPX 12 HP	2-4		424_EPOS2 24/2 (DC/EC)	
26_	Max. axial load (dynamic)	N	0.1	119_GPX 14 A/C	3-4		424_EPOS2 Module 36/2	
27_	Max. force for press fits (static)	N	30	120_GPX 14 LN/LZ	3-4			
	(static, shaft supported)	N	120	121_GPX 14 HP	4			
28_	Max. radial load [mm from flange]	N	0.8 [5]					
Other specifications				Configuration				
29_	Number of pole pairs		1	Bearing: Sleeve bearings/ball bearings preloaded				
30_	Number of commutator segments		7	Commutation: Precious metal brushes with or without CLL				
31_	Weight of motor	g	16	Flange front/back: Standard flange/Flange with thread holes/no flange				
32_	Typical noise level	dBA	44	Shaft front/back: Length				
				Electric connection: Terminals or cable/cable length/connector type				

xdrives.maxonmotor.com

xdrives.maxonmotor.com

April 2016 edition / provisional data / subject to change

maxon X drives 67

11.12 Master Motor Encoder

Sensor - ENX10 EASY 512IMP



Type	
Counts per turn	512
Number of channels	3
Line Driver	RS422
Max. outer diameter	10 mm
Max. housing length	8.5 mm
Max. electrical speed	90000 rpm
Max. speed	30000 rpm
Technical data	
Supply voltage, typical	5 V
Supply voltage tolerance +/-	10 %
Output signal driver	Differential, EIA RS 422
Current per cable	-20...20 mA
Min. state length	45 °el
Min. state length	135 °el
Signal rise time/Signal fall time	20/20 ns
Min. state duration	125 ns
Direction of rotation	A for B, CW
Index position	A low & B low
Index synchronously to AB	yes
Index pulse width	90 e°
Typical current draw at standstill	23 mA
Max. moment of inertia of code wheel	0.05 gcm ²
Weight (Standard cable length)	7.1 g
Operating temperature range	-40...100 °C
Number of autoclave cycles	0

Datasheet: http://www.maxonmotor.com/medias/CMS_Downloads/DIVERSES/ENXEASY_en.pdf

12 APPENDIX C ENGINEERING DRAWINGS